THE IDENTIFICATION OF NOVEL MUTATIONS CAUSING FAMILIAL ALS AND THE ELUCIDATION OF COMMON DISEASE MECHANISMS

Midhat Salman

In partial fulfilment of the requirements for the degree of Doctor of Philosophy

Division of Brain Sciences

Department of Medicine

Imperial College London

2018

ABSTRACT

Amyotrophic lateral sclerosis (ALS) is a late onset fatal disease resulting from upper and lower motor neuron degeneration. The lack of an effective treatment for ALS indicates the need for a greater understanding of the pathogenesis underlying the disease. We, therefore, started this thesis with the aim of characterising putative novel familial ALS mutations for elucidating the mechanisms through which they contribute to the disease pathogenesis. We focused on the mutations obtained from the Imperial College FALS cohort and selected mutations in two genes, *RUBCN* and *CLCN6* for characterisation. We performed expression profiling of *RUBCN* in spinal cord samples from SALS cases and found a significant difference in the expression of *RUBCN* compared to controls at both mRNA and protein levels. This encouraged us to characterise the mutation in lymphoblastoid cell lines (LCLs) derived from the individuals of the relevant FALS pedigree. We were highly encouraged by a significant downregulation at basal levels in the mRNA expression of three genes that belong to different neuroprotective pathways in the presence of the mutation. In the case of *CLCN6,* we found a significant downregulation in its protein expression with the presence of ER stress in SALS cases. In LCLs derived from the individuals of relevant FALS pedigree, we found a significant downregulation in mRNA and protein expression of the UPR pathway genes in the presence of the mutation under cell stress. We also found a significant decrease in cell survival at basal and under cell stress conditions. We concluded that the disruption of the UPR pathway is the molecular mechanism underlying the pathogenesis caused by the *CLCN6* mutation leading to cell death. Hence, our novel findings in SALS and FALS for the mutations in both genes provide a strong evidence of their association with Familial ALS.

DECLARATION

I declare that this thesis is my own composition and the data presented in it is my own original work. The contribution of two other researchers, Alexandra Rother and Ayesha Hashmi, has been appropriately credited within this thesis and all other work is appropriately referenced.

Midhat Salman

COPYRIGHT DECLARATION

Midhat Salman

DEDICATION

This thesis is dedicated to my parents as a symbol of love and appreciation especially to my father whose prayers and strength made me finish this journey despite his departure from this world during the last stages of my PhD degree.

ACKNOWLEDGEMENT

I would like to express my deep gratitude to Professor Jacqueline de Belleroche for her supervision of my PhD degree. I am grateful to her for her invaluable input and guidance throughout my PhD studies and for her ready availability whenever I needed. Her kind nature helped me strive through stressful times during PhD.

Many thanks to everyone in the Neurogenetics group especially to Alex Morris, Intan Bakhtiar, Luigi Montibeller, Roxy Zhang, for their friendship and support and to Alexandra Rother and Ayesha Hashmi for their contribution. Thanks to Maria T Cencioni for her help in cell culture, FACS experiments and for being a lovely friend. Many thanks to Effrosyni Tsafa, Ilaria Palimisano, Rehiana Ali, Felwah Al-Zaid, Mariam Albahrani, Rean Mohammed and Mai Al-Zaydi for their friendship. They all made my time spent at Imperial College London a lovely experience.

Most of all, I am extremely grateful to my family for their unconditional love and support. To my mother for her prayers and dedication to my education and my father for his love and strength that always gave me the courage to go after my dreams. His prayers and strength will stay with me forever despite his absence. To my brother and sister, Khursund and Iflaah, for their support, friendship and well wishes.

I would also like to thank Imperial College London for awarding me with the prestigious 'President's PhD scholarship' to undertake the PhD degree, to the Edith Evelyn Wali Mohammad Memorial Fund and the Charles Wallace Pakistan Trust for awarding the grant for the PhD write-up stage.

TABLE OF CONTENTS

LIST OF FIGURES

LIST OF TABLES

ABBREVIATIONS

ALS	Amyotrophic lateral sclerosis
FALS	Familial amyotrophic lateral sclerosis
SALS	Sporadic amyotrophic lateral sclerosis
UMN	Upper motor neurons
LMN	Lower motor neurons
FTD	Frontotemporal dementia
SorCS2	Sortilin-related receptor CNS expressed 2
TDP-43	TAR DNA-binding protein 43
FUS	Fused in sarcoma
C9orf72	Chromosome 9 open reading frame 72
EMG	Electromyography
NCS	Nerve conduction studies
MRI	Magnetic resonance imaging
GWAS	Genome wide association studies
DNA	Deoxyribonucleic acid
RNA	Ribonucleic acid
QGSY-rich region	Glutamine-glycine-serine-tyrosine)-rich region
RGG domain	Arg-Gly-Gly repeats
DPRs	Dipeptide repeat proteins
$PI(3,5)P_2$	Phosphatidylinositol 3,5-bisphosphate
ER	Endoplasmic reticulum
hiPSC	Human induced pluripotent stem cells
UPR	Unfolded protein response

UPS	Ubiquitin–proteasome system
ERAD	ER-associated protein degradation
IRE1	Inositol-requiring enzyme-1
PERK	Double stranded RNA-activated protein kinase (PKR)-like ER kinase
ATF6	Activating transcription factor 6
eIF2α	Eukaryotic initiation factor-2
Nrf2	Nuclear factor erythroid 2-related factor 2
CHOP	C/EBP-homologous protein
CMA	Chaperone mediated autophagy
mTOR	Mechanistic target of rapamycin
ULK	Unc-51-Like Kinases
DENN	Differentially expressed in normal and neoplastic cells
GEF	Guanine-nucleotide exchange
NEFH	Neurofilament heavy subunit
ROS	Reactive oxygen species
$O_2{\cdot}^-$	Superoxide radical anion
·NO	Nitric oxide radical
·OH	Hydroxyl radical
H_2O_2	Hydrogen peroxide
Na^+	Sodium ion
Ca^{2+}	Calcium ions
Cl^-	Chloride ion
H^+	Proton
miRNA	MicroRNA

LCLs	Lymphoblastoid cell lines
mRNA	Messenger RNA
PCR	Polymerase chain reaction
qPCR	Quantitative PCR
$MgCl_2$	Magnesium chloride
ExoSAP	Exonuclease I - Shrimp Alkaline Phosphatase
SDS-PAGE	Sodium dodecyl sulphate-polyacrylamide gel electrophoresis
RIPA buffer	Radioimmunoprecipitation assay buffer
BSA	Bovine serum albumin
TBST	Tris Buffer Saline Tween 20
PBST	Phosphate buffer Saline Tween 20
ECL substrate	Enhanced luminol-based chemiluminescent substrate
FITC	Fluorescein isothiocyanate
PS	Phospholipid phosphatidylserine
PI	Propidium iodide
EDTA	Ethylenediaminetetraacetic acid
NaCl	Sodium chloride
ddH_2O	Double distilled water
TEMED	Tetramethylethylenediamine
KCl	Potassium chloride
EVS	Exome Variant Server
CCD	coiled-coiled domain
NADPH	Nicotinamide adenine dinucleotide phosphate
LPS	Lipopolysaccharide
NCL	Neuronal ceroid lipofuscinosis

SEM	Standard error of the mean
PIK3C3	Phosphatidylinositol 3-kinase catalytic subunit type 3
EBV	Epstein-Barr virus
ECACC	The European Collection of Authenticated Cell Cultures
GAPDH	Glyceraldehyde 3-phosphate dehydrogenase
FACS	Fluorescence-activated cell sorting
TN	Tunicamycin
TG	Thapsigargin
R	Rapamycin
DMSO	Dimethyl sulfoxide
WT	Wild type
SD	Standard deviation
t-BH	Tertiary-butyl hydroperoxide
LAP	LC3-associated phagocytosis
PE	Phosphatidylethanolamine
n-BP	n-butylidenephtalide
ClC	Chloride channels
veh	Vehicle
PRR	Pattern-recognition receptors
DAPI	4′,6-diamidino-2-phenylindole

Chapter 1: Introduction

Amyotrophic lateral sclerosis (ALS) was a term first coined by Jean Martin Charcot. Amyotrophic means no muscle nourishment and lateral sclerosis means the hardening of tissues in the lateral spinal cord. ALS is a rapidly progressing late onset neurodegenerative disease that occurs due to the degeneration of upper and lower motor neurons in brain and spinal cord resulting in muscle spasticity, stiffness and atrophy. Muscle spasticity and stiffness occur due to the failure of upper motor neurons (present in motor cortex) and muscle atrophy occurs due to the degeneration of lower motor neurons (brain stem and spinal cord) (Brown and Al-Chalabi, 2017).

The disease often becomes fatal due to respiratory failure within 3-5 years of symptom onset (Cox et al., 2010) but the variability in the disease course is large with some patients dying within months and others surviving for two decades or more after symptom onset (Robberecht and Philips, 2013). The incidence and prevalence of the disease increases with age. In the United States and Europe, 1 or 2 people are affected per 100,000 each year with the total number of cases of 3 to 5 per 100,000 each year (Chio et al., 2013). The disease is classified as sporadic or familial with approximately 10% of the cases with a family history of the disease and thus have familial (FALS) form of ALS while the remaining do not have a family history and so have sporadic ALS (SALS). Men are more frequently affected than women with a ratio of 2:1 in sporadic ALS, whereas, the ratio is similar between men and women in familial ALS. The mean age of the disease onset is mid to late 50s, whereas, familial ALS may also have an onset in late teen or early adulthood and such types of ALS are called juvenile ALS (Brown and Al-Chalabi, 2017, Baumer et al., 2010)

Research has shown that the disease is caused by a combination of genetic, epigenetic and environmental factors (Dolinar et al., 2018). There is no known cause for sporadic ALS but

various studies have reported potential environmental risk factors associated with the development of sporadic ALS including military service, agricultural work, football, heavy metals, smoking, electric shock, geography and pesticides. Apart from the environmental risk factors, many mutations found in FALS have also been found in SALS (Ingre et al., 2015, Al-Chalabi and Hardiman, 2013). A possible genetic contribution is likely to be present in most patients with ALS with a complex range of effect sizes extending from classical Mendelian patterns of inheritance to multiple rare variants acting in combination where environmental effects provide the age-dependant succeeding steps required for the disease appearance (Talbot et al., 2018). Sporadic ALS and familial ALS show similarities in their clinical and pathological features which suggests the presence of common cellular and molecular disease mechanisms between both types of the disease (Brown and Al-Chalabi, 2017).

1.1 Clinical presentation

There are four main clinical presentations of ALS depending on the population of motor neurons involved (Ludolph et al., 2015).

1. Primary lateral sclerosis: It involves upper motor neurons (UMN), corticopontine and corticospinal motor neurons, with mild lower motor neuron (LMN) dysfunction. It shows a slow progression of severe spastic muscle stiffness and shows mild muscle atrophy. It may also involve prominent bulbar symptoms (Gordon et al., 2006, Brown and Al-Chalabi, 2017).
2. Limb-onset ALS/Flail arm (Vulpian Bernhard) syndrome and Flail leg syndrome: It involves both upper and lower motor neurons. A minimum of two body regions are involved at onset in this form of ALS (Ludolph et al., 2015).

3. Progressive muscular atrophy: It has predominant involvement of lower motor neurons with little or no involvement of upper motor neuron and slight spasticity (Brown and Al-Chalabi, 2017).
4. Progressive bulbar palsy/bulbar-onset ALS: It involves the dysfunction of both upper and lower motor neurons. It initially starts with difficulties in speech and swallowing and then shows limb features later during the disease course. Symptoms of emotional lability defined by the outbursts of laughing or crying are also prominent (Ludolph et al., 2015, Gordon et al., 2006).

ALS symptoms include the combination of upper and lower motor neuron. Upper motor neuron signs include slow movement, hyperreflexia and increased muscle tone. Symptoms of lower motor neurons include weakness, muscle atrophy, hyporeflexia and fasciculations (Ferguson and Elman, 2007). ALS may have a bulbar onset or limb onset. The symptoms of ALS start with a progressive unilateral weakness in the distal legs and arms. Patients with bulbar onset experience difficulties with speaking, chewing and swallowing and may also experience muscle cramps or twitches (Hulisz, 2018). Patients with limb onset experience difficulties with their gait and with other simple daily activities such as buttoning a shirt or holding a cup. The higher mental functions such as reasoning, understanding, problem solving and remembering are usually retained. Patients do not always show a linear progression of the disease and may sometimes have a duration of limited or no function loss during the disease progression. ALS reversals and arrests have also been reported in some cases where the patient shows recovery of the lost functions but this has been observed only in less than 1% of the patients (Hulisz, 2018). Prefrontal and temporal cortex neurons can also be affected in ALS resulting in frontotemporal dementia (FTD) in about 15% of the patients (Robberecht and Philips, 2013).

1.2 Pathological features

The main pathological feature of ALS is the death of motor neurons in motor cortex and spinal cord. There is a degeneration and loss of Betz cells in the motor cortex (Hammer et al., 1979). The spinal cord frequently shows atrophy of the anterior nerve roots. The loss of myelinated axons in the lateral and anterior columns of the spinal cord causes thinning and scarring (sclerosis) of the lateral aspects of the spinal cord. As the disease progresses, there is atrophy of the muscles of the tongue, oropharynx, and limbs (Brown and Al-Chalabi, 2017). Patients having ALS with frontotemporal dementia also show neuronal degeneration in frontal and/or temporal cortex (Murphy et al., 2007). Motor neuron degeneration is also accompanied by neuroinflammation around the area of degeneration causing the proliferation of microglia, astroglia and oligodendroglial cells (Philips and Rothstein, 2014, Kang et al., 2013, McGeer and McGeer, 2002, Schiffer and Fiano, 2004).

The presence of Bunina bodies and Lewy body-like inclusions in neuronal cells formed by the abnormal accumulation of protein aggregates are a characteristic pathological feature of ALS in both sporadic and familial ALS (Mizuno et al., 2011). Bunina bodies are found in the cytoplasm of motor neurons and are round to oval small (2–4 μm in diameter) intracellular inclusions in the motor neurons of the brain stem and spinal cord (Tomonaga et al., 1978). They are positive for cystatin c, transferrin, peripherin and sortilin-related receptor CNS expressed 2 (SorCS2) but negative for proteins commonly associated with neurodegeneration (Mizuno et al., 2011, Mizuno et al., 2006, Mori et al., 2015). Lewy body-like hyaline inclusions and skein-like inclusions are ubiquitin-positive and are found in the cytoplasm of motor neurons in the anterior horn of spinal cord. They are rounded structures composed of bundles of thick filaments and have a thread-like structure (Mizusawa, 1993, Saberi et al., 2015). Apart from motor neurons, the inclusions can also be found in glial cells (Arai et al., 2003). Some of the proteins present in inclusions are common in most of the disease cases such as ubiquitinated

TDP-43 protein aggregate inclusions where the loss of nuclear TDP-43 leads to the formation of aggregates in the cytoplasm (Giordana et al., 2010). Other types of protein aggregates are detected only in specific ALS subtypes depending on the genetic cause such as SOD1 aggregates, FUS positive aggregates, and C9orf72 aggregates all showing distinctive neuropathological signature for example the ALS cases with *SOD1* mutations show SOD1 positive inclusions that are negative for TDP-43 (Kato et al., 2000).

1.3 Diagnosis

The symptoms of ALS can be similar to a few other diseases in the early stages of the disease, so multiple tests are performed to exclude the possibility of other conditions. The tests used to exclude other conditions include laboratory tests, electromyography (EMG), nerve conduction studies (NCSs) and Magnetic resonance imaging (MRI) (Ferguson and Elman, 2007, Brown and Al-Chalabi, 2017, Al-Chalabi et al., 2016). The laboratory tests performed include complete blood count, liver and thyroid function tests, electrolytes, creatine kinase, erythrocyte sedimentation rate, rheumatoid factor, antinuclear antibody, vitamin B12, serum protein electrophoresis with immunofixation, anti-GM1 ganglioside antibody, and 24-hour urine protein electrophoresis with immunofixation (Ferguson and Elman, 2007). The EMG findings for ALS include positive sharp waves, neurogenic potentials, fasciculation potentials and fibrillation potentials (Ludolph et al., 2015). The NCS findings for ALS are normal or slightly abnormal with an absence of motor conduction block. Patients also have normal sensory nerve action potentials (Ferguson and Elman, 2007). Sophisticated structural MRI studies can be used to indicate disease-related changes within the interhemispheric white matter projections, primary motor cortices and corticospinal tracts (Muller et al., 2016).

After other diagnosis has been excluded, the revised El Escorial criteria–2015 is used for diagnosis and is currently the clinical standard for ALS diagnosis. The criteria require the

evidence of the progression of UMN and LMN dysfunction in at least one limb or region of the body, or LMN deficits in one body region identified by clinical examination or in two body regions by EMG (Ludolph et al., 2015).

Genetic testing is also used if the patient has a first or a second-degree relative diagnosed with ALS or FTD within 3 generations. Such a patient will have the familial form of ALS. On identification of a pathogenic mutation in a disease-causing gene in the patient that segregates with the disease in the family the term hereditary or primary genetic ALS is used instead of familial ALS. The genetic variant gene serves as a substitute for upper motor neuron dysfunction or a second limb or region in such cases (Ludolph et al., 2015).

1.4 Treatment

The current treatments available for ALS slow the progression of the disease but do not offer a substantial clinical benefit to the patients. Two drugs, riluzole and edaravone, have been approved by the Food and Drug Administration for the treatment of ALS (Oskarsson et al., 2018). Riluzole has been the only drug in routine clinical use. It is known to block voltage-sensitive Na+ channels and reduce the release of glutamate. It is taken in the form of a pill by the patient. Edaravone was approved for ALS treatment in 2017. It is a free radical scavenger and acts by supressing oxidative stress. It helps in reducing the rate of patient immobility (Brown and Al-Chalabi, 2017, Talbot et al., 2018). It is given to the patients via intravenous infusion. Apart from drug treatment, care is provided to manage the symptoms of patients with ALS which include the use of ventilatory support, nasogastric feeding and prevention of aspiration (Brown and Al-Chalabi, 2017). Several new approaches are also under progress as a potential therapy for the disease such as antisense oligonucleotides targeting C9orf72 (Jiang et al., 2016), transplantation of spinal cord-derived neural stem cells and the use of embryonic stem cell-derived astrocytes (Glass et al., 2016, Barbeito, 2018).

Currently, the diagnosis of the disease is through assessment of clinical symptoms which occur only after a large number of motor neurons have already died. Thus, the available drugs will only be more effective if the disease is diagnosed earlier to prevent further damage to motor neurons. A lot of efforts are being put into discovering biomarkers for early disease diagnosis though no reliable molecular biomarker has been identified so far. Additionally, new pathogenic pathways underlying the disease are being uncovered with the advances in the discovery of genetic causes that also contribute to the identification of potential biomarkers and drug targets (Chia et al., 2018).

1.5 Genetics

Most forms of familial ALS are transmitted with an autosomal dominant pattern of inheritance but it can also be inherited in an autosomal recessive or X-linked manner. In some cases, the same gene may show a different pattern of inheritance in different families depending on the sequence variant involved (Andersen and Al-Chalabi, 2011). The pace of gene discovery has greatly accelerated in the last few years through which there has been a rapid advancement in the understanding of the genetic causes of ALS. This has mainly been possible due to the advances in genotyping and sequencing technologies. Currently, large sample sets are being used to search for genes linked to ALS using genome wide association studies (GWAS) and next-generation sequencing technologies such as whole-genome sequencing and whole-exome sequencing especially for patients with the availability of few DNA samples from their families or with no family history of ALS (Leblond et al., 2014, Renton et al., 2014). Whole exome or whole genome sequencing technologies produce a huge amount of sequencing data as a result of large scale parallel DNA sequencing allowing the identification of many potential ALS associated DNA variants (Marangi and Traynor, 2015). Variants present in multiple independent families and cohorts, with increased burden in cases compared to controls are the strongest candidates for having an association with ALS (Brown and Al-Chalabi, 2017).

The identification of the first causative gene of ALS, *SOD1*, in 1993 indicated the involvement of a genetic factor in ALS and directed the focus of research towards the identification of genetic causes of the disease for the better understanding of the pathogenesis of the disease and for the identification of possible therapeutic targets (Rosen et al., 1993). The second cause of ALS, *TARDBP*, was identified in 2008 after a big gap since the discovery of *SOD1* (Sreedharan et al., 2008). The genetic cause of about 70% of familial and up to 10% of sporadic cases have now been found to date (Volk et al., 2018) with more than 25 genes discovered (Brown and Al-Chalabi, 2017) with the number rapidly increasing each year. A general belief is that the disease occurs as a result of an interplay between environmental and genetic factors but it is also believed that all cases occur primarily as a result of the involvement of genetic factors. In addition, ALS has also been suggested to be a multistep process (Al-Chalabi et al., 2014). The identified ALS genes can generally be clustered into three categories with genes that are (1) involved in protein homeostasis (2) involved in RNA homeostasis and trafficking (3) involved in cytoskeletal dynamics (Figure 1-1) (Brown and Al-Chalabi, 2017, Peters et al., 2015). All these mechanisms are interlinked such as protein aggregates formed by alteration in protein homeostasis may sequester proteins involved in RNA binding and subsequently disturbing RNA trafficking and homeostasis (Brown and Al-Chalabi, 2017).

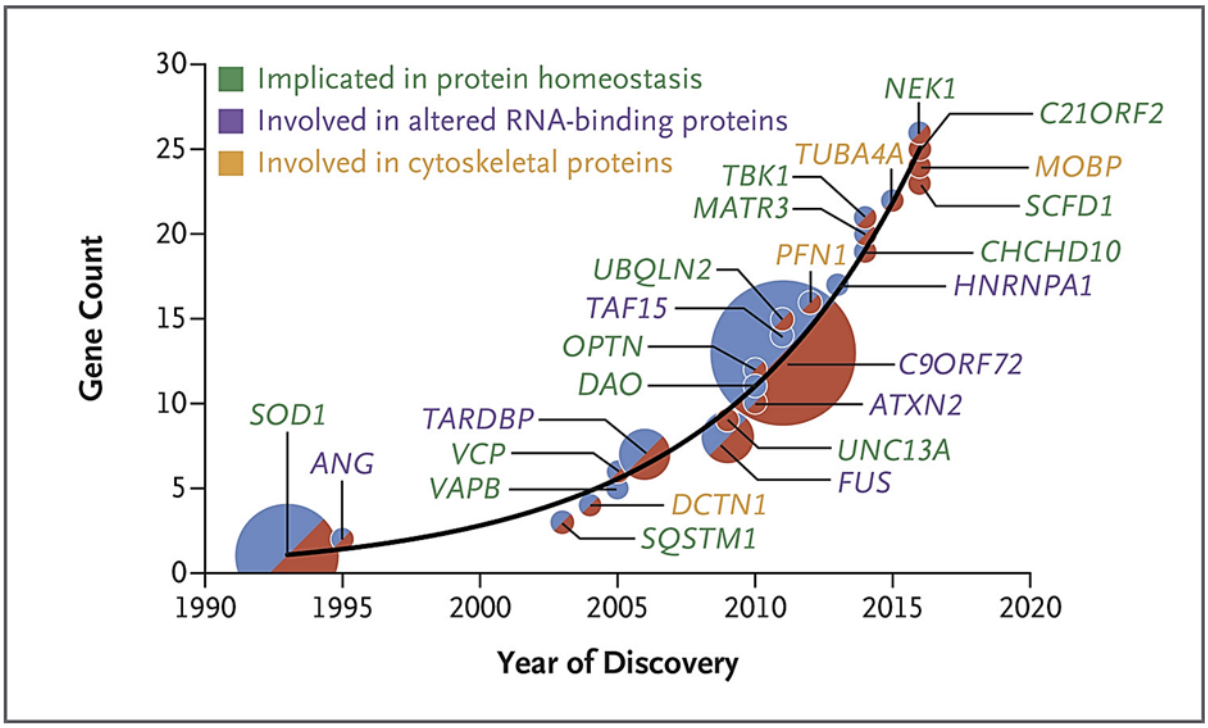

Figure 1-1 The ALS genes identified to date

Multiple ALS genes have been identified to date starting from *SOD1* in 1993. The graph indicates the sequence of gene discovery during the period. The colour of the gene name indicates the role it performs. The size of the circles indicates the proportion of ALS cases associated with the relevant gene. Blue circles show link of the gene with familial ALS, red circles show link with sporadic ALS and the presence of both colours in a circle indicate the link of the gene with both familial and sporadic ALS (Brown and Al-Chalabi, 2017)

1.5.1 Major ALS-related genes

C9ORF72, *SOD1*, *TARDBP* and *FUS* are the most common genes involved in causing ALS in Asian and European populations but the genetic landscape is different between Asian and European populations (Zou et al., 2017). The function of these genes and the related pathogenic mechanisms contributing to the disease are described below.

1.5.1.1 *SOD1*

Superoxide dismutase 1 (*SOD1*) was the first gene identified as a cause of familial ALS by linkage analysis in 1993 (Rosen et al., 1993). More than 200 mutations have been reported in *SOD1* in patients with ALS since then (Wroe et al., 2008). Mutations in *SOD1* cause ALS in about 20% of familial and in about 1-4% of sporadic ALS cases (Pasinelli and Brown, 2006). ALS causing mutations in the gene are mostly missense but insertions, deletions and nonsense mutations have also been reported (Chen et al., 2013). Nonsense mutations were identified at the C-terminal of the protein which suggested that most of the molecule is required for the enzyme to show its pathogenic effect (Robberecht and Philips, 2013).

Patients with mutant SOD1 usually present with limb onset ALS that starts from lower limb but few also show bulbar onset. SOD1 ALS patients show a lot of variation in their clinical phenotype, severity of the disease, age of onset and progression of disease that indicates a possible involvement of environmental factors along with genetic factors (Chen et al., 2013). For example, the $SOD1^{D90A}$ mutation has been linked to autosomal dominant ALS in some groups while to autosomal recessive ALS in a Scandinavian population. Patients with $SOD1^{A4V}$ mutation have a short survival span of about one year after symptom onset (Pasinelli and Brown, 2006) compared to patients with $SOD1^{D90A}$ mutation who have a long survival of about 10 years (Andersen et al., 1996). Similarly, the $SOD1^{I113T}$ mutation has a variable age of onset, clinical phenotype, penetrance and disease progression (Lopate et al., 2010).

SOD1 protein is a homodimer that consists of 153 amino acids, a copper and a zinc atom (Turner et al., 2013). Zinc contributes to the structural stability of the protein and copper is required for the activity of SOD1 enzyme. It is a cytoplasmic protein which functions as an antioxidant that converts superoxide radicals to hydrogen peroxide and oxygen (Turner et al., 2013). Since SOD1 detoxifies superoxides, mutation in the protein may lead to oxidative stress. If zinc component of the protein is affected, it becomes misfolded. Mutant SOD1 performs inefficient cellular buffering and inefficient zinc and copper trafficking. Numerous hypotheses have been proposed to explain the mechanisms by which *SOD1* mutations lead to ALS pathology such as oxidative stress, endoplasmic reticulum stress, mitochondrial dysfunction, protein aggregation, glutamate excitotoxicity and inflammation (Turner et al., 2013, Estevez et al., 1999, Tiwari et al., 2005, Morfini et al., 2013). Neuronal inclusions with SOD1 protein aggregates are a hallmark of *SOD1* related ALS and could be a primary pathogenic mechanism underlying the disease (Kato et al., 2000, Ekhtiari Bidhendi et al., 2018). These aggregates are formed when mutant SOD1 protein misfolds and is ubiquitinated to be targeted for degradation (Basso et al., 2006) but instead of degradation, it accumulates in the cytoplasm forming protein aggregates that harm the cellular functions with toxic gain of function (Figure 1-2) (Bendotti et al., 2012, Chen et al., 2012). Mutant SOD1 shows prion-like spread of protein aggregates with an ability to sequester the wild-type SOD1 protein (Polymenidou and Cleveland, 2012) which can misfolded when oxidised and is aggregation-prone (Ezzi et al., 2007).

In vitro and in vivo models of SOD1 mutations are widely used for the investigation of pathogenic mechanisms underlying ALS. Various cellular functions have been reported to fail in mutant SOD1 mouse models including axonal transport and mitochondrial function leading to axonal retraction and denervation ultimately causing cell death (Ilieva et al., 2009). $SOD1^{G93A}$ transgenic mice are the commonly used model for such studies (Gurney, 1997). Compared to SOD1 knockout mice that do not develop ALS, $SOD1^{G93A}$ transgenic mice

develop the disease and also show active SOD1 enzyme indicating that toxic gain of function is responsible for the degeneration of motor neurons in these mice (Massilamany et al., 2013). Latest study also reported the involvement of loss of function contributing to ALS in C. elegans model showing that both gain and loss of function of SOD1 contribute to ALS pathogenesis by affecting different neuronal populations (Baskoylu et al., 2018). SOD1 models have been very useful in elucidating the cellular mechanisms on the one hand but they have not been very helpful in selecting agents for human trials on the other (Ludolph et al., 2007). This is mainly due to the fact that the pathology of SOD1 ALS is distinct from the other ALS cases where TDP-43 or FUS pathology is present indicating different disease mechanisms involved (Mackenzie et al., 2007).

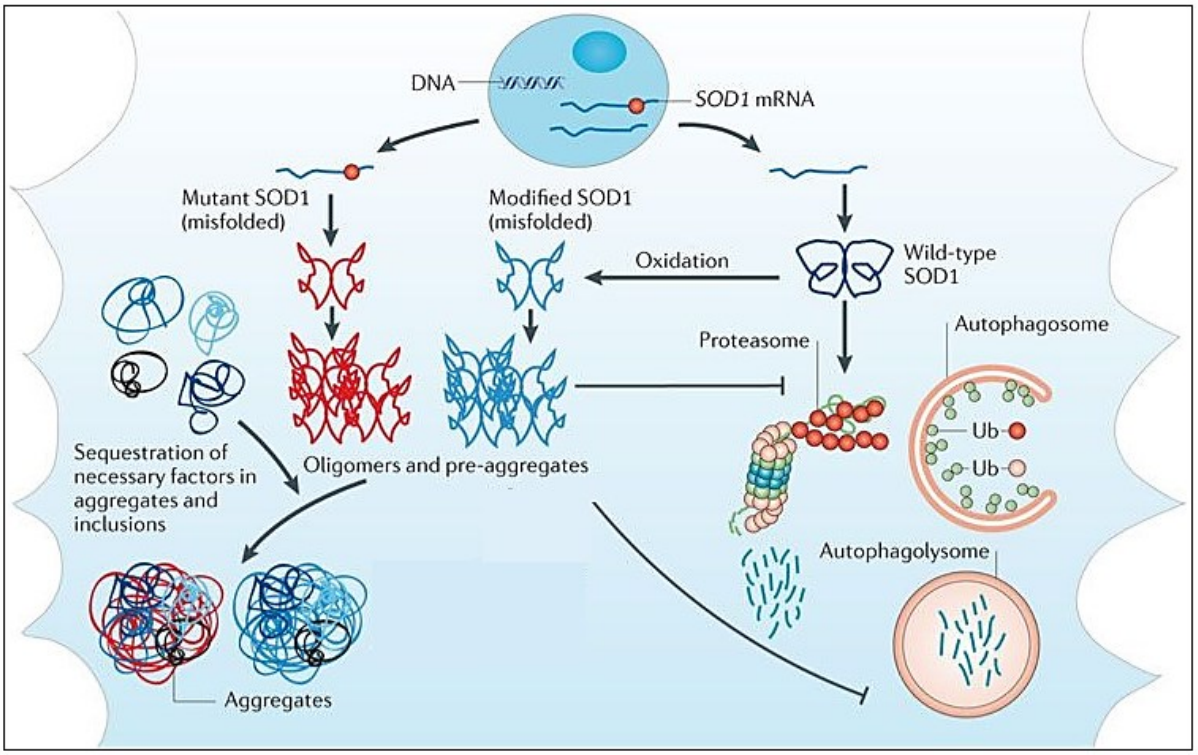

Figure 1-2 Pathogenic mechanisms in ALS associated with SOD1

Mutant SOD1 and oxidised misfolded wild-type SOD1 are able to escape the cellular degradation machinery leading to the formation of protein aggregates inside cell. These aggregates by gain of toxic function impair the cellular protein degradation pathways, sequester essential proteins required in cellular functions and disrupt other cellular processes such as axonal transport and mitochondrial respiration. Adapted from (Robberecht and Philips, 2013).

1.5.1.2 *TARDBP*

After a long gap from the discovery of *SOD1* in 1993, mutations in *TARDBP* were identified in 2008 (Sreedharan et al., 2008). *TARDBP* encodes for TAR DNA binding protein (TDP-43). Ubiquitinated TDP-43 is a major component of neural inclusions and is present in almost 95% ALS cases. TDP-43 inclusions are thus a hallmark for ALS (Sreedharan et al., 2008, Ludolph et al., 2015, Hans et al., 2018). Frequency of mutations in *TARDBP* on the other hand are much lower than the TDP-43 neuropathology accounting for about 4% of familial ALS and about 2% of sporadic ALS cases (Chio et al., 2012). More than 50 missense mutations have been described in the *TARDBP* gene to date and have been identified in C-terminal end of the protein that is involved in ribonucleoprotein binding and mRNA splicing. A few deletion mutations at the C-terminal end of the protein have also been reported (Lee et al., 2011, Kapeli et al., 2017). Patients with *TARDBP* associated ALS predominantly present with limb onset ALS with a variable age of disease onset and disease duration (Sreedharan et al., 2008).

The functional consequences of TDP-43 in ALS pathogenesis are not currently fully known (Miguel et al., 2018). TDP-43 belongs to the family of heterogenous ribonucleoproteins and is located in the nucleus. It shuttles between the nucleus and the cytoplasm as it contains a nuclear localization signal and a nuclear export signal (Robberecht and Philips, 2013). It is a DNA/RNA binding protein and is involved in transcriptional and post-transcriptional regulation (Buratti and Baralle, 2010). It consists of two RNA recognition motifs and binds to GU-rich sequences in the introns that are present in many pre-mRNAs thus targeting about 6000 mRNAs. TDP-43 knock down studies reported changes in the abundance and splicing of hundreds of mRNAs and microRNAs (Tollervey et al., 2011, Polymenidou et al., 2011, Kawahara and Mieda-Sato, 2012). RNAs whose levels were affected the most by the reduction in TDP-43 levels were encoded by genes containing long intronic regions producing proteins involved in synaptic activity of neurons. Many TDP-43 target transcripts are also associated

with neurodegenerative diseases such as transcripts for valosin containing protein (VCP) and fused in sarcoma (FUS) indicating that TDP-43 may have an essential role in the regulation of splicing of genes required in central nervous system (Buratti and Baralle, 2010, Polymenidou et al., 2011). TDP-43 has also been shown to interact with mutant SOD1 indicating a link between the two distinct pathogenic mechanisms (Higashi et al., 2010).

Under stress conditions, TDP-43 is mainly present in the cytoplasm associated with stress granules which are formed under stress and are composed of repressed translational complexes. After the stress has been resolved inside the cell, TDP-43 relocates to the nucleus after stress granules disaggregate. It has been proposed that mutant TDP-43 modifies dynamics of stress granules which in turn leads to the formation of cytoplasmic inclusions and hence, contributing to the TDP-43 proteinopathies observed in ALS by acting as a sink for RNAs or proteins (Liu-Yesucevitz et al., 2010, Dewey et al., 2011). Sequestering of TDP-43 in the stress granules also result in nuclear depletion of TDP-43 leading to loss of function in nucleus. TDP-43 also undergoes secondary modifications inside the cytoplasm which might also contribute to its pathogenicity in ALS (Lee et al., 2011, Hans et al., 2018).

Numerous animal models of TDP-43 have been generated expressing human wild-type protein or mutants linked to ALS that display motor neuron degeneration (Tsao et al., 2012). TDP-43 over expression and deficiency both have been suggested harmful for the cells in *in vitro* and *in vivo* models indicating the importance of tight control of TDP-43 levels in the cell (Robberecht and Philips, 2013). For example, upregulated TDP-43 levels in TDP-43 transgenic mice disrupted RNA metabolism in the motor neurons by altering mRNA splicing and stability and lead to the formation of TDP-43 inclusions (Tsao et al., 2012). TDP-43 is involved in autoregulating its own expression by binding to and enhancing the splicing of an intron in the 3' untranslated region of its own mRNA inducing its degradation (Polymenidou et al., 2011). TDP-43 self-regulation might also be affected by the TDP-43 protein aggregation thus

contributing to the disease pathogenesis (Ayala et al., 2011). Hence, factors that affect the *TARDBP* expression may cause harm to the cell even in the absence of TARDBP mutation by inducing TDP-43 aggregate formation inside the cytoplasm contributing to ALS pathogenesis observed in majority of the cases of ALS (Robberecht and Philips, 2013).

1.5.1.3 *FUS*

Fused in sarcoma (*FUS*) mutation was first identified as a cause of ALS in a family of Cape Verdean origin as a recessive mutation but later dominant missense mutations in FUS were commonly identified (Kwiatkowski et al., 2009). Most of the mutations affect the C-terminal end of the protein and may lead to C-terminal end truncation (Bosco et al., 2010a, Lagier-Tourenne et al., 2010). Mutations in *FUS* account for almost 5% cases of familial ALS and less than 1% cases of sporadic ALS (Lanson and Pandey, 2012, Zou et al., 2017). Most of the cases show lower motor neurons symptoms without the involvement of bulbar region (Chen et al., 2013). Patients with *FUS* mutations show a wide variation in the age of onset of the disease with more than 60% of the cases showing disease onset before 45 years of age and many of them even presenting with juvenile ALS (Bäumer et al., 2010).

FUS and TDP-43 share functional homology but they do not localise in the cytoplasmic aggregates together. ALS cases with FUS mutations show FUS positive inclusions and indicate the involvement of distinct pathogenic mechanisms from TDP-43 positive inclusions (Sun et al., 2011b, Lagier-Tourenne et al., 2012, Shang and Huang, 2016). FUS is predominantly located in the nucleus and is an RNA binding protein like TDP-43 (Kwiatkowski et al., 2009). Mutations at the C-terminal end of FUS disrupt the nuclear localisation signal affecting the nuclear transport of FUS, which leads to the cytoplasmic localisation of the protein and its assembly in stress granules formed in cytoplasm in response to cell stress (Bosco et al., 2010a). Mutant FUS aggregates then cause toxicity by binding RNA and proteins in the aggregates in

a similar manner to TDP-43 aggregates but unlike TDP-43, FUS contains an RGG domain which is critical for FUS aggregation. FUS also contains QGSY-rich region and a glycine rich region which establishes the prion-like domain leading to the formation of FUS aggregates and inclusions (Sun et al., 2011b) and therefore, FUS toxicity or aggregation propensity is not enhanced by mutations in the gene (Sun et al., 2011b).

FUS binds to more than 5000 genes and is involved in splicing of about 1000 mRNAs by binding to the long intronic sequences similar to TDP-43 but mostly targets different genes and mRNAs than TDP-43. Several of the FUS target genes encode neuronal proteins (Lagier-Tourenne et al., 2012) and so, the mutations in FUS raise the possibility of the involvement of defects in RNA homeostasis in neurons by loss of function contributing to the ALS pathogenesis (Shang and Huang, 2016). Several genetic modifiers have been identified that also contribute to FUS-mediated neurodegeneration such as *PINK1* and Parkin, the genes important for mitochondrial quality control, and intermediate length ATNX2 polyQ expansions (Farg et al., 2013).

Many transgenic animal models have been generated to understand the disease mechanisms caused by FUS mutations and have shown that mutant FUS protein leads to neurodegeneration (Shang and Huang, 2016). For example, in studies performed on transgenic mouse and transgenic Drosophila models, overexpression of mutant FUS protein led to progressive motor neuron damage (Huang et al., 2011, Chen et al., 2011). Downregulation of the proteins improved the locomotive functions and survival rates in transgenic flies (Chen et al., 2016a). A study on FUS knockout transgenic mouse lines reported the gain of function by mutant FUS causing motor neuron degeneration instead of loss of FUS function (Sharma et al., 2016). The present studies therefore indicate the gain of toxic function as a major contributor to FUS-related ALS pathology.

1.5.1.4 *C9ORF72*

A ground-breaking discovery towards the genetic causes of ALS was made with the discovery of a hexanucleotide repeat expansion (GGGGCC) in the intronic region of the *C9ORF72* gene as the most frequent genetic cause of ALS in 2011 (DeJesus-Hernandez et al., 2011, Renton et al., 2011). *C9ORF72* accounts for almost 33% of familial ALS and 8% of sporadic ALS cases and shows a wide range in the age of onset and duration of the disease (Woollacott and Mead, 2014, Farg et al., 2014). In most healthy individuals, the hexanucleotide sequence is repeated ≤11 times while in ALS cases, the length of repeats considered toxic is still uncertain. An arbitrary cut-off of 30 repeats is considered pathological and has been observed to range from several hundred to thousand (Balendra and Isaacs, 2018). Patients with repeat expansions show TDP-43 positive inclusions in brain and spinal cord but there may also be other inclusions containing p62 or ubiquilin-2 (Brettschneider et al., 2012).

C9orf72 is involved in the regulation of autophagy and endocytosis and also has been shown to reside in lysosomes where it affects their function (Farg et al., 2014, Amick et al., 2016). C9orf72 is colocalised with Rab proteins, that are involved in autophagy and endosomal pathways, in the motor neurons of C9ORF72 ALS patients compared to controls (Farg et al., 2014). This suggested a possibility of a dysregulation in Rab-mediated cellular trafficking in patients bearing the *C9ORF72* repeat expansion (Farg et al., 2014). The expanded GGGGCC repeats form nuclear RNA foci by a bidirectional transcription forming sense and antisense RNA (Lagier-Tourenne et al., 2013, Mizielinska et al., 2013). These repetitive RNAs produce different dipeptide repeat proteins (DPRs) by translation in different reading frames namely poly-PR, poly-GR, poly-GP, poly-GA and poly-PA (Mori et al., 2013). These dipeptide repeat proteins are also present in p62 positive inclusions but are absent from TDP-43 inclusions (Mann et al., 2013, Davidson et al., 2016).

The use of *in vitro* and *in vivo* models has contributed to the present understanding of the role of *C9ORF72* mutations in the pathology of ALS (Balendra and Isaacs, 2018). Three different mechanisms have been proposed contributing to the pathogenesis of the disease (1) loss of function of the C9orf72 protein (2) toxic gain of function from C9orf72 repeat RNA (3) toxic gain of function from dipeptide repeat (DPRs) proteins produced by repeat-associated non-ATG translation (Balendra and Isaacs, 2018). Loss of function mutation by the knockdown of C9orf72 in *in vitro* and *in vivo* models inhibited autophagy induction and led to the formation of P62 and TDP-43 cytoplasmic aggregates (Sellier et al., 2016, Sullivan et al., 2016). It also led to reduced endocytosis (Farg et al., 2014). It has also been shown to elevate glutamate receptor levels and increase sensitivity of neurons to excitotoxicity (Selvaraj et al., 2018). Gain of function mutation by the overexpression of C9orf72 in cell lines induced the formation of stress granules (Farg et al., 2014). The C9orf72 repeat RNA led to the formation of nuclear RNA foci in neurons and reduced survival in *in vivo* and *in vitro* models (Wen et al., 2014, Zhang et al., 2015). Studies in Drosophila models showed the involvement of DPR in neurotoxicity. In one study, neurodegeneration was inhibited when the repeats were interrupted by stop codons which prevented the production of DPRs. In another study, the intron containing the repeat was spliced out to stop the production of DPRs and as a result, no evidence of neurodegeneration was observed (Balendra and Isaacs, 2018). The highly toxic nature of DPRs affect multiple downstream pathways involved in a range of cellular functions ultimately leading to disease progression (Balendra and Isaacs, 2018).

1.5.2 Other ALS-related genes

Many other ALS-associated genes have been identified which are as follows:

1.5.2.1 *OPTN*

OPTN encodes for optineurin. Mutations in *OPTN* were initially identified in a Japanese family causing autosomal recessive ALS. A missense, nonsense and a deletion mutation were identified in the study (Maruyama et al., 2010). OPTN is involved in a variety of cellular processes such as protein secretion, cell division, membrane trafficking, Golgi organization and in immunity against pathogens depending on its subcellular localization and interaction with other proteins (Bansal et al., 2015). It is also involved in the activation of the autophagy-lysosomal pathway for the degradation of protein aggregates (Korac et al., 2013). Mutations in OPTN were shown to affect the inhibitory role of OPTN on the nuclear factor kappa B activation (NF-kappaB) pathway and led to the formation of TDP-43 and OPTN containing cytoplasmic inclusions (Maruyama et al., 2010). Hence, it is involved in neurotoxicity through loss of function mutation. Mutations in OPTN have also been reported in sporadic ALS cases in addition to familial ALS (van Blitterswijk et al., 2012).

1.5.2.2 *VCP*

VCP encodes for valosin-containing protein. In 2010, VCP was the first gene identified as a genetic cause of familial ALS by exome sequencing. It was also identified in sporadic cases of ALS (Koppers et al., 2012). Mutations in VCP account for 1–2% of familial ALS cases (Johnson et al., 2010). VCP plays a role in multiple cellular functions including mediating degradation of proteins via the ubiquitin-proteasome system and autophagy, assembly of peroxisomes, Golgi biogenesis and vesicle transport and fusion (Meyer and Weihl, 2014, Johnson et al., 2010). Using fibroblasts from patients, mutations in the VCP were shown to cause mitochondrial uncoupling leading to reduction of cellular ATP production making them vulnerable to high energy-demanding processes and eventually contributing to cell death (Bartolome et al., 2013).

1.5.2.3 *UBQLN2*

UBQLN2 is located on the short arm of chromosome X and encodes for ubiquilin 2 protein. It causes X-linked juvenile and adult-onset ALS (Deng et al., 2011). *UBQLN2* mutations are a rare cause of familial ALS (Daoud et al., 2012). It is involved in the regulation of ubiquitin-proteasome system (UPS) thus mutations in *UBQLN2* disrupt this pathway leading to abnormal protein aggregation and neurodegeneration. Mutations in *UBQLN2* also disrupts RNA metabolism through loss of binding of UBQLN2 to hnRNP proteins (Gilpin et al., 2015). UBQLN2 positive inclusions are found in patients with familial and sporadic ALS with and without *UBQLN2* mutations (Daoud and Rouleau, 2011, Deng et al., 2011).

1.5.2.4 *SQSTM1*

SQSTM1 encodes for p62 protein and was identified as a cause of ALS in a 2011 study (Fecto et al., 2011). P62 regulates ubiquitin binding and is involved in protein degradation by targeting proteins to the proteasome system or autophagy for degradation. It is a major component of the protein inclusions found in motor neurons of patients with ALS. Mutations of *SQSTM1* have been found in both familial and sporadic ALS cases. It accounts for about 1% of familial ALS cases (Fecto et al., 2011, Teyssou et al., 2013). *SQSTM1* knockdown in a zebrafish model showed behavioural abnormalities, shorter motor neuronal axons and disrupted autophagy (Lattante et al., 2015).

1.5.2.5 *PFN1*

PFN1 encodes for Profilin 1. Multiple mutations in *PFN1* were identified in several large ALS kindreds in 2012 (Wu et al., 2012). PFN1 converts monomeric actin to filamentous actin. Hence, cells with mutant PFN1 show defective cytoskeletal architecture of the neuron since they have decreased levels of bound actin which affects axonal growth (Wu et al., 2012, Boopathy et al., 2015). PFN1 is also a stress granule-associated protein and mutations

in the gene led to altered stress granule dynamics in a study on mouse primary cortical neurons and human cell lines (Figley et al., 2014). Cells with *PFN1* mutations also show ubiquitinated TDP-43 protein aggregates (Boopathy et al., 2015).

1.5.2.6 *VAPB*

VAPB was identified as a causative gene of ALS in a study performed on a large Brazilian family (Nishimura et al., 2004). The gene encodes for vesicle associated membrane protein associated protein B and is involved in vesicle-trafficking, the unfolded protein response (UPR) and lipid transport. It is an integral membrane protein of endoplasmic reticulum (Chen et al., 2010). *VAPB* mutations disrupt many functions inside the cell such as causing decreased ER anchoring of lipid-binding proteins, defective calcium homeostasis of mitochondria and an impaired ability of the protein to initiate UPR (Morotz et al., 2012, Kanekura et al., 2006).

Apart from the above mentioned genes, several other genes have been identified in ALS patients but were identified in one or few pedigrees and thus are a rare cause of ALS. These genes include the following:

1.5.2.7 *SETX*

Mutations in *SETX* cause autosomal dominant juvenile ALS with distal muscle weakness. The bulbar and respiratory symptoms are absent. Patients usually have slow disease progression and pass a normal life (Hirano et al., 2011). *SETX* encodes a DNA/RNA helicase protein which plays a role in DNA repair, replication, transcription and RNA processing and the mutations in the gene have been suggested to cause motor neuron degeneration by aberrant RNA processing (Chen et al., 2004, Skourti-Stathaki et al., 2011).

1.5.2.8 *ATXN2*

ATXN2 encodes for Ataxin-2 protein which is an RNA binding protein and is involved in RNA processing. It is localised to ER, Golgi apparatus and stress granules. *ATXN2* contains a polyglutamine (polyQ) tract that usually has 22–23 repeats but in case of ALS, intermediate length polyQ expansions (23–34 repeats) were found strongly associated with the disease (Elden et al., 2010, Borghero et al., 2015). ATXN2 interacts with TDP-43 to form an RNA-dependent complex and the longer polyQ repeats increase the interaction between the two proteins leading to increased dislocation of TDP-43 into the cytoplasm that forms TDP-43 aggregates (Elden et al., 2010). In addition, intermediate length ATXN2 polyQ expansions have been identified as a modifier of mutant TDP-43 toxicity (Hart and Gitler, 2012). Ataxin-2 also interacts with FUS and the presence of intermediate length polyQ expansions contribute towards enhanced FUS related pathology in ALS patients (Farg et al., 2013).

1.5.2.9 *FIG4*

Mutations in *FIG4* were identified in a genetic screen in sporadic and familial ALS cases (Chow et al., 2009). FIG4 is involved in the regulation of $PI(3,5)P_2$ complex inside cell, a lipid located on the surface of late endosome and involved in the retrograde trafficking of endosomes to Golgi network (Chow et al., 2009). The mutant protein shows mislocalisation and an inability to bind to the $PI(3,5)P_2$ complex (Alsultan et al., 2016) resulting in neurodegeneration of motor cortex and striatum (Chen et al., 2013)

1.5.2.10 *DAO*

A missense mutation was identified in *DAO* gene encoding for D-amino acid oxidase in a three-generation pedigree in 2010. The patients showed rapid progression of the disease with bulbar involvement (Mitchell et al., 2010). DAO is highly expressed in brain stem and spinal

cord (Mitchell et al., 2010, Paul et al., 2014). The presence of the mutation impairs the enzyme activity of D-amino acid oxidase. Studies on *in vitro* models showed increased ubiquitinated protein aggregate formation and increased apoptotic cell death in the presence of the mutation (Paul et al., 2014) and transgenic studies on the pathogenic mutation showed that the mutation caused significant loss of spinal cord motor neurons (Kondori et al., 2018).

1.5.2.11 Alsin

ALS2/Alsin was identified in consanguineous families from Saudi Arabia and Tunisia (Hadano et al., 2001, Yang et al., 2001). Most of the identified mutations introduce premature stop codon and cause protein truncation leading to a loss of function of the gene. Alsin has been suggested to play a neuroprotective role. It is involved in activating Rab5 GTPases required for endosomal trafficking and mutations in the gene may disrupt this function (Hadano et al., 2001, Otomo et al., 2008). Studies on mice models with knocked-out alsin displayed signs of corticospinal track degeneration but did not show characteristic features of ALS indicating that alsin mutations could be a risk factor for motor neuron degeneration rather than being a direct cause (Cai et al., 2008, Gros-Louis et al., 2008).

1.5.2.12 *hnRNPA1*

Mutations in *hnRNPA1* have been detected in ALS cases (Kim et al., 2013). The gene encodes for heterogeneous nuclear ribonucleoprotein A1 which interacts with TDP-43 and ubiquilin-2 (Gilpin et al., 2015, Honda et al., 2015). Mutation screening in some other studies did not find mutation in the gene indicating it to be a very rare cause of ALS (Alsultan et al., 2016).

1.5.2.13 *ANG*

Mutations in *ANG* were found segregating with both sporadic and familial ALS (Greenway et al., 2006). *ANG* encodes for angiogenin which is a neuroprotective protein. Mutations in the gene were reported to affect the ability of neurons to make contact with their neighbouring cells and led to neurodegeneration in cell culture model (Subramanian et al., 2008).

Some other genes have also been reported but their link to ALS is not fully convincing. For example, ***CHMP2B*** was discovered in a Danish family with FTD and was also found in two other FALS cases. Mutations in *CHMP2B* can disrupt endosomal structure but the data available to support its link to ALS pathogenesis is not enough (Cox et al., 2010, Skibinski et al., 2005). A mutation in ***DCTN1*** was found in a large pedigree showing convincing segregation of ALS with the mutation (Puls et al., 2003). Mutations in the gene disrupt axonal transport in motor neurons leading to neurodegeneration (Lai et al., 2007). ***SPG11*** encodes for spatacsin and mutations in the gene commonly cause juvenile onset recessive familial ALS with slow progression (Orlacchio et al., 2010). iPSC-derived neuronal cells showed that the *SPG11* mutations cause axonal instability and defective axonal transport (Perez-Branguli et al., 2014). ***SIGMAR1*** was first reported to be linked to juvenile ALS in a family from Saudi Arabia (Al-Saif et al., 2011). The gene encodes for Sigma nonopioid intracellular receptor 1 which is an ER chaperone and a subunit of potassium channel and the mutant protein reduces mitochondrial ATP production and causes cytoplasmic aggregate formation but its link to ALS is not fully elucidated yet (Luty et al., 2010, Fukunaga et al., 2015).

1.5.3 Recently identified ALS genes

Apart from the above mentioned genes, seven novel genes associated with ALS have been identified in the last 5 years that include *MATR3*, *CHCHD10*, *TUBA4A*, *TBK1*, *NEK1*, *CCNF*

and *KIF5A* (Volk et al., 2018). All of these genes were identified using genome-wide association studies, whole-genome sequencing or whole-exome sequencing technologies (Chia et al., 2018). The details are given below.

1.5.3.1 *MATR3*

MATR3 was reported to be associated with familial ALS in a study on families from European descent (Johnson et al., 2014). Mutations in *MATR3* were also identified in sporadic ALS cases afterwards. It has been reported to be a rare cause of ALS (Chia et al., 2018). Patients with *MATR3* mutations show signs of both upper and lower motor neurons and a survival of 2-12 years after symptom onset (Marangi et al., 2017). MATR3 is a DNA/RNA binding nuclear protein involved in regulation of gene expression (Coelho et al., 2015). The protein interacts with the other two ALS associated RNA binding proteins, TDP-43 and FUS (Johnson et al., 2014, Yamaguchi and Takanashi, 2016). Transgenic mice overexpressing human MATR3 were reported to develop hind-limb paralysis with hind-limb and forelimb muscle atrophy indicating the importance of the regulation of MATR3 levels in neuromuscular function (Moloney et al., 2016).

1.5.3.2 *CHCHD10*

Mutations in *CHCHD10* were reported in familial ALS in a large French family in 2014 and have been reported to be a rare cause of ALS. The gene encodes for the coiled-coil-helix-coiled-coil-helix domain-containing 10 protein (Bannwarth et al., 2014, Dols-Icardo et al., 2015). About 20 missense mutations in the exon 2 of the gene have been identified so far that encodes for an internal hydrophobic helical segment. CHCHD10 is a mitochondrial protein and is enriched in cristae junctions of mitochondria where it is involved in the maintenance of mitochondrial dynamics (Woo et al., 2017). The helical segment plays a role in mitochondrial membrane binding, therefore, the mutations in this region may affect the helical structure and

subsequently membrane binding of the protein (Modjtahedi et al., 2016). Fibroblasts from the patients with mutant CHCHD10 indicated mitochondrial DNA deletions, defects in mitochondrial structure and the respiratory chain (Bannwarth et al., 2014). Abnormalities arising in mitochondrial dynamics as a result of the mutant CHCHD10 protein are similar to those seen in cases of mutant TDP-43. This is because wild-type CHCHD10 associates with endogenous TDP-43 retaining TDP-43 inside the nucleus but mutant CHCHD10 is unable to retain TDP-43 in the nucleus leading to its accumulation in the cytoplasm (Woo et al., 2017).

1.5.3.3 *TUBA4A*

TUBA4A encodes for a cytoskeletal protein and was reported in familial ALS in 2014 using data from American and European ALS patients and healthy controls (Smith et al., 2014b). It has the highest expression in brain tissue and has been identified in both sporadic and familial ALS. It is a rare cause of ALS and the patients show signs of both upper and lower motor neurons (Smith et al., 2014b, Pensato et al., 2015). Most of the ALS-associated mutations identified in the gene are missense mutations affecting tubulin polymerisation that result in disturbed microtubular dynamics and structural stability in motor neurons (Smith et al., 2014b).

1.5.3.4 *TBK1*

In 2015, two independent studies identified *TBK1* in familial ALS. TBK1 is a multidomain protein that is involved in phosphorylation of proteins involved in autophagy, neuroinflammation, ubiquitin-proteasome system and many proteins from the ALS associated genes such as *SQSTM1*, *OPTN* and *UBQLN2* (Oakes et al., 2017, Cirulli et al., 2015, Freischmidt et al., 2015). *TBK1* mutations show a wide range in clinical phenotypes including variable age of onset, duration and progression of the disease. These mutations account for approximately 1% of familial ALS and sporadic ALS cases (Chia et al., 2018). Patients with TBK1-associated ALS show p62 and TDP43-positve inclusions (Gijselinck et al., 2015). Most

of the identified *TBK1* mutations have been found in the kinase and the coiled-coil domains of the protein suggesting a possible alteration in the downstream regulatory pathways of TBK1 (Chia et al., 2018, Freischmidt et al., 2015).

1.5.3.5 *NEK1*

NEK1 was reported to be a major cause of ALS in two independent studies in familial ALS cases and has been suggested to account for about 2% of familial ALS (Kenna et al., 2016b, Brenner et al., 2016). *NEK1* mutations have also been implicated in sporadic ALS (Cirulli et al., 2015). NEK1 is involved in several cellular functions including mitochondrial membrane permeability, axonal polarity, cilia formation, DNA repair, mitotic checkpoint control and neuronal morphology. It was also shown to interact with two other proteins associated with ALS namely VAPB and ALS2/Alsin (Kenna et al., 2016b). Mutations in *NEK1* impaired DNA damage response resulting in increased DNA damage in hiPSC-derived motor neurons (Higelin et al., 2018).

1.5.3.6 *CCNF*

CCNF was discovered as a causative ALS gene in a large European family and transmitting in an autosomal dominant pattern of inheritance. It accounts for about 4% of familial and 2% of sporadic ALS cases. *CCNF* encodes cyclin F which is a component of the Skp1-cullin-F-box E3 ubiquitin-ligase complex involved in tagging proteins with ubiquitin to direct them to ubiquitin-proteasome system for degradation (Williams et al., 2016). Mutant CCNF expression in neuronal cells caused accumulation of ubiquitinated proteins including TDP-43 suggesting the impairment of the ubiquitin-proteasome pathway resulting in abnormal proteostasis leading to neuronal degeneration (Williams et al., 2016).

1.5.3.7 *KIF5A*

KIF5A has been reported to be a cause of ALS very recently. A missense mutation and two splice-site mutations located in the C-terminus of the protein leading to aberrant splicing were identified in familial ALS. In addition, a non-synonymous single nucleotide variant also located at the c-terminus end of protein was also identified in FALS cases. Loss of RNA expression and haploinsufficiency were suggested to be the most possible pathogenic mechanisms underlying *KIF5A*-associated ALS (Brenner et al., 2018).

Although these genes have been identified as a genetic cause of ALS, the precise mechanisms contributing to the disease pathogenesis are not currently clear for all of them especially in the case of the newly discovered genes. More *in vivo* and *in vitro* functional studies are required for such genes in order to better understand the disease processes (Chia et al., 2018). The discovery of the genetic causes of ALS has increased our understanding of the molecular pathways underlying the pathogenesis of the disease. Many of the identified genes in ALS also have been reported to cause FTD which indicates the existence of a genetic link between the two diseases.

1.6 Pathogenic mechanisms underlying ALS

Different pathogenic mechanisms underlie ALS including dysregulation of protein homoeostasis, dysregulation of RNA binding and processing, defects in cytoskeletal functions, mitochondrial dysfunction, oxidative stress, ER stress, exitotoxicity and epigenetic changes. All these changes contribute to the death of motor neurons.

1.6.1 Protein homeostasis (proteostasis)

Proteins are folded in a tertiary structure after synthesis to perform function inside cell. Some of the proteins, however, during the process are misfolded and are required to be

refolded. Cells have a protein quality control system that detects and refolds these misfolded proteins or direct them for degradation in order to avoid protein aggregation and for maintaining protein homeostasis. This maintenance of protein homeostasis inside the cell is termed as protein proteostasis (Ruegsegger and Saxena, 2016). The protein quality control system includes different pathways for removal of misfolded proteins namely the unfolded protein response (UPR) pathway, autophagy and ubiquitin proteasome system. Proteins that have been identified in neurodegenerative diseases are only slightly stable at physiological conditions and have thus a high probability of misfolding. Misfolded proteins have exposed beta sheets and are aggregation prone and thus result in protein aggregate formation which may be resistant to proteolytic pathways leading to the formation of inclusion bodies (Hipp et al., 2014). Defects in proteostasis result in the inability of the cell to refold proteins properly or degrade misfolded proteins leading to the formation of protein aggregates and neurodegeneration (Takalo et al., 2013). The protein degradation pathways are more important in the case of neurons since they are differentiated cells with polarised cell-bodies. The presence of protein aggregates can cause disruption in the movement of material across the neurons and their post-mitotic nature means that the protein aggregates will not be diluted by cell division resulting in the development of neurodegenerative diseases (Ghavami et al., 2014).

1.6.1.1 Protein aggregates

An important theme underlying ALS pathogenesis is the dysfunction of several proteins leading to formation of protein aggregates. Dense aggregates of ubiquitinated proteins are observed in later stages of motor neuron disease and are a hallmark of ALS. SOD1, TDP-43 or FUS aggregates are commonly found in ALS. It is unclear whether the aggregates become toxic to the cell leading to cell death or instead they are formed in response to some primary pathology in the cell for the protection of the cell (Peters et al., 2015).

ALS usually begins focally and spreads in a prion-like manner from cell to cell. Such a cell-to-cell spread and propagation of misfolding proteins has been reported for both mutant and wild type SOD1 (Munch and Bertolotti, 2011, Guo and Lee, 2014). Similarly, TDP-43 and FUS also have prion-like domains that enhance their aggregate formation and spread (Gitler and Shorter, 2011). Many prion-like domains containing proteins are components of stress granules that are formed in response to cell stress. The interactions between these domains facilitate the fast assembly of the stress granules (King et al., 2012). Many ALS-associated RNA/DNA binding proteins incorporate into these granules along with several other RNAs and proteins. An abnormally strong interaction between these proteins result in the persistent sequestration of the RNA and proteins inside granules leading to the formation of cytoplasmic inclusions observed in ALS (Peters et al., 2015).

ALS patients with *SOD1* mutations display mutant SOD1 protein aggregates in inclusion bodies present in the spinal motor neurons (Shibata et al., 1993) and in cell culture (Prudencio et al., 2009). In addition to aggregates, mutant SOD1 also forms oligomers which are often soluble and may be more toxic to the cells than visible aggregates (Peters et al., 2015). Aggregates with misfolded oxidised wild-type SOD1 are also detected in spinal cord of ALS patients (Bosco et al., 2010b).

Ubiquitinated TDP-43 aggregates are a hallmark of ALS. Hyperphosphorylated TDP-43 leaves nucleus and accumulates in the cytoplasm of neurons assembling into inclusions. These protein aggregates first accumulate in the motor neurons in spinal cord but then spread throughout central nervous system as the disease progresses becoming toxic to the cell both by the gain of function in the cytoplasm by aggregate formation and loss of function as a result of depletion from the nucleus (Brettschneider et al., 2013, Lagier-Tourenne et al., 2010).

Mutant FUS also forms protein aggregates and is found in cytoplasmic inclusions. It is a major component of the stress granules and of ubiquitin-positive and p62-positive cytoplasmic inclusions found in both neurons and glial cells in brain and spinal cord (Vance et al., 2009). Compared to TDP-43 inclusions, the frequency of FUS positive inclusions are low in ALS cases (Neumann et al., 2009).

Mutant C9orf72 is also a part of cytoplasmic protein inclusions. The hexanucleotide repeat expansions of C9orf72 found in ALS cases produce cytoplasmic protein inclusions as well as nuclear RNA foci produced from sense and antisense transcripts across the repeat expansions (Lee et al., 2013). Patients with hexanucleotide repeat expansions also have cytosolic aggregates composed of dipeptide repeat proteins produced from the translation of all possible reading frames of the hexanucleotide repeats as explained earlier in the genetics section of this chapter (Mori et al., 2013). In addition to the intranuclear RNA foci, patients with repeat expansions also show TDP-43, p62 or ubiquilin-2 positive inclusions (Brettschneider et al., 2012).

1.6.1.2 Protein degradation and protein quality control system

The protein quality control system is responsible for degradation of misfolded proteins. Many identified familial ALS-associated mutations directly affect proteostasis networks by disrupting protein quality control system affecting ubiquitin–proteasome system (UPS), autophagy and UPR pathway.

1.6.1.2.1 ER stress and UPR

The endoplasmic reticulum (ER) is an important compartment in the cell involved in protein synthesis and their secretion to the proper target site inside the cell. ER has contact points with other organelles inside the cell including Golgi apparatus, plasma membrane, nucleus and mitochondria. Apart from protein folding and synthesis, lipid biogenesis and calcium

regulation also occurs inside the ER lumen. Proteins after undergoing glycosylation in the ER are transported to Golgi apparatus for further maturation (Schroder and Kaufman, 2005). Some proteins are improperly folded during the protein folding processes and are either refolded by protein chaperones inside the ER or are released to the cytoplasm to be degraded by the ubiquitin-proteasome system mediated by the ER-associated protein degradation (ERAD) pathway or by autophagy (Hetz and Mollereau, 2014, Hosoi et al., 2017). If the influx of proteins to the ER exceeds its folding capacity or if there is accumulation of misfolded proteins inside ER, the physiological state of ER is disturbed leading to ER stress. In order to alleviate ER stress, unfolded protein response is activated inside the cell which may end with adaptive or apoptotic outputs. There are three major branches of the unfolded protein response (UPR) pathway activated in response to ER stress namely inositol-requiring enzyme-1 (IRE1) pathway, double stranded RNA-activated protein kinase (PKR)-like ER kinase (PERK) pathway and activating transcription factor 6 (ATF6) pathway. IRE1α, PERK and ATF6 are ER transmembrane stress sensors activated when protein accumulation exceeds above a threshold level in order to restore homeostasis. The pathways reduce the protein load entering the ER by inhibiting total protein synthesis, increasing the ER efficiency to handle misfolded proteins, increasing the expression of protein chaperones and facilitating the transport of misfolded proteins outside the ER for degradation. The restoration of protein homeostasis corresponds to the adaptive output of UPR. If the UPR fails to alleviate ER stress then the apoptotic response is triggered inside the cell resulting in cell death (Shore et al., 2011).

When activated, the PERK phosphorylates the eukaryotic initiation factor-2 (eIF2α) or nuclear factor erythroid 2-related factor 2 (Nrf2) that leads to the inhibition of general protein translation to protect the ER from the load of newly synthesized proteins (Harding et al., 1999, Cullinan and Diehl, 2006). Activation of IRE1α pathway leads to the splicing

of XBP1 (X-box binding protein 1) which increases the expression of genes involved in ERAD pathway. ER stress translocates ATF6 to Golgi apparatus where it is activated by cleavage and then is transported to the nucleus activating UPR-related genes (Figure 1-3) (Walter and Ron, 2011).

SOD1 aggregates are considered one of the causes of ER stress as an ER chaperone, GRP78/HSPA5 was found bound to and colocalised with mutant SOD1 in mouse models of ALS (Wate et al., 2005). GRP78 normally binds to the ER stress sensors but on accumulation of misfolded proteins in the ER, dissociates from these protein sensors and binds to misfolded proteins leading to the activation of the UPR pathways (Kaufman, 1999). In sporadic ALS cases and mouse models of ALS, increased amounts of IRE1 and ATF6 were observed indicating the presence of ER stress and activated UPR pathways (Atkin et al., 2008, Chen et al., 2010, Lautenschlaeger et al., 2012). Deposition of granular material in ER lumen indicative of accumulation of misfolded proteins was reported in SALS patients (Sasaki, 2010). Changes in ER morphology were observed including detachment of ribosomes and fragmentation of rough endoplasmic reticulum in SALS patients (Oyanagi et al., 2008).

Examples of ALS-associated genes involved in ER stress and UPR pathways include TDP-43 and VAPB. In a study performed on NSC-34 cells transfected with human wild-type TDP-43, ER stress induction was observed (Suzuki et al., 2011). Mutations in *VAPB* have been associated with familial ALS. VAPB is a protein localised to ER and is involved in ER protein transport, maintenance of ER structure, lipid biogenesis and the UPR. Mutations in *VAPB* induce protein aggregation and disorganisation of endoplasmic reticulum eventually inducing cell death (Chen et al., 2010).

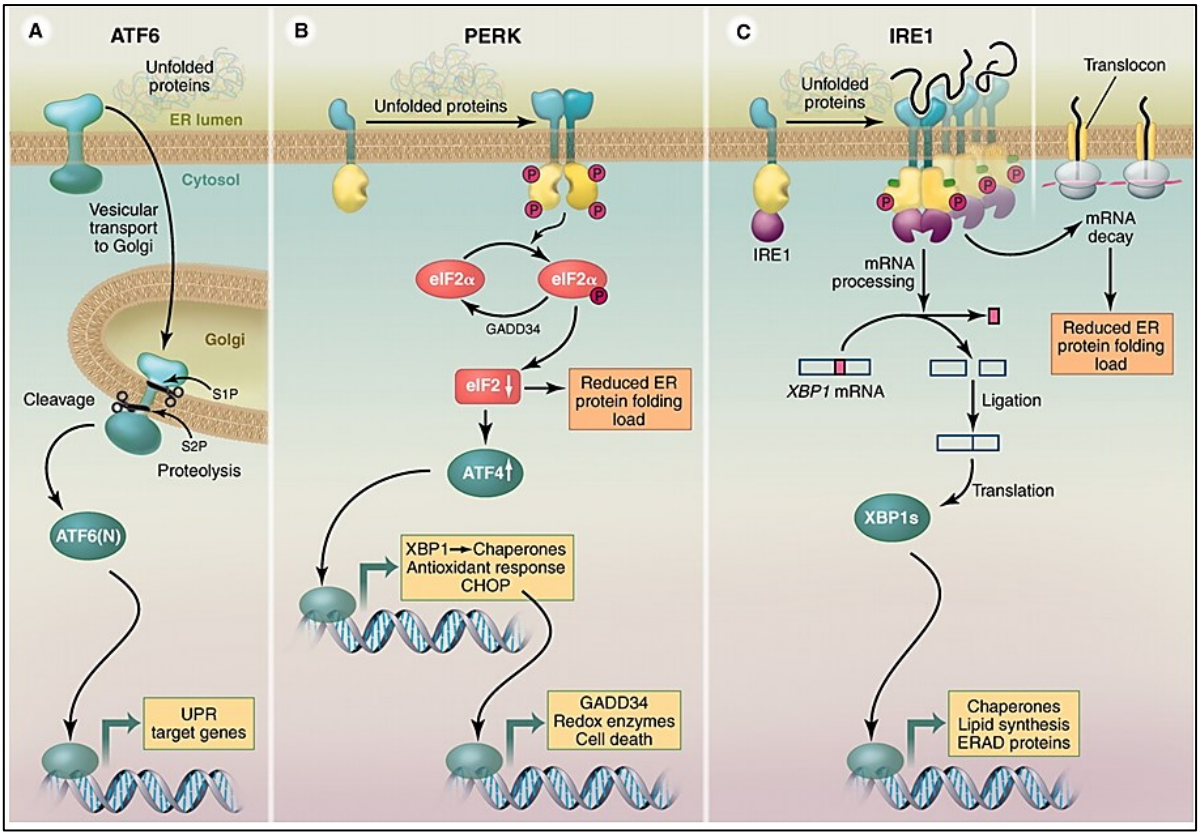

Figure 1-3 The three branches of the UPR pathway

Accumulation of misfolded proteins above a threshold level in ER activates the UPR transmembrane sensors activating transcription factor 6 (ATF6), protein kinase RNA-like ER kinase (PERK) and inositol-requiring enzyme 1 (IRE1). a) On activation, ATF6 is translocated to Golgi apparatus where it is activated by cleavage and then is transported to the nucleus for the activation of UPR target genes. b) On activation, PERK phosphorylates eukaryotic translation initiation factor 2α (eIF2α) which inhibits protein translation to reduce ER protein load and expresses ATF4. ATF4 translocates to the nucleus and induces the expression of genes related to autophagy, oxidative response, amino acid metabolism, ER chaperones and C/EBP-homologous protein (CHOP). c) Activation of IRE1 induces the splicing of XBP1 mRNA. The active XBP1s then increases the expression of ER chaperones, genes involved in ERAD pathway and genes involved in lipid synthesis (Walter and Ron, 2011).

1.6.1.2.2 Ubiquitin proteasome system (UPS)

In order to eliminate the misfolded proteins formed during folding process from the secretary pathway, endoplasmic reticulum-associated degradation (ERAD) machinery is employed by ER for the subsequent degradation of the misfolded proteins in the cytosol by ubiquitin proteasome system (UPS) (Nassif et al., 2010). UPS is a proteolytic system in which misfolded proteins are tagged with several ubiquitin molecules leading to the degradation of substrate by the proteasome (Ciechanover and Brundin, 2003). The misfolded protein substrate is first ubiquitinated in an ATP-dependent enzymatic process that involves three enzymes namely Ub-activating enzyme E1, Ub-conjugating enzyme E2 and the Ub ligase E3 for the specific recognition and subsequent ubiquitination of the substrates. Substrates are ubiquitinated at lysine 48 and translocated to proteasome for degradation. The proteasome is made up of a 20S core subunit and two 19S regulatory subunits at both sides of the core subunit. ATPases make up the 19S particle and are responsible for the recognition and unfolding of poly-ubiquitinated proteins and their subsequent translocation to the 20S catalytic core for degradation into shorter peptides (Clague and Urbe, 2010). Apart from misfolded proteins, short-lived cellular proteins are also degraded by UPS system (Ravid and Hochstrasser, 2008). Like other neurodegenerative diseases, dysfunction of UPS is also linked to ALS (Bendotti et al., 2012).

Example of ALS-linked genes involved in UPS pathway include ubiquilin-2 (*UBQLN2*). Ubiquilin-2 regulates the ubiquitination of the target proteins for degradation. Mutations in ubiquilin-2 cause defects in the protein degradation pathway and abnormal protein aggregation (Deng et al., 2011). Another example is *VCP* which is involved in the proteosomal degradation of ubiquitinated proteins. Mutations in *VCP* also cause defects in the ubiquitination/protein degradation pathways (Johnson et al., 2010). $SOD1^{G93A}$ mice

model also show decreased constitutive proteasome levels indicating the involvement of proteasome impairment in the toxicity of mutant SOD1 (Cheroni et al., 2005).

1.6.1.2.3 Autophagy

Cells have another process for protein degradation apart from UPS called autophagy which is a common ALS associated pathway. Autophagy is involved in the degradation of long-lived proteins, protein aggregates and damaged or old organelles (Mizushima and Komatsu, 2011). There are three major types of autophagy namely macroautophagy, microautophagy and chaperone mediated autophagy (CMA). Macroautophagy involves the degradation of cellular components and misfolded protein aggregates via autophagosome formation. Microautophgay involves the direct uptake and degradation of components from cytosol and their degradation in lysosomes without the formation of autophagosomes (Glick et al., 2010). In CMA, a pentapeptide sequence is recognised in target substrate by Hsp70 followed by binding the binding of Hsp70 to the protein. This substrate-chaperone complex is then recognised by LAMP2A. The whole complex is thereafter degraded in lysosome (Arias and Cuervo, 2011).

Macroautophagy (autophagy) is mainly regulated through mTOR which inhibits autophagy under physiological conditions by inhibiting ULK kinase activity. There are more than 30 ATG proteins involved in the process. The autophagy process involves initiation, elongation and maturation steps followed by the fusion of autophagosomes with lysosomes forming autolysosomes. The process initiates with the formation of a pre-autophagosomal structure called phagophore which then elongates to engulf selected organelles or a region of cytoplasm and matures into a double membrane structure called autophagosome. Several protein complexes are involved in the initiation step. Cell stress, like starvation, inhibits mTOR activating ULK1-ATG13-FIP200 complex which further activates beclin-1 interacting

complex consisting of BCL-2 family proteins, beclin-1, class III phosphatidylinositol 3-kinase (PI3KC3) and ATG14L, all of which are involved in the formation of autophagosomes (Ganley et al., 2009). At the same time, two additional specialised conjugation systems control the elongation step, the ATG5–ATG12 conjugation system which is facilitated by ATG7, ATG10, and ATG12 (Hanada et al., 2007) and the second LC3–ATG8 conjugation system which is facilitated by ATG3 and ATG4. ATG4 cleaves the C-terminal of LC3 to from LC3I which is lipidated to from LC3II and is embedded on the autophagosome membrane (Ghavami et al., 2012). Beclin1-PI3KC3 complex depending on the interacting proteins activates or represses autophagy. The interaction with Atg14L promotes formation of autophagosomes, the interaction with UVRAG promotes the maturation of autophagosomes, while the interaction of UVRAG containing PI3KC3 complex with Rubicon suppresses the maturation of autophagosomes (Matsunaga et al., 2009). The autophagosomes after formation at random sites in the cytoplasm are transported to the microtubule organizing-center for their fusion with lysosomes to generate autolysosomes and for the subsequent degradation of the cargo (Figure 1-4). The autopahgosomes may also fuse with late endosomes before fusing with lysosomes to generate an amphisome (Tan et al., 2014).

Disruption in autophagy machinery has been implicated in many neurodegenerative diseases including ALS. In sporadic ALS patients, accumulation of autophagosomes was observed which was suggestive of the dysfunction of autophagy in ALS (Morimoto et al., 2007). $SOD1^{G93A}$ mice spinal cord samples also showed upregulated autophagy (Li et al., 2008). Many causative ALS genes are involved in the autophagy pathway and mutations in the genes lead to disruption of the pathway activity. Some examples of genes involved in the autophagic system include p62, optineurin, VCP, ubiquilin 2, TBK1 and C9orf72. Mutations in P62 can block its association with ubiquitinated substrates or with autophagosomes (Pankiv et al., 2007). Similarly, mutations in autophagy receptor optineurin can affect the autophagy mediated

degradation of ubiquitinated protein aggregates (Shen et al., 2015). TBK1 is involved in the phosphorylation and activation of the autophagy adaptors p62 and OPTN and therefore, mutations in the gene can impair the activation of p62 or OPTN disrupting autophagy (Freischmidt et al., 2015). C9orf72 is involved in the regulation of autophagy as the knockdown of C9orf72 in *in vitro* and *in vivo* models inhibited autophagy induction and led to the formation of P62 and TDP-43 cytoplasmic aggregates (Sellier et al., 2016).

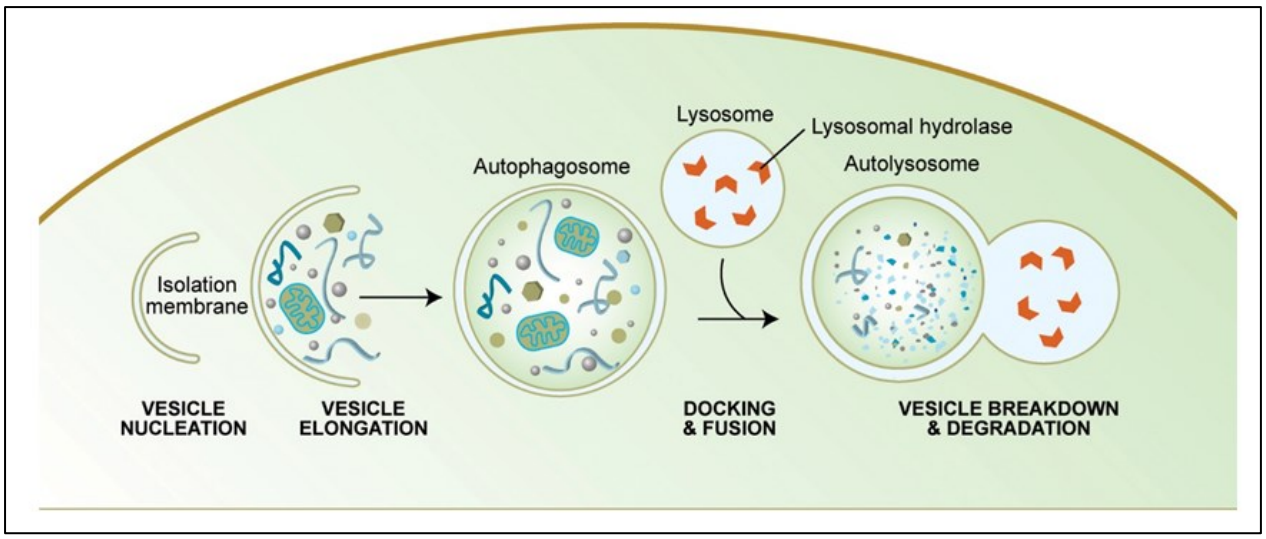

Figure 1-4 Steps of autophagy pathway

The autophagy process begins with the formation of isolation membrane also called phagophore. The phagophore elongates by the action of multiple proteins that make core autophagy machinery and lead to the formation of autophagosomes that encloses proteins or cellular compartments for degradation. The autophagosomes mature and then either fuse with late endosomes to form amphisomes which later fuses with lysosomes or directly fuse with lysosomes forming autolysosomes where the final degradation of cargo takes place (Melendez and Levine, 2009).

1.6.1.2.4 Endosomal pathway

Endosomal pathway consists of membrane-enclosed vesicular structures involved in internalization and recycling of molecules in cells. The different endosomal compartments in the pathway include early endosomes, recycling endosomes, and late endosomes (Huotari and Helenius). The pathway ends with the fusion of late endosomes with lysosomes. Endocytosis usually starts with the internalization of clathrin coated pits forming double membrane vesicles derived from the plasma membrane. After formation, the vesicles either fuse with each other or with the pre-existing early vesicles to form early endosomes. Early endosomes have slightly acidic pH to allow the dissociation of receptors from cargo and are usually formed in the peripheral cytoplasm. They act as a sorting station for receptors to be recycled back to the plasma membrane by recycling endosomes, or proteins to be transported to the trans-Golgi network and for the remaining cargo to be transferred into degradation pathway. The early endosomes mature into late endosomes by the switching of Rab5 in early endosomes to Rab7 in late endosomes that takes place during the maturing process (Stenmark, 2009, Hu et al., 2015). The late endosomes eventually fuse with lysosomes for the degradation of cargo. A stable pH gradient is maintained during the process with early endosomes having a pH of 6.5, late endosomes with pH 5.5 and lysosomes with a pH of 4.5 compared to the cytosol which has a pH of around 7 (Figure 1-5) (Diering and Numata, 2014).

Disruption in the pathway has been associated with ALS. Examples of ALS-associated genes involved in endosomal pathway include *alsin* and *C9orf72* (Yang et al., 2001). Alsin contains three guanine-nucleotide exchange (GEF) domains and mutations in the gene disrupt the protein impairing Rab 5 mediated endocytic trafficking in neurons (Lai et al., 2009). Similarly, pathogenic hexanucleotide repeat expansion in C9orf72 result in disruption of endosomal trafficking. C9ORF72 contains a DENN domain that functions as a GEF for Rab GTPases and

colocalises with Rab proteins in the endosomal system. The inhibition of C9orf72 disrupted the endosomal trafficking of Shiga toxins indicating its importance in endocytosis (Farg et al., 2014). Loss of function of TDP-43 disrupts endosomal trafficking especially with reduced number and motility of recycling endosomes in neuronal cell culture (Schwenk et al., 2016). Considering the important role played by the endosomal pathway in transferring molecules required for normal function and survival of cells, it is evident that alterations in the pathway can affect proteostasis or the correct localization of cargo molecules leading to neurodegeneration (Schreij et al., 2016).

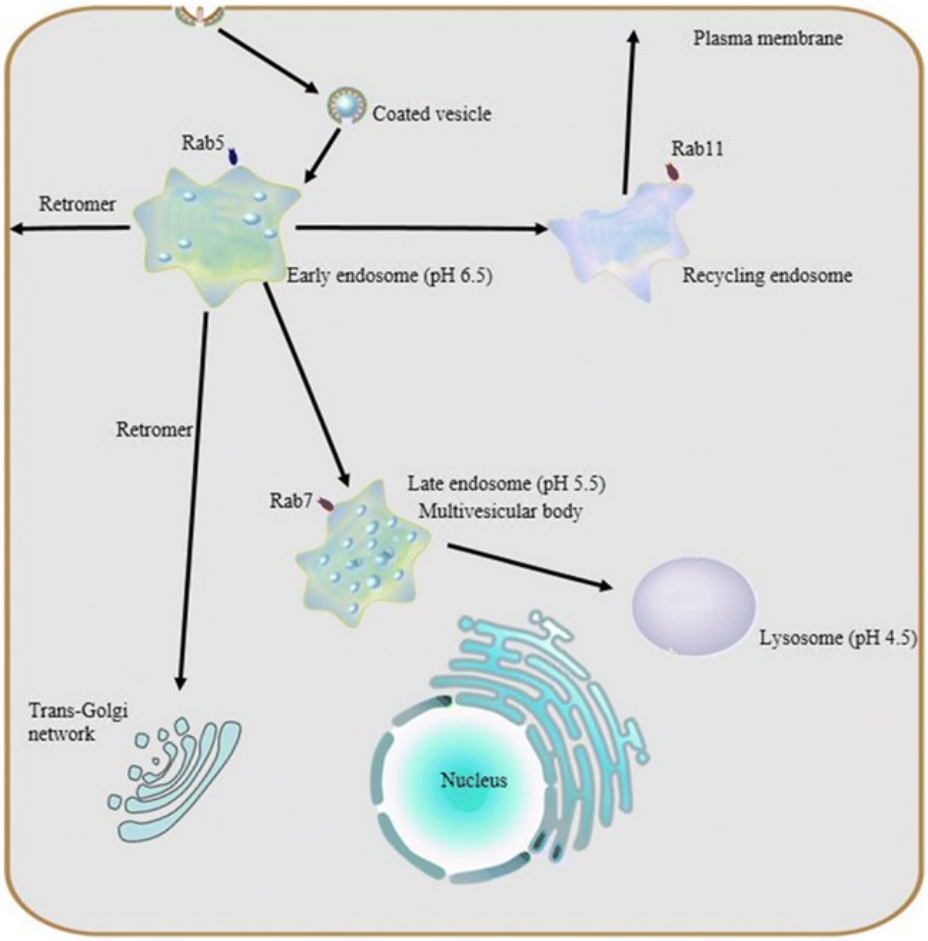

Figure 1-5 Endocytic pathway

Endocytosis consists of three endosomal compartments including early endosomes, recycling endosomes, and late endosomes. Protein internalization usually starts with clathrin coated pits that form double membrane vesicles. After internalization, the cargo proteins are transported to early endosomes which have slightly acidic pH of 6.5. Early endosomes act as a sorting station for receptors to be recycled back to the plasma membrane by recycling endosomes, or for proteins to be transported to the trans-Golgi network. The remaining cargo is transferred to the late endosome which has a pH of 5.5. The cargo is finally transferred for degradation to lysosomes which have a pH of about 4.5. A stable pH gradient is maintained in endosomal compartments compared to cytosol which has a pH of about 7 (Hu et al., 2015).

1.6.2 Dysregulation of RNA homeostasis and trafficking

Several DNA/RNA binding proteins have been discovered as a cause of familial ALS and include both the common and rare causes of ALS. The common examples include TDP-43, FUS and C9orf72 and the rare examples include SETX, ANG, ataxin and hnRNPA1. TDP-43 and FUS are both DNA and RNA binding nuclear proteins that are involved in RNA transcription, splicing, transport and processing (Peters et al., 2015). Under normal cellular conditions, these proteins e.g., TDP-43, FUS, hnRNPA1, are mainly localized in nucleus with translocation to cytoplasm for the transport of RNA but under cell stress may become a component of stress granules in cytoplasm. The mutant variants associated with ALS usually mislocalise to the cytoplasm making protein aggregates leaving the nucleus depleted of them. Thus they contribute to the pathogenesis of the disease by both loss of function in the nucleus and gain of the cytotoxic function in the cytoplasm in the form of protein aggregates that disrupt normal cellular functions (Paez-Colasante et al., 2015). The ALS associated expanded G_4C_2 repeats of C9orf72 form nuclear RNA foci containing both sense and antisense RNA transcripts causing reduced survival of neurons in *in vitro* and *in vivo* studies (Zhang et al., 2015, Lagier-Tourenne et al., 2013). These repetitive RNAs also produce different dipeptide repeat proteins (DPRs) which become neurotoxic by affecting multiple downstream pathways involved in a range of cellular functions (Balendra and Isaacs, 2018).

1.6.3 Cytoskeletal defects

The structure of motor neurons makes them highly dependent on intracellular transport mechanisms for transport of molecules across the axons, which is sustained by the cytoskeletal structure inside the cell. Some identified ALS causing genes are a part of the cytoskeleton machinery and the axonal transport system required for the proper functioning of neurons for example, neurofilament heavy subunit (NEFH), *TUBA4A*, *DCTN1* and *PFN1*. Neurofilaments

are intermediate filaments found in neurons and form the neuronal cytoskeleton together with microtubules and microfilaments. Mutations have been reported in the NEFH subunit of neurofilament in sporadic and familial cases which disrupt the cross-linking properties of the neurofilaments (Figlewicz et al., 1994, Al-Chalabi et al., 1999). Mutation in *TUBA4A* effect tubulin polymerisation disrupting the microtubule dynamics and structural stability in motor neurons (Smith et al., 2014b). DCTN1 is involved in binding vesicles and organelles to dynein, a cytoskeletal motor protein. Mutations in the gene disrupt axonal transport in motor neurons leading to neurodegeneration (Lai et al., 2007). PFN1 is involved in the conversion of monomeric actin to filamentous actin. Mutant protein is unable to perform its role resulting in the defective cytoskeletal architecture of the neuron (Boopathy et al., 2015).

1.6.4 Mitochondrial dysfunction

Mitochondria play multiple roles in cells including ATP production, calcium homeostasis, phospholipid biogenesis and apoptosis. Therefore, maintenance of healthy mitochondria is important for the survival and proper functioning of neurons and their dysfunction has been linked to ALS. Many defects in mitochondria have been found contributing to the progression of ALS such as defective bioenergetics, altered morphology, abnormal calcium homeostasis, defective mitochondrial transport and reactive oxygen species (ROS) production (Smith et al., 2017b).

Defective mitochondrial morphology with altered structure and mitochondrial accumulation in different parts of the motor neurons have been observed in sporadic ALS cases (Sasaki and Iwata, 2007). Overexpression of ALS related mutant genes have also shown defects in mitochondrial morphology and transport. Overexpressed wild-type and mutant TDP-43 in primary motor neurons result in reduced mitochondrial length and density in motor neurons (Wang et al., 2013). Similar results were observed with studies on mice expressing mutant

TDP-43. Overexpression of mutant SOD1 in $SOD1^{G93A}$ transgenic mice also showed similar effects on mitochondrial morphology and transport (Higgins et al., 2003, Magrane et al., 2014). Overexpressed mutant FUS also resulted in shortening of mitochondria in cultured motor neurons (Tradewell et al., 2012). Mitochondrial damage caused by the mutant SOD1, TDP-43 and FUS could be due to the interaction these proteins have with mitochondria that has been shown in various studies (Deng et al., 2015, Higgins et al., 2002, Wang et al., 2016). Mutations in ALS-associated *CHCHD10*, whose product is localised to mitochondrial membrane, results in disruption of mitochondrial cristae effecting the mitochondrial structure (Genin et al., 2016).

Reduced cellular respiration and ATP production has been observed in spinal cord samples of sporadic ALS patients (Wiedemann et al., 2002) and in the brain and spinal cord samples from $SOD1^{G93A}$ transgenic mice (Mattiazzi et al., 2002). Disrupted calcium homeostasis has also been reported in SOD1, TDP-43 and FUS related ALS models (Damiano et al., 2006, Stoica et al., 2014, Stoica et al., 2016). Mutations in *VAPB* have also shown defects in calcium homeostasis and axonal transport of mitochondria (Morotz et al., 2012).

Accumulation of defective mitochondria in cells may occur as a result of defective mitophagy which is a type of autophagy that removes damaged mitochondria from cells. Mitophagy requires autophagy receptors, optineurin and P62, activated when phosphorylated by TBK1. ALS related mutations in these genes effect autophagy as explained earlier and hence, may also be disrupting mitophagy (Smith et al., 2017b) leading to the accumulation of damaged mitochondria inside the cells that can induce oxidative stress. Mitochondrial dysfunction has been detected early in the pathogenesis of ALS in animal models which suggests an important role played by mitochondria in progression of the disease (Smith et al., 2017b).

1.6.5 Oxidative stress

Reactive oxygen species (ROS) are produced as a by-product of aerobic metabolism inside a cell. The major source of cellular ROS is the oxidative phosphorylation taking place in the mitochondrial respiratory chain that produces hydrogen peroxide (H_2O_2) and superoxide radical anion ($O_2^{\cdot -}$). $O_2^{\cdot -}$ react with nitric oxide radicals (·NO) to form peroxynitrite. Similarly, H_2O_2 partially reduces to further generate hydroxyl radical (·OH) (Siân C el al., 2006). ROS are highly reactive and cause oxidative damage to DNA, proteins and lipids. Damage caused by ROS affects cellular processes resulting in mitochondrial damage, protein aggregate formation, ER stress, apoptosis, excitotoxicity and induction of inflammatory response (Andersen, 2004).

There is substantial evidence that links the damage caused by oxidative stress to motor neuron death in ALS. ALS patients have shown elevated levels of oxidative stress biomarkers in biofluids and post-mortem tissues (Bogdanov et al., 2000, Mitsumoto et al., 2008). Oxidative damage to cellular components has also been widely reported in cell and animal models of ALS for example, damage to DNA and RNA by oxidation has been reported in $SOD1^{G93A}$ mouse model occurring early in the disease (Chang et al., 2008). Oxidation of wild-type SOD1 has also been reported leading to misfolding of SOD1 and aggregate formation. SOD1 is involved in detoxifying superoxide radicals and is localized to mitochondrial intermembranous space (Rakhit et al., 2002) and therefore, damage to SOD1 by oxidation or by mutations in *SOD1* gene subsequently disrupts mitochondrial function resulting in increased superoxide production (Pickles et al., 2016). Similarly, oxidative stress has been proposed to promote TDP-43 aggregate formation resulting from cysteine oxidation and disulphide bond formation causing TDP-43 cross-linking (Colombrita et al., 2009, Cohen et al., 2012). Damage of neurofilaments by oxidation result in aggregation of neurofilament subunits leading to cytoskeletal dysfunction (Kim et al., 2004). ROS induces inflammatory response by crossing

the cell membrane of motor neurons and spreading to the neighbouring cells activating astrocytes and microglia and producing more ROS resulting in further spread of the damage to neighbouring cells (Kawamata et al., 1992). Hence, oxidative stress causes immense damage to motor neurons either directly or by cross-talk with other mechanisms leading to motor neuron degeneration.

1.6.6 Glutamate excitotoxicity

Glutamate is a neurotransmitter that is released from the presynaptic neuron into synapse and activates glutamate receptors present on the postsynaptic neuron. Activation of the receptors result in the influx of Na^+ and Ca^{2+} ions inside the cell, leading to the generation of an action potential. Excitotoxicity occurs as a result of over-stimulation of the glutamate receptors triggering increased calcium signalling leading to neuronal degeneration (Rothstein et al., 1990). Motor neurons are specifically vulnerable to the excitotoxicity mediated by AMPA receptors. The influx of calcium inside cells causes the uptake of calcium by mitochondria generating ROS which can exit the cells and damage glutamate transporters of neighbouring cells disrupting the re-uptake of glutamate into the astrocytes which results in increased levels of glutamate in synapse. This causes excessive stimulation of glutamate receptors and increased influx of Na^+ and Ca^{2+} inside the surrounding neurons which are again taken up by the mitochondria of those neurons and thus starts a vicious feed-forward cycle that amplifies the excitotoxic damage to motor neurons (Rao and Weiss, 2004).

Excitotoxicity has been linked to ALS in a number of early studies. Increased glutamate signalling has been observed in ALS patients and animal models (Rothstein et al., 1990, Howland et al., 2002). In mouse models of SOD1, Ca^{2}+ up-take by atypical AMPA receptors in motor neurons promoted misfolding and aggregate formation of mutant SOD1 and death

of motor neuron (Tateno et al., 2004). Decreased glutamate transport was observed in synaptosomes in the brain and spinal cord samples of patients with sporadic ALS resulting in neurotoxic levels of extracellular glutamate (Rothstein et al., 1990). The ALS-associated *DAO* gene regulates the levels of D-serine which is an activator at the NMDA receptor of glutamate. Mutations in *DAO* result in increased levels of synaptic D-serine leading to an excessive activation of the receptor and consequently excitotoxicity (Paul et al., 2014).

In vivo treatments studies on $SOD1^{G93A}$ mice that interfered with glutamate excitotoxicity reported prolonged survival of mice by delaying motor neuron death (Rembach et al., 2004). A good example of such treatments is riluzole, the drug used for the treatment of ALS that slows the progression of the disease and prolongs survival by its anti-excitotoxic properties (Bensimon et al., 1994). It inhibits the release of glutamate by inactivating Na^+ channels on nerve terminals and by the inhibition of postsynaptic NMDA and AMPA receptors (Doble, 1996, Albo et al., 2004).

1.6.7 Epigenetic mechanisms

In addition to the genetic factors, epigenetic changes also contribute to ALS such as histone modifications, DNA methylation, microRNA (miRNA) expression and regulation. The involvement of epigenetic mechanisms in disease progression has been strongly supported by studies on monozygotic twins showing disease discordance (Dolinar et al., 2018). In a study on five monozygotic twin pairs with one affected twin in each case and lacking the known genetic variations in ALS-associated genes, widespread changes in methylation patterns were found especially within genes and pathways related to neurobiological functions such as glutamate metabolism and the Golgi apparatus (Young et al., 2017). In a study on SALS patients, methylation levels were compared between patients and controls in brain regions. 38 methylation sites were found with hypo- or hyper-methylation and a majority was associated

with genes involved in oxidative stress, calcium homeostasis and neurotransmission (Morahan et al., 2009).

miRNA are short non-coding RNAs that regulates mRNA expression by translational repression (Jonas and Izaurralde, 2015). Multiple studies have shown dysregulation in miRNA expression pattern in ALS. In a study on peripheral blood leukocytes of SALS patients, abnormal miRNA expression patterns for miRNAs that are associated with various neurodegenerative processes were observed (Chen et al., 2016b). Similarly, a study on human post-mortem spinal cord tissues reported dysregulation of miRNAs and their gene targets implicated in pathways involved in the pathogenesis of ALS (Figueroa-Romero et al., 2016).

The modification of histone tails and globular domains by methylation and acetylation has been implicated in ALS. The reduced gene expression of C9orf72 with hexanucleotide repeat expansions was reported to occur as a result of histone trimethylation. In the brain tissues of patients with ALS, trimethylated lysines at sites 9, 27, and 79 within histone H_3 and at site 20 within H_4 were found strongly bound to expanded repeats resulting in lower levels of C9orf72 owing to the tighter binding of mutated DNA to the histones (Belzil et al., 2013). Dysregulation of histone-modifying enzymes can also contribute towards disease progression. Histone deacetylase 4 was found upregulated in the muscle samples of ALS patients presented with rapid disease progression (Bruneteau et al., 2013). Epigenetic mechanisms are certainly involved in the progression of the disease but whether these changes are a cause of the disease or a consequence remains arguable (Dolinar et al., 2018, Albo et al., 2004).

1.6.8 Apoptosis

There has been a lot of evidence suggesting that the motor neuron death occurs from apoptosis in ALS (Guégan and Przedborski, 2003). Apoptosis is a programmed cell death and is characterized by a series of morphological changes that includes cell shrinkage, chromatin

condensation, nuclear fragmentation, membrane blebbing and the formation of apoptotic bodies with an absence of inflammatory response. Apoptosis employs the activation of upstream-effector caspases which activate the downstream executioner caspases (Ashe and Berry, 2003). These caspases are cysteine proteases and their substrates include cytoskeletal proteins and DNA.

Apoptotic cell death can be triggered from three main pathways that are death receptor-mediated pathway, mitochondrial-mediated pathway, or endoplasmic-reticulum-mediated pathway. The death receptor mediated pathway activates caspase-8 and caspase-10 which either directly activates downstream caspase-3, 6 and 7 leading to cell death or further mediates mitochondria-mediated apoptotic pathway. The mitochondria-mediated apoptotic pathway involves the release of cytochrome c into cytosol where it activates caspase-9 leading to the activation of caspase-3 and cell death. Endoplasmic-reticulum-mediated pathway involves the activation of caspase-12 as a result of unresolved ER stress that further activates caspase-9 leading to the activation of caspase-3 in a cytochrome c independent manner or by triggering caspase-8 resulting in the activation of mitochondrial-mediated cell death (Figure 1-6) (Sano and Reed, 2013, Sathasivam and Shaw, 2005).

Ca^{2+} plays an important role in apoptosis signalling in relation to ALS. Ca^{2+} overload or perturbation of intracellular Ca^{2+} compartmentalization causes cytotoxicity and triggers apoptosis. Ca^{2+} overload occurring as a result of excessive activation of post-synaptic receptors during excitotoxicity can cause damage to the cell and trigger apoptotic pathway. Ca^{2+} concentration in the cytoplasm can also increase as a result of damage caused by oxidative stress to the Ca^{2+} transporting system of the ER and mitochondria (Orrenius et al., 2003). Mutations in SOD1 have been reported to promote apoptotic cell death by converting SOD1 from anti-apoptotic to a pro-apoptotic enzyme in the presence of oxidative stress (Rabizadeh et al., 1995). In a study on SOD1 transgenic mice, mutant SOD1 was selectively recruited to

mitochondria in the affected tissues implicating the mitochondria-mediated apoptotic cascade in motor neuron death (Liu et al., 2004). Overexpression of the anti-apoptotic Bcl-2 protein in SOD1 transgenic mice delayed disease onset and prolonged survival by reducing spinal cord motor neurodegeneration (Kostic et al., 1997). The deletion of two pro-apoptotic BCL-2 family proteins, Bax and Bak, halted neuronal loss and prevented neuronal degeneration in $SOD1^{G93A}$ mice by blocking the mitochondrial apoptotic pathway and preserving the motor neuron viability and function. It also indicated that mitochondrial apoptotic pathway is activated early in ALS and contributes to motor neuron degeneration. Inhibition of apoptosis upstream of mitochondrial permeabilization was thus suggested to be a possible therapeutic strategy for ALS (Reyes et al., 2010).

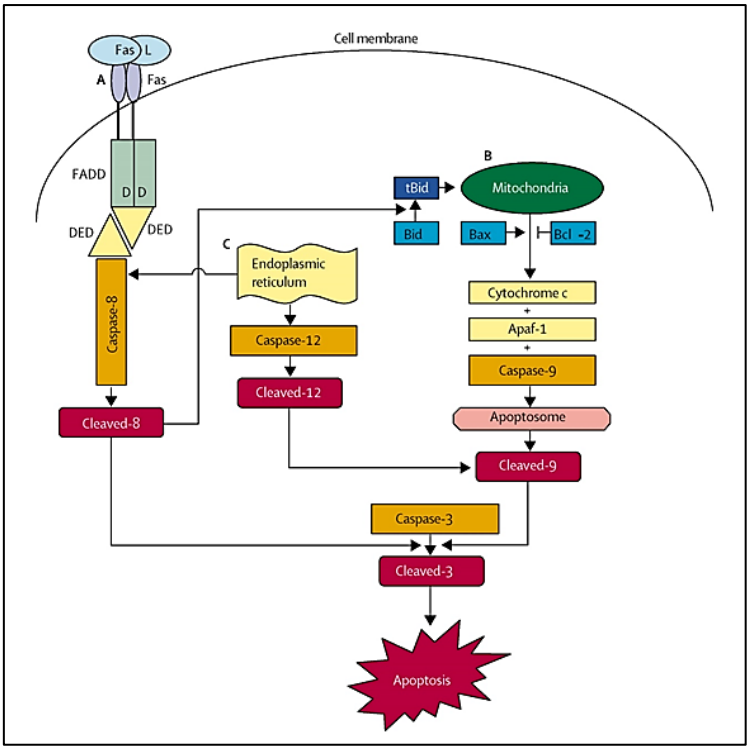

Figure 1-6 Pathways for caspase activation in apoptotic cell death

Three main pathways can trigger apoptotic cell death namely death receptor-mediated pathway, mitochondrial-mediated pathway, or endoplasmic-reticulum-mediated pathway. A) The Fas–Fas-ligand pathway is the major death receptor mediated pathway and is activated by Fas ligand (FasL) that attaches to Fas and recruits Fas-associated death domain protein (FADD) that contains a death domain (DD) and a death-effector domain DED) activating caspase-8 which either directly activate downstream caspase-3 leading to cell death or further mediates mitochondria-mediated apoptotic pathway. B) The mitochondria-mediated apoptotic pathway involves the release of cytochrome c into cytosol where it activates apoptosis activating factor-1 (Apaf-1) and caspase-9 leading to the activation of caspase-3 and cell death. C) Endoplasmic-reticulum-mediated pathway involves the activation of caspase-12 that further activates caspase-9 leading to the activation of caspase-3 in a cytochrome c independent manner or by triggering caspase-8 resulting in the activation of mitochondrial-mediated cell death (Sathasivam and Shaw, 2005).

1.7 Hypothesis of the study

We hypothesised that the identified novel mutations disrupt the normal cellular mechanisms within neurons leading to motor neuron death in patients with familial ALS.

1.8 Aims of the study

Our study involved the following aims

(1) Sanger sequencing to confirm the presence of mutations and their transmission with the disease.

(2) Expression profiling of selected candidate genes and the marker proteins of cellular pathways involved in the action of candidate genes in spinal cord samples from sporadic ALS cases.

(3) Functional characterization of selected mutations in lymphoblastoid cell lines obtained from FALS patients harbouring the mutations and healthy controls lacking the mutations from the same pedigree.

Chapter 2: Material and methods

2.1 Samples

For this thesis project, we had blood samples or buffy coats from FALS families with multiple affected individuals. We also had lymphoblastoid cell lines (LCLs) from these families. In addition to FALS cases, we had spinal cord tissue samples from controls (22) and SALS (12) cases for gene expression (mRNA and protein) profiling in ALS. This study was initially approved by the Riverside Research Ethic Committee.

NRES committee Fulham, Genetics of Motor Neurone Disease/ Amyotrophic Lateral Sclerosis. REC reference: 12/LO/0902.

NRES Committee Yorkshire and the Humber, Gene expression in Motor Neurone Disease/ Amyotrophic Lateral Sclerosis. Reference: 12/YH/0281.

2.2 Genomic DNA extraction

Genomic DNA from whole blood, buffy coat layer (leukocyte layer) or LCLs was extracted using the QIAamp® DNA Midi kit (Qiagen) according to the manufacturer's protocol provided with the kit. 100-200 µl of Qiagen Protease was mixed with 1 ml of cell suspension or blood sample. 1.2-2.4 ml of buffer AL was added in the same tube and mixed thoroughly by inverting the tube several times followed by vigorous shaking to ensure sufficient lysis of cells. The tube was incubated at 70^{o}C for 10 min to maximise DNA yield after cell lysis. 1-2 ml of absolute ethanol was added to the tube and the tube was inverted several times to precipitate DNA. After transferring to a QIAamp Midi column the solution was centrifuged at 3000 rpm for 3 min. Filtrate was discarded from the column and 2 ml of buffer AW1 was added to the column followed by centrifugation at 5000 rpm for 1 min. 2 ml of buffer AW2 was then added to the column and centrifuged at 5000 rpm for 15 min. The filtrate was discarded and the column was

placed in a new tube. 200-300 µl of buffer AE was added directly to the column membrane and the column was incubated at room temperature for 5 min followed by centrifugation at 5000 rpm for 2 min. Extracted DNA was transferred to a DNase/RNase free tube and stored at -20ºC for short-term and -80ºC for long-term storage. The DNA was run on agarose gel to check the quality and purity as explained in the section 2.6 of this chapter.

2.3 Measurement of extracted DNA

To check the purity and concentration of extracted DNA, DNA was quantified using a ND-1000 spectrophotometer (NanoDrop®). Optical density (OD) readings were obtained at 260 nm and 280 nm. A DNA sample with a 260/280 OD ratio of approximately 1.8 or greater was considered a good quality DNA.

2.4 Primer designing

For sequencing genomic DNA or studying the expression of genes, complementary primers were designed to amplify the target sequence using Primer3 program (http://bioinfo.ut.ee/primer3-0.4.0/) and were ordered from Sigma-Aldrich. Primer length was kept between 18-22 bps and the product size was kept less than 500 bps. A maximum of 4 consecutive identical nucleotides were allowed in the primers and forward and reverse primers were designed with a maximum of 5ºC difference in their melting temperature (Tm).

Primers were reconstituted to a concentration of 100 µM with sterile water. A concentration of 10 µM was used for DNA sequencing and 6 µM for qPCR. The primers were stored at -20ºC. The primer sequences have been specified in the methodology section of respective chapters.

2.5 Polymerase chain reaction (PCR)

DNA fragments were amplified by PCR using gene specific primer pairs. A temperature gradient PCR was used to find the optimal annealing conditions for the primer pairs followed

by conventional PCR to amplify target fragments. For each PCR reaction, a standard 30 µl solution was prepared that contained 1X GoTaq buffer (Promega), $MgCl_2$ (Promega), dNTPs (Invitrogen), forward and reverse primer, Go*Taq* DNA polymerase (Promega) and template DNA (Table 2-1).

Table 2-1 PCR reaction preparation

Reagents	Stock concentration	Required concentration	Volume required per reaction
GoTaq Buffer	5X	1X	6 µl
$MgCl_2$	25 mM	1.5 mM	1.8 µl
dNTPs	10 mM	0.1 mM	0.3 µl
Forward primer	10 µM	0.5 µM	1.5 µl
Reverse primer	10 µM	0.5 µM	1.5 µl
Go*Taq*	5 U/µl	0.02 U/µl	0.1 µl
template	5 ng/µl	0.5 ng/µl	1 µl
water			**17.8 µl**
total			30 µl

Reagents required for a standard PCR reaction. The stock for dNTP mix contained 10 mM each of the four nucleotides (dTTP,dGTP, dCTP, dATP).

PCR reactions were performed in a thermocycler (Techne) using the following steps: Initial denaturation at 94ºC for 3 min. This was followed by 35 cycles (for most reactions) each of which had denaturation at 94ºC for 30 sec, annealing at an optimised temperature for 30 sec and extension at 72ºC for 45 sec. A final extension step at 72ºC for 5 min.

2.6 Agarose gel electrophoresis

PCR products were visualised by separating them according to their sizes on agarose gel. 2 µl of orange G, used as a tracking dye, was added to 8 µl of PCR product. 2% agarose gel was prepared by adding 11g of agarose powder to 0.5X TBE buffer. The solution was placed in a microwave oven for 5 to 10 min in order to dissolve the agarose powder completely. The mixture was cooled to about 60ºC and 1% ethidium bromide (10 µl) was added to the solution to visualize DNA under UV light. The mixture was poured into a gel casting tray with the insertion of combs for making wells and left at room temperature to solidify for an hour. Combs were removed and the gel was transferred to the electrophoresis tank containing 0.5X TBE buffer for loading DNA samples. A size marker, ΦX174 DNA/BsuRI (HaeIII) (Fermentas) was run along the samples to confirm the size of the amplified DNA product. Samples were run at 210V for 1 hour. The gel was visualised under UV transilluminator using gel documentation system (Geldoc).

2.7 Enzymatic clean-up

For Sanger sequencing, PCR products were cleaned using Exonuclease I - Shrimp Alkaline Phosphatase (ExoSAP) protocol. ExoSAP contains exonuclease I (New England Biolabs) for the removal of unused primers and Shrimp Alkaline Phosphatase (SAP) (Sigma-Aldrich) for the removal of remaining unused dNTPs from the PCR products before DNA sequencing.

10 µl of ExoSAP mix was prepared for each sample. The mix contained 0.025 µl Exonuclease I, 0.25 µl of SAP and 9.725 µl of sterile distilled water. This mixture was added to 22 µl of PCR product. The 32 µl mixture was then incubated at 37ºC for 30 minutes followed by 95ºC for 5 minutes in a thermocycler.

2.8 DNA Sequencing

DNA was sequenced using the Sanger Sequencing method. 1.2 µl of 10 µM forward or reverse primer was added to 10 µl of purified PCR products and sent for sequencing to the MRC CSC Genomic Core Laboratory at Imperial College London. The sequencing files were read using CodonCode aligner software.

2.9 Total RNA extraction

To check the expression of target genes at the transcriptional level, RNA was extracted from spinal cord samples, whole blood or LCLs using a Direct-zol™ RNA mini prep kit (Zymo Research,) according to the protocol provided by the manufacturer. The extraction was performed in a sterile and RNase-free environment using RNase AWAY decontaminant reagent to decontaminate surfaces and labware from RNase. Tissue samples or cells were lysed by adding TRIzol® reagent and a homogenous solution was made. The samples were kept at room temperature for 5 min and centrifuged at 12000 rpm for 1 min. The supernatant was transferred to new RNase free tubes. An equal amount of molecular grade absolute ethanol was added to the sample homogenates and was mixed thoroughly. The solution was then transferred into Zymo-Spin™ IIC columns placed in collection tubes and was centrifuged at 12000 rpm for 1 min. The flow-through was discarded and the samples were treated with DNase I. For this step, a DNase I mixture was prepared that contained 5 µl of DNase I and 75 µl of DNase I reaction buffer for each sample in an RNase free tube. 80 µl of DNase I mixture was then

directly added to the column matrix for each sample and the columns were incubated for 15 min at room temperature. 400 µl of Direct-zol™ RNA PreWash was added to the columns afterwards and the columns were centrifuged for 1 min. The RNA PreWash addition step was repeated and 700 µl of RNA Wash buffer was added to the columns followed by centrifugation of 3 min for a complete removal of Wash buffer from the columns. Columns were transferred to RNase-free tubes. 40 µl of DNase/RNase-free water was added to the columns to elute the RNA and the columns were left at room temperature for 5 min. Columns were then centrifuged at maximum speed for 1 min. The RNA samples stored at -80ºC.

Purity and concentration of RNA was checked using a ND-1000 spectrophotometer (NanoDrop®). RNA samples with 260/280 OD ratio of approximately 2.0 were considered good quality RNA extracts.

2.10 cDNA synthesis

cDNA is a complementary DNA that is synthesized from RNA by reverse transcription. To perform qPCR for gene expression analysis, cDNA was synthesised from extracted RNA using random hexamer primers (Invitrogen) and AMV reverse transcriptase (New England Biolabs), 10X RT buffer (New England Biolabs) and dNTP mix (invitrogen). The RT buffer provides the optimal reaction conditions for cDNA synthesis.

For cDNA synthesis, an RNA mix and an enzyme mix were prepared. The RNA mix was prepared in an RNase-free tube by adding 2 µl of dNTP mix (10 mM), 1 µl of random hexamers (50 ng/µl), 5 µl of nuclease-free water and 9 µl of total RNA. The RNA mix was incubated for 5 min at 65ºC for denaturation. The tubes were vortexed and left on ice. The enzyme mix was prepared in a separate RNase-free tube by adding 2 µl of 10X RT buffer and 1 µl of AMV reverse transcriptase (10000 U/ml). The enzyme mix was added to the RNA mix for each sample and the solution was incubated in thermocycler for 10 min at 25ºC followed by an

incubation of 42°C for 1 hour and a final step of 90°C for 5 min, which inactivates the enzyme. The newly synthesized cDNA was then stored at -20°C for further use.

2.11 Quantitative real-time PCR (qPCR)

qPCR is a widely used efficient technique for gene expression analysis as it allows to monitor the amplification of a gene product in real time. A fluorescent reporter is used in qPCR, which can bind to a double stranded DNA produced during the amplification. The detected fluorescent signal from the reporter is indicative of the number of PCR products synthesized in a reaction. With each PCR cycle the fluorescence increases, so the higher the signal, the more is the PCR product.

We amplified template cDNA by quantitative real-time PCR (qPCR) to analyse the target gene expression in spinal cord tissue samples, lymphocytes and LCLs. For each qPCR reaction, a standard 20 µl solution was prepared that contained 10µl of 2X PowerUp™ SYBR® Green Master Mix (ThermoFisher scientific), 1 µl of forward (6 µM) and 1 µl of reverse primer (6 µM), 1 µl of template cDNA and 7 µl of sterile distilled water. The 2X PowerUp™ SYBR® Green Master Mix is made up of dNTPs, Taq DNA Polymerase, SYBR Green dye, ROX reference dye, and buffer.

Primers for qPCR were optimised using a temperature gradient PCR to find the optimal annealing conditions prior to performing qPCR. qPCR was performed in Mx3000P qPCR System using the following steps: Initial denaturation step at 95°C for 10 min. This was followed by 35 cycles of denaturation at 95°C for 30 sec, annealing at an optimised temperature for 30 sec and extension at 72°C for 45 sec. A final step of 1 cycle with denaturation at 95°C for 1 minute, annealing at an optimised temperature for 30 sec and extension at 95°C for 45 sec. For quality control checks, non-template control reactions were included in each qPCR

run. The qPCR products were run on 2% agarose gel to confirm the amplification of the required product.

2.12 Protein extraction

Radioimmunoprecipitation assay buffer (RIPA) is a preferred buffer for extracting proteins from whole cells. To run protein samples on SDS-PAGE gel for detecting the proteins of interest, spinal cord tissues and cells were lysed with RIPA buffer to isolate proteins. Tissues or cells were re-suspended in 100–200 µl of RIPA buffer and homogenised. Samples were left at 4^{o}C with gentle agitation for 30 min (cells) to 2 hours (tissues) followed by centrifugation at 12000 rpm for 20 min at 4^{o}C. The supernatant was transferred to a fresh tube and the protein extract was frozen at -80^{o}C for long-term storage.

2.13 Bradford assay

The Bradford assay is used for measuring the concentration of proteins in a sample. The Bradford dye reagent contains Coomassie Brilliant blue G which undergoes an absorbance shift from 465 to 595 nm on binding to proteins. Hence, if a sample has more proteins than more Coomassie will bind and will have a higher absorbance at 595 nm.

We used Pierce™ bovine serum albumin (BSA) (Thermo Scientific) as a protein standard for determining the protein concentration of cell or tissue samples. 1 mg/ml was the initial concentration of BSA standard and serial dilutions were prepared. In a 96 well plate, 5 µl of BSA standard/sample dilution was added followed by 195 µl of quick start™ Bradford 1X dye reagent (Boi-Rad). Absorbance of samples was measured with a VersaMax Microplate Reader (Molecular Devices) at 595 nm. The protein concentration of samples was then calculated by comparison to the standard curve produced from BSA dilutions.

2.14 Sample preparation for gel loading

Protein extracts (40 to 50 µg/20 µl for spinal cord tissue and 20 µg/20 µl of LCLs) were mixed with Laemmli SDS sample buffer (Alfa Aesar) which denatures proteins, reduces disulphide bonds, gives them a negative charge and helps in monitoring the run on a gel. RIPA buffer or double distilled water was used to make up the final required volume of samples. The samples were heated at 95ºC for 10 min before loading on a SDS-PAGE gel.

Sodium dodecyl sulphate polyacrylamide gel electrophoresis (SDS-PAGE)

Sodium dodecyl sulphate-polyacrylamide gel electrophoresis (SDS-PAGE) is a technique used to separate proteins based on their molecular weight. SDS is an ionic detergent that denatures the proteins and masks their intrinsic charge by giving them a uniform negative charge. The proteins, therefore, travel from the negatively charged to the positively charged electrode based only on their molecular weight.

SDS-PAGE gels are made of a stacking and a resolving gel layer. The resolving gel was prepared (8-12.5%) according to the size of the protein of interest (Table 2-2) and was poured in the assembled glass plates. After the polymerisation of resolving gel, stacking gel was prepared and poured over it and a comb was inserted. The gel was left to polymerise. The gel apparatus was assembled and 1X running buffer was poured in the gel tank. The comb was removed from the gel and protein samples were loaded. A molecular weight marker (Thermo Scientific) was also loaded along the samples to estimate the size of proteins separated by the gel. The gel was electrophoresed at 80 V for 70 minutes.

Table 2-2 Percentage of resolving gel

Protein size (kDa)	Gel percentage (%)
4-40	20
12-45	15
10-70	12.5
15-100	10
25-200	8

2.15 Western blotting

Western blotting is a technique used to identify proteins of interest among other proteins that have been separated by gel electrophoresis based on their molecular weight. The proteins from the gel are transferred to a membrane and incubated with primary and secondary antibodies. The unbound antibodies are washed off and the protein of interest is detected using a substrate that binds to the enzyme conjugated with secondary antibody producing chemiluminiscence. The chemiluminiscence is then detected by developing a film or by using a chemiluminescence imaging system.

After performing SDS-PAGE, proteins were transferred to a nitrocellulose membrane by either a semi-dry transfer or a wet transfer system. The semi-dry transfer was performed using a Pierce power blotter (Thermo Scientific) and 1-step™ transfer buffer (Thermo Scientific) after assembling a gel-membrane-filter paper package according to the manufacturer's protocol. The wet transfer was performed for an hour or overnight using home-made 1X transfer buffer. After protein transfer, the membrane was stained with Ponceau S solution (Sigma-Aldrich) to assess the success of protein transfer. The membrane was destained by repeated washing with Tris Buffer Saline Tween 20 (TBST) or Phosphate buffer Saline Tween 20 (PBST) before further use.

The nitrocellulose membrane was blocked with a 5% blocking buffer that was made either with non-fat milk or BSA for an hour under gentle agitation. This step prevents non-specific binding of the primary or secondary antibody to the membrane. After blocking, the membrane was incubated overnight with primary antibody diluted in blocking buffer at a recommended concentration, at 4^{o}C under gentle agitation. The membrane was washed 3 times with TBST/PBST for 5 minutes to remove any unbound antibody. This was followed by an incubation with anti-IgG secondary antibody diluted in blocking buffer for an hour under gentle

agitation at room temperature. The membrane was again washed 3 times with TBST/PBST for 5 minutes. The membrane was finally incubating in Pierce™ ECL western blotting substrate (Thermo Scientific) for 5 minutes and immediately imaged using Syngene GeneGnome XRQ chemiluminescence imaging system.

The relative density of the candidate protein between different samples was quantified using ImageJ software and the samples were normalised against a housekeeping gene.

2.16 Cell culture

EBV transformed lymphoblastoid cell lines were cultured in RPMI 1640 medium (Gibco) containing 10% Fetal bovine serum (Sigma-Aldrich), 1% penicillin/Streptomycin (Gibco) and 1% glutamax (Gibco). The cells stored in liquid nitrogen were thawed and suspended in 5 ml of culture medium. The cells were centrifuged at 1500 rpm for 10 min at 37ºC. The supernatant, containing dead cells, was discarded and the cells were resuspended in 10 ml of fresh culture medium. The cells were incubated at 37ºC, 5% CO_2. After 24 hours, cells were centrifuged and the media was doubled to 20 ml and were left at the same conditions for incubation. After about 48 hours, the media was replaced and increased to 40 ml and incubated at the same conditions. After 24 to 48 hours, the cells were passaged by centrifuging the cell culture and dividing the pellet in two flasks both containing 40 ml of medium. After another 24 to 48 hours, cells were counted and centrifuged. The cells that were required for further experiments were treated accordingly and the remaining were frozen in a freezing solution (10% FBS and 10% DMSO). For freezing cells, $1x10^7$ to $3x10^7$ cells were taken and resuspended in 1 ml of freezing solution per cryovial. The cryovials were stored at -80ºC or in liquid nitrogen for long-term storage.

For counting cells, a hemocytometer was used. The cell suspension was diluted with trypan blue which is used to distinguish viable cells from dead cells. Trypan blue penetrates the cell membrane of dead cells and colours them blue, whereas, it cannot penetrate the cell membrane

of viable cells, so they stay unstained. After counting the number of live cells, cell concentration was calculated using the following formula:

$$\text{Total cells/ml} = \text{Total cells counted} \times \frac{\text{dilution factor}}{\text{\# of Squares}} \times 10{,}000 \text{ cells/ml}$$

2.17 LCL drug treatment

LCLs were treated with drugs in order to artificially induce autophagy and ER stress in the cells. This was done to study the effect of mutations under basal and cell-stressed conditions. The drugs used were tunicamycin (Sigma-Aldrich, UK), thapsigargin (Sigma-Aldrich, UK), rapamycin (Sigma-Aldrich, UK) and staurosporine (Sigma-Aldrich, UK).

LCLs were first grown for 8 to 10 days at 37^{o}C, 5% CO_2 before treatment with the drugs. Cells were seeded in a 24 well plate with 3 x 10^6cells/ml in each well for mRNA and protein expression studies and 1 x 10^6cells/ml in each well for FITC-Annexin V analysis. The cells were incubated in the plate for few hours before starting the drug treatment. The drug treatment has been explained in detail in the respective chapters.

For mRNA and protein expression studies, cells were centrifuged at 2000 G for 5 min and the pellets were frozen at -80^{o}C for later use. For cell survival studies, cells were stained with FITC-Annexin V for analysis with flow cytometry.

2.18 Flow cytometry

Flow cytometry is a method used for analysing the expression of molecules on the cell surface or inside the cell in a heterogeneous population of cells. It measures fluorescence intensity produced by fluorescent-labelled ligands that bind to specific molecules such as the binding of FITC- Annexin V to the phospholipid phosphatidylserine (PS) on the surface of apoptotic cells.

We used flow cytometry for the detection of the cells undergoing apoptosis using FITC-Annexin V assay. Apoptosis is a process characterised by distinct morphological features that start from the loss of plasma membrane asymmetry and end at the cleavage of DNA. On loss of plasma membrane asymmetry, PS translocates to the outer side of the membrane from the cytoplasmic side of the membrane. This results in exposure of PS to the external cellular environment. Annexin V, which has a high affinity for PS, binds to the exposed PS. This hallmark stage of apoptotic cell is examined using flow cytometry (van Engeland et al., 1996). Fluorescein isothiocyanate (FITC) is a sensitive probe that is used to label Annexin V for the flow cytometric analysis of cells undergoing apoptosis. Annexin V is used in conjunction with Propidium iodide (PI) that binds to DNA. The damaged and dead cells are permeable to PI but the viable cells with intact membrane are not, so the PI reaches the DNA of damaged cells and labels them. Hence, viable cells are AnnexinV negative and PI negative; early apoptotic cells are Annexin V positive and PI negative; late apoptotic cells are Annexin V positive and PI positive; and dead cells are Annexin V negative and PI positive.

LCLs were grown and treated with drugs. The treatment was inhibited and the cells were centrifuged at 200 G for 5 min. Cells were then stained for FITC-Annexin V assay for flow cytometric analysis. FITC-Annexin V assay staining of cells was performed using FITC-Annexin V Apoptosis Detection kit 1 (BD Biosciences) according to manufacturer's protocol. In summary, the cells were resuspended in 1 ml of 1X binding buffer with a cell concentration of 1 x 10^6cells/ml. 100 ul (1 x 10^5 cells) of the cell suspension was transferred to a 5 ml culture tube. 5 ul of FITC-Annexin V was added to the tube followed by 5 ul of PI. The tubes were vortexed gently and incubated for 15 min at room temperature (25^{o}C) in dark. Finally, 400 ul of 1X binding buffer was added to each tube. The cells were then analysed using 2 Laser FacsCalibur Flow Cytometer (BD Biosciences) within an hour of cell staining.

For the flow cytometric analysis, four tubes were prepared as experimental controls. The cells were taken from the LCL of a healthy individual whose gene did not harbour the mutation present in FALS cases. The experimental controls were prepared as follows:

1. 100 ul (1 x 10^5 cells) of cell suspension without the addition of FITC Annexin V and PI.
2. 100 ul (1 x 10^5 cells) of cell cell suspension with FITC-Annexin V only.
3. 100 ul (1 x 10^5 cells) of cell cell suspension with PI only.
4. 100 ul (1 x 10^5 cells) of cell cell suspension with both FITC-Annexin V and PI.

Acquired data was analysed using FlowJo 10.1 software.

2.19 Statistical analysis

GraphPad Prism software was used for performing statistical tests and for producing graphs. Paried Student's t-test was used for analysing the effect of drugs. Unpaired Student's t-test (parametric) or Mann-Whitney test (non-parametric) was used for examining the effect of mutation and 2-way ANOVA with post-hoc tests was used for flow cytometric analysis.

2.20 Stock Solutions

Table 2-3 Recipes for stock solutions

Solution	Volume	Components
Stock solution for agarose gel electrophoresis		
10X TBE buffer	1 L	Tris-base, 108 g Boric acid, 55 g 0.5 M EDTA pH 8.0, 40 ml Distilled water, to 1L
0.5M EDTA	100 ml	EDTA salt, 18.61 g Distilled water, 80 ml Adjust pH to 8
Stock solutions for Western blotting		
RIPA	100 ml	150 mM NaCl, 8.76 g 1% NP-40 or Triton X-100, 1 ml 0.5% sodium deoxycholate, 0.5 g 0.1% SDS, 0.1 g 50 mM Tris-base , pH 8.0, 0.61g 10% complete protease inhibitor cocktail 10% complete phosphatase inhibitor cocktail
8% Resolving Gels of SDS-PAGE	8 ml	ddH_2O, 3.7 ml 30% acrylamide, 2.13 ml 1.5 M Tris (pH 8.8), 2 ml 10% SDS, 80 µl 10% ammonium persulfate, 80 µl TEMED, 8 µl
4% Stacking gels for SDS-PAGE	5 ml	ddH_2O, 3 ml 30% acrylamide, 670 µl 0.5 M Tris (pH 6.8), 1.25 ml 10% SDS, 50 µl 10% ammonium persulfate, 50 µl

		TEMED, 10 µl
1X Running buffer	1 L	25 mM Tris-base, 3.03 g 192 mM glycine, 14.4 g 0.1% SDS, 1.0 g ddH_2O to make volume to 1000 ml Adjust pH to 8.3
Wet Transfer buffer	1 L	25 mM Tris-base, 3.03 g 192 mM glycine, 14.4 g 10%-20% methanol, 100-200 ml ddH_2O to make volume to 1000 ml
1X TBS	I L	20 mM Tris-base, 2.42 g 150 mM NaCl, 8.76 g 50mM KCl, 3.73 g ddH_2O to make volume to 1000 ml Adjust pH to 7.6
1X PBST/TBST	1 L	1X PBS/TBS, 1000 ml Tween 20, 1 ml

Chapter 3: Selection of genes for study/confirmatory Sanger sequencing and transmission with the disease

3.1 Introduction

3.1.1 Exome sequencing in FALS Sequencing Consortium

The Familial Amyotrophic Lateral Sclerosis (FALS) gene identification project was initiated by our group in 1991. 208 families including affected and unaffected individuals were recruited to participate in this project and the data obtained from these participants contributed to the identification and characterisation of important pathological mutations in *SOD1, TARDBP, FUS, VAPB, SQSTM1, C9ORF72, DAO, TUB4A, TBK1, NEK1, CCNF, ANXA11* and *KIF5A*. Previously, linkage analysis for gene discovery required large pedigrees with multiple affected individuals but recently the process has been greatly facilitated by the advent of whole exome sequencing and whole genome sequencing technologies. Mutations have been identified in over 70% of FALS cases with generally large families while the remaining families with undiscovered disease causative genes are generally smaller and sometimes have the availability of only one index case. Hence, in order to enhance gene discovery in such small pedigrees, it has become essential to form large international consortia. Our group, therefore, embarked on the whole exome analysis of families where the gene was not yet identified in a collaboration with Professor Christopher Shaw (Kings College London), funded by a Programme Grant from the MRC, with a focus on families where DNA was available from 2 or more affected individuals. We subsequently joined the first International FALS sequencing consortium consisting of laboratories from eight countries (USA, UK, Canada, Australia, Italy, Spain, The Netherlands, The Republic of Ireland).

This thesis is focused on the predicted pathogenic mutations obtained from the Imperial College FALS cohort data that was contributed to studies performed by the FALS sequencing consortium. The discovery cohort for exome sequencing used by the FALS sequencing consortium initially consisted of ~363 index FALS cases from laboratories in eight countries (USA, UK, Canada, Australia, Italy, Spain, The Netherlands, The Republic of Ireland). These index cases lacked mutations or repeat expansions in ALS genes that were already known at the time that this study was started (*C9orf72*, *SOD1*, *FUS*, *TARDBP*, *UBQLN2*, *PFN1*, *OPTN*, *ANG* and *VCP*). Target bases (3.2×10^9) were sequenced on average per sample to an average depth of 90.4x in the study. Control exome data of 4,300 European Americans was also included that was available through the Exome Variant Server (EVS) of NHLBI. In addition, control exome data from 31 internally sequenced samples was also included. For identifying putatively damaging variants, different bioinformatics tools (GERP, SIFT, phyloP and MutationTaster) were used.

The formation of the consortium enabled the identification of several new FALS genes (~1% frequency) that would not have been possible without combining the cohorts of different research laboratories e.g., *TUBA4A* (Smith et al., 2014b), *TBK1* (Cirulli et al., 2015) and *NEK1* (Kenna et al., 2016a).

3.1.2 Selection of candidate genes for characterisation

Our work was focused on pathogenic mutations present in the Imperial College FALS cohort where the putative pathogenic mutations were present either in multiple families or in more than one family member diagnosed with the disease. Information about further mutations found in our selected candidate genes in other families from the consortium was available. We screened for mutations that were the top hits in gene-based rare variant analysis (Smith et al., 2014b).

The selection of pathogenic mutations was based on satisfying the following criteria:

1. Absent from or rare in large control cohorts (e.g., *RUBCN*: 0/120,758 chromosomes, *CLCN6*: 1/121,406 chromosomes).
2. Mutation predicted to be pathogenic
3. Expressed in central nervous system.
4. Functionally relevant to known ALS pathogenic pathways (RNA processing and proteostasis)
5. Confirmed to be present in the index case by Sanger Sequencing.
6. Present in all family members with FALS indicating transmission with disease

Among our selected genes (*CLCN6, SMAD6, HEATR6*, *PKD1L1*, *RUBCN* and *NCOR1*), two genes (*PKD1L1* and *NCOR1*) appeared in the top 8 hits in the gene-based rare variant analysis because of having highly significant scores by multiple statistical tests performed by Smith et al in 2014 (Smith et al., 2014b)

3.1.3 Objectives

To perform Sanger sequencing on all individuals available from the affected families to

1. confirm presence of mutation in the index case.
2. establish transmission of mutation with the disease within a family.

3.2 Methods

We had three families in which we identified six short listed genes from the analysis performed by Smith et al (Smith et al., 2014a) for establishing the transmission of mutation with disease. We performed Sanger sequencing to confirm the mutation and its transmission with the disease.

3.2.1 Sanger Sequencing

Genomic DNA was extracted from the buffy coat layer obtained from whole blood using the QIAamp® DNA Midi kit (Qiagen, UK) and was quantified using a NanoDrop ND-1000 spectrophotometer. Genomic DNA fragments for sequencing were amplified by conventional PCR using primer pairs given in Table 3-1. The specificity of PCR to yield a single product was checked by agarose gel electrophoresis. PCR products were purified using Exonuclease I –Shrimp Alkaline Phosphatase (ExoSAP) protocol. Purified PCR products were then sequenced using Sanger Sequencing method by MRC CSC Genomic Core Laboratory at Imperial College London. The sequencing files were read using CodonCode aligner software.

Table 3-1 Primer sequences for the amplification of genomic DNA

Gene	Primers	Product size (bp)
HEATR6	Forward: CCAGGCCAGCTTATATATTCGA Reverse: TCATGGTAGAGATCGAGGACA	480
SMAD6	Forward: GCGCCATATTTCCTGAGGACA Reverse: CGATCTTGCTGCGCGTTCG	378
CLCN6	Forward: CATTCCAAGCAAGACCAGGA Reverse: ACACAGCAGAGAAGGCACAA	281
NCOR1	Forward: CCAAAAGGTGACAGTACTCTCCA Reverse: CGATAAACCTCGCCTGCAGT	394
PKD1L1	Forward: TGTGCAACTGTATGGGTCACA Reverse: GTGTGCTTGCTCAGACTCCA	388
RUBCN	Forward: AGGAGAATGCCCACTTCAGC Reverse: CAGGTTCTTGGTGCGGATTT	182

To confirm presence of mutation and transmission with disease of six short listed genes in our project, gene segments containing the mutation were sequenced using primer pairs given in the table above.

3.3 Results

CLCN6, SMAD6, HEATR6 and *PKD1L1* were sequenced in pedigree SM821. *RUBCN* was sequenced in pedigree SM331 and *NCOR1* was sequenced in pedigree SM86. The novel DNA variants identified by whole-exome sequencing were first confirmed by Sanger sequencing in the index cases. Once their presence was confirmed, the remaining available DNA samples from the family were sequenced to determine the segregation pattern of the mutation with disease.

3.3.1 Pedigree SM821

Blood samples were available from 10 individuals in this family. Only one individual in addition to the index case was diagnosed with FALS at the time of sample collection and the other individuals were healthy (Figure 3-1). The age of onset in II 1 and III 1 FALS cases was 61 years and 35 years respectively and the disease duration was 14 years and 5 years respectively.

CLCN6, SMAD6, HEATR6 and *PKD1L1* genes were amplified with the respective primer pairs and the amplified DNA fragments were sequenced.

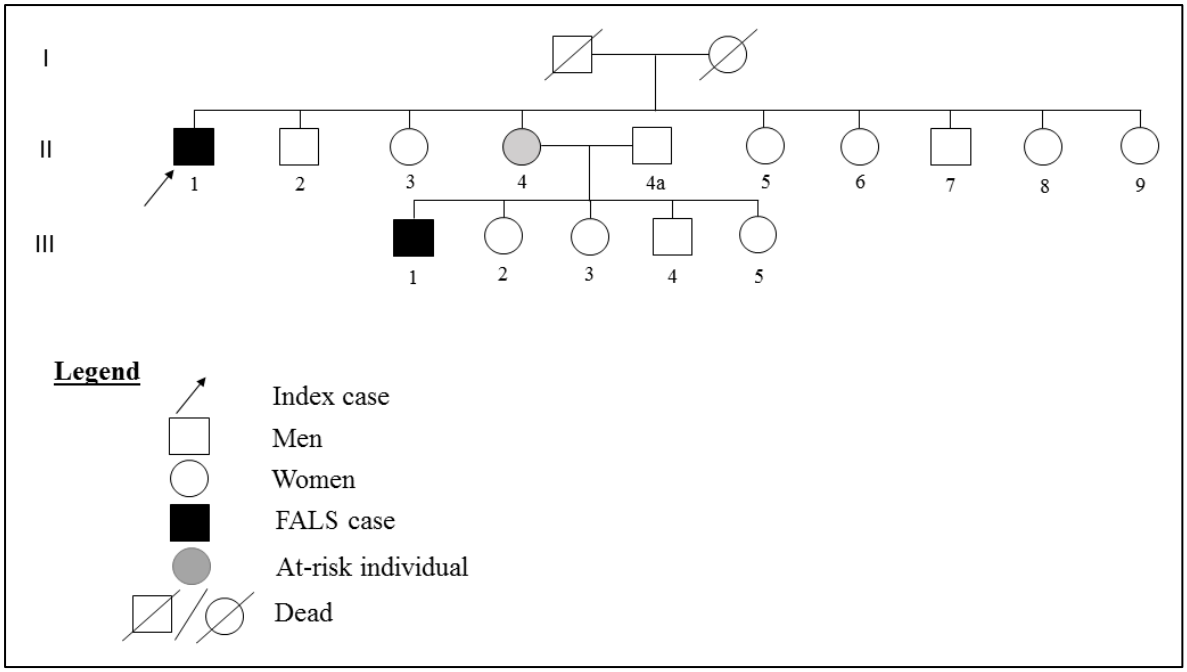

Figure 3-1 Pedigree SM821 with FALS cases and controls.

Blood samples were available from 10 individuals of this pedigree including the two affected FALS cases. The index case is indicated by an arrow. Out of 8 control cases, 4 individuals carried the mutation in *CLCN6* gene, identified by DNA sequencing, in addition to 2 FALS cases putting them at risk of developing the disease at some stage of their life.

3.3.1.1 *CLCN6*

CLCN6 [Acc:2024] is on chromosome 1 and encodes a 869 amino acid protein. The predicted novel DNA variant converts a cytosine residue to a guanine (Figure 3-2) resulting in an amino acid change from leucine to valine in protein. The mutation was identified as non-synonymous and Novel/ very rare in control cohorts (ExAC browser): 1/ 121,406 chromosomes. The position of the mutation is as follows:

NM_001286: exon15: c.C1423G: p.L475V, ENST00000346436

The mutation was confirmed in the index case (II 1) and identified in another affected family member (III 1) and the obligate carrier (II 4). The mutation was also identified in three other family members (II 2, II 3 and II 6) putting them at a risk of developing the disease later in their life (Figure 3-1). The mutation transmitted in an autosomal dominant pattern of inheritance. Overall, 6 out of 10 individuals screened for the mutation carried the mutation. As the mutation in this gene fulfilled the criteria of transmission with the disease, it was selected for further studies.

3.3.1.2 *SMAD6*

*SMAD*6 is on chromosome 15 and encodes a 496 amino acid protein. The predicted novel DNA variant converts a guanine residue to adenine (Figure 3-3) resulting in an amino acid change from cysteine to tyrosine in protein. The position of mutation is as follows:

NM_001142861: exon 4:c.G212A:p.C71Y

NM_005585: exon4: c.G995A:p.C332Y

The presence of the mutation was confirmed in the index case (II 1). It was also identified in the obligate carrier (II 4) but it was absent from the other affected family member (III 1) (Figure

3-1). Hence, the mutation did not fulfil the criteria of transmission with the disease and thus, was not selected for further studies.

3.3.1.3 *HEATR6*

HEATR6 is on chromosome 17 and encodes a 1181 amino acid protein. The identified novel DNA variant converts cytosine to thymine in the exonic region (Figure 3-4). This mutation results in protein truncation as it removes arginine and introduces a stop codon. The position of the mutation is as follows:

NM_022070: exon17:c.C2617T:p.R873X

The presence of the mutation was confirmed in the index case (II 1) and in the obligate carrier (II 4) but it was absent in the other affected member (III 1) (Figure 3-1) and hence, did not segregate with disease. Hence, the mutation did not fulfil the criteria of transmission with the disease and was not selected for further studies.

3.3.1.4 *PKD1L1*

PKD1L1 is on chromosome 7 and encodes a 2849 amino acid protein. The identified mutation changes a cytosine residue to guanine (Figure 3-5). This mutation results in protein truncation as it removes glutamic acid and introduces a stop codon. The position of mutation is as follows:

NM_138295: exon9 c.G1279T: p.E427X, ENST00000289672

The presence of the mutation was confirmed in the index case (II 1) and the obligate carrier (II 4) but it was absent from the other affected member of the family (III 1) (Figure 3-1), which showed that it was not segregating with disease. Hence, the mutation did not fulfil the criteria of transmission with the disease and was not selected for further studies.

Therefore, out of the four genes short-listed in the family, only *CLCN6* fulfilled the criteria of transmission with the disease and was thus selected for further studies.

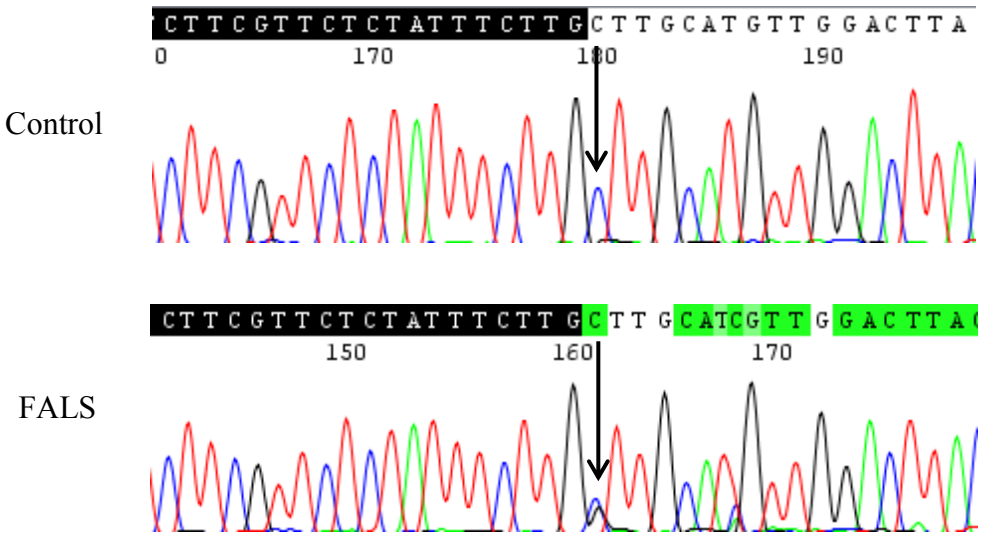

Figure 3-2 Chromatograms of *CLCN6* sequence indicating the nucleotide transversion in FALS case compared to a control

DNA was extracted from lymphocytes of ten individuals from pedigree SM821 including two FALS cases. A *CLCN6* gene segment containing the mutation was sequenced using primer set given in Table 3-1. The two chromatograms shown here indicate the difference between the DNA sequence of *CLCN6* in a control and a FALS case. The position of a heterozygous transversion, C to G, present in a FALS case compared to a control has been indicated by arrows.

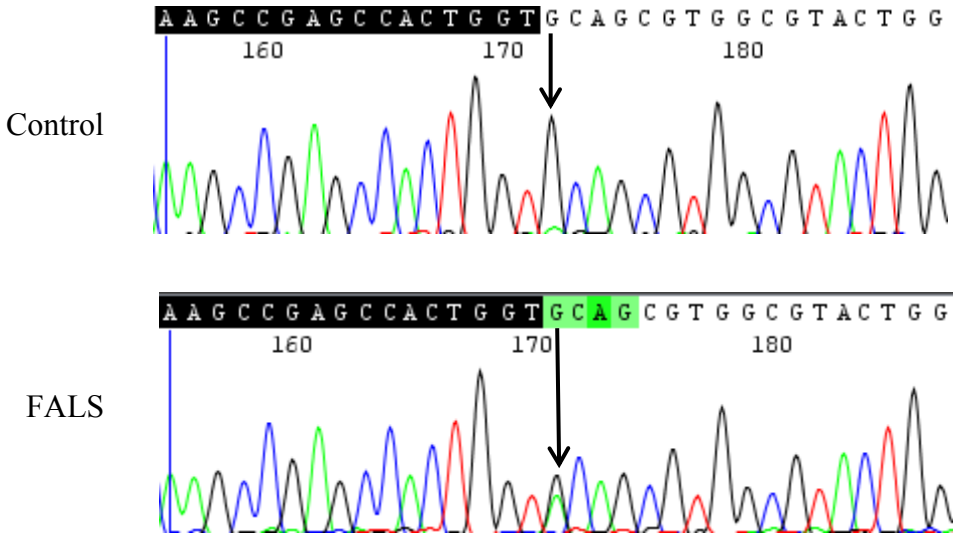

Figure 3-3 Chromatograms of *SMAD6* sequence indicating the nucleotide transition in FALS case compared to a control

DNA was extracted from lymphocytes of two FALS cases, three at-risk individuals and five controls from pedigree SM821. A *SMAD6* gene segment containing the mutation was sequenced using primer set given in Table 3-1. The two chromatograms shown here indicate the difference between the DNA sequence of *SMAD6* in a control and a FALS case. The position of a heterozygous transition, G to A, present in a FALS case compared to a control has been indicated by arrows.

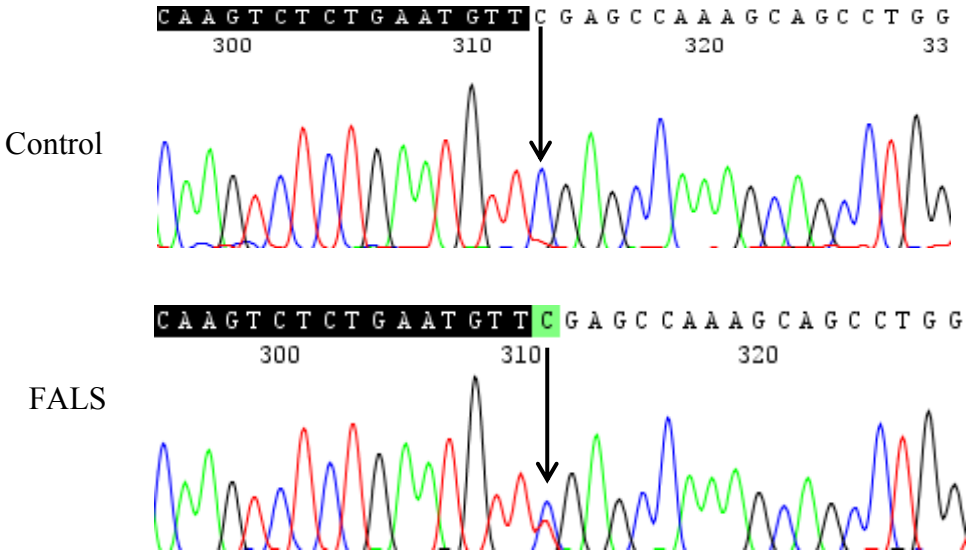

Figure 3-4 Chromatograms of *HEATR6* sequence indicating the nucleotide transition in FALS case compared to a control

DNA was extracted from lymphocytes of two FALS cases, three at-risk individuals and five controls from pedigree SM821. A *HEATR6* gene segment containing the mutation was sequenced using primer set given in Table 3-1. The two chromatograms shown here indicate the difference between the DNA sequence of *HEATR6* in a control and a FALS case. The position of a heterozygous transition, C to T, present in a FALS case compared to a control has been indicated by arrows.

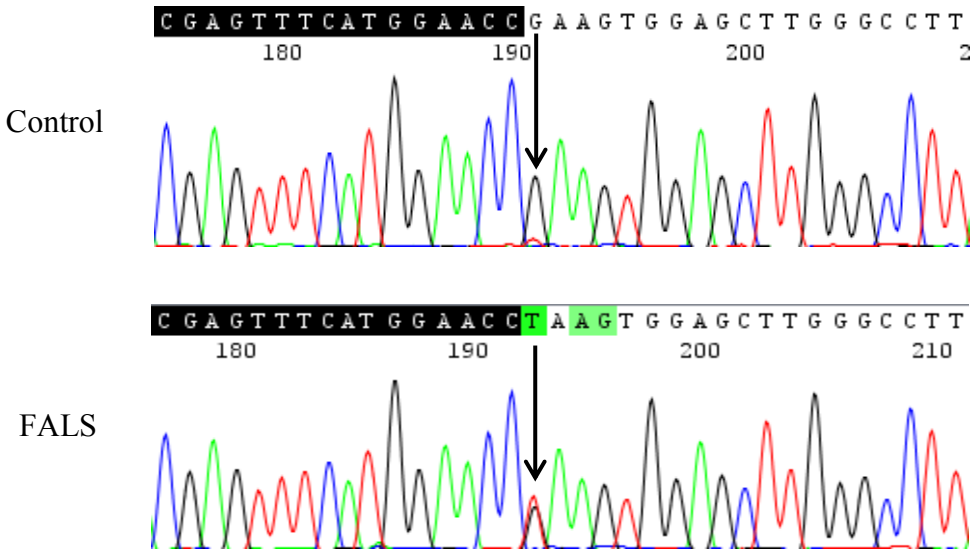

Figure 3-5 Chromatograms of *PKD1L1* sequence indicating the nucleotide transversion in FALS case compared to a control

DNA was extracted from lymphocytes of two FALS cases, three at-risk individuals and five controls from pedigree SM821. A *PKD1L1* gene segment containing the mutation was sequenced using primer set given in Table 3-1. The two chromatograms shown here indicate the difference between the DNA sequence of *PKD1L1* in a control and a FALS case. The position of a heterozygous transversion, G to T, present in a FALS case compared to a control has been indicated by arrows.

3.3.2 Pedigree SM331

Blood samples were available from 8 individuals in this family. Only one individual in addition to the index case was diagnosed with FALS at the time of sample collection and the other individuals were healthy (Figure 3-6). The age of onset in III 4 and III 8 FALS cases was 65 years and 61 years respectively and the disease duration was 4 years and 2 years respectively. Only one gene, *RUBCN*, was amplified in this family and the amplified DNA fragments were sequenced.

3.3.2.1 *RUBCN*

RUBCN [Acc:28991] is on chromosome 3 and encodes a 972 amino acid protein. The mutation converts cytosine residue to adenine in exonic region (Figure 3-7) resulting in an amino acid change of cysteine to phenylalanine in protein. The mutation was identified as non-synonymous and novel, being absent from control cohorts (ExAC browser): 0/120,758 chromosomes (927 aa), 0/120,764 chromosomes (972 aa). The position of mutation in two main transcripts is as follows:

NM_001145642: exon 11:c.G1415T :p.C472F, ENST00000273582 (927 aa)

NM_014687: exon 10:c.G1550T :p.C517F, ENST00000296343 (972 aa)

Mutation was predicted to be pathogenic by following software programs:

Sift score: DAMAGING: 0.05

(SIFT scores predicts the effect of the amino acid changes on protein)

PP2DIV: probably damaging: 0.958

PP2VAR: possibly damaging: 0.584

(Poly phe 2 (PP2) analysis predict the effects of the mutation on protein structure)

The presence of the mutation was confirmed in the index case (III 4) and the other affected member of the family (III 8) (Figure 3-6). It was also identified in two other family members (III 2, III 6) putting them at a risk of developing the disease later in their life. The mutation transmitted in an autosomal dominant pattern of inheritance. Overall, 4 out of 8 individuals screened for the mutation carried the mutation. As this mutation fulfilled the criteria of transmission with the disease, it was selected for further studies. Other mutations were also identified in this gene in five other FALS index cases from the FALS sequencing consortium.

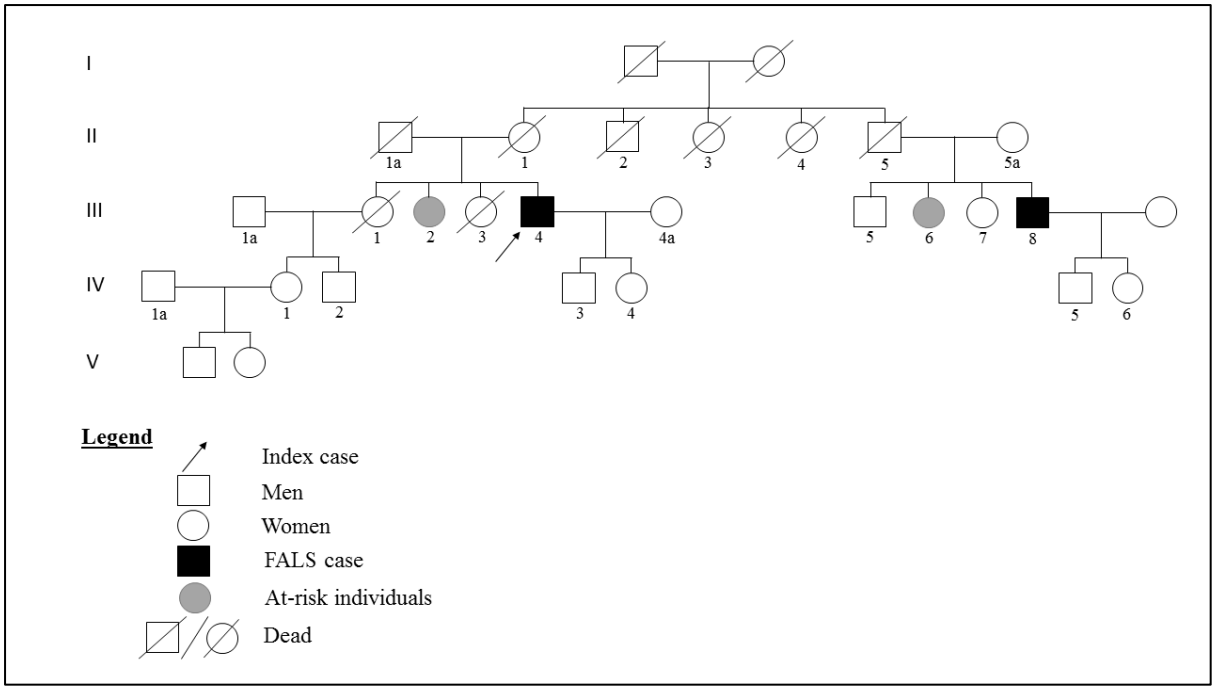

Figure 3-6 Pedigree SM331 with FALS cases and controls

Blood samples were available from 8 individuals of pedigree SM331 including the two affected FALS cases. The index case is indicated by an arrow. Out of 6 control cases, 2 individuals carried the mutation in *RUBCN* gene, as identified by DNA sequencing, in addition to 2 FALS cases putting them at risk of developing the disease at some stage of their life.

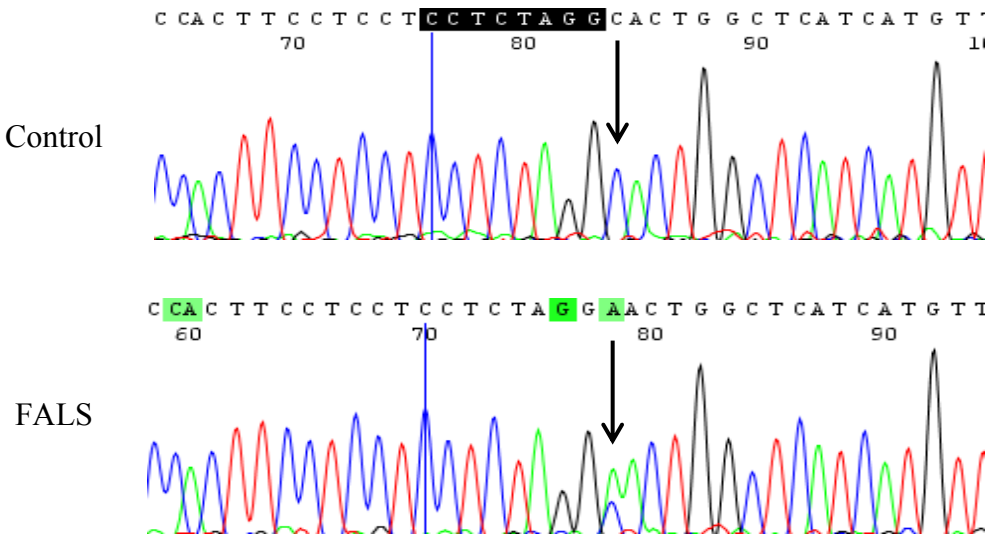

Figure 3-7 Chromatograms of *RUBCN* sequence indicating the nucleotide transversion in FALS case compared to a control

DNA was extracted from lymphocytes of two FALS cases, two at-risk individuals and four controls from pedigree SM331. A *RUBCN* gene segment containing the mutation was sequenced using primer set given in Table 3-1. The two chromatograms shown here indicate the difference between the DNA sequence of *RUBCN* in a control and a FALS case. The position of a heterozygous transversion, C to A, present in a FALS case compared to a control has been indicated by arrows.

3.3.3 Pedigree SM86

3.3.3.1 NCOR1

Whole-exome sequencing identified a mutation in *NCOR1* in the FALS index case of pedigree 68. *NCOR1* is on chromosome 17. The mutation converts cytosine residue to guanine in exonic region. The position of mutation in different transcripts is as follows:

NM_001190440: exon 31: c.C4684G : p.P1550A, ENST00000395851

NM_006311: exon 32: c.C4600G: p.P1534A, ENST00000268712

The presence of the mutation was not confirmed in the index case by Sanger sequencing (Figure 3-8) and therefore, no other family member was sequenced. Hence, the mutation was not selected for further studies.

FALS index case

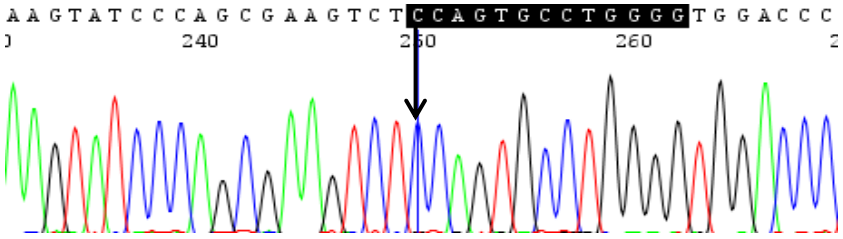

Figure 3-8 Chromatogram of *NCOR1* sequence indicating the wild-type nucleotide sequence of the gene in the index case of pedigree SM86.

DNA was extracted from lymphocytes of the index case of pedigree SM86. A *NCOR1* gene segment containing the mutation was sequenced using primer set given in Table 3-1. The chromatogram shown here indicates the DNA sequence of *NCOR1* in the FALS index case. Presence of mutation in *NCOR1* gene initially identified by exome sequencing by FALS sequencing consortium was not confirmed by Sanger sequencing.

3.4 Discussion

This thesis project was focused on the predicted pathogenic mutations obtained from the Imperial College FALS cohort, which fulfilled the initial short-listing criteria for further studies. The criteria included the following points: mutation would be rare in controls, is predicted to be pathogenic, is expressed in central nervous system and is functionally relevant to known ALS pathogenic pathways such as RNA processing and proteostasis.

We started this PhD project by confirming the presence of mutation in the respective genes in the index cases by Sanger Sequencing. This is important because the massive parallel sequencing and the different read depths in exome sequencing may result in errors. The occurrence of errors means that not all mutations identified by exome sequencing can be replicated by Sanger sequencing. The mutation in *NCOR1* could not be replicated by Sanger sequencing and was thus excluded from the study. Sanger sequencing was also performed on DNA from other family members from the pedigrees for establishing the transmission of mutation with the disease. This was another important short-listing criterion for selection of mutations whose effects could be further investigated at the functional level.

Finally, out of the total six genes sequenced by Sanger sequencing, the identified mutation was found transmitting with the disease in only two genes, *CLCN6* and *RUBCN*. We, therefore, selected these two genes based on satisfying all the criteria (Table 3-2) for functional studies to elucidate the effects of the mutation on viability, ER stress, autophagy, endosomal function and oxidative stress.

Table 3-2 Selection criteria for novel mutation in a gene

Selection Criteria	***SMAD6***	***HEATR6***	***PKD1L1***	***NCOR1***	***CLCN6***	***RUBCN***
Mutation would be rare in controls	●	●	●	●	●	●
Predicted to be pathogenic	●	●	●	●	●	●
Gene expressed in central nervous system	●	●	●	●	●	●
Mutation functionally relevant to known ALS pathways	●	●	●	●	●	●
Mutation presence confirmed by Sanger Sequencing in index case	●	●	●	○	●	●
Mutation transmitted with the disease	○	○	○	○	●	●

Selection of novel mutations in genes had to fulfil criteria listed in the table above to be selected for functional studies for investigating their putative association with FALS.

Chapter 4: Gene expression characterisation of putative genes (*RUBCN, CLCN6*) and the pathways that are involved in the action of these genes in spinal cord samples from SALS.

4.1 Introduction

We selected two genes based on satisfying the criteria described in table 4.2 for further studies, *RUBCN* and *CLCN6*.

4.1.1 *RUBCN*

The gene for Rubicon, *RUBCN*, is located on chromosome 3q29. The gene has several isoforms produced by alternative splicing but there is only one canonical sequence that is translated into a protein consisting of 972 amino acids with a molecular weight of 108.6 kDa (https://www.uniprot.org/uniprot/Q92622). Rubicon**,** RUN and cysteine rich domain containing Beclin 1-interacting protein, localises to the late endosome/lysosome compartments of the cell (Matsunaga et al., 2009). It is expressed ubiquitously in most tissues of the body and is very abundant in the cerebral cortex (Wong et al., 2017). The protein comprises of multiple domains including the RUN domain, a coiled-coiled domain (CCD) and FYVE-like domain (Sun et al., 2010b). These domains interact with different proteins e.g. the RUN domain interacts with Vps34, CCD interacts with UVRAG and Beclin 1 and the FYVE-like domain and C-terminal region interact with RAB7 to enable downstream processes (Figure 4-1) (Yang et al., 2012).

Rubicon is involved in many signalling pathways and cellular responses. It associates with the UVRAG-Beclin-Vps34 complex to negatively regulate the maturation step of autophagy and the endocytic pathway (Zhong et al., 2009, Matsunaga et al., 2009, Sun et al., 2010b). It is

involved in LC3-associated phagocytosis where it is an essential positive regulator of the NADPH oxidase complex that induces potent antimicrobial responses (Martinez et al., 2015). Rubicon is also involved in the feedback inhibition of CARD9-mediated PRR-signal transduction by targeting CARD9 to disrupt the CBM complex to prevent excessive pro-inflammatory responses (Yang et al., 2012). Defects in the protein have been reported to cause recessive ataxia (Assoum et al., 2013), LPS-induced stroke (Zi et al., 2015) and non-alcoholic fatty liver disease (Tanaka et al., 2016).

4.1.2 *CLCN6*

The gene *CLCN6* is located on chromosome 1p36 and encodes for Chloride transport protein 6. It consists of 869 amino acid residues and has a molecular weight of 97.3 kDa. The protein is localised on endoplasmic reticulum (Buyse et al., 1998) and late endosome membranes (Ignoul et al., 2007) and functions as a Cl^-/H^+ antiporter (Neagoe et al., 2010). The protein is widely expressed in many different tissues (Brandt S et al., 1995) but predominantly in the nervous system (Poet M et al, 2006). ClC family members, ClC-3 to ClC-7, that are localised on the membrane of the endosomal-lysosomal system are thought to facilitate the acidification of the endosomal-lysosomal compartments by providing an electric shunt for the efficient pumping of the H^+-ATPase (Jentsch et al., 2002). Single nucleotide variants in *CLCN6* have been linked to benign partial epilepsies in infancy (Yamamoto et al., 2015). In addition, disruption of the ClC-6 protein has been linked to mild forms of neuronal ceroid lipofuscinosis (NCL), a lysosomal storage disease (Poet et al., 2006).

In this chapter, we have focused on the expressional profiling of proteins involved in ER stress-activated UPR, autophagy and endosomal pathways as these are the main pathways involved in the action of our candidate genes. In addition, defects in these pathways have been linked to

many neurological disorders specifically ALS (Hetz and Mollereau, 2014, Schreij et al., 2016, Menzies et al., 2017).

4.1.3 Objectives

To perform gene expression profiling of putative ALS genes and the pathways involved in the action of these proteins in order to characterise the function of these pathways in spinal cord post-mortem samples from sporadic ALS cases compared to healthy individuals.

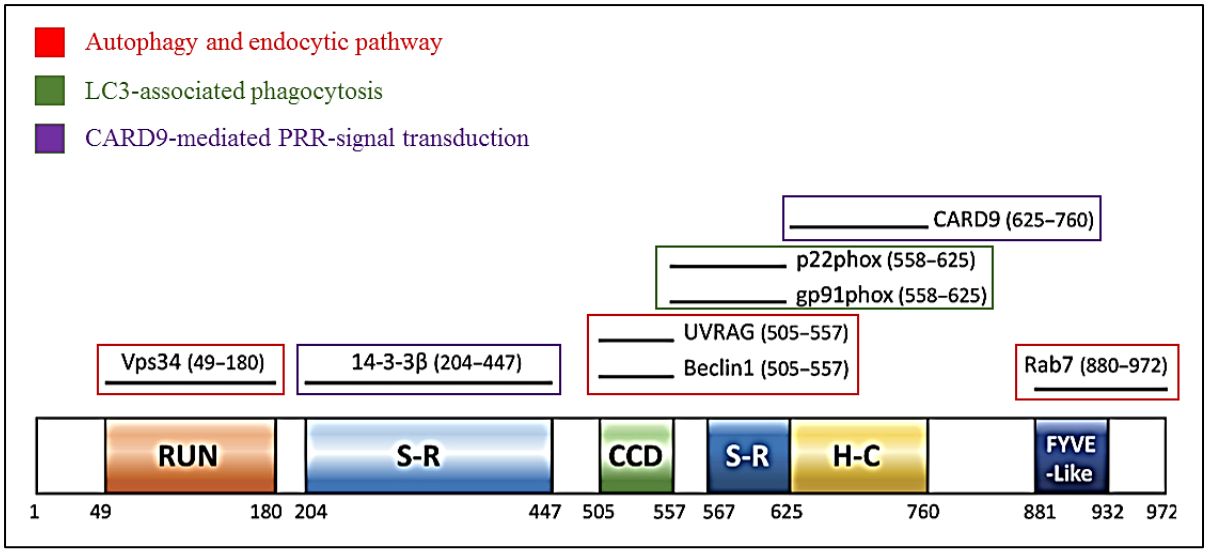

Figure 4-1 Structure of Rubicon protein.

The schematic structure of human Rubicon protein and the sites of interaction of its binding proteins from various pathways (Wong et al., 2017).

4.2 Materials and Methods

4.2.1 Samples

We used spinal cord tissue samples from controls and SALS cases (Table 4-1).

Table 4-1 Spinal cord tissues from controls and SALS cases

Group	n	Age at death (years) Median (range)	Post-mortem delay (hours) Median range
Controls	17 (12 males, 5 females)	66 (20-91)	11 (3-19)
SALS	32 (21 males, 11 females)	68 (24-85)	14 (5-25)

The number of controls and SALS cases used in this study with the age at death of patients diagnosed with SALS and of healthy individuals (controls) and the post-mortem delay between the time of death and collection of spinal cord tissue.

4.2.2 RNA extraction and cDNA synthesis

RNA was extracted from frozen spinal cord tissue samples using a Direct-zolTM RNA miniprep kit (Zymo Research, USA) according to the manufacturer's protocol. Extracted RNA was eluted with 40 µl of DNase/RNase-free water and stored at -80^{o}C. RNA was quantified using a NanoDrop spectrophotometer ND-1000 to check the purity/quality of total RNA samples. The measurement of 260/280 absorbance ratio in all mRNA extractions was in the range of 1.83 to 1.94 (mean = 1.89).

For performing qPCR, cDNA was synthesised from extracted RNA using AMV reverse transcriptase (New England Biolabs), 10X RT buffer (New England Biolabs), random

hexamers (Invitrogen) and dNTP mix according to the protocol explained in section. cDNA was stored at -20^{o}C for further use.

4.2.3 Quantitative real-time PCR (qPCR) and gel electrophoresis

We analysed the expression of target genes in spinal cord tissue at the mRNA level by qPCR. We used the Power Up™ SYBr™ Green Master Mix with 6 µM of primers for preparing qPCR reactions. The Stratagene® MX3000p qPCR system was used for qPCR. The primers used to amplify required gene products are given in tables (Table 4-2 and Table 4-3). The amplification of the required single gene product was confirmed by analysis of thermal dissociation profiles generated from the qPCR reaction and by separating the PCR products on 2% agarose gels (Figure 4-2 and Figure 4-3).

4.2.4 Protein extraction and western blotting

Sections from frozen spinal cord tissue blocks were homogenised and lysed with RIPA buffer. Protein extracts were kept at -80^{o}C. A Bradford assay was performed to determine the concentration of proteins in each sample and samples were equalised to a concentration of 50 µg/40 µl with the addition of 1X Laemmli SDS sample buffer (Alfa Aesar). Proteins were separated using 8% SDS-PAGE and blotting was carried out using conditions optimised for each antibody.

The following primary and secondary antibodies were used:

Primary antibodies: rabbit polyclonal anti-CLCN6 antibody (1:250, Abcam), rabbit polyclonal anti-rubicon antibody (1:2000, Abcam), rabbit polyclonal anti-LAMP2 antibody (1:50, Abcam), mouse monoclonal anti-GAPDH antibody (1:2000, Santa Cruz).

Secondary antibodies: peroxidase labelled anti-mouse IgG (H+L) (Vector laboratories), peroxidase labelled anti-rabbit IgG (H+L) (Vector laboratories)

4.2.5 Statistical analysis

Statistical analysis of gene expression in SALS compared to control spinal cord samples was performed using the Student's t-test (GraphPad Prism 5 software). The normality of the data distribution was tested by the D'Agostino-Pearson test. Results are represented as means ± standard error of mean (SEM). The changes in gene expression are given as fold change (FC) values. For both mRNA and protein expression analysis, values were normalised against a house-keeping gene in order to compensate for the differences in the quantity of starting material loaded in different samples. Non-normally distributed data was analysed using the Mann-Whitney U test. The Grubbs outlier test was performed to remove outliers from the data. When the qPCR analysis was carried out in two batches for the expression of a single gene on different samples, a normalisation factor was applied after comparing the means of the two groups.

Table 4-2 Primer sequences used for the cDNA amplification by qPCR

Gene	Primers	Product size (bp)
Autophagy genes		
RAB7A	Forward: CACTCATGAACCAGTATGTG Reverse: CATATCTGCATTGTGACTAGC	118
LAMP2	Forward: CGTTCTGGTCTGCCTAGTCC Reverse: CAGTGCCATGGTCTGAAATG	173
SQSTM1	Forward: CAGTCCCTACAGATGCCAGA Reverse: TCTGGGAGAGGGACTCAATC	142
CLCN6	Forward: GAGTCTTAGAGAGCCTCCTTGTGTC Reverse: ACACAGCAGAGAAGGCACAA	365
BECN1	Forward: TGTCACCATCCAGGAACTCA Reverse: CTGTTGGCACTTTCTGTGGA	180
ATG14L	Forward: ATGAGCGTCTGGCAAATCTT Reverse: CCCATCGTCCTGAGAGGTAA	192
ER stress genes		
XBP1 total	Forward: GCTCAGACTGCCAGAGATCG Reverse: TCTTCAGCAACCAGGGCATC	188
XBP1 spliced	Forward: AGAGTCTGATATCCTGTTGG Reverse: AGTTCATTAATGGCTTCCAG	189
HSPA5	Forward: TCAAGTTCTTGCCGTTCAAGG Reverse: AAATAAGCCTCAGCGGTTTCTT	148
DNAJB9	Forward: TTTCCAGACACGCCAGGATG Reverse: GTCCTGCAGTGCTTGCTAGA	195
House-keeping gene		
ACTB	Forward: GACAACGGCTCCGGCATGTG Reverse: CCTTCTGACCCATGCCCAC	121
GAPDH	Ready-made primer pair ordered from Primer design	118

Table 4-3. Primer sequences used for the cDNA amplification by qPCR of *RUBCN* transcripts

Transcripts	Primers	Product size (bp)
Both 972aa and 927aa	Forward: GAGAATGCCCACTTCAGCAT Reverse: CAGGTTCTTGGTGCGGATTT	180
972aa	Forward: GAATGGAGCTCGGAGGCGGCGA Reverse: CGGATAAGCCCGTGATAGAG	193
927aa	Forward: GCCCCAGGAATATCACCATT Reverse: AGAGCTGGGTGTGCTGACTT	122

Different primer pairs used to amplify different *RUBCN* transcripts. The positions of the primer pairs are indicated in Figure 4-7.

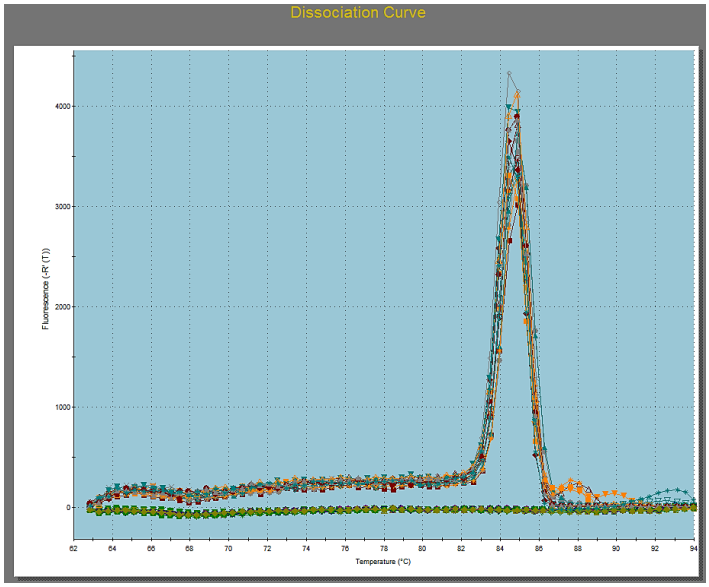

Figure 4-2 Dissociation curve from a qPCR reaction

A representative qPCR dissociation curve profile of *RUBCN* cDNA amplification from a qPCR reaction performed on post-mortem spinal cord samples from SALS cases and healthy individuals. Dissociation curve analysis helps in determining the specificity of the PCR reaction and shows the melting temperature at which double-stranded DNA is denatured.

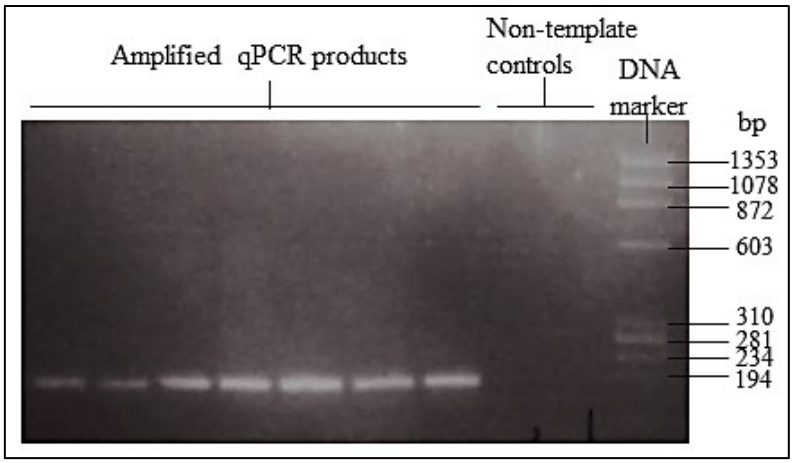

Figure 4-3 Rubicon amplified qPCR products

The amplified qPCR products of *RUBCN* and the non-template controls from the same qPCR plate. The gel picture confirms the specificity of the primer pair used to for the amplification of the gene segment.

4.3 Results

As the first step of our functional studies, we wanted to explore the changes in gene expression in the pathways involved in the actions of our candidate genes in ALS cases. In order to do this, we performed studies on the expression of genes involved in the autophagy pathway, ER stress-activated UPR pathway and endosomal pathway on the spinal cord post-mortem samples derived from cases of sporadic amyotrophic lateral sclerosis (SALS) and healthy individuals. In addition to our putative ALS genes, *RUBCN* and *CLCN6*, we selected autophagy pathway proteins Atg14L and Beclin 1; ER stress marker proteins spliced form of XBP1, DNAJB9, and HSPA5; the endosomal pathway marker Rab7; lysosomal pathway markers LAMP1 and LAMP2.

4.3.1 Gene expression of components of autophagy/endosomal pathways with relevance to *RUBCN*

mRNA expression levels of *BECN1, ATG14L, RAB7, LAMP1* and LAMP2 were similar in both SALS cases and healthy individuals (Figure 4-4). A small change in the expression of LAMP2 protein was observed but it was non-significant (p=0.0506) (Figure 4-5).

We found a substantial upregulation in the mRNA expression of *RUBCN* in SALS cases compared to healthy controls using a primer pair that amplifies both 972 amino acid and 927 amino acid transcripts in addition to other isoforms of *RUBCN* (FC=2.85). A significant upregulation in SALS was also observed using the primer pair specific for the 972-amino-acid transcripts (FC=1.52). The expression of *RUBCN* found using the primer pair specific for the 927-amino-acid isoform however, was similar in both SALS cases and healthy controls (Figure 4-6). At the protein level, we observed a significant downregulation in Rubicon protein expression level in SALS cases (FC=1.84) (Figure 4-8).

A significant negative correlation was found between *RUBCN* and *LAMP2* mRNA levels in SALS cases (p=0.045, r=-0.52) (Figure 4-11). This could be an indication of the activation of the autophagy/ endosomal pathways resulting in an increased lysosomal activity due to a decrease in *RUBCN* expression, the negative regulator of autophagy/endocytosis pathways.

4.3.2 Gene expression of components of the ER stress-activated UPR pathway

We investigated the activation of ER stress-activated UPR pathways in spinal cord post-mortem samples derived from SALS cases and healthy controls. We found a significant upregulation in the expression of the transcription factor spliced *XBP1* (*XBP1s*) and its target genes *HSPA5* and *DNAJB9* (Figure 4-9). This indicated the activation of ER stress in SALS.

4.3.2.1 Gene expression of endosomal-lysosomal pathway genes with relevance to *CLCN6*

mRNA expression levels of endosomal pathway marker *RAB7A* and lysosomal markers *LAMP1,* and *LAMP2* were similar in both SALS cases and healthy individuals (Figure 4-4 and Figure 4-5). We also observed no difference in the mRNA expression of *CLCN6* between SALS cases and controls, however, we observed a significant downregulation in the expression level of CLCN6 protein (FC=0.41) (Figure 4-10).

Since *RUBCN* and *CLCN6* are both localised in the late endosome, we wanted to determine whether there was a correlation between mRNA levels of these two genes. We were encouraged to find a significant positive correlation between the mRNA expression levels of *CLCN6* and *RUBCN* in SALS cases (p=0.002, r=0.813) (Figure 4-11), which indicates a similar change in gene expression of both the genes in SALS cases.

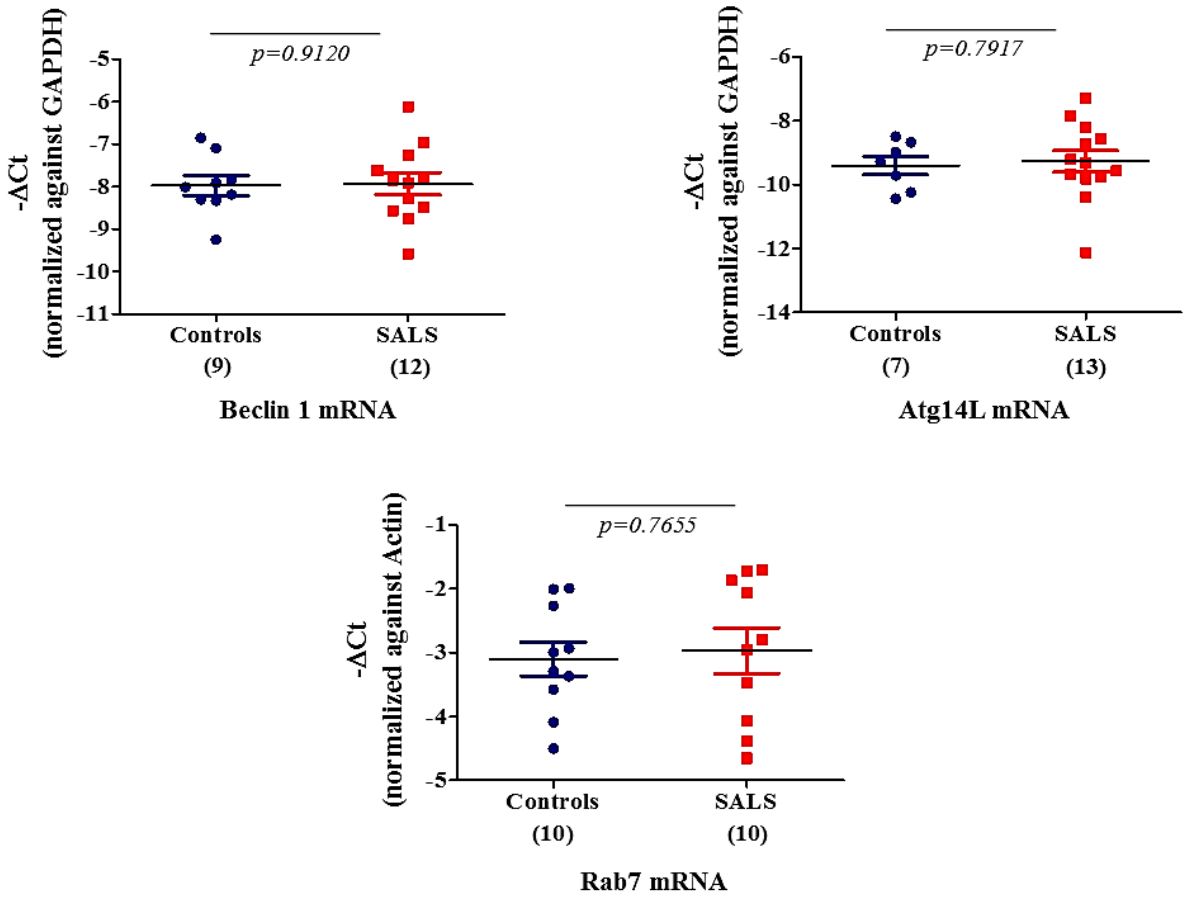

Figure 4-4 mRNA expression of autophagy/endosomal pathway genes in spinal cord samples.

mRNA expression level of autophagy pathway genes (*BECN1*, *ATG14L*) and the endosomal pathway gene (*RAB7A*) in spinal cord post-mortem samples derived from healthy individuals (controls, blue) and cases of sporadic amyotrophic lateral sclerosis (SALS, red). The number of samples analysed is indicated in brackets along the X-axis. The values of gene expression normalised to the house-keeping gene, β-actin (-delta Ct) are represented by means and SEMs. Circles and squares represent individual samples. All data is normally distributed according to the D'Agostino and Pearson normality test. The unpaired Student's t-test was used for analysing the data; *$p<0.05$.

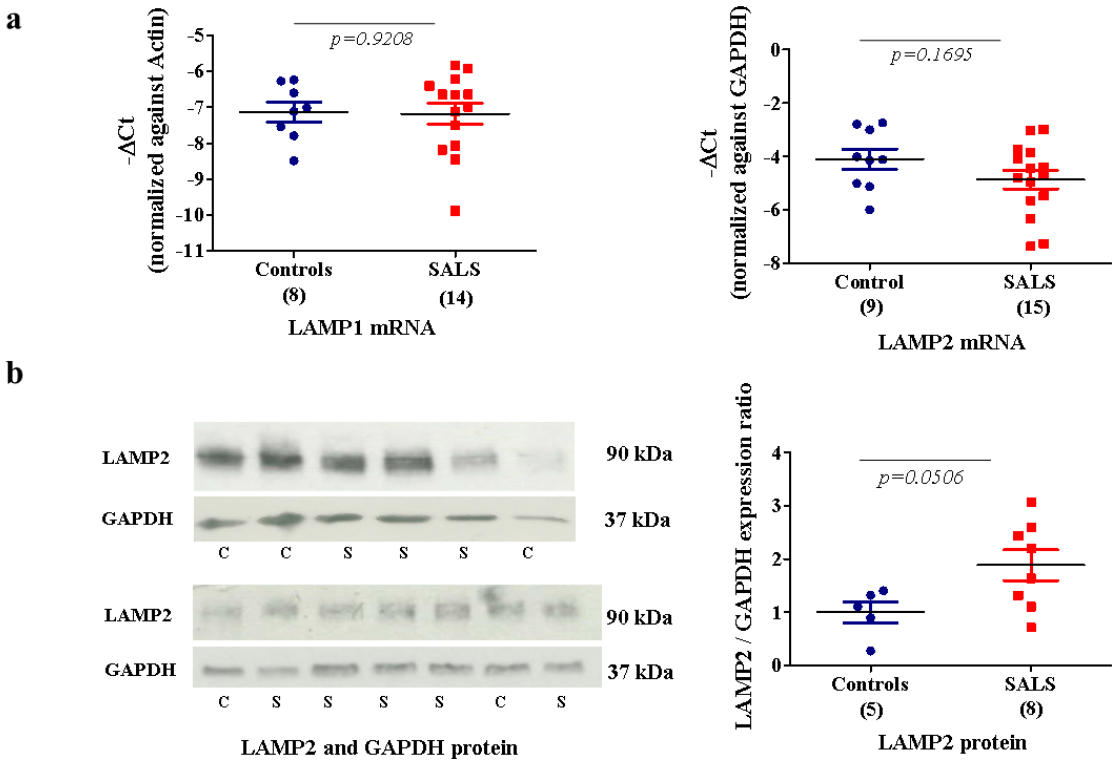

Figure 4-5 mRNA and protein expression levels of lysosomal pathway genes in spinal cord samples.

a) mRNA expression level of lysosomal pathway genes (*LAMP1* and *LAMP2*) in spinal cord post-mortem samples derived from healthy individuals (controls, blue) and cases of sporadic amyotrophic lateral sclerosis (SALS, red). The number of samples analysed is indicated in brackets along the X-axis. The values of gene expression normalised to the house-keeping gene β-actin (-delta Ct) are represented by means and SEMs. b) Western blots for LAMP2 protein and GAPDH in spinal cord post-mortem samples derived from healthy individuals, C, and cases of sporadic amyotrophic lateral sclerosis, S. The graph shows the number of samples analysed in brackets along X-axis. The values of protein expression normalised to the house-keeping gene, GAPDH, are represented by means and SEMs. Circles and squares represent individual samples; controls, blue; SALS, red. All data is normally distributed according to D'Agostino and Pearson normality test. The unpaired Student's t-test was used for analysing the data; *$p<0.05$.

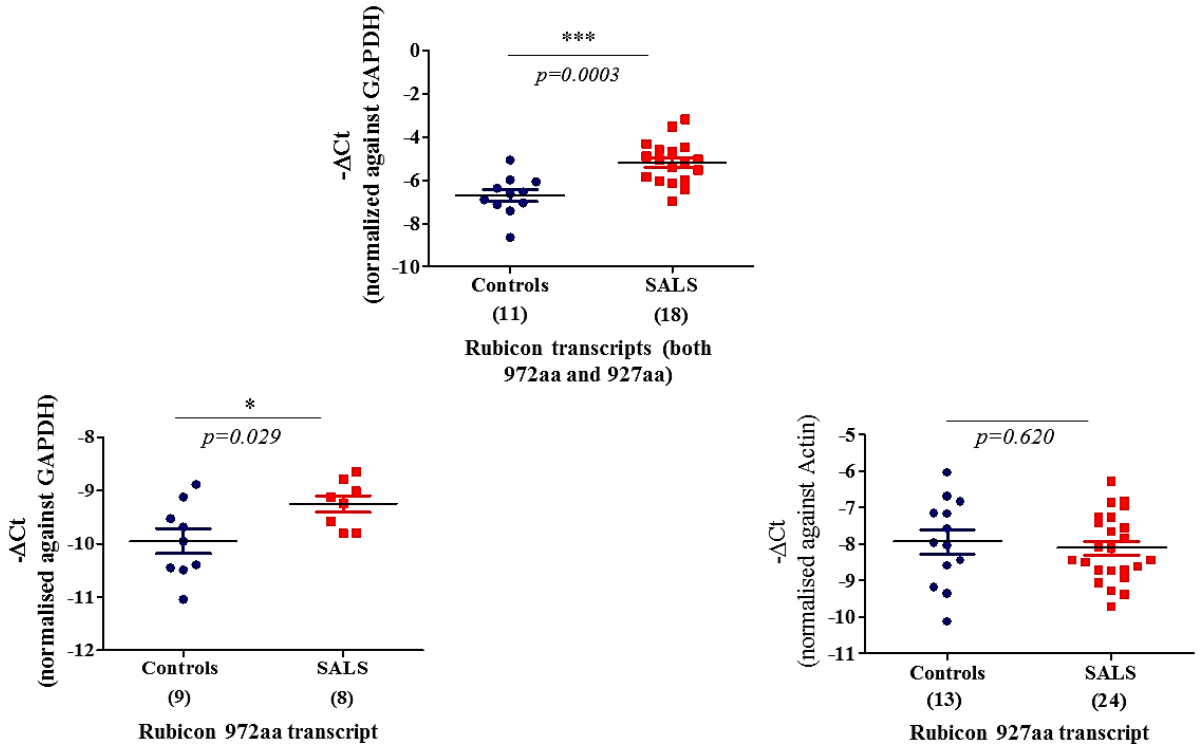

Figure 4-6 mRNA expression levels of *RUBCN* in spinal cord samples.

mRNA expression levels of different *RUBCN* transcripts produced by alternative splicing in spinal cord post-mortem samples derived from healthy individuals (controls, blue) and cases of sporadic amyotrophic lateral sclerosis (SALS, red). The position of the primer pairs used for the amplification of these transcripts are indicated in Figure 4-7. The number of samples analysed is indicated in brackets along the X-axis. The values of gene expression normalised to the house-keeping gene *GAPDH* (-delta Ct) are represented by means and SEMs. Circles and squares represent individual samples; controls, blue; SALS, red. All data is normally distributed according to the D'Agostino and Pearson normality test. The unpaired Student's t-test was used for analysing the data; *p<0.05; ***p<0.0005

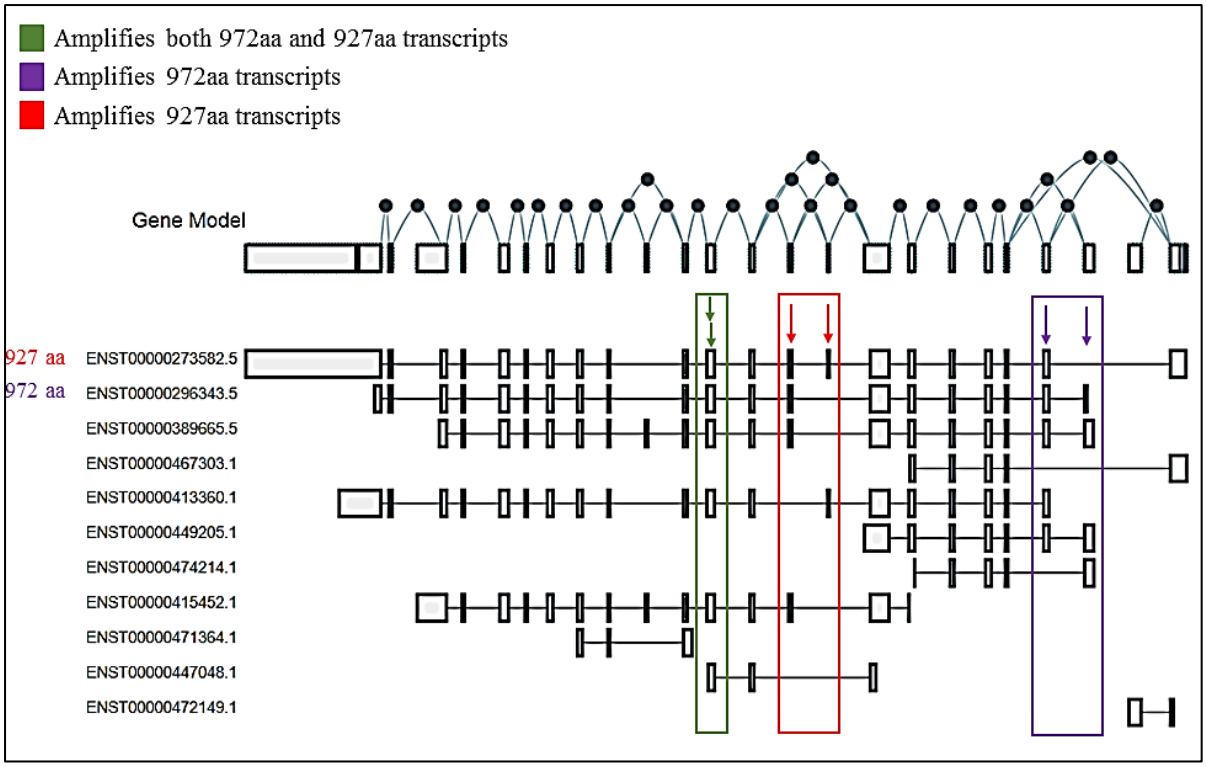

Figure 4-7 *RUBCN* isoforms and position of primer pairs used for amplification

There are different isoforms produced by alternative splicing of *RUBCN*. The two main isoforms that have been characterised are the 972-amino-acid (972aa) transcript and the 927-amino-acid (927aa) transcript. Three sets of primer pairs were designed for the amplification of these two isoforms. The pair indicated by green arrows could amplify both of these isoforms. The pair indicated by red arrows could only amplify 927aa transcript. The pair indicated by purple arrows could amplify only the 972aa transcript. The primer pairs for the amplification of both transcripts together and the one for 972aa transcript could also amplify some other isoforms but they are not known to be expressed in spinal cord. Adapted from GTEx portal.

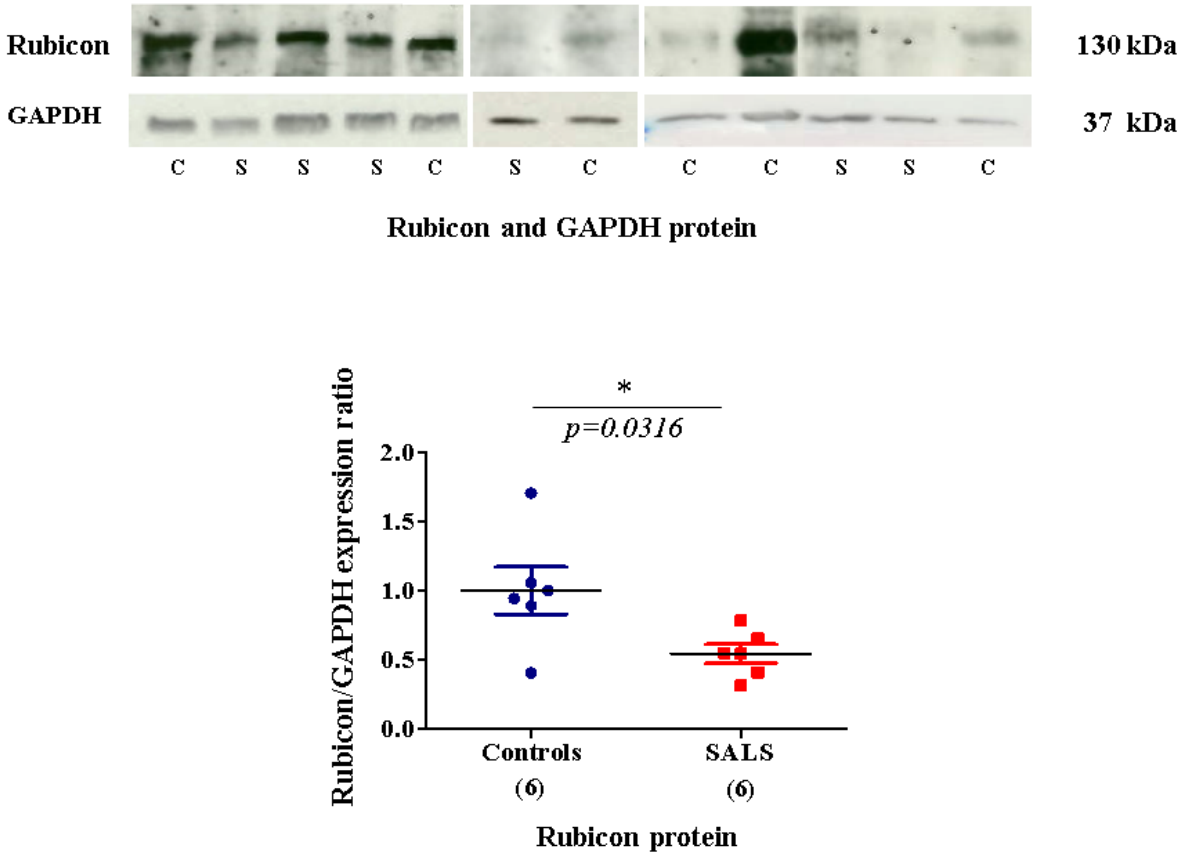

Figure 4-8 Protein expression levels of Rubicon in spinal cord samples.

Western blots for Rubicon protein and GAPDH in spinal cord post-mortem samples derived from healthy individuals, C, and cases of sporadic amyotrophic lateral sclerosis, S. The graph shows the number of samples analysed in brackets along the x-axis. The values of protein expression normalised to the house-keeping gene, GAPDH, are represented by means and SEMs. Circles and squares represent individual samples; controls, blue; SALS, red. All data is normally distributed according to the D'Agostino and Pearson normality test. The unpaired Student's t-test was used for analysing the data; *$p<0.05$.

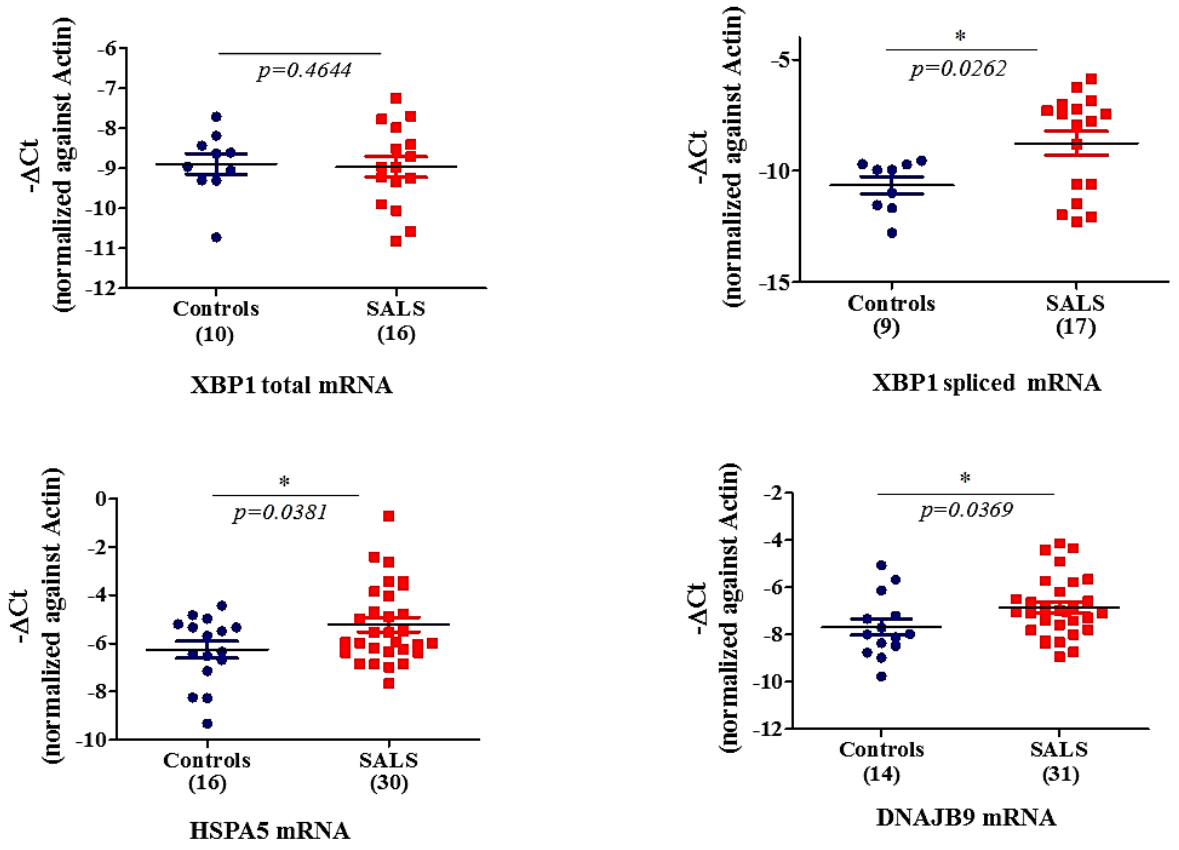

Figure 4-9 mRNA expression level of ER stress-activated genes in spinal cord samples.

mRNA expression levels of ER stress-activated genes (*XBP1* and its spliced form, *HSPA5*, and *DNAJB9*) in spinal cord post-mortem samples derived from healthy individuals (controls, blue) and cases of sporadic amyotrophic lateral sclerosis (SALS, red). The number of samples analysed is indicated in brackets along the x-axis. The values of gene expression normalised to the house-keeping gene β-actin (-delta Ct) are represented by means and SEMs. Circles and squares represent individual samples. All data is normally distributed according to D'Agostino and Pearson normality test. The unpaired Student's t-test was used for analysing the data; *$p<0.05$.

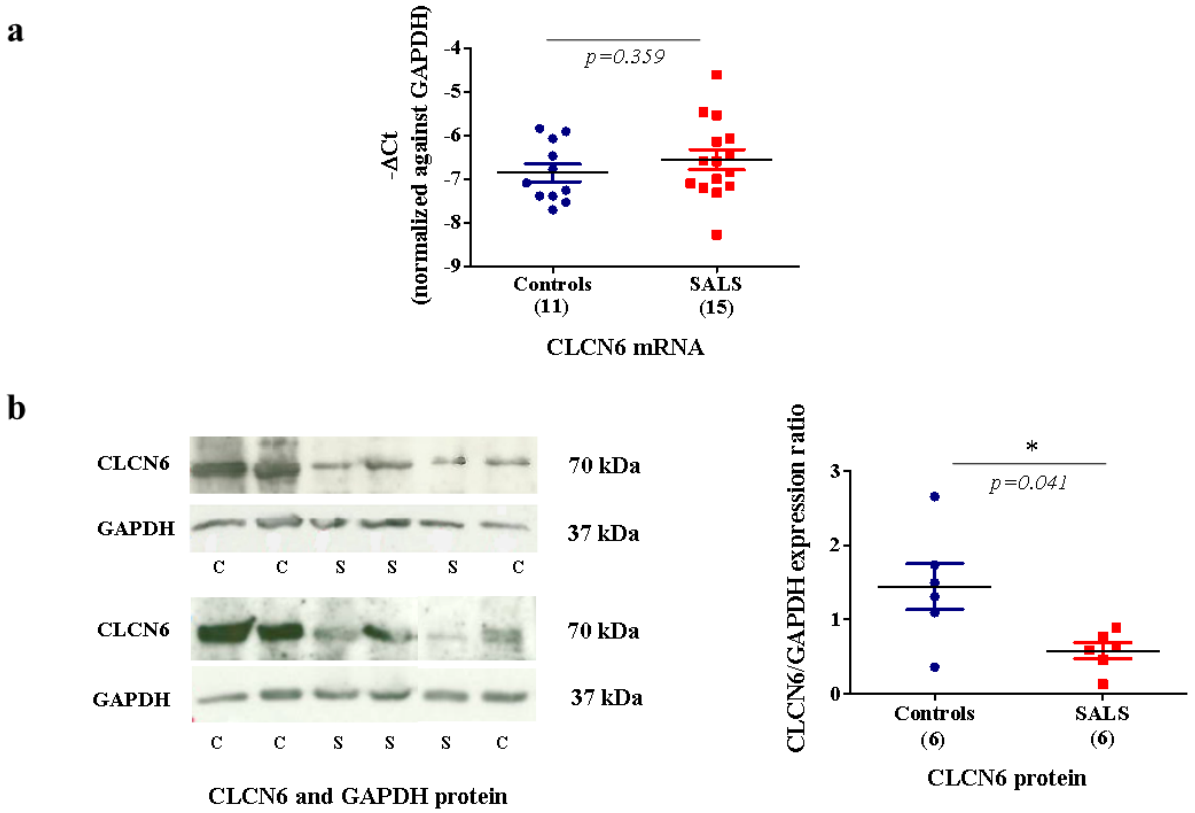

Figure 4-10 mRNA and protein expression levels of *CLCN6* in spinal cord samples.

a) mRNA expression level of *CLCN6* in spinal cord post-mortem samples derived from healthy individuals (controls, blue) and cases of sporadic amyotrophic lateral sclerosis (SALS, red). The number of samples analysed is indicated in brackets along the X-axis. The values of gene expression normalised to the house-keeping gene *GAPDH* (-delta Ct) are represented by means and SEMs. b) Western blots for CLCN6 protein and GAPDH in spinal cord post-mortem samples derived from healthy individuals, C, and cases of sporadic amyotrophic lateral sclerosis, S. The graph shows the number of samples analysed in brackets along X-axis. The values of protein expression normalised to the house-keeping gene, GAPDH, are represented by means and SEMs. Circles and squares represent individual samples; controls, blue; SALS, red. All data is normally distributed according to the D'Agostino and Pearson normality test. The unpaired Student's t-test was used for analysing the data; *$p<0.05$.

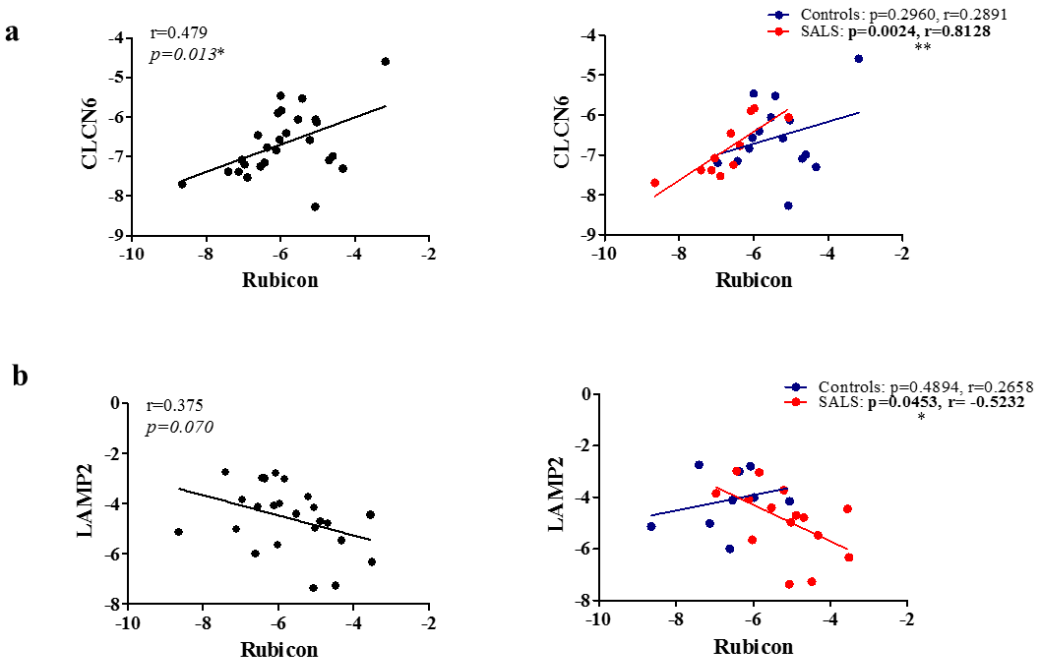

Figure 4-11 Correlation of the mRNA expression level of shortlisted candidate genes, autophagy genes and lysosomal marker in spinal cord samples.

Correlation between the mRNA expression levels of different genes in spinal cord post-mortem samples derived from healthy individuals (controls, blue) and cases of sporadic amyotrophic lateral sclerosis (SALS, red). a) Correlation between the mRNA expression of two candidate genes shortlisted for further investigation, *RUBCN*, and *CLCN6*. The first graph includes SALS cases and control individuals together shown in black circles (n=26) while the second graph shows SALS cases (red circles, n=11) and controls (blue circles, n=15). b) Correlation between the mRNA expression of the lysosomal marker, *LAMP2*, and *RUBCN*. The first graph includes SALS cases and control individuals together shown in black circles (n=24) while the second graph shows SALS cases (red circles, n=15) and controls (blue circles, n=9). The values used were of gene expression normalised to the house-keeping gene β-actin (-delta Ct). Each circle represents an individual sample. All data is normally distributed according to the D'Agostino and Pearson normality test. Pearson's correlation (r) values are indicated with each graph; *p<0.05, **p<0.005.

4.4 Discussion

4.4.1 *RUBCN*

Rubicon is a negative regulator of autophagy and endosomal pathways and is found in a complex with PI3KC3 in both endosomes and autophagosomes (Matsunaga et al., 2009, Sun et al., 2010b). Because of the crucial role autophagy and endosomal trafficking play in cell survival, disruption in both pathways has been linked to neurodegenerative diseases. We, therefore, performed expression profiling of genes involved in autophagy and endosomal pathways specifically the ones involved in the complex with which Rubicon interacts. We studied the expression of *ATG14L*, *BECN1*, *RAB7A*, *LAMP1* and *LAMP2* alongside the expression levels of Rubicon. Beclin 1 was selected being a core component of the PI3KC3 complex and Atg14L as a known positive regulator of autophagosome formation. Rab7 is a marker for endocytosis and interacts with Rubicon. LAMP1and LAMP2 are marker proteins for lysosomal activity.

There are three distinct Class III PI3K (PI3KC3) complexes that are involved in autophagy (Figure 4-12). The main components of PI3KC3 complex consist of VPS34, Beclin 1 and VPS15 and the specificity of the complex is determined by the different components that bind to this complex via Beclin 1 (Sun et al., 2011a). The first complex consists of Atg14L. The binding of Atg14L to the complex is required for the starvation-induced autophagy and leads to autophagosome formation (Matsunaga et al., 2009). The second complex consists of UVRAG instead of Atg14L. This complex is involved in autophagosome formation and/or autophagosome maturation (Liang et al., 2008, Itakura et al., 2008). This complex is also involved in endosome maturation. The third complex contains Rubicon in addition to UVRAG. Under nutrients rich condition, Rubicon negatively regulates autophagy by binding to UVRAG

containing PI3KC3 complex subsequently inhibiting autophagy (Kim et al., 2015b). The third complex also negatively regulates endosomal pathway by inhibiting endosome maturation.

UVRAG in the UVRAG containing PI3KC3 complex positively regulates the class C-VPS/HOPS complex (Liang et al., 2008). The Class C-VPS/HOPS complex contains the guanine nucleotide exchange factor (GEF) for Rab7 and leads to Rab 7 activation by promoting the transition of Rab7 GDP to GTP (Markgraf et al., 2007). For early endosomes to mature to late endosomes, Rab7 has to be activated and recruited to displace Rab5 on early endosomes (Rink et al., 2005). Rubicon is highly enriched on Rab5-positive early endosomes and leads to inhibition of endosome maturation by sequestering UVRAG and subsequently preventing UVRAG interaction with C-VPS/HOPS complex localised at late endosome. Active Rab7 competes for Rubicon binding releasing UVRAG and promoting UVRAG interaction with C-VPS/HOPS to further activate Rab7. This results in amplification of Rab7 activity leading to autophagosome and late endosome maturation (Sun et al., 2010a).

Autophagy and endosomal pathways are interlinked and dependent on each other. Autophagosomes may also first fuse with endosomes to form amphisomes before fusing with lysosomes instead of directly fusing with lysosomes as has been observed in a study in rat hepatocytes where five times as many amphisomes as autolysosomes were found (Stromhaug et al., 1998). Overall, during autophagosome and endosome maturation, UVRAG is required for activating both PI3KC3 and HOPS complexes but the interaction of Rubicon with the UVRAG containing PI3KC3 complex inhibits its activity. Active Rab7 can release UVRAG from Rubicon sequestration and thereby, promotes lysosomal degradation (Lin and Zhong, 2011).

In our studies on spinal cord post-mortem samples from SALS cases and healthy individuals (controls), we found similar mRNA expression levels of *BECN1, ATG4L, RAB7*, *LAMP1* and

LAMP2 between SALS cases and controls, which indicates that the activity of these proteins most probably remains undisturbed in SALS cases.

In the case of *RUBCN*, we were highly encouraged to find a substantial upregulation in the mRNA expression of *RUBCN* in SALS cases compared to healthy controls that was equivalent to a fold change of 2.85. There are only two well-characterised transcripts for *RUBCN* (https://www.ensembl.org/Homo_sapiens/Gene/Summary?db=core;g=ENSG00000145016;r=3:197671393-1977497270). The primer pair that showed a highly significant upregulation in SALS (p=0.0003, FC=1.52) amplifies both 927-amino-acid and 972-amino-acid transcripts in addition to four other transcripts (Figure 4-7). The other four transcripts have very low abundance in brain and are probably degraded. The primer pair used for 972-amino-acid transcript amplifies two other transcripts in addition to 972, which have very low expression in brain. The expression of 972-amino-acid transcript has not been detected in any of the tissues whose data is available on GTEx portal. The primer pair used for the amplification of 927-amino-acid transcript only amplifies this specific transcript (Figure 4-7) (https://www.gtexportal.org/home/gene/KIAA0226#spliceVizBlock).

A significant negative correlation between the mRNA expression of *LAMP2* and *RUBCN* was observed which may be suggestive of an increased autophagy/endosomal pathway activity where a decrease in negative regulator results in the increased activity of the pathway as has been illustrated by the upregulation of LC3II expression in SALS cases in a previous study (Hetz et al., 2009). Compared to mRNA, at the protein level the expression of Rubicon was significantly lower in SALS cases compared to controls. The difference in the expression levels of mRNA and protein could be due to the post-transcriptional modifications of mRNA before it is translated to protein. The increased *RUBCN* expression in the case of mRNA levels and a decreased protein expression may actually be due to the fact that only the 972-amino-acid transcript is translated into protein since this is the only transcript that contains the exon 2 that

contains the first part of protein sequence and is absent in the other major transcript detected by qPCR. The 972 protein is the canonical protein which has been reported in the literature and no shorter form of protein has been described to our knowledge. In GTEx portal several transcripts are abundant in brain and lymphocytes. The most abundant 927-amino-acid transcript, reported by GTEx portal, has not been detected at mRNA level in our experiment. The fact that it is has not been detected at mRNA level may reflect the different methodology used for the data available on GTEx portal compared to ours.

4.4.2 *CLCN6*

ClC-6 protein is localised on membranes of the endoplasmic reticulum and late endosomes. Previous studies have indicated the presence of ER stress in spinal cord post-mortem samples from SALS cases (Hetz et al., 2009, Atkin et al., 2008, Ilieva et al., 2007). We, therefore, determined if the same was true for our spinal cord post-mortem samples from SALS. To determine the presence of ER stress and the activation of ER stress-activated UPR pathways, we analysed the mRNA expression levels of different UPR markers that included *XBP1* (a key UPR transcription factor), *HSPA5* (XBP1 activated chaperone) and *DNAJB9* (a co-chaperone of HSPA5). We found a substantial increase in the expression levels of all the three UPR markers (Montibeller and de Belleroche, 2018).

Although the mRNA expression level of our candidate gene, *CLCN6*, was similar in SALS cases and controls, the protein expression level of *CLCN6* was significantly downregulated in SALS cases compared to the healthy controls equivalent to a fold change of 0.41. Since ClC-6 is a Cl^-/H^+ antiporter, low expression of CLCN6 in SALS may be an indication of the disturbance in ER leading to ER stress and disrupted endosomal pathway in SALS cases. The presence of unresolved ER stress and abnormalities of the endosomal-lysosomal system have

been established to be involved in causing neurodegenerative diseases in many previous studies (Montibeller and de Belleroche, 2018, Cabral-Miranda and Hetz, 2018, Schreij et al., 2016).

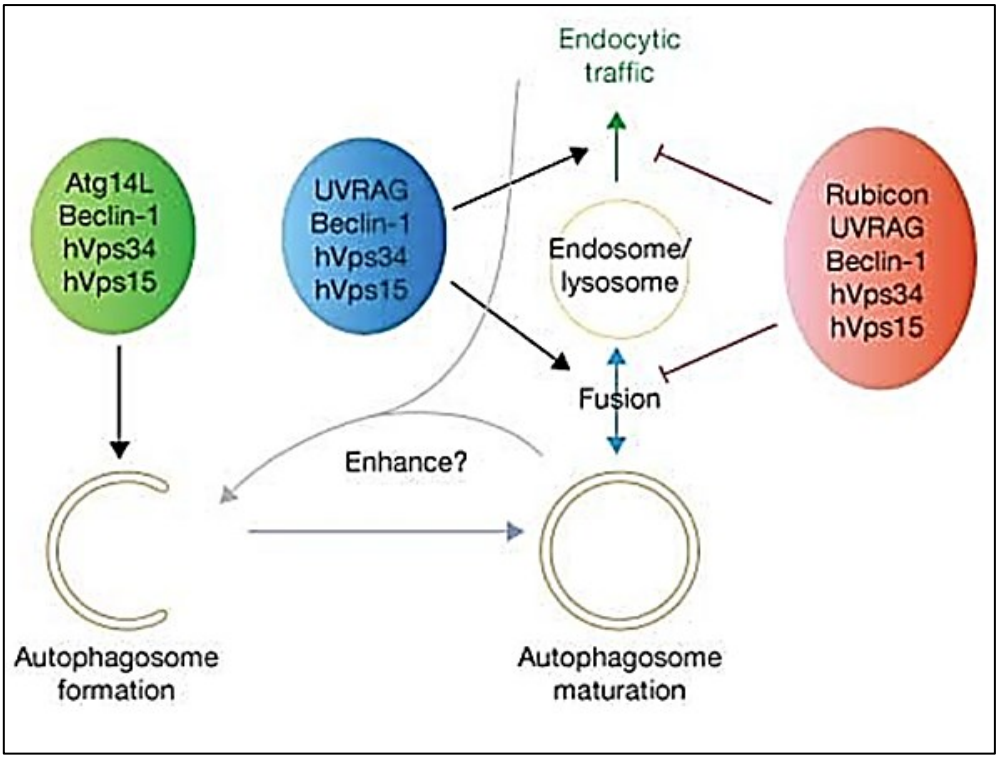

Figure 4-12 The role of Rubicon in autophagosome and endosome maturation

The three distinct Class III PI3K (PI3KC3) complexes. The PI3KC3 complex with Atg14L is involved in autophagosome formation. The complex with UVRAG is involved in autophagosome and endosome maturation. The complex contacting Rubicon in addition to UVRAG is involved in suppressing autophagosome and endosome maturation step (Matsunaga et al., 2009).

Chapter 5: Functional characterisation of *RUBCN* in FALS lymphoblastoid cell lines (LCLs): effect of ER stress

5.1 Introduction

Rubicon is a negative regulator of autophagy/endosomal pathways activated by the UPR in ER stress and is a positive regulator of non-canonical autophagy. Two different complexes are involved in these pathways and Rubicon interacts with both. The first complex leads to autophagosome /endosome maturation and the other leads to the initiation of ROS production via non-canonical autophagy. In this chapter, our focus is on the ER stress and UPR initiated pathways of autophagy/endocytosis. We will focus on the non-canonical autophagy pathway leading to ROS production in the next chapter.

We performed functional studies on lymphoblastoid cell lines (LCLs) from unaffected and affected individuals from the pedigree SM331 harbouring the mutation to identify the molecular mechanism through which the identified mutation in *RUBCN*, coding for Rubicon, is linked to FALS. LCLs were previously established by in-vitro infection of B cells from peripheral blood with Epstein-Barr virus (EBV) which results in immortalisation of B cells. This provides an unlimited source of cells for performing various molecular studies (Hussain and Mulherkar, 2012). Expression of *RUBCN* is known to be the highest in this tissue compared to other tissues (GTEx Portal), which makes them an excellent model to investigate the effect of the mutation. We investigated the effect of the mutation on ER stress activated UPR pathways, autophagy/endocytosis pathways and on cell survival.

In order to explore the effects of the identified mutation in *RUBCN*, we initially investigated the known actions of *RUBCN* that have been established in the regulation of autophagy and endocytosis. We then investigated the effect of the mutation on *RUBCN* relevant pathways by

inducing cell stress using drugs in LCLs. Various drugs are available that trigger or inhibit autophagy in cells by either mTOR - dependent (starvation) or mTOR-independent pathways. ER stress can also be used to induce autophagy as recent studies have shown the induction of autophagy under ER stress (Adolph et al., 2013).

5.1.1 ER stress

The drugs we used to induce autophagy by ER stress in our study were tunicamycin and thapsigargin. Tunicamycin was used to induce a mild ER stress. It inhibits protein N-glycosylation that results in the accumulation of misfolded proteins in ER leading to ER stress (Banerjee et al., 2011). Thapsigargin was used to induce a strong ER stress. It inhibits the endoplasmic reticulum calcium pump, which leads to the accumulation of calcium in cytoplasm. Chaperones perform a critical role in protein folding in endoplasmic reticulum (ER) and require calcium ions for their activity but the absence of calcium ions in ER causes their activity to fail. This leads to the accumulation of misfolded proteins in the ER resulting in ER stress (Thastrup et al., 1990, Hetz and Mollereau, 2014). In order to alleviate ER stress, ER transmembrane stress sensors are activated which initiate the unfolded protein response (UPR) (Hetz et al., 2015). Upon activation, UPR modulates diverse processes inside the cell such as increased expression of protein chaperones, reduced protein synthesis, activation of ER-associated degradation of misfolded proteins (ERAD) pathway and activation of autophagy (Rashid et al., 2015, Hoyer-Hansen and Jaattela, 2007, Hetz, 2012, Ron and Walter, 2007). One of the stress sensors in ER membrane is IRE1α which upon activation splices the mRNA of X box-binding protein 1 (XBP1) and converts it into its active spliced form (XBP1s). The spliced form of XBP1 is a transcription factor that activates the transcription of HSPA5, DNAJB9 and other genes involved in the ERAD pathway (Lee et al., 2003). HSPA5/BiP is the most abundant ER chaperone and an established ER stress marker (Kaufman, 2002). It is

localised in the ER and is involved in protein folding and protein assembly. DNAJB9 is also localised within the ER. It acts as a co-chaperone of HSPA5 and regulates its activity (Nakanishi et al., 2004). The marker proteins of ER stress pathways that we selected to test the effect of the *RUBCN* mutation were XBP1, HSPA5 and DNAJB9.

If UPR fails to restore ER homeostasis, then an apoptotic response is triggered which leads to cell death (Hoyer-Hansen and Jaattela, 2007).

5.1.2 Autophagy

We used rapamycin in order to induce autophagy by the mTOR dependent pathway. It acts on the mTORC1 complex and inhibits its activity resulting in the induction of autophagy (Sarkar, 2013). Autophagy (macroautophagy) is initiated with the formation of the phagophore that encloses the targeted substrates from cytoplasm leading to the formation of an autophagosome. After the formation of the autophagosome, a stepwise process of autophagosome maturation takes place that ends with the fusion of the autophagosome with a lysosome to enable the degradation of the cargo carried by them (Kang et al., 2011). The marker proteins of the autophagy pathway that we selected to test the effect of the *RUBCN* mutation were *SQSTM1*/p62 and LC3II. We also selected LAMP2 as a marker of lysosomal activity that indicates the completion of the pathway with cargo degradation carried by autophagosomes.

5.1.3 Endocytosis

Autophagy, endosomal and lysosomal pathways are interlinked and dependent on each other. The endosomal pathway starts with the internalisation of extracellular components by vesicle formation. The cargo contained in the vesicles is then sorted in a series of sequential steps from early to late endosomes. During these steps, some of the components are returned to the cell surface while others are sent to the trans-Golgi network. The remaining components ultimately

fuse with the lysosome for degradation (Elkin et al., 2016). Alterations in this pathway can affect the correct localisation of some cellular components, cell proteostasis and cell survival (Tsvetanova, 2013).

Rab7A is an established marker of late endosomes and thus we have used it in our study to investigate the effects of mutation on endosomal pathway. Rab7A converts the early endosome to late endosome in the endosomal pathway (Rink et al., 2005). It is also involved in the regulation of ER stress where the defects in Rab7A can lead to ER stress and eventually to defects in the endosomal pathway (Mateus et al., 2018).

5.1.4 Apoptosis

Apoptosis is a programmed cell death pathway whereby the cell undergoes shrinkage followed by chromatin condensation and cell fragmentation resulting in the formation of apoptotic bodies. The apoptotic bodies are finally removed by phagocytosis (Kerr et al., 1972). Apoptosis is commonly found in neurodegenerative diseases. When UPR and autophagy fail to maintain cellular homeostasis under prolonged stress conditions, apoptosis is triggered by the cell (Hetz and Mollereau, 2014, Yonekawa and Thorburn, 2013).

5.1.5 Objectives

We hypothesized that the mutation in *RUBCN* would affect the autophagy/endosomal pathways by affecting expression of different pathway genes and may ultimately also affect cell viability. Hence, the following functional studies were performed to investigate the effects of the mutation:

1. Analysis of the changes in the gene expression using two techniques: quantitative PCR (qPCR) and western blot analysis.
2. Analysis of cell survival using flow cytometry with FITC- Annexin V assay.

We designed these experiments to test the effects of the mutation under both basal and cell stress conditions. We used tunicamycin and thapsigargin to induce ER stress activated UPR pathways and rapamycin to induce autophagy.

5.2 Methods

5.2.1 Lymphoblastoid cell lines culture

Lymphocytes were prepared from blood samples donated by 8 members of the family in which the *RUBCN* mutation was found and used for EBV transformation by ECACC (HPA, Porton). Informed consent was taken from all the members of the family who gave blood samples and the study was performed following the Research Governance regulations of Imperial College London. ER stress and autophagy pathways were induced in these lymphoblastoid cell lines (LCLs) for investigating the effect of mutation in presence and absence of cell stress. LCLs were grown in RPMI 1640 medium (Gibco) containing 10% Foetal bovine serum (Sigma-Aldrich), 1% penicillin/Streptomycin (Gibco) and 1% glutamax (Gibco). The cells were grown in RPMI 1640 medium. Four LCLs were from controls, two were from FALS and two from at-risk individuals harbouring the same gene mutation that was present in FALS patients. The cell lines were grown for 8 to 10 days at 37ºC, 5% CO_2 until appropriate number of cells was obtained before treatment with the drugs. Cells were counted and transferred to a 24 well plate. The remaining cells were centrifuged and resuspended in freezing solution (FBS and 10% DMSO) with $1x10^7$ to $3x10^7$ cells per cryovial. The cryovials were stored in liquid nitrogen for future use.

5.2.2 Drug treatment of LCLs

The following drugs were used: tunicamycin (Sigma-Aldrich), thapsigargin (Sigma-Aldrich), rapamycin (Sigma-Aldrich). Staurosporine (Sigma-Aldrich) was only used in FITC-Annexin V assay as a positive control for apoptotic cell death. Working concentrations used were: tunicamycin at 2 μg/ml, thapsigargin at 0.5 μM, rapamycin at 0.2 μM and staurosporine at 5 uM. Working concentration of drugs was prepared by serial dilutions using DMSO as a solvent.

A 24 well plate was used for treatment of cells with drugs. For gene expression analysis, 1 ml of culture medium containing 3 x 10^6 cells was transferred into each well. The experiment was set up for a total of 48 hours. The cells were incubated at 37ºC, 5% CO_2 for 24 hours before starting drug treatment. After 24 hours incubation in the 24 well plate, the cells were treated with tunicamycin and rapamycin for 24 hours and with thapsigargin for 6 hours. A no-drug medium control and vehicle controls (DMSO was used as the drug vehicle) were included in the experiment. The vehicle was added either at 24 hours or 6 hours to provide appropriate controls the drugs used.

For FITC annexin V assays, 1 x 10^6 cells were added in each well. The cells were incubated in a plate for 6 hours before starting cell treatment and the experiment was set up for a total of 30 hours. In addition to tunicamucin, thapsigargin and rapamycin treatment as stated above, cells were also treated with staurosporine for 4 hours with a corresponding vehicle control.

For inhibiting drug treatment, 400 µl of cold phosphate buffer saline (PBS) was added to each well. The cells were transferred from plates into eppendorf tubes and centrifuged for 5 min at 2000g. Supernatants were discarded and the step was repeated with the addition of 400 ul of cold PBS. The pellets were then stored at -80ºC for RNA or protein extraction or were subsequently used for FITC-Annexin V assay.

5.2.3 DNA extraction and sequencing

The DNA sequence of LCLs was confirmed before starting functional studies. Genomic DNA was extracted from LCLs using the QIAamp® DNA Midi kit (QIAGEN) according to the manufacturer's protocol. A PCR technique was used to amplify DNA fragments using a gene specific primer pair (Table 5-1). PCR products were visualised by separating them on agarose gel according to their sizes and then the products were purified using Exonuclease I - Shrimp Alkaline Phosphatase (ExoSAP) protocol. Samples for Sanger sequencing were analysed in the

MRC CSC Genomic Core Laboratory at Imperial College London. The acquired sequencing files were read using CodonCode aligner software.

Table 5-1 *RUBCN* Primer Sequence

Gene	Primers	Product size (bp)
RUBCN	Forward: AGGAGAATGCCCACTTCAGC Reverse: CAGGTTCTTGGTGCGGATTT	182

Sequence of forward and reverse primers used to amplify *RUBCN* for DNA sequencing.

5.2.4 RNA extraction and cDNA synthesis

RNA was extracted from the lymphocytes and cell lines using a Direct-zol^{TM} RNA mini prep kit (Zymo Research, USA) according to the manufacturer's protocol which has been explained in detail in Chapter 2. 40 µl of DNase/RNase-free water was used to elute extracted RNA. RNA was quantified using NanoDrop spectrophotometer ND-1000 and stored at -80^{o}C.

For performing qPCR, cDNA was synthesised from extracted RNA using AMV reverse transcriptase (New England Biolabs), 10X RT buffer (New England Biolabs), random hexamers (Invitrogen) and dNTP mix according to the protocol explained in Chapter 2. cDNA was stored at -20^{o}C for further use.

5.2.5 Quantitative real-time PCR (qPCR)

We analysed the expression of target genes in lymphocytes and LCLs at the mRNA level by quantitative real-time PCR (qPCR) as explained in Chapter 2. The primers used to amplify required gene products are given in Table 5-2. For quality control checks, non-template controls were included in each qPCR plate. The experiment contained replicates for the expression of each candidate gene. The amplification of the required gene product was

confirmed by analysing dissociation curves generated from the qPCR reaction and by separating the PCR products on 2% agarose gels (Figure 5-1).

5.2.6 Protein extraction and sample preparation for SDS-PAGE

Proteins were extracted from lymphocytes and LCLs by re-suspending cells in 200µl of RIPA buffer. Samples were left at 4 ºC for 30 minutes on a shaker and centrifuged at 4ºC for 20 minutes at 12000 rpm. Supernatants were transferred to fresh tubes and protein extracts were kept at -80ºC. A Bradford assay was performed to determine the concentration of proteins in each sample and samples were equalised to a concentration of 20 µg/25 µl with the addition of 1X Laemmli SDS sample buffer (Alfa Aesar).

Table 5-2 Primer sequences for qPCR

Gene	Primers	Product size (bp)
Candidate gene		
RUBCN	Forward: GAGAATGCCCACTTCAGCAT Reverse: CAGGTTCTTGGTGCGGATTT	180
ER stress genes		
XBP1 total	Forward: GCTCAGACTGCCAGAGATCG Reverse: TCTTCAGCAACCAGGGCATC	188
XBP1 spliced	Forward: AGAGTCTGATATCCTGTTGG Reverse: AGTTCATTAATGGCTTCCAG	189
HSPA5	Forward: TCAAGTTCTTGCCGTTCAAGG Reverse: AAATAAGCCTCAGCGGTTTCTT	148
DNAJB9	Forward: TTTCCAGACACGCCAGGATG Reverse: GTCCTGCAGTGCTTGCTAGA	195
Autophagy genes		
LAMP2	Forward: CGTTCTGGTCTGCCTAGTCC Reverse: CAGTGCCATGGTCTGAAATG	173
SQSTM1 (P62)	Forward: CAGTCCCTACAGATGCCAGA Reverse: TCTGGGAGAGGGACTCAATC	142
Endosomal pathway gene		
RAB7A	Forward: CACTCATGAACCAGTATGTG Reverse: CATATCTGCATTGTGACTAGC	118
House-keeping gene		
ACTB	Forward: GACAACGGCTCCGGCATGTG Reverse: CCTTCTGACCCATGCCCAC	121
GAPDH	Ready-made primer pair ordered from Primer design	118

Primer sequences used to amplify exome sequences of genes by qPCR in order to study the expression of genes at the mRNA level for investigating the effect of the mutation in LCLs from individuals of pedigree SM331.

a

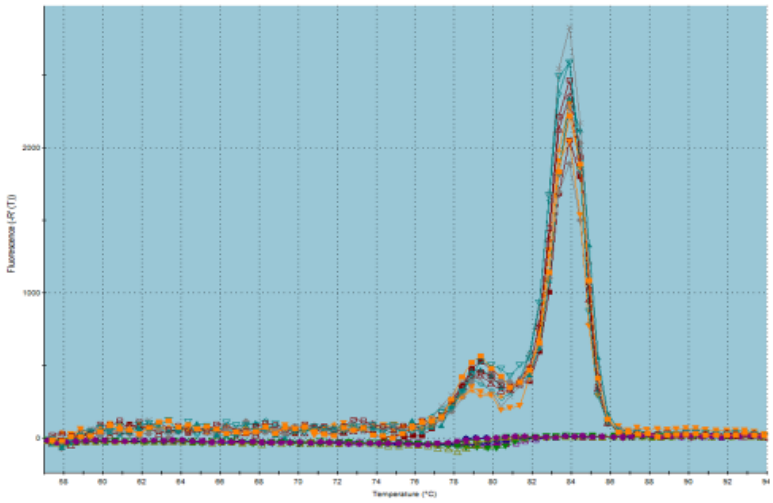

b

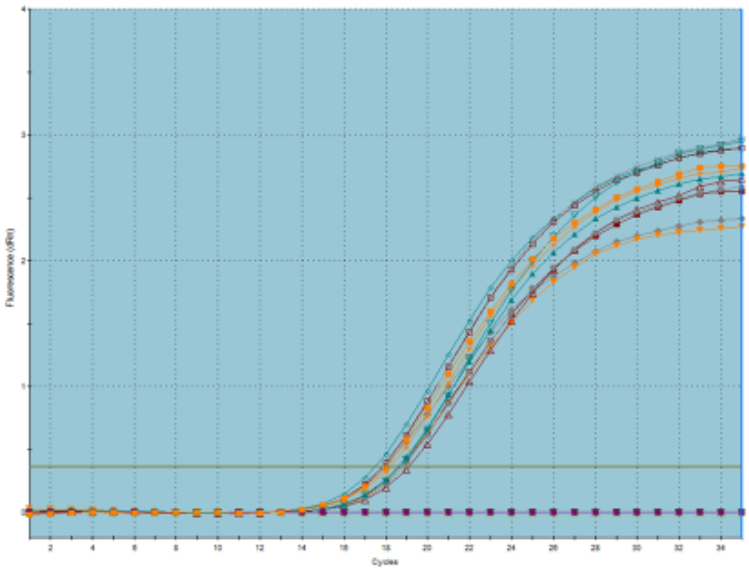

Figure 5-1 Dissociation curve and amplification plot from a qPCR reaction

The dissociation curve and amplification plot profiles of β-actin cDNA amplification from a qPCR reaction performed on two LCLs, a mutant (index case) and a wild-type individual of pedigree SM331 treated with tunicamycin, thapsigargin and rapamycin. a) Dissociation curve analysis helps in determining the specificity of the PCR reaction and shows the melting temperature at which double-stranded DNA is denatured. b) Amplification plot indicates the threshold cycle for each sample and the total amplification obtained from the given number of amplification cycles during a qPCR reaction.

5.2.7 Western blotting

SDS-PAGE gels were prepared. Samples were boiled for 10 minutes at 95ºC and loaded along with a protein marker. Electrophoresis was performed at 70 V for approximately 2 hours. Proteins were transferred from the gel to a nitrocellulose membrane using a Pierce Power Blotter (Thermo Scientific) and a successful transfer was confirmed with Ponceau S solution (Sigma-Aldrich). The nitrocellulose membranes were blocked with 5% blocking buffer for 1 hour with gentle agitation. This was followed by incubation of membranes with primary antibody at 4ºC and gentle agitation for the optimised time. The membranes were washed 3 times with TBST/PBST for 5 minutes and incubated at room temperature with secondary antibody for 1 hour with gentle agitation. The membranes were washed 3 times with TBST/PBST for 5 minutes. The membrane was finally incubated in Pierce™ ECL western blotting substrate (Thermo Scientific) for 5 minutes and immediately imaged using a Syngene GeneGnome XRQ chemiluminescence imaging system.

The relative density of candidate gene expression between samples was quantified using ImageJ software and the samples were normalised against a housekeeping gene, GAPDH.

5.2.7.1 Antibodies used in Western blotting

Primary antibodies: rabbit polyclonal anti-rubicon antibody (1:500, Abcam), rabbit polyclonal anti-SQSTM1/P62 antibody (1:1000, Abcam), rabbit polyclonal anti-LAMP1 antibody (1:1000, Abcam), rabbit polyclonal anti-Rab7 antibody (1:1000, Cell Signalling), rabbit polyclonal anti-LC3B antibody (1:2000, Sigma Aldrich), mouse monoclonal anti GAPDH antibody (1:2000, Santa Cruz).

Secondary antibodies: peroxidase labelled anti-mouse IgG (H+L) (Vector laboratories), peroxidase labelled anti-rabbit IgG (H+L) (Vector laboratories)

5.2.8 FITC-Annexin V assay staining

After growing and treating cells, the cells were stained using a FITC Annexin V Apoptosis Detection kit 1 (BD Biosciences). The cells were then analysed for apoptotic cell death using 2 Laser FacsCalibur Flow Cytometer (BD Biosciences).

5.2.9 Statistical analysis

Two-way ANOVA along with a Bonferroni post-hoc test was used to analyse the effect of the interaction of drug and mutation on cell survival. The paired Student's t-test was performed to analyse the effect of drug treatment and the unpaired Student's t-test was performed to analyse the effect of mutation. Results were given as mean ± Standard error of mean (SEM). The changes in gene expression have been given as fold change (FC) value. For both mRNA and protein expression analysis, values were normalised against a house-keeping gene in order to compensate for the differences in the quantity of starting material loaded in different samples. Non-normally distributed data was analysed by non-parameteric Mann-Whitney test. GraphPad Prism 5 software was used for performing the tests and for drawing graphs. Inverse of ΔCt values were used to draw graphs as the inverse represents the right direction of the gene expression change compared to ΔCt values.

5.3 Results

5.3.1 Confirmation of DNA sequence in LCLs

The DNA sequence of LCLs from all eight cell lines was determined and the presence of the mutation in the index case and a further family member with FALS, found through lymphocyte sequencing, was confirmed in LCLs and in addition was present in two 'at risk' individuals but absent from four further individuals (Figure 5-2). This provided the two groups for the functional studies, four cell lines with mutation and four without (see chapter 3 for further details).

5.3.2 Expression of *RUBCN* in lymphocytes

In order to confirm the comparability of our studies on LCLs with lymphocytes, we analysed the expression of *RUBCN* in lymphocytes at basal levels using qPCR before proceeding with the studies on LCLs. qPCR was performed on RNA extracted from all eight blood samples available from pedigree SM331 (Figure 5-3). Electrophoresis of the amplified products from qPCR on agarose gels confirmed the amplification of the gene of interest, *RUBCN*.

5.3.3 Investigation of effect of mutation on cellular pathways

After analysing the expression of *RUBCN* in lymphocytes in controls and FALS cases, we proceeded with the investigation of the effect of the putative ALS associated mutation on the autophagy/endosomal pathways in LCLs obtained from pedigree SM331. We performed the functional characterisation of the mutation by exposing tissues to cell stress *in vitro* using ER stress inducers, tunicamycin and thapsigargin, which activate UPR pathways and ultimately autophagy pathway and also by using an autophagy inducer, rapamycin, to induce the mTOR-dependent autophagy pathway.

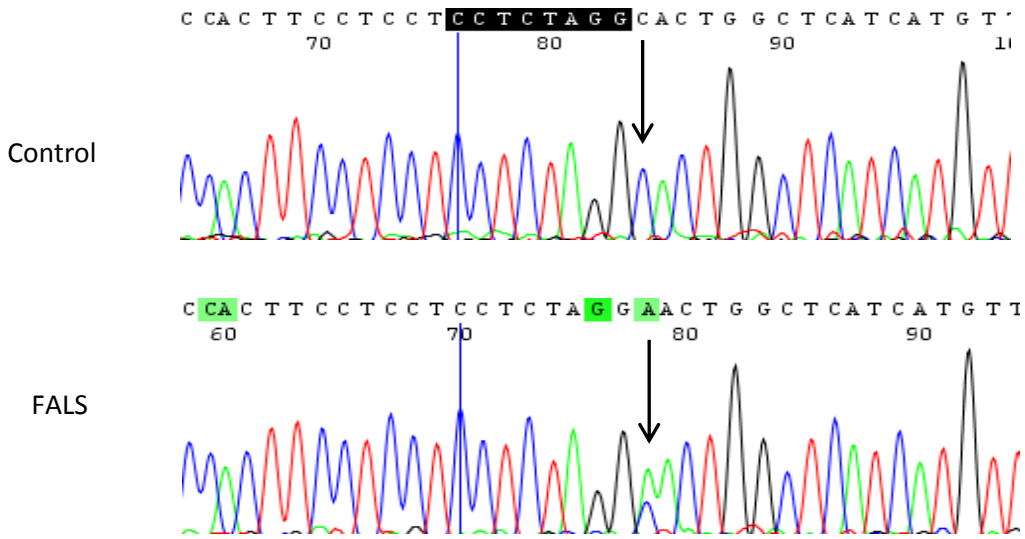

Figure 5-2 Chromatograms of *RUBCN* sequences indicating the nucleotide transversion in a FALS case compared to a control from pedigree SM331.

DNA was extracted from the LCLs of two FALS cases, two at-risk individuals and four controls from pedigree SM331. A *RUBCN* gene segment containing the mutation was sequenced using primer set given in Table 5-1. The two chromatograms shown here indicate the difference between the DNA sequence of *RUBCN* in LCLs from a control and a FALS case. The arrows indicate the position of a heterozygous transversion, C to A, present in a FALS case compared to a control.

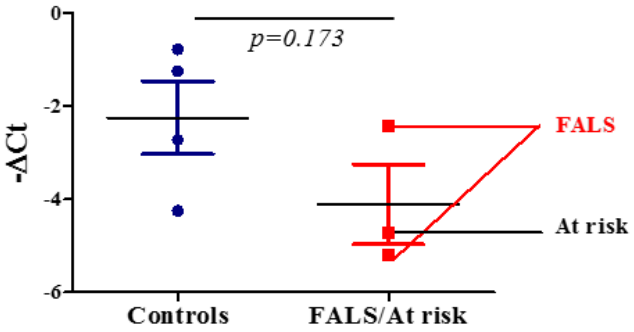

Figure 5-3 *RUBCN* mRNA expression levels in lymphocytes.

Expression levels of *RUBCN* mRNA from eight LCLs, four mutant and four wild type individuals, of pedigree SM331 to investigate the effect of mutation on the expression of *RUBCN*. The values of *RUBCN* expression normalised to the house-keeping gene *GAPDH* are represented by means and SEMs. Circles and squares show individual samples. An unpaired Student's t-test was used.

5.3.3.1 Expression of UPR genes at the mRNA level

5.3.3.1.1 Effect of drugs

We observed a significant upregulation of ER stress markers; XBP1s, *XBP1*total and *HSPA5* (p=<0.05), in control cell lines (FC=2.9, 3.5, 4.9 respectively) and in mutant cell lines (FC=3.0, 4.4, 6.2 respectively) with tunicamycin. A significant upregulation was also observed with thapsigargin in the expression of *XBP1*s and *XBP1* total in both control LCLs (FC=2.2, 2.0 respectively) and in mutant LCLs (FC=2.3, 2.5 respectively). In the case of *HSPA5* and *DNAJB9*, a significant upregulation was observed only in mutant LCLs (FC=2.3, 1.7) with thapsigargin. The upregulation of ER stress marker genes confirmed the activation of UPR pathways (Table 5-3).

5.3.3.1.2 Effect of mutation

We did not observe a significant effect of mutation on the expression of any of the ER stress markers investigated (Table 5-4). These findings illustrate that the ER stress is unaffected by the mutation at the mRNA level in *RUBCN* and that the mutation is not interfering with the UPR pathways.

5.3.3.2 Expression of autophagy and endosomal genes at the mRNA level

5.3.3.2.1 Effect of drugs

We observed a significant upregulation of *SQSTM1*, *RAB7A* and *LAMP2* with tunicamycin (p=<0.05) both in control cell lines (FC=4.1, 2.3, 2.0) and in mutant cell lines (FC=4.1, 4.7, 2.5). A significant change in gene expression was not observed with thapsigargin and rapamycin (Table 5-3). These results suggest that tunicamycin induced autophagy.

5.3.3.2.2 Effect of mutation

We did not find a significant effect of the mutation on the expression of any of the pathway genes investigated though a small change in the mRNA expression of *RAB7A* was observed ($p=0.06$) towards decreased expression at basal levels but it was non-significant (Table 5-4) (Figure 5-4). These findings illustrate that although autophagy/endosomal pathways are not significantly affected by the mutation, the mutation still may have some effects that requires a further investigation.

Table 5-3 Investigation of the effect of drug treatment on cellular pathways at the mRNA level.

	Wild type			Mutant		
	TN	TG	R	TN	TG	R
LAMP2	0.017 ↑	0.257	0.913	0.038 ↑	0.412	0.245
RUBCN	0.136	0.176	0.119	0.932	0.624	0.689
DNAJB9	0.136	0.094	0.499	0.201	0.030 ↑	0.545
HSPA5	0.016 ↑	0.786	0.314	0.002 ↑	0.021 ↑	0.368
***XBP1* total**	0.002 ↑	0.026 ↑	0.348	0.015 ↑	0.005 ↑	0.678
***XBP1* spliced**	0.001 ↑	0.009 ↑	0.385	0.009 ↑	0.002 ↑	0.337
RAB7A	0.040 ↑	0.619	0.424	0.024 ↑	0.165	0.349
SQSTM1	0.028 ↑	0.160	0.423	0.021 ↑	0.106	0.135

P-values obtained from paired t-tests for investigating the effect of drug treatment on cellular pathways. LCLs were treated with tunicamycin and rapamycin for 24 hours and thapsigargin for 6 hours with the addition of vehicle in the relevant experimental controls simultaneously. The values of gene expression were normalised to the house-keeping gene β-actin. TN, tunicamycin treatment; TG, thapsigargin treatment; R, rapamycin treatment. Arrows indicate an upregulation or downregulation in the expression of the gene. Values in red indicate significant values, $p<0.05$.

Table 5-4 Investigation of the effect of the *RUBCN* mutation on cellular pathways at the mRNA level.

P values obtained by comparing wild-type LCLs to mutant LCLs under different drug treatments						
	Medium	**DMSO 24 hr**	**DMSO 6 hr**	**TN**	**TG**	**R**
LAMP2	0.995	0.624	0.353	0.543	0.886	0.541
RUBCN	0.849	0.627	0.486	0.462	0.627	0.192
DNAJB9	0.922	0.467	0.297	0.600	0.166	0.577
HSPA5	0.600	0.133	0.576	0.762	0.165	0.325
XBP1 total	0.282	0.203	0.1.00	0.650	0.409	0.746
***XBP1* spliced**	0.541	0.698	0.467	0.777	0.518	0.656
RAB7A	0.748	0.059	0.969	0.667	0.798	0.827
SQSTM1	0.4868	0.706	0.565	0.652	0.939	1.000

P-values obtained from unpaired t-test for investigating the effect of *RUBCN* mutation on the autophagy/endosomal pathways in eight LCLs, four mutant and four wild-type control individuals, of pedigree SM331. LCLs were treated with tunicamycin for 24 hours and thapsigargin for 6 hours with the addition of vehicle, DMSO, simultaneously in the relevant experimental controls. The values of gene expression were normalised to the house-keeping gene β-actin. TN, tunicamycin treatment; TG, thapsigargin treatment; R, rapamycin treatment.

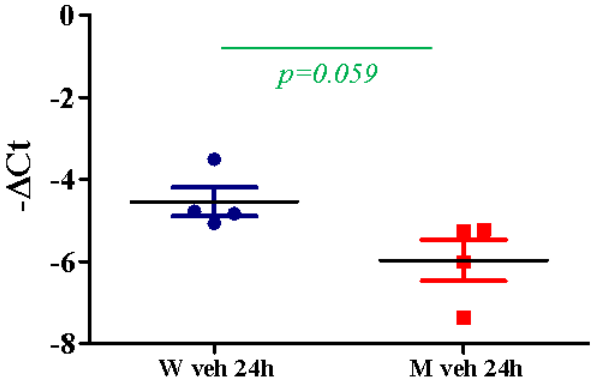

Figure 5-4 The effect of the mutation on the endosomal pathway marker, *RAB7A*, at basal levels in LCLs.

The effect of the mutation on the mRNA expression level of the endosomal pathway marker *RAB7A* in eight LCLs, four mutant and four wild type individuals, of pedigree SM331 at basal levels. The values of *RAB7A* expression normalised to the house-keeping gene β-actin (-delta Ct) are represented by means and SEMs. Circles and squares represent individual samples. W, wild type; M, mutant; veh 24h, vehicle added for 24 hours. Unpaired Student's t-tests was used for investigating the effect of the mutation.

5.3.3.3 Expression of Autophagy and endosomal pathway genes at the protein level

5.3.3.3.1 Effect of drugs

At the protein level**,** tunicamycin caused a significant upregulation on the expression of Rubicon (p=<0.05) in wild type cell lines (FC=2.6). A small increase in the protein expression of LC3II was observed in wild type and mutant cell lines but it was non-significant (p=0.06 and 0.07 respectively). Thapsigargin caused a significant upregulation of LC3II proteins (p=<0.05, FC=1.5) in mutant cells lines but not in wild type cell lines, which suggests a possible increase in the autophagy pathway in mutant cell lines treated with thapsigargin. Rapamycin caused a significant downregulation in the expression of Rubicon in mutant cell lines (p=0.007, FC=0.09) but not in wild type cell lines. Rapamycin also caused a small change in the protein expression of P62 and LAMP1 in wild type cell lines but it was non-significant (Table 5-5).

5.3.3.3.2 Effect of mutation

We observed a small upregulation in the *RUBCN* protein expression at basal levels (p=0.06) in the presence of the mutation but it was non-significant. This trend was absent under cell stress. The protein expression of other autophagy pathway proteins was not affected by the presence of mutation (Table 5-6) (Figure 5-5). This suggests that the mutation did not significantly affect the pathways investigated.

Table 5-5 Investigation of the effect of drug treatment on autophagy/endosomal pathways at the protein level.

	Wild type			Mutant		
	TN	**TG**	**R**	**TN**	**TG**	**R**
Rubicon	0.0442 ↑	0.1006	0.1663	0.2521	0.7899	0.0068 ↓
P62	0.4857	0.7808	0.0592	0.7811	0.4608	0.5879
LC3II	0.0601	0.2465	0.4087	0.0676	0.0127 ↑	0.1903
Rab7	0.5319	0.4600	0.7059	0.8422	0.2004	0.6857
LAMP1	0.1449	0.3501	0.0758	0.4355	0.1252	0.2419

P-values obtained from paired T-Test for investigating the effect of drug treatment on autophagy/endosomal pathways. LCLs were treated with tunicamycin and rapamycin for 24 hours and thapsigargin for 6 hours with the addition of vehicle in the relevant experimental controls simultaneously. Quantitative analysis was performed by densitometry and each protein was normalised against a reference gene, GAPDH. TN, tunicamycin treatment; TG, thapsigargin treatment; R, rapamycin treatment. The paired Student's t-test was used for investigating the effect of drugs. Arrows indicate an upregulation or downregulation in the expression of the gene. Values in red indicate significant values, $p<0.05$.

Table 5-6 Investigation of the effect of *RUBCN* mutation on autopahgy/endosomal pathways at the protein level.

P values obtained by comparing wild-type LCLs to mutant LCLs under different drug treatments				
	M	**TN**	**TG**	**R**
Rubicon	0.0604	0.4266	0.9165	0.9727
P62	0.5069	0.9616	0.7216	0.3301
LC3II	0.4873	0.5056	1.000	0.8171
Rab7	0.9873	0.4532	0.9784	0.6959
LAMP1	0.5559	0.3533	0.4169	0.4744

P-values obtained from unpaired T-Test for investigating the effect of *RUBCN* mutation on autophagy/endosomal pathway. LCLs were treated with tunicamycin and rapamycin for 24 hours and thapsigargin for 6 hours with the addition of vehicle in the relevant experimental controls simultaneously. Quantitative analysis was performed by densitometry and each protein was normalised against a reference gene, GAPDH. M, no drug medium (basal levels); TN, tunicamycin treatment; TG, thapsigargin treatment; R, rapamycin treatment. The unpaired Student's t-test was used for investigating the effect of the mutation. Arrows indicate an upregulation or downregulation in the expression of the gene.

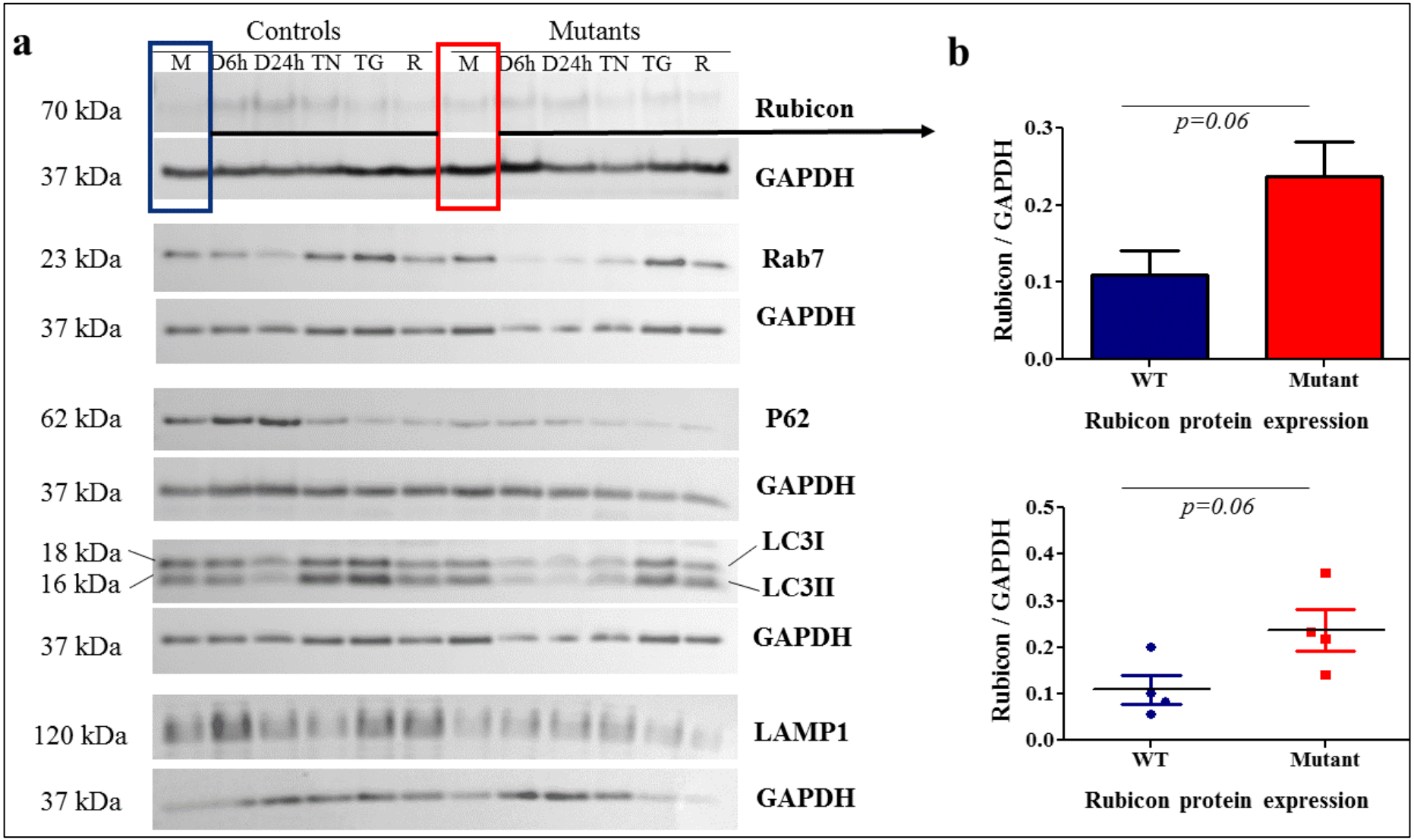
a
Controls
Mutants
M
D6h
D24h
TN
TG
R
M
D6h
D24h
TN
TG
R
70 kDa
Rubicon
37 kDa
GAPDH
23 kDa
Rab7
37 kDa
GAPDH
62 kDa
P62
37 kDa
GAPDH
18 kDa
16 kDa
LC3I
LC3II
37 kDa
GAPDH
120 kDa
LAMP1
37 kDa
GAPDH
b
p=0.06
Rubicon / GAPDH
0.3
0.2
0.1
0.0
WT
Mutant
Rubicon protein expression
p=0.06
Rubicon / GAPDH
0.5
0.4
0.3
0.2
0.1
0.0
WT
Mutant
Rubicon protein expression

Figure 5-5 Western blots of the autophagy/endosomal pathway genes in LCLs.

a) Western blot analysis for investigating the protein levels of candidate gene, *RUBCN*; autophagy markers, P62 and LC3II; endosomal pathway marker, Rab7; and lysosomal marker, LAMP2 in LCLs of pedigree SM331 treated with tunicamycin, thapsigargin and rapamycin. LCLs were treated with tunicamycin and rapamycin for 24 hours and thapsigargin for 6 hours with the addition of vehicle, DMSO, simultaneously in the relevant experimental controls. The figure shows a representative control and a representative mutant cell line in each blot with all treatments. Quantitative analysis of protein bands was performed by densitometry and each protein was normalised against reference gene GAPDH. M, untreated LCLs; D6h, Vehicle addition for 6 hours; D24h, vehicle added for 24 hours; TN, tunicamycin treatment; TG, thapsigargin treatment; R, rapamycin treatment.

b) Protein level analysis of Rubicon at basal levels in untreated LCLs, four mutant and four wild type individuals, of pedigree SM331. One sample from each group is indicated in a blue and a red box in part a. The data is represented by means and SEMs. Quantitative analysis of protein bands was performed by densitometry and the values were normalised against reference gene GAPDH. WT, wild type. The unpaired Student's t-test was used for investigating the effect of mutation.

5.3.4 Investigation of the effect of mutation on cell survival

We performed flow cytometry analysis of LCLs to investigate the effect of mutation on the cell survival under basal and stressed conditions. We hypothesized that the presence of the mutation could lead to increased cell death under cell stress conditions. LCLs were exposed to ER stress by tunicamycin and thapsigargin and autophagy was induced by rapamycin. Staurosporine was used as a positive control for apoptotic cell death. We observed a significant increase in cell death with staurosporine, tunicamycin and thapsigargin. The presence of the mutation did not affect cell survival under cell stress conditions (Table 5-7) (Figure 5-6 to Figure 5-9).

Table 5-7 Investigation of the effect of mutation on cell survival

Stage	Interaction between mutation and drug	Effect of drug	Effect of mutation
TN total apoptosis	0.4811	P<0.0001 ↑	0.9599
TN early apoptosis	0.7810	0.0043 ↑	0.6762
TN late apoptosis	0.4014	0.0005 ↑	0.3682
TN viable cells	0.5155	P<0.0001 ↓	0.9429
TG total apoptosis	0.5705	0.0090 ↑	0.5682
TG early apoptosis	0.7216	0.0721	0.5462
TG late apoptosis	0.5801	0.0044 ↑	0.8999
TG viable cells	0.6140	0.0192 ↓	0.6783
R total apoptosis	0.3738	0.1996	1.0000
R early apoptosis	0.2763	0.3625	0.8840
R late apoptosis	0.8018	0.5560	0.7973
R viable cells	0.3682	0.1538	0.9943
S total apoptosis	0.9225	0.0223 ↑	0.7545
S early apoptosis	0.6199	0.0350 ↑	0.7922
S late apoptosis	0.4795	0.1448	0.7387
S viable cells	0.9539	0.0224 ↓	0.7464

P values obtained from a two-way ANOVA test along with Bonferroni post-hoc correction for investigating the effect of the interaction of drug and *RUBCN* mutation on cell survival. Eight LCLs, four mutant and four wild type individuals of pedigree SM331, were treated with staurosporine for 4 hours, thapsigargin for 6 hours, tunicamycin and rapamycin for 24 hours with the addition of vehicle, DMSO, simultaneously in the relevant experimental controls. Fluorescence-activated cell sorting (FACS) was performed with FITC-Annexin V assay for cell survival analysis. Values in red indicate significant values, $p<0.05$. Arrows indicate the effect of drug on cell survival.

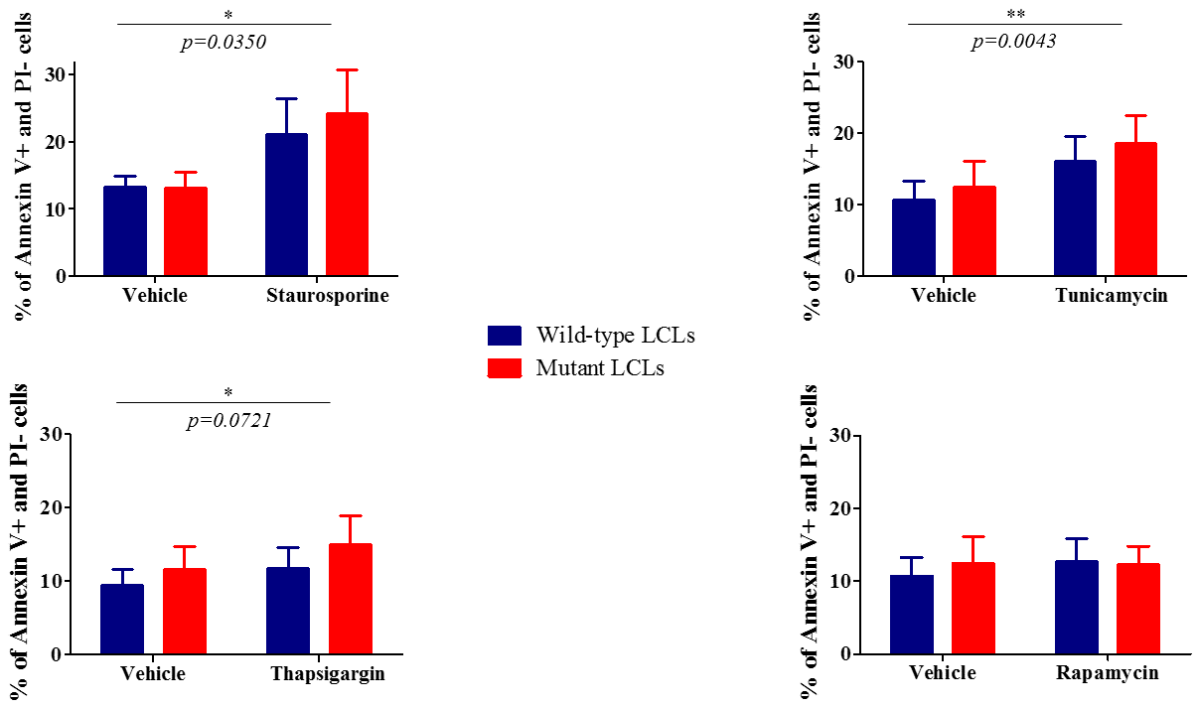

Figure 5-6 Investigation of the effect of RUBCN mutation on early apoptosis

Annexin V positive cells undergoing early apoptosis measured from fluorescence-activated cell sorting (FACS) profiles in eight LCLs, four mutant and four wild type individuals of pedigree SM331, to investigate the effect of mutation on cell viability. LCLs were treated with staurosporine for 4 hours, thapsigargin for 6 hours, tunicamycin and rapamycin for 24 hours with the addition of vehicle, DMSO, simultaneously in the relevant experimental controls. The data is represented by means and standard deviation (SD). Two-way ANOVA along with a Bonferroni post-hoc test was used to analyse the effect of the interaction of drug and *RUBCN* mutation on cell survival. P-values indicate the effect of drug *p<0.05; **p<0.005.

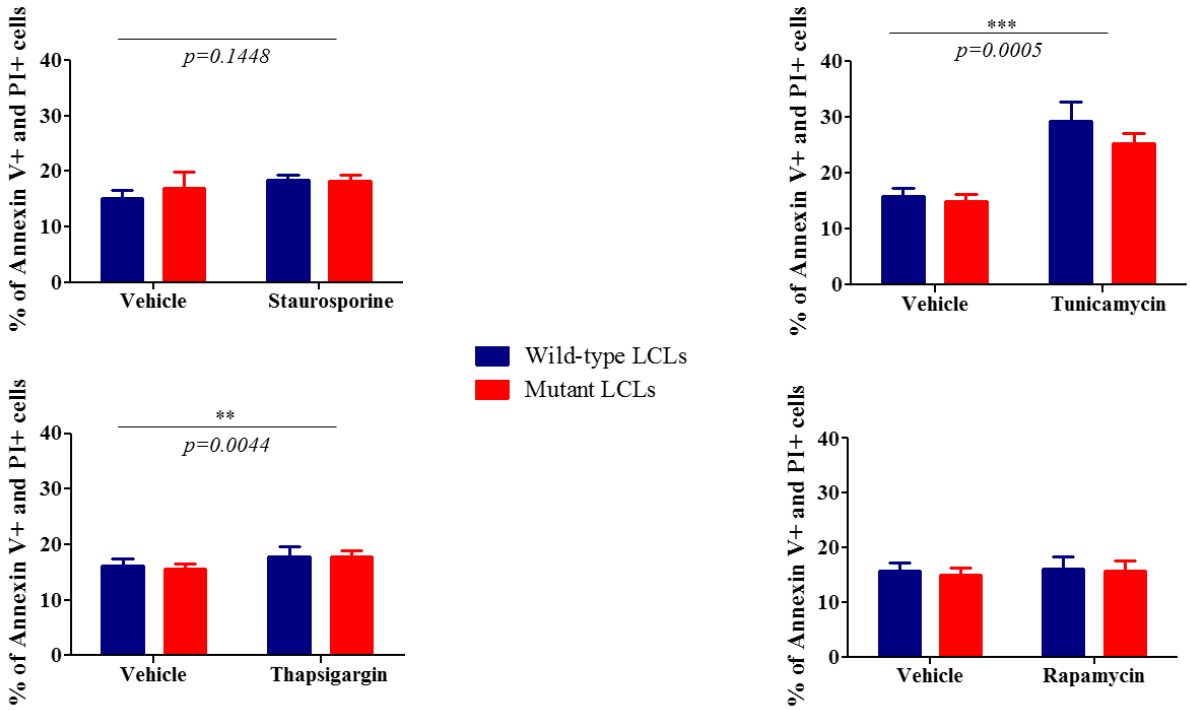

Figure 5-7 Investigation of the effect of *RUBCN* mutation on late apoptosis

Annexin V positive cells undergoing late apoptosis measured from fluorescence-activated cell sorting (FACS) profiles in eight LCLs, four mutant and four wild type individuals of pedigree SM331, to investigate the effect of mutation on cell viability. LCLs were treated with staurosporine for 4 hours, thapsigargin for 6 hours, tunicamycin and rapamycin for 24 hours with the addition of vehicle, DMSO, simultaneously in the relevant experimental controls. The data is represented by means and standard deviation (SD). Two-way ANOVA along with a Bonferroni post-hoc test was used to analyse the effect of the interaction of drug and *RUBCN* mutation on cell survival. P-values indicate the effect of drug ** $p<0.005$; ***$p<0.0005$.

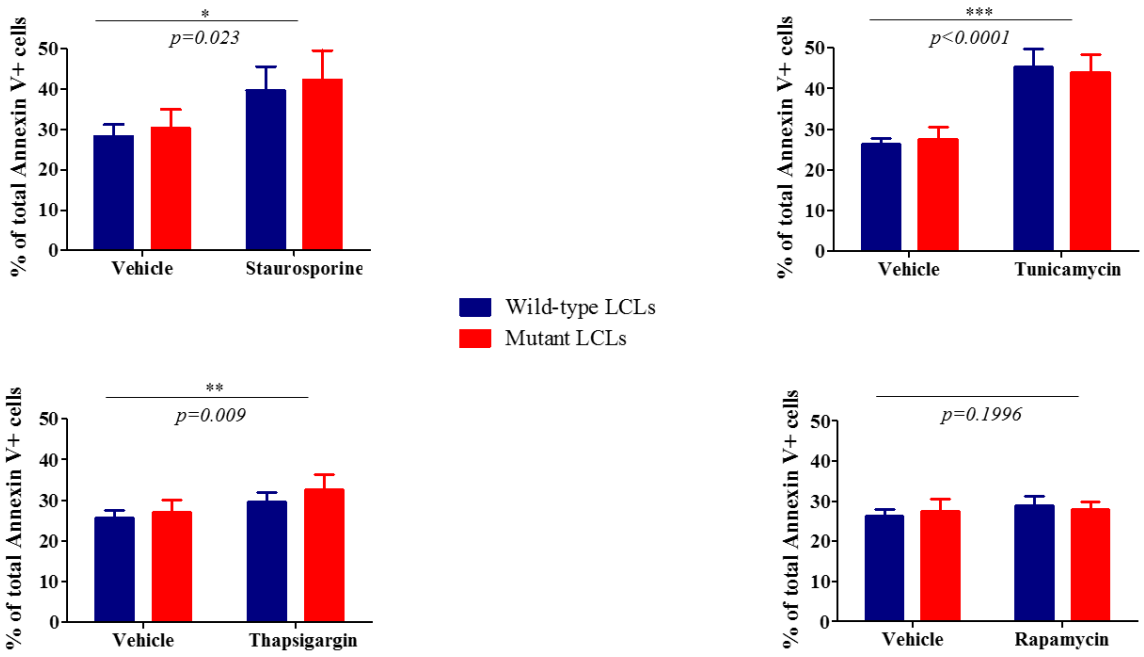

Figure 5-8 Investigation of the effect of *RUBCN* mutation on total Annexin V positive cells

Sum of Annexin V positive cells undergoing both early and late apoptosis measured from fluorescence-activated cell sorting (FACS) profiles in eight LCLs, four mutant and four wild type individuals of pedigree SM331, to investigate the effect of mutation on cell viability. LCLs were treated with staurosporine for 4 hours, thapsigargin for 6 hours, tunicamycin and rapamycin for 24 hours with the addition of vehicle, DMSO, simultaneously in the relevant experimental controls. The data is represented by means and standard deviation (SD). Two-way ANOVA along with a Bonferroni post-hoc test was used to analyse the effect of the interaction of drug and *RUBCN* mutation on cell survival. P-values indicate the effect of drug *p<0.05; **p<0.005; ***p<0.0005.

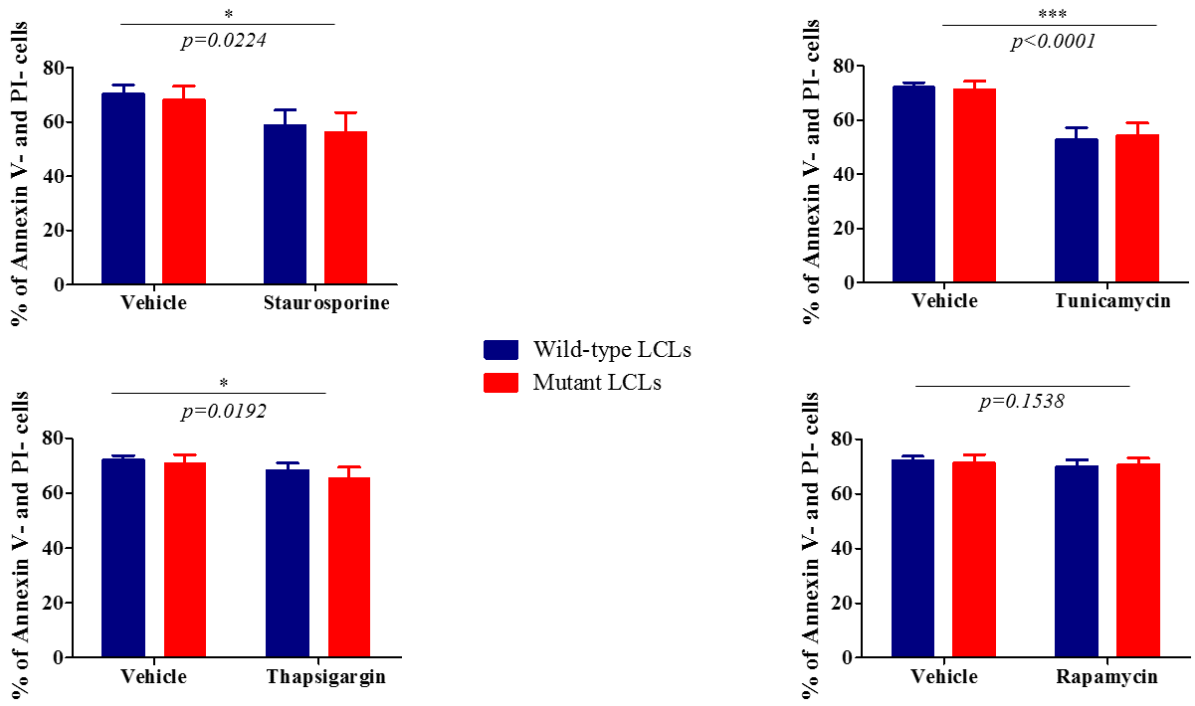

Figure 5-9 Investigation of the effect of *RUBCN* mutation on viable cells

Annexin V and PI negative viable cells that did not undergo apoptosis measured from fluorescence-activated cell sorting (FACS) profiles in eight LCLs, four mutant and four wild type individuals of pedigree SM331, to investigate the effect of mutation on cell viability. LCLs were treated with staurosporine for 4 hours, thapsigargin for 6 hours, tunicamycin and rapamycin for 24 hours with the addition of vehicle, DMSO, simultaneously in the relevant experimental controls. The data is represented by means and standard deviation (SD). Two-way ANOVA along with a Bonferroni post-hoc test was used to analyse the effect of the interaction of drug and *RUBCN* mutation on cell survival. P-values indicate the effect of drug *p<0.05; ***p<0.0005.

5.4 Discussion

Our candidate gene, *RUBCN*, is involved in autophagy and endosomal pathways as a negative regulator of autophagosome and endosome maturation (Sun et al., 2010a, Matsunaga et al., 2009, Zhong et al., 2009). In this chapter we have investigated the effects of the *RUBCN* mutation identified in FALS in pedigree SM331 on cell viability and the cellular pathways linked to *RUBCN* activity that include ER stress, autophagy and endosomal pathway.

We selected markers for ER stress (*XBP1*, *DNAJB9*, *HSPA5*), autophagy pathway (LC3II and *SQSTM1*), endosomal pathway (*RAB7A*) and lysosomal pathway (*LAMP1* or *LAMP2*) for investigating the effect of mutation on these pathways. We used tunicamycin, a mild ER stress inducer; thapsigargin, a strong ER stress inducer and rapamycin, autophagy inducer to induce these pathways. The concentration of these drugs for inducing the related pathways was selected based on dose-response curves produced by Intan Barul Akma Bakhtiar previously in our lab (unpublished data).

Under basal conditions, *RUBCN* negatively regulates autophagy and endocytosis by downregulating autophagosome and endosome maturation (Sun et al., 2011a, Zhong et al., 2009, Matsunaga et al., 2009). Considering its role, we hypothesized that if the mutation is a loss of function mutation then Rubicon should lose its inhibitory effect on the maturation of autophagosomes/endosomes and thus an upregulation of autophagy/endocytosis should be observed at basal levels. Under cell stress, however, there may not be an effect of *RUBCN* mutation on activity of the pathways as Rubicon does not inhibit autophagosome/endosome maturation under cell stress. We therefore designed this experiment such that our hypothesis could be tested both under basal and cell stress conditions.

In order to confirm the comparability of our studies on LCLs with lymphocytes, we analysed the mRNA expression of *RUBCN* in lymphocytes at basal levels before proceeding with the

studies on LCLs and we found comparable results of the effect of mutation on the expression of *RUBCN* between lymphocytes and LCLs. This confirmed LCLs as a good model for functional characterisation of the *RUBCN* mutation in addition to the known highest expression of *RUBCN* in LCLs compared to other tissues.

5.4.1 Effect of drugs on cellular pathways

We observed a significant upregulation in the expression of ER stress and autophagy markers with tunicamycin in control and mutant LCLs at both mRNA and protein levels. Thapsigargin also showed significant upregulation in an ER stress marker in both control and mutant LCLs at mRNA levels. It also showed a significant upregulation in the LC3II protein expression. Hence, ER stress was induced by both the drugs used. The differences observed on the expression of genes under tunicamycin and thapsigargin treatment could be due to the difference in the mode of action of the two drugs. The upregulation of autophagy markers by tunicamycin and thapsigargin confirms the activation of autophagy by ER stress which has been illustrated in previous studies (Rashid et al., 2015). Rapamycin treatment showed a significant effect on the expression of an autophagy gene, *RUBCN*, at protein levels. The observed effects by drug treatments signified the efficiency of our model under both basal and cell stress conditions for investigating the effects of the mutation.

5.4.2 Effect of the mutation on cellular pathways

We did not find a significant effect of the mutation in *RUBCN* on the expression of the marker genes or other autophagy related genes under basal or stressed conditions at mRNA levels, except for a small but non-significant change in the mRNA expression of *RAB7A* ($p=0.06$) and in the protein expression of Rubicon at basal levels ($p=0.06$).

Since the mutation we have identified is present at the site that interacts with UVRAG and Beclin 1 (Figure 5-10), we anticipated that the presence of the mutation may affect the binding of Rubicon protein with these two proteins of the Class III PI3K (PI3KC3) complex and would eventually affect the binding of Rubicon with the PI3KC3 complex. This could lead to a subsequent loss of inhibitory function of Rubicon resulting in an upregulation of autophagy and endosomal pathway. Our findings from the functional studies performed in this chapter, however, have not illustrated an effect on the autophagy markers, P62 and LC3II, or the lysosomal activity marker, LAMP1. This suggests that the mutation is perhaps not affecting the binding of Rubicon to the proteins of the PI3KC3 complex and thus the negative regulatory role of Rubicon on the pathways remains intact. On the other hand, even if the binding of Rubicon to UVRAG or Beclin 1 is affected, Rubicon may still be interacting with the PI3KC3 complex by its direct binding to VPS34, as the stability of the complex is dependent on VPS34, the catalytic subunit of PI3KC3 complex (Martinez-Vicente, 2015, Sun et al., 2011a). VPS34 interacts with Beclin 1, which further binds to UVRAG, resulting in a complete complex able to perform its inhibitory role in the presence of Rubicon (Figure 5-11Figure 5-11). There is a strong possibility for the later since the proteins in the complex are involved in multiple interactions with each other such as VPS34 interacts with Beclin1, Rubicon, and Rab7. Beclin 1 interacts with VPS34, Rubicon and UVRAG. UVRAG binds to Rubicon and Beclin 1 (GeneCards; STRING). As Rubicon does not have an inhibitory role on pathways under cell stress conditions, it was not surprising to find no effect of the mutation on the expression of any of the genes investigated from autophagy and endocytic pathway under cell stress conditions. However, the mutation in *RUBCN* may have an effect on the cell in some way especially on pathways in which it is involved as a positive regulator. Rubicon is involved as a positive regulator in LC3-associated phagocytosis where its presence leads to the activation

of the complex responsible for ROS production (Martinez-Vicente, 2015). This part of our project has been covered in detail in the next chapter.

At this point, it is important to study the changes in *UVRAG* gene expression in presence of the *RUBCN* mutation since even if Beclin 1 and Rubicon do not interact directly, as has been suggested by Sun et al. (Sun et al., 2011a), the *UVRAG* expression may give an important clue to the effect of mutation on the activity of the complex. This is especially important since Rubicon interacts exclusively with the UVRAG containing PI3KC3 complex although only to a subpopulation of this complex (Matsunaga et al., 2009). In this case, the inhibitory role of Rubicon may only be affecting a subpopulation of the UVRAG containing PI3KC3 complexes.

We wanted to investigate the effect of mutation on Beclin 1 protein levels but unfortunately, the antibody used gave many non-specific bands in LCL tissues and made the quantitative analysis of Beclin 1 protein bands extremely difficult. We have thus excluded Beclin 1 protein expression results from our analysis.

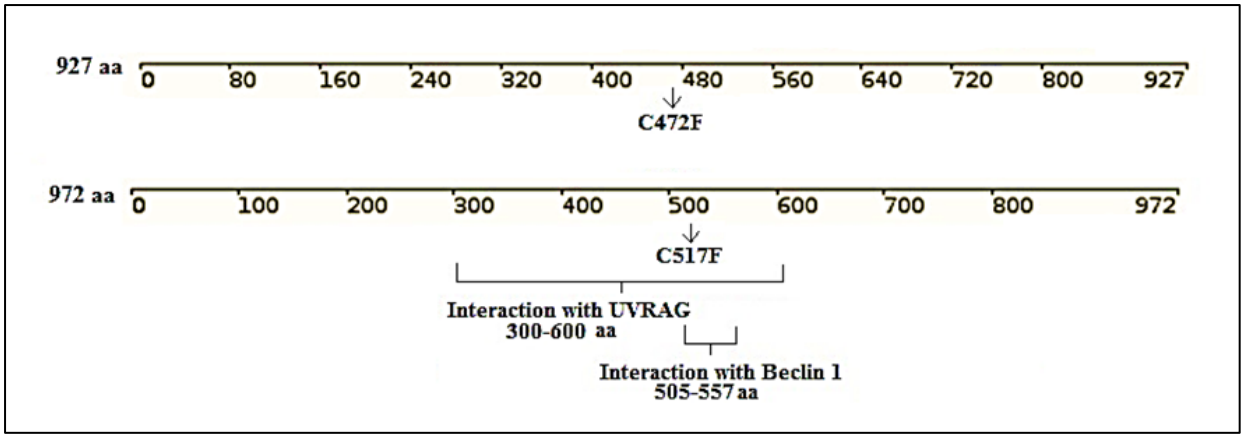

Figure 5-10 The two main transcripts of *RUBCN*.

The protein map shows the site of amino acid change from cysteine (C) to phenylalanine (F) in two major transcripts of *RUBCN* (927 and 972 amino acid transcripts) as a result of the mutation we have detected in pedigree SM331. It also indicates the two proteins that interact with Rubicon on the mutated site.

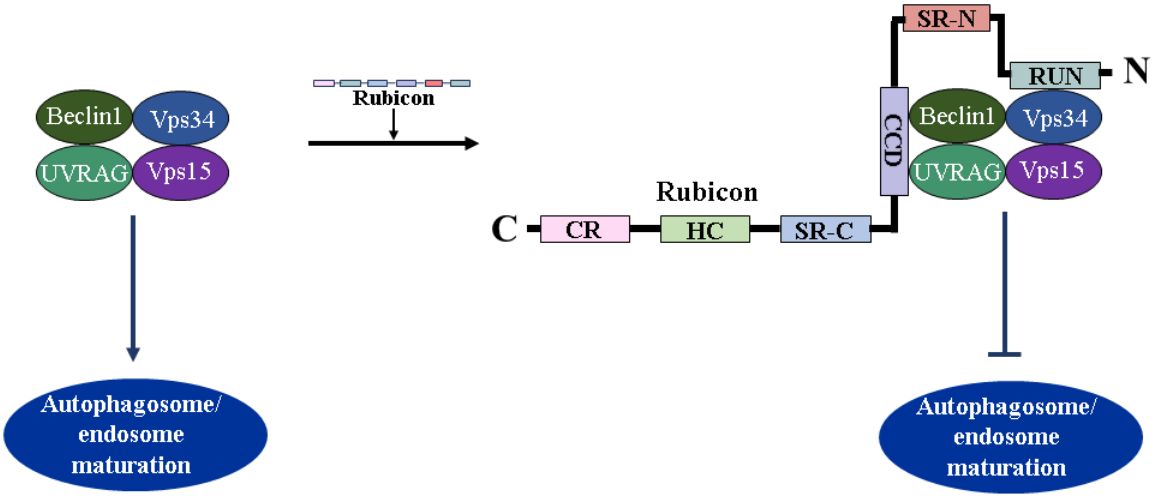

Figure 5-11 Interaction of Rubicon with UVRAG containing PI3KC3 complex

UVRAG positively regulates the PI3KC3 complex to undergo autophagosome/endosome maturation while the presence of Rubicon in the complex inhibits the formation of autophagosomes/endosomes, which ultimately inhibits the autophagy/endosomal pathway. Rubicon interacts with multiple proteins of the complex including Vps34, the catalytic subunit of the complex. Hence, even if the mutation we have detected in Rubicon affects the interaction of Rubicon with UVRAG and Beclin 1, Rubicon may still bind to the complex through its interaction with VPS34. VPS34 in turn interacts on its own with other components of PI3KC3 complex.

5.4.3 Effect of mutation on cell survival

We also investigated effects of mutation on cell survival. In this experiment, we treated cells with staurosporine in addition to tunicamycin, thapsigargin and rapamycin. Staurosporine is an inhibitor of protein kinases and this leads to induction of apoptosis. It is used in assays of apoptosis as a positive control for apoptosis induction (Kabir et al., 2002) as it induces cell death by both caspase-dependant and caspase-independent apoptotic pathways. We hypothesized that the presence of mutation could disrupt the normal cellular processes by the formation of protein aggregates as the misfolded protein from mutated *RUBCN* may be aggregation prone and thus non-degradable leading to increased cell death. On the other hand, as the role of the gene is to act as a negative regulator of autophagy, a loss of function mutation at basal levels could result in an upregulated level of autophagy. Continuous upregulated autophagy may be a signal of an unresolved problem inside the cell triggering apoptotic cell death. We wanted to investigate if the mutation leads to an increased cell death compared to wild type under cell stress. The presence of a constant ER stress leads to apoptosis, so we studied the effects of cell death under both ER stress and rapamycin effects.

In our LCL model, stauropsporine, tunicamycin and thapsigargin showed a significant increase in cell death. Since the mode of action of rapamycin is not directly related to induction of apoptosis, rapamycin is not necessarily expected to kill cells. Our results suggest that the presence of the mutation does not affect cell viability.

In conclusion, the identified mutation in *RUBCN* is not affecting the cell survival and the unfolded protein response, autophagy and endosomal pathways according to our investigation based on the genes studied from the pathways.

Chapter 6: Functional characterisation of *SM331* in FALS lymphoblastoid cell lines (LCLs): effect of oxidative stress

6.1 Introduction

In this chapter, we have focused on oxidative stress in relation to canonical autophagy, macroautophagy, and the non-canonical autophagy pathway, LC3-associated phagocytosis, that includes ROS production. In addition to oxidative stress, we have repeated ER stress and autophagy induction in order to understand the effect of the *RUBCN* mutation on these pathways in more detail.

6.1.1 Oxidative stress

Oxidative stress is a known central feature of neurodegenerative diseases (Kim et al., 2015a). An imbalance between the oxidants and antioxidants in the cell leads to oxidative stress. This imbalance is caused by reactive oxygen species (ROS) and reactive nitrogen species (RNS) produced as by-products of cellular metabolic process. These species cause damage to lipids, protein and nucleic acids inside the cell by oxidising and removing electrons from these molecules that promotes cell death. Different mechanisms such as autophagy are employed by cells to maintain redox signalling homeostasis by removing ROS and RNS. Autophagy is induced by oxidative stress especially the mitophagy pathway as the damaged mitochondria are considered to be the main source of abundant ROS production. Other damaged molecules are also primarily cleared by autophagy (Pajares et al., 2018).

We have used tertiary-butyl hydroperoxide (t-BH) to induce oxidative stress *in vitro* in order to induce autophagy in our cellular model of lymphoblastoid cell lines (LCLs) in order to study the effect of the *RUBCN* mutation. Tert-Butyl hydroperoxide (t-BH) is commonly used to

induce oxidative stress in cells as it causes ROS production. t-BH is detoxified to tert-butanol and GSH which is further oxidised to its disulphide form (GSSG) (Kučera et al., 2014).

6.1.2 LC3-associated phagocytosis (LAP)

LC3-associated phagocytosis (LAP) is a non-canonical autophagy pathway that induces cell tolerance to exogenous threats and is induced by different stimuli such as dying cells, pathogens and immune complexes (Henault et al., 2012, Martinez et al., 2011). LAP shares part of its machinery with canonical autophagy but is functionally distinct from it. LAP is initiated upon the engulfment of a particle through involvement of extracellular receptors e.g., Toll-like receptors. A single membraned vesicle, LAPosome, is formed after initiation of the pathway, which recruits parts of autophagy machinery for the embedding of LC3-II on the LAPosome membrane. Although Rubicon is inhibitory for autophagy, it is essential for LAP. The Rubicon containing PI3KC3 complex containing VPS34, UVRAG, and Beclin-1, but lacking the canonical autophagy components ATG14 and Ambra1 translocates to the LAPosome and produces PI(3)P in response to LAP stimuli (Martinez J et al., 2015). PI(3)P in turn recruits downstream autophagic proteins (ATG7, ATG3, ATG5, ATG12, and ATG16L) (Mizushima, 2007) and also stabilizes and activates the NOX2 complex (Martinez et al., 2015). The active NOX2 complex produces reactive oxygen species (ROS) in the lumen of phagosomes. This leads to the conjugation of LC3-II to the LAPosome facilitating the fusion of LAPosomes with lysosomes for the degradation of the cargo carried by them, resulting in the initiation of an immune response (Figure 6-1) (Martinez et al., 2015).

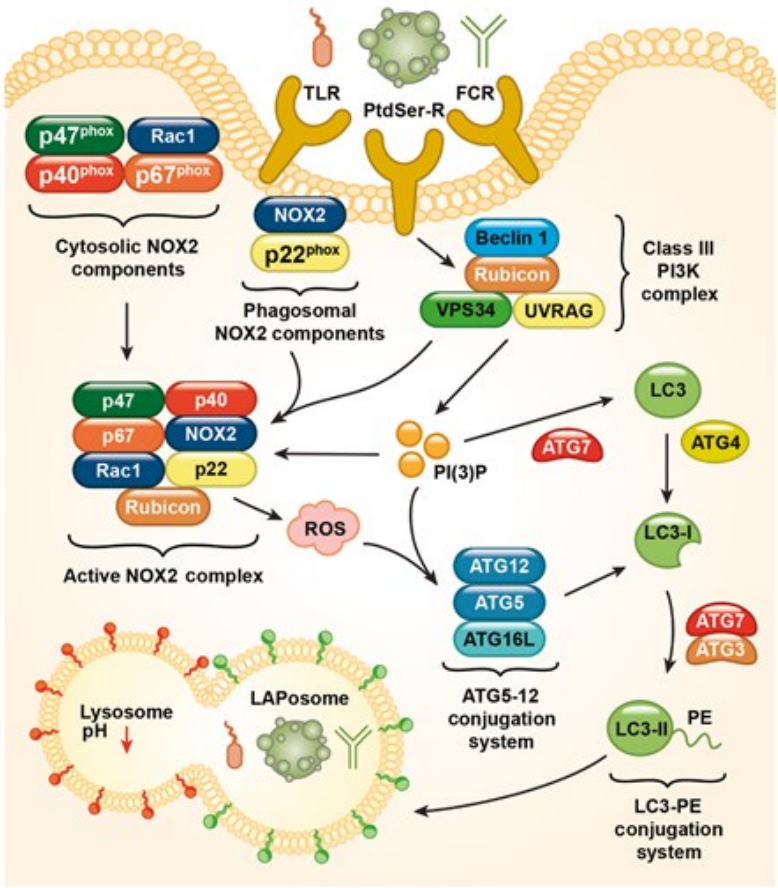

Figure 6-1 LC3-associated phagocytosis pathway

Components of the LC3-associated phagocytosis (LAP) pathway are recruited to the LAPosome when the stimuli that activate cell surface receptors (Toll-like receptors, TLR; Fc receptors, FCR; phosphatidylserine receptors) are engulfed by the cell. This leads to the association of the Rubicon containing PI3KC3 complex with the LAPosome and causes the production of PI(3)P. PI(3)P in turn performs two roles: it recruits the downstream ATG5-12 and LC3-PE conjugation systems and stabilises and activates the NOX2 complex (cytosolic NOX2 components join phagosomal NOX2 components) for ROS production. Rubicon is also required for the stability of the NOX2 complex. Both PI(3)P and ROS then lead to the embedding of LC3-II on the LAPosome membrane, which results in subsequent fusion of mature LAPosomes to lysosomes for the degradation of the cargo contained by the LAPosomes (Wong et al., 2018).

6.1.3 ER stress and autophagy

We used tunicamycin for inducing ER stress and rapamycin for inducing autophagy. The details of the importance of these pathways in relation to *RUBCN* and the effects of these drugs on these pathways has already been explained in detail in chapter 6. In addition to autophagy induction, we studied the effect of the mutation on autophagy by using an autophagy inhibitor. We used n-butylidenephtalide (nBP) to inhibit autophagy. n-BP has been shown to inhibit autophagy through the mTOR signalling pathway (Zhou et al., 2017, Hsueh et al., 2016).

6.1.4 Objectives

We hypothesized that the mutation in *RUBCN* would affect the LC3-associated phagocytosis which is linked to oxidative stress in addition to autophagy/endosomal pathways by affecting expression of different pathway genes and may ultimately affect cell viability. Hence, the following functional studies were performed to investigate the effects of the mutation:

1. Analysis of changes in gene expression using quantitative PCR (qPCR) which is a gold standard for gene expression analysis at the mRNA levels.
2. Analysis of cell survival using flow cytometry with FITC-Annexin V assay.

We designed these experiments to test the effects of the mutation under both basal and cell stress conditions.

6.2 Materials and methods

The materials and methods used for the experiments mentioned in this chapter were the same as previously described in Chapter 5. The only difference in this chapter is that we have not performed studies on the expression of genes at the protein level due to time limitations. The experiments described in this chapter were performed together with Alexandra Rother, an MSc Translational Neuroscience student, as part of her research project under my supervision.

The expression of genes studied in this chapter and the drugs and concentrations used for inducing cell stress are given in Table 6-1 and Table 6-2 respectively. Drugs were purchased from Sigma-Aldrich (rapamycin, tertiary-butyl hydroperoxide, tunicamycin, Staurosporine) and Alfa Aeser (n-butylidenephtalide).

Table 6-1 Primer sequences for qPCR

Gene	Primers	Product size (bp)
Candidate gene		
RUBCN	Forward: GAGAATGCCCACTTCAGCAT Reverse: CAGGTTCTTGGTGCGGATTT	180
ER stress genes		
XBP1 spliced	Forward: AGAGTCTGATATCCTGTTGG Reverse: AGTTCATTAATGGCTTCCAG	189
DNAJC10	Forward: CAGTGAAATATCATGGAGACAG Reverse: ATTTCCTGTCCAAAGTTCTG	95
Autophagy genes		
LAMP2	Forward: CGTTCTGGTCTGCCTAGTCC Reverse: CAGTGCCATGGTCTGAAATG	173
SQSTM1 (P62)	Forward: CAGTCCCTACAGATGCCAGA Reverse: TCTGGGAGAGGGACTCAATC	142
UVRAG	Forward: AGGGTTATTCAAATGCTCAG Reverse: GTAGCAAAGAGAAGACATCG	87
VPS34	Forward: CTGTGCTGGATATTGCGTGATC Reverse: AAGTCTATGTGGAAGAGTTTGCCT	102
Endosomal pathway gene		
RAB7A	Forward: CACTCATGAACCAGTATGTG Reverse: CATATCTGCATTGTGACTAGC	118
Oxidative stress/ LC3-associated phagocytosis gene		
NOX2	Forward: AAGATCTACTTCTACTGGCTG Reverse: AGATGTTGTAGCTGAGGAAG	124
House-keeping gene		
ACTB	Forward: GACAACGGCTCCGGCATGTG Reverse: CCTTCTGACCCATGCCCAC	121

Primer sequences used to amplify exonic sequences of genes by qPCR in order to study the expression of genes at the mRNA level in order to investigate the effect of the mutation in LCLs from individuals of pedigree SM331.

Table 6-2 Drug treatments used

Drug	DMSO	TN	n-BP	R	DMSO	ST	t-BH
Duration [hr]	24	24	24	24	4	4	4
Volume [µL]	4	2	2	2	4	5	4
Stock concentration	-	1 mg/mL	5 mg/mL	100 µM	-	1 mM	12.5 mM
Working concentration	-	2 µg/mL	10 µg/mL	0.2 µM	-	5 µM	50 µM

Drugs with their incubation duration, volume used, concentrations of the stock solutions and final drug concentration in 1 mL of complete RPMI1640 medium. Dimethyl sulfoxide, DMSO; Rapamycin, R; tertiary-butyl hydroperoxide, t-BH; tunicamycin, TN; Staurosporine, ST; n-butylidenephtalide, n-BP.

6.3 Results

6.3.1 Investigation of the effect of the mutation on cellular pathways

We proceeded with the investigation of the effect of the *RUBCN* mutation on the autophagy/endosomal pathway and LAP pathway in LCLs from pedigree SM331 in response to oxidative stress and autophagy inhibition, in addition to repeating ER stress with tunicamycin and autophagy induction with rapamycin, for investigating the effect of mutation on the expression of additional pathway proteins.. We used t-BH to induce oxidative stress and n-BP for autophagy inhibition.

We investigated the effect of the mutation on these pathways at the mRNA level only due to time constraints.

6.3.1.1 Expression of the UPR pathway genes at the mRNA level

6.3.1.1.1 Effect of drugs

Tunicamycin caused a significant upregulation of the ER stress marker *XBP1*s ($p<0.05$, FC=2.62) in wild type LCLs but the effect was diminished in mutant LCLs. With rapamycin, a significant downregulation in DNAJC10 was observed in wild type LCLs (FC=0.52) but the effect was reduced in mutant LCLs. A small change was observed in the mRNA levels of *XBP1*s in mutant LCLs ($p=0.057$) but it was non-significant. t-BH did not have any effect on the expression of UPR genes. With n-BP, a significant downregulation was observed in the expression of *XBP1*s in mutant LCLs (FC=0.5) (Table 6-3).

6.3.1.1.2 Effect of mutation

We observed a significant downregulation in the expression of *DNAJC10* ($p<0.05$, FC=0.53) in the presence of mutation at basal levels with vehicle added for 4 hours (Figure 6-2) (Table 6-5).

6.3.1.2 Expression of autophagy and endosomal genes at the mRNA level

6.3.1.2.1 Effect of drugs

VPS34 was significantly upregulated by tunicamycin ($p<0.05$, FC=1.43) in wild type LCLs but the effect was diminished in mutant LCLs. A small change in mRNA expression was observed for *RUBCN* ($p=0.069$) but it was non-significant. With rapamycin, a significant downregulation ($p<0.05$) was observed in the expression of *RUBCN* mRNA in both wild type (FC=0.43) and mutant LCLs (FC=0.20) but only in wild type LCLs for *VPS34* (FC=0.49), *UVRAG* (FC=0.35) and *RAB7A* (FC= 0.21) (Table 6-3 and Table 6-4).

6.3.1.2.2 Effect of mutation

A significant downregulation was observed in the expression of *RAB7A* at basal levels with no vehicle added ($p<0.05$, FC=0.38) (Table 6-5) (Figure 6-2).

6.3.1.3 Expression of the LAP-associated phagocytosis genes at the mRNA level

6.3.1.3.1 Effect of drugs

With tunicamycin, the expression of NOX2 was significantly upregulated ($p<0.05$, FC=1.97) in mutant LCLs. t-BH had no effect on the mRNA expression of *NOX2* (Table 6-3 and Table 6-4).

6.3.1.3.2 Effect of mutation

We observed a significant downregulation (p=0.015, FC=0.43) in the expression of *NOX2* at basal levels with vehicle added for 4 hours in the presence of the mutation (Table 6-5) (Figure 6-2).

6.3.1.4 Correlation between the expressions of different genes at the mRNA level.

6.3.1.4.1 Correlation between *NOX2* and *RUBCN* expression in the absence and presence of mutation

Since the effect of the mutation was observed on the expression of both *RUBCN* and *NOX2*, we checked the correlation between the expressions of *NOX2* with *RUBCN*. The correlation was studied at basal levels and under oxidative stress. A strong correlation between *NOX2* and *RUBCN* was observed at basal levels with vehicle added for 4 hours and under oxidative stress in wild type LCLs while this correlation was diminished in the presence of the mutation (Figure 6-3). This indicates the possible effect of the *RUBCN* mutation on the expression of *NOX2*.

6.3.1.4.2 Correlation between *VPS34* and *XBP1*s expression in the absence and presence of mutation

Since the expression profiles of *VPS34* and *XBP1*s looked very similar in the q-RT-PCR experiments, especially under TN induced ER stress, correlation of the expression of these two genes was investigated. A strong positive correlation was observed between the mRNA expression of the two genes in wild type cell lines at basal levels with the addition of vehicle for 24 hours and under ER stress, and in mutant cell lines at basal levels and also under ER stress (Figure 6-4Figure 6-4). This experiment indicates a positive correlation between *VPS34* and *XBP1*s mRNA expression at basal levels and under ER stress independent of the presence of the mutation.

6.3.2 Investigation of the effect of mutation on cell survival

We performed flow cytometry analysis of LCLs to investigate the effect of mutation on the cell survival under basal and stressed conditions. We hypothesized that the presence of the mutation could lead to increased cell death under basal or cell stressed conditions. LCLs were exposed to oxidative stress by t-BH, ER stress by tunicamycin and autophagy was induced by rapamycin. n-BP was used to inhibit autophagy. Staurosporine was used as a positive control for apoptotic cell death. We observed a significant increase in cell death with t-BH and tunicamycin (Table 6-6) (Figure 6-5 to Figure 6-8). Staurosporine also caused a significant increase in cell death ($p < 0.05$) (figures are not shown here as the effects of staurosporine have already been shown in chapter 5).

The presence of the mutation did not affect cell survival under basal or cell stress conditions (Table 6-6) (Figure 6-5 to Figure 6-8).

Table 6-3 Investigation of the effect of 24 hr drug treatment on cellular pathways

	Wild type			Mutant		
	TN	n-BP	R	TN	n-BP	R
RUBCN	0.6118	0.9488	0.0073↓	0.0686	0.0614	0.0072↓
LAMP2	0.9552	0.6113	0.5075	0.1197	0.6323	0.4705
VPS34	0.0284↑	0.5827	0.0424↓	0.6288	0.2824	0.1610
UVRAG	0.9990	0.9591	0.0355↓	0.1660	0.5288	-
RAB7A	0.6914	0.2621	0.0144↓	0.8808	0.0507	0.4279
DNAJC10	0.2717	0.7078	0.0168↓	0.7488	0.0939	0.0637
XBP1s	0.0318↑	0.7720	0.1841	0.2399	0.0200↓	0.0566
NOX2	0.1123	0.9073	0.1031	0.0197↑	0.1920	-

P-values obtained from paired t-tests investigating the effect of drug treatment on autophagy/endosomal and LAP pathways in eight LCLs, four mutant and four wild-type control individuals, of pedigree SM331. LCLs were treated with tunicamycin, n-BP and rapamycin for 24 hours with the addition of vehicle in the relevant experimental controls simultaneously. The values of gene expression were normalised to the house-keeping gene β-actin. TN, tunicamycin treatment; n-BP, n-butylidenephtalide treatment; R, rapamycin treatment. Arrows indicate an upregulation or downregulation in the expression of the gene. Values in red indicate significant values, $p<0.05$. Where sample number was less than 3, statistical analysis could not be performed and a hyphen is marked in the table instead.

Table 6-4 Investigation of the effect of 4 hr drug treatment on cellular pathways

	Wild-type	**mutant**
	t-BH	t-BH
RUBCN	-	0.3639
LAMP2	0.2628	0.3562
VPS34	-	0.1554
UVRAG	-	0.9412
RAB7A	-	0.3777
DNAJC10	-	0.4941
XBP1s	-	0.2979
NOX2	-	0.2815

P-values obtained from paired t-tests investigating the effect of drug treatment on autophagy/endosomal and LAP pathways in eight LCLs, four mutant and four wild-type control individuals, of pedigree SM331. LCLs were treated with t-BH for 4 hours with the addition of vehicle in the relevant experimental control simultaneously. The values of gene expression were normalised to the house-keeping gene β-actin. t-BH, tert-Butyl hydroperoxide treatment. Arrows indicate an upregulation or downregulation in the expression of the gene. Where sample number was less than 3, statistical analysis could not be performed and a hyphen is marked in the table instead.

Table 6-5 Investigation of the effect of the *RUBCN* mutation on cellular pathways.

P values obtained by comparing wild-type LCLs to mutant LCLs under different drug treatments							
	Medium	**DMSO 24 hr**	**DMSO 4 hr**	**TN**	**n-BP**	**R**	**t-BH**
RUBCN	0.6509	0.1213	0.0812	0.4072	0.3394	0.6366	0.1790
LAMP2	0.9520	0.3480	0.7485	0.3344	0.8512	0.3091	0.2962
VPS34	0.1984	0.4219	0.1017	0.4960	0.9040	0.4282	-
UVRAG	0.6818	0.8336	0.1693	0.1693	0.3031	0.2893	0.7622
RAB7A	0.0154↓	0.4817	0.9381	0.4842	0.4849	0.2910	0.8632
DNAJC10	0.9519	0.1074	0.0308↓	0.9968	0.3803	0.2539	0.2476
XBP1s	0.8628	0.3508	0.1726	0.7166	0.3791	0.2539	0.2234
NOX2	0.7419	0.2702	0.0146↓	0.3547	0.4512	-	0.0994

P-values obtained from unpaired t-tests investigating the effect of *RUBCN* mutation on the autophagy/endosomal and LAP pathways in eight LCLs, four mutant and four wild-type control individuals, of pedigree SM331. LCLs were treated with t-BH for 4 hours and tunicamycin, n-BP and rapamycin for 24 hours with the addition of vehicle in the relevant experimental controls simultaneously. The values of gene expression were normalised to the house-keeping gene β-actin. TN, tunicamycin treatment; n-BP, n-butylidenephtalide treatment; R, rapamycin treatment; t-BH, tert-Butyl hydroperoxide. Arrows indicate an upregulation or downregulation in the expression of the gene. Values in red indicate significant values, $p<0.05$.

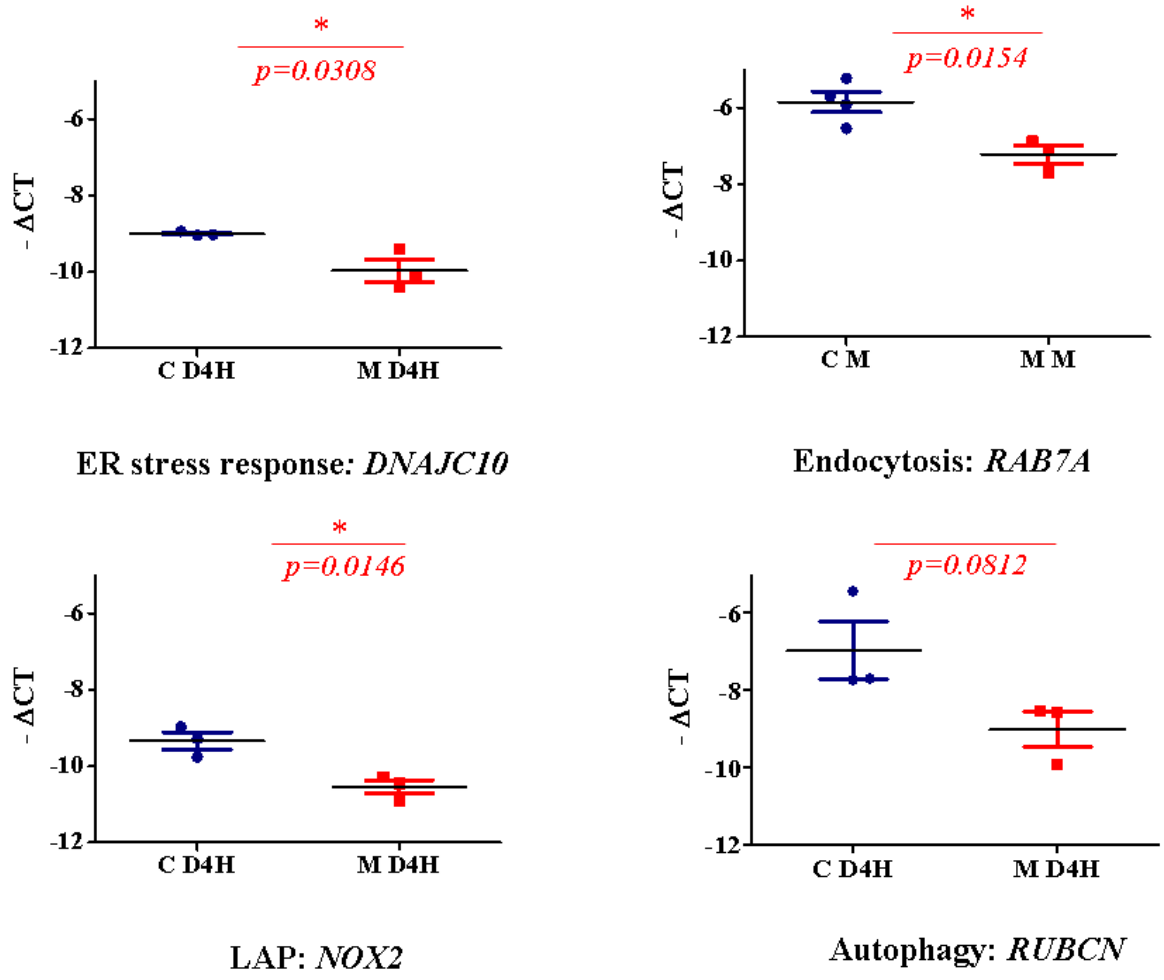

Figure 6-2 The mutation effects at basal levels

mRNA expression levels of selected genes, *RUBCN*, endosomal, ER stress and LAP markers in eight LCLs, four mutant and four control individuals, of pedigree SM331 to investigate the effect of mutation on endosomal and autophagy pathway. The values of *RUBCN, RAB7A*, *DNAJC10* and *NOX2* expression normalised to the house-keeping gene β-actin (-delta Ct) are represented by means and SEMs. Circles represent individual samples. DMSO was used in the experimental controls. C, control; M, mutant; D, DMSO. Unpaired Student's t-tests was used for investigating the effect of the mutation. *p<0.05. Red asterisk with p-value represent the significant effect of the mutation.

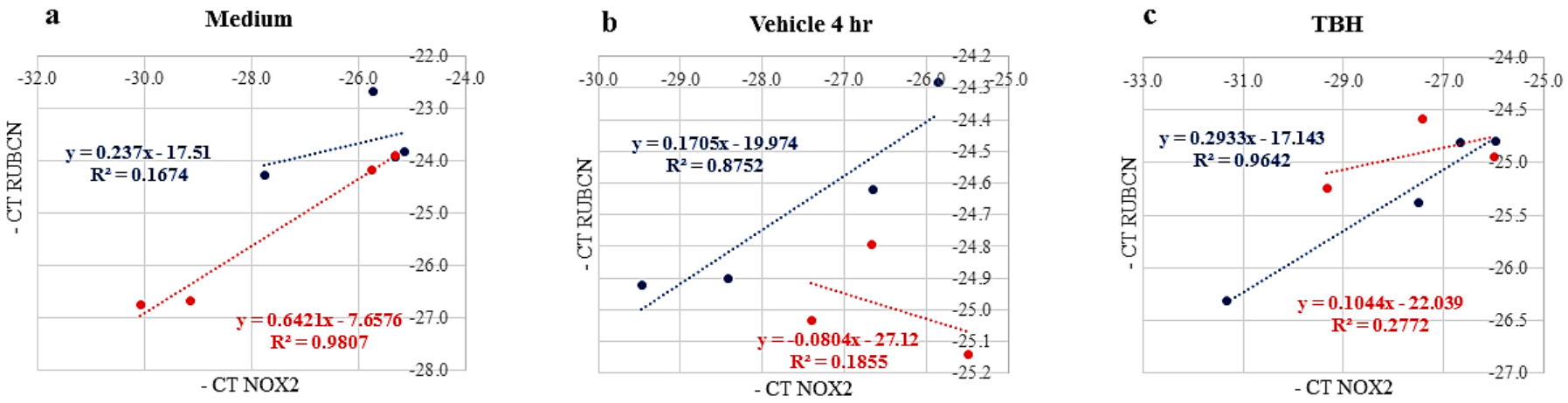

Figure 6-3 Correlation between the mRNA expression levels of *RUBCN* and *NOX2* in LCLs.

Correlation between the mRNA expression levels of *RUBCN* and *NOX2* in eight LCLs, four mutant and four control individuals, of pedigree SM331 a) in the medium without addition of vehicle b) in the medium with the addition of vehicle, DMSO, for 4 hours c) with TBH treatment. The values used were inverse of delta Ct values (-Ct). Blue circles represent control samples and red circles represent mutant samples. Pearson's correlation (r) values are indicated with each graph.

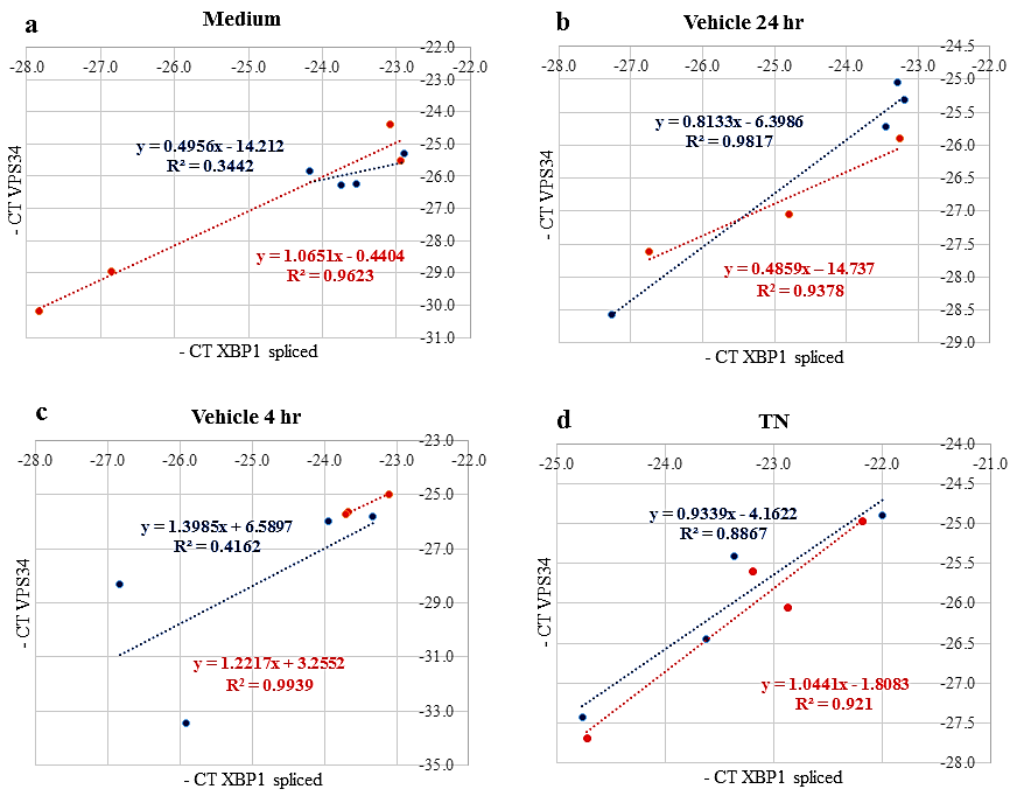

Figure 6-4 Correlation between mRNA expression levels of *XBP1s* and *VPS34* in LCLs.

Correlation between mRNA expression levels of *XBP1* spliced and *VPS34* in eight LCLs, four mutant and four control individuals, of pedigree SM331 a) in medium without addition of vehicle b) in medium with the addition of vehicle, DMSO, for 24 hours c) in medium with the addition of vehicle, DMSO, for 4 hours D) with TN treatment. The values used were inverse of delta Ct values (-Ct). Blue circles represent control samples and red circles represent mutant samples. Pearson's correlation (r) values are indicated in each graph.

Table 6-6 Investigation of the effect of mutation on cell survival

Stage	Interaction between mutation and drug	Effect of drug	Effect of mutation
TN total apoptosis	0.7820	0.0063 ↑	0.4990
TN early apoptosis	0.6715	0.0030 ↑	0.6353
TN late apoptosis	0.5298	0.0178 ↑	0.5576
TN viable cells	0.7930	0.0067 ↓	0.4438
n-BP total apoptosis	0.4852	0.9933	0.5574
n-BP early apoptosis	0.8274	0.8794	0.9204
n-BP late apoptosis	0.4774	0.9091	0.5120
n-BP viable cells	0.3420	0.9139	0.5273
R total apoptosis	0.3861	0.6156	0.7364
R early apoptosis	0.1485	0.8897	0.4721
R late apoptosis	0.6115	0.5876	0.3796
R viable cells	0.5676	0.5676	0.4624
TBH total apoptosis	0.8126	0.0008 ↑	0.8501
TBH early apoptosis	0.2281	0.0142 ↑	0.7881
TBH late apoptosis	0.4347	0.0018 ↑	0.7360
TBH viable cells	0.5337	0.0004 ↓	0.6914

P values obtained from a two-way ANOVA test along with Bonferroni post-hoc correction for investigating the effect of the interaction of drug and *RUBCN* mutation on cell survival. Eight LCLs, four mutant and four wild type individuals of pedigree SM331, were treated with TBH for 4 hours and with tunicamycin, n-BP and rapamycin for 24 hours with the addition of vehicle, DMSO, simultaneously in the relevant experimental controls. Fluorescence-activated cell sorting (FACS) was performed with FITC-Annexin V assay was for cell survival analysis. Arrows indicate an upregulation or downregulation in the expression of the gene. Values in red indicate significant values, $p<0.05$.

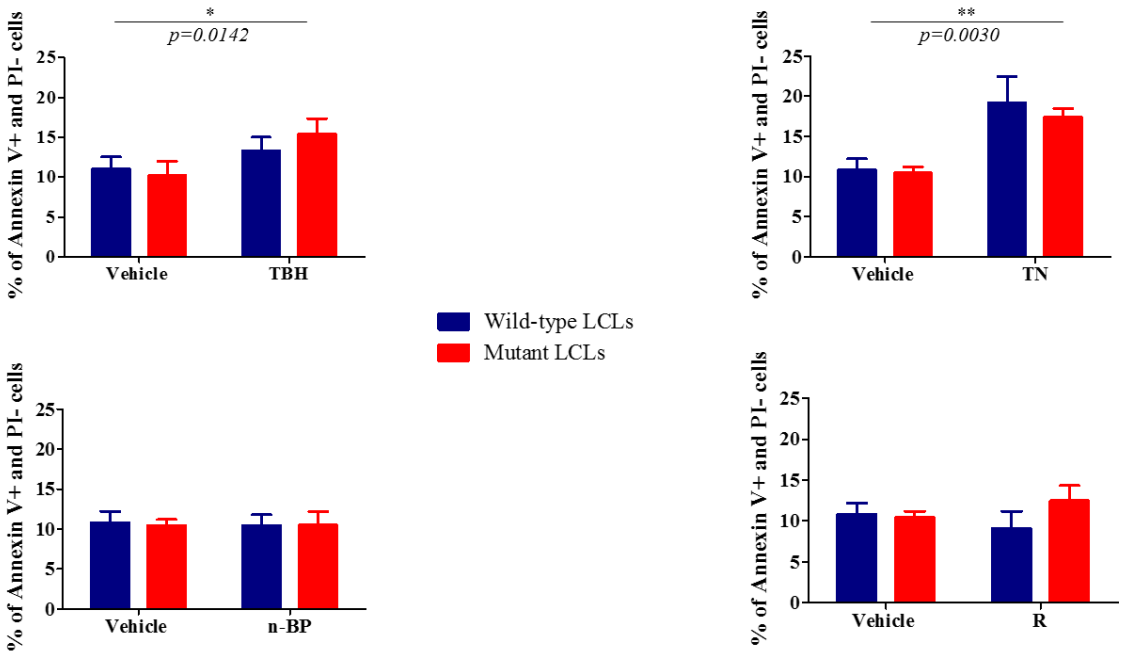

Figure 6-5 Investigation of the effect of the *RUBCN* mutation on early apoptosis

Annexin V positive cells undergoing early apoptosis measured from fluorescence-activated cell sorting (FACS) profiles in eight LCLs, four mutant and four wild type individuals of pedigree SM331, to investigate the effect of mutation on cell viability. LCLs were treated with TBH for 4 hours and with tunicamycin, n-BP and rapamycin for 24 hours with the addition of vehicle, DMSO, simultaneously in the relevant experimental controls. The data is represented by means and standard deviation (SD). Two-way ANOVA along with a Bonferroni post-hoc test was used to analyse the effect of the interaction of drug and *RUBCN* mutation on cell survival. P-values indicate the effect of drug *p<0.05; **p<0.005.

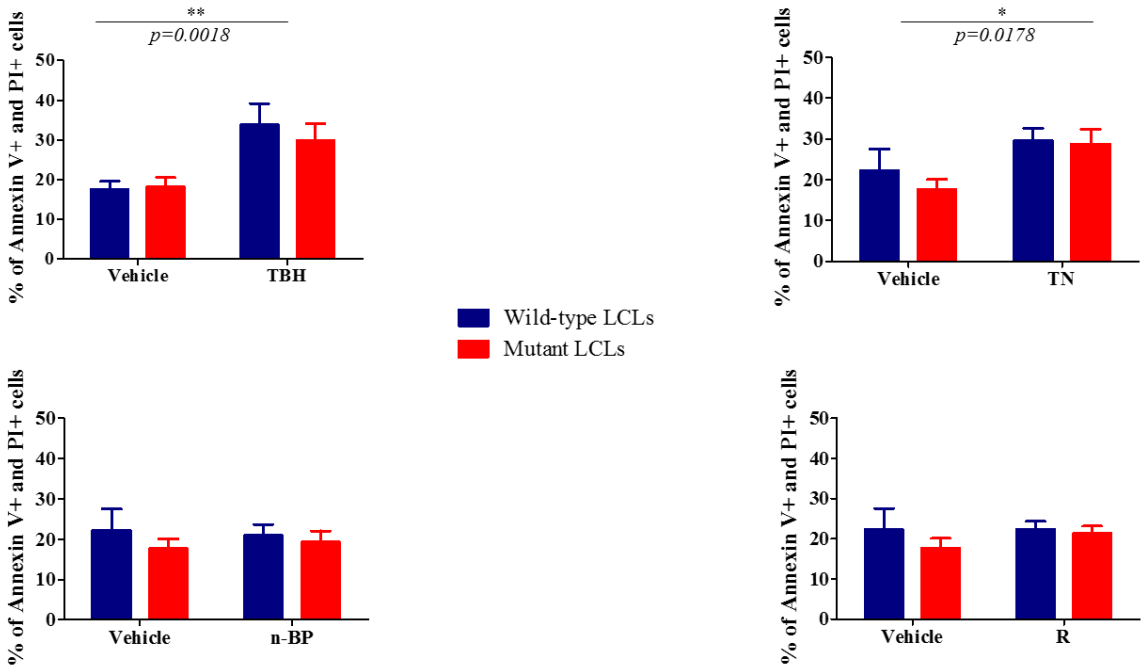

Figure 6-6 Investigation of the effect of the *RUBCN* mutation on late apoptosis

Annexin V positive cells undergoing late apoptosis measured from fluorescence-activated cell sorting (FACS) profiles in eight LCLs, four mutant and four wild type individuals of pedigree SM331, to investigate the effect of mutation on cell viability. LCLs were treated with TBH for 4 hours and with tunicamycin, n-BP and rapamycin for 24 hours with the addition of vehicle, DMSO, simultaneously in the relevant experimental controls. The data is represented by means and standard deviation (SD). Two-way ANOVA along with a Bonferroni post-hoc test was used to analyse the effect of the interaction of drug and *RUBCN* mutation on cell survival. P-values indicate the effect of drug *p<0.05; **p<0.005.

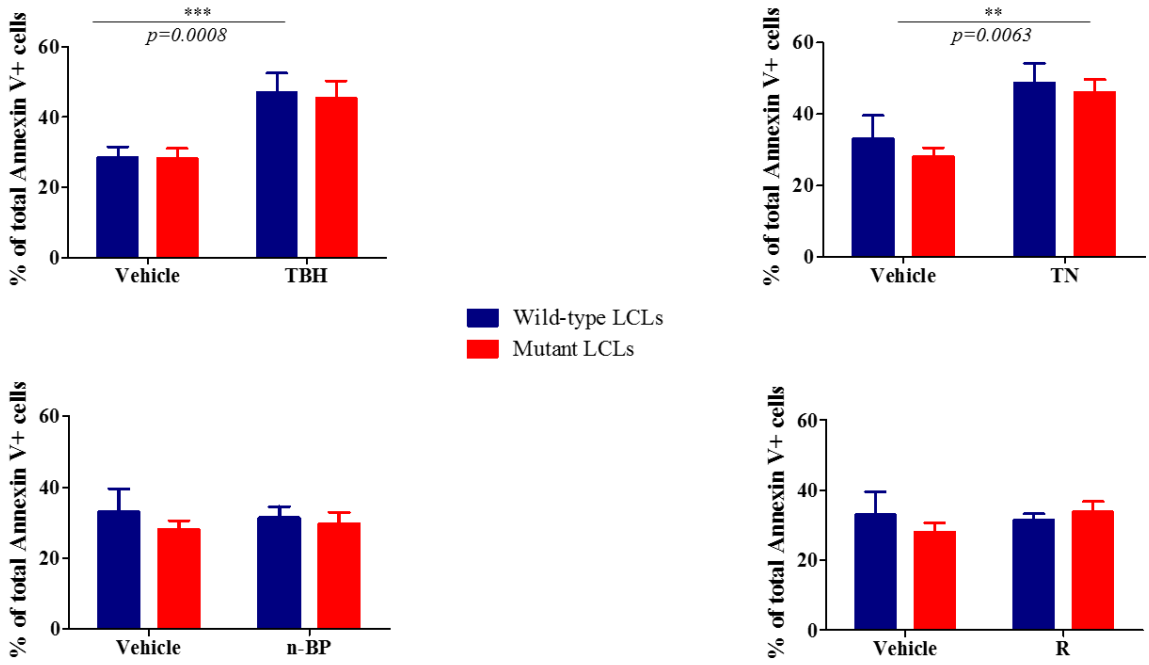

Figure 6-7 Investigation of the effect of the *RUBCN* mutation on total Annexin V positive cells

Annexin V positive cells undergoing total apoptosis measured from fluorescence-activated cell sorting (FACS) profiles in eight LCLs, four mutant and four wild type individuals of pedigree SM331, to investigate the effect of mutation on cell viability. LCLs were treated with TBH for 4 hours and with tunicamycin, n-BP and rapamycin for 24 hours with the addition of vehicle, DMSO, simultaneously in the relevant experimental controls. The data is represented by means and standard deviation (SD). Two-way ANOVA along with a Bonferroni post-hoc test was used to analyse the effect of the interaction of drug and *RUBCN* mutation on cell survival. P-values indicate the effect of drug *p<0.05; **p<0.005.

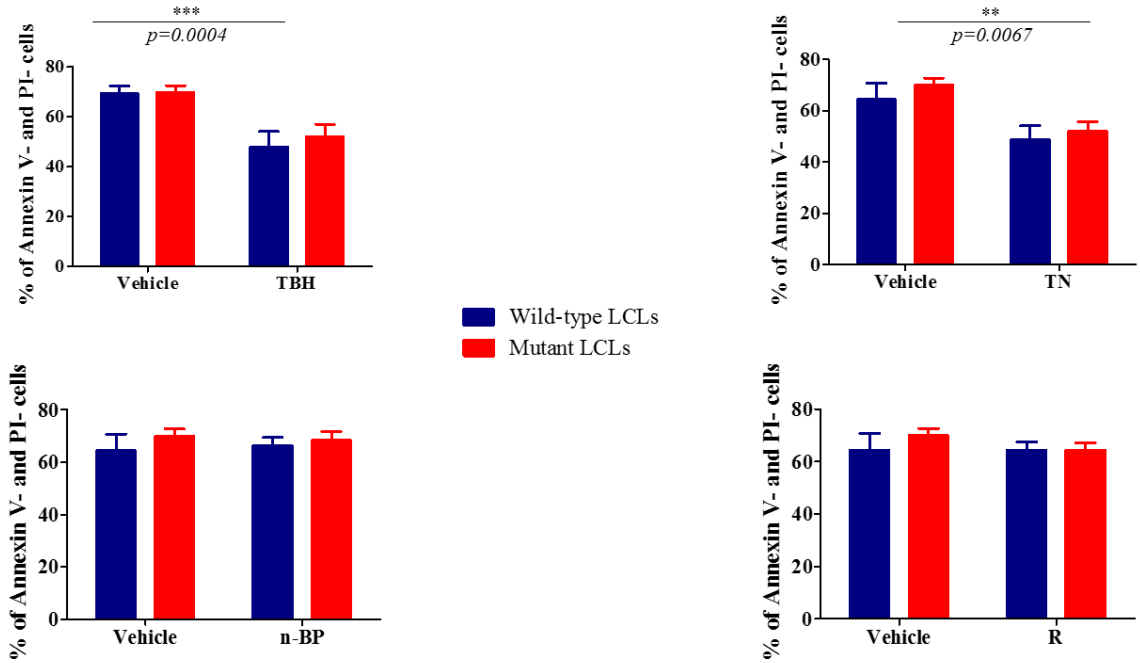

Figure 6-8 Investigation of the effect of the *RUBCN* mutation on viable cells

Annexin V and PI negative viable cells that did not undergo apoptosis measured from fluorescence-activated cell sorting (FACS) profiles in eight LCLs, four mutant and four wild type individuals of pedigree SM331, to investigate the effect of mutation on cell viability. LCLs were treated with TBH for 4 hours and with tunicamycin, n-BP and rapamycin for 24 hours with the addition of vehicle, DMSO, simultaneously in the relevant experimental controls. The data is represented by means and standard deviation (SD). Two-way ANOVA along with a Bonferroni post-hoc test was used to analyse the effect of the interaction of drug and RUBCN mutation on cell survival. P-values indicate the effect of drug *p<0.05; **p<0.005.

6.4 Discussion

In order to investigate the effect of mutation on pathways relevant to Rubicon function, we selected different drugs to induce or inhibit autophagy/endosomal pathways and LC3-associated phagocytosis. We selected markers for ER stress (*XBP1*, *DNAJC10*), autophagy pathway proteins (*VPS34*, *UVRAG*), endosomal pathway (*RAB7A*), lysosomal pathway (*LAMP2*) and LC3-associated phagocytosis pathway protein (*NOX2*) in addition to the candidate gene (*RUBCN*). Compared to the experiments from chapter 6, we selected additional proteins from ER stress activated UPR and autophagy pathways in this experiment in order to understand the effect of the mutation on these pathways in detail in addition to investigating the effect of mutation in LC3-associated pathways. We used tunicamycin, a mild ER stress inducer; t-BH, oxidative stress inducer and rapamycin, autophagy inducer to induce these pathways. We also used n-BP to inhibit autophagy. The concentration of these drugs for inducing the related pathways was based on dose-response curves generated by other members of the group (Intan Barul Akma Bakhtiar and Luigi Montibeller: unpublished data).

6.4.1 Effect of drugs on cellular pathways

Tunicamycin showed induction of ER stress and autophagy as evident by the significant upregulation of *XBP1* and *VPS34* in control LCLs. We did not observe any significant effects of the autophagy inhibitor, n-BP on the expression of any of the genes studied in control LCLs although a significant downregulation of *XBP1* was observed in mutant LCLs. We also observed a significant downregulation in the expression of *RUBCN* with rapamycin treatment in both control and mutant LCLs which was not observed before (Chapter 5 experiments) as the data obtained previously showed greater variation, whereas, the data obtained in the present experiment was very close and showed a significant effect of the drug. Downregulation of *RUBCN*, the negative regulator of autophagy/endocytosis, indicates a possible upregulation of

these pathways. A significant downregulation was also observed in the expression of *DNAJC10*, *VPS34*, *UVRAG* and *RAB7A* in control LCLs with rapamycin. We could not observe the effect of t-BH at the mRNA level in control LCLs because of the lower number of samples ($n<3$) as the statistical analysis could not be performed. In mutant LCLs, t-BH did not show any significant effect on the expression of the genes studied. This might have resulted from the lower drug exposure time or the lower drug concentration used.

6.4.2 Effect of mutation on cellular pathways

At basal levels, we observed a significant downregulation in the expression of *RAB7A* with no added vehicle in the presence of mutation. A significant downregulation was also observed in the expression of *DNAJC10* and *NOX2*, and a small though non-significant change in *RUBCN* with vehicle added for 4 hours. Since the mutation effects were either present in medium without vehicle or in medium with added vehicle but not both, it may indicate that the vehicle, DMSO, might be interfering with the activity of the pathways in some way although we found no significant effect of DMSO on the expression of any gene. We, therefore, analysed the effect of drugs with their relevant vehicle controls to find the effect of the drug. Since a significant downregulation was observed in the expression of *DNAJC10*, *NOX2* and *RAB7A* at least in one of the basal levels studies, this indicates that the mutation is most probably affecting these pathways to a certain extent and hence, the effect of the mutation on these pathways should be focused more in further studies.

One interesting and important observation is that the mutation did not affect the expression of proteins that interact with Rubicon at the N-terminal (Vps34 and UVRAG), whereas, there is a strong effect of the mutation on genes that interact with Rubicon near the C-terminal of protein (*NOX2* and *RAB7A*). This might indicate that even if the mutation affects the protein structure of Rubicon, Rubicon might still be able to interact with UVRAG and other

components of the PI3KC3 complex via Vps34 with which it interacts via its RUN domain (Sun et al., 2011a) near the N-terminal (Figure 6-9). This might explain why the mutation shows no effect on the genes from the autophagy pathway. The interaction of Vps34 with other components of PI3KC3 complex has been explained in detail in the discussion section of chapter 5. This indicates the importance of testing the protein-protein interaction of Rubicon with all the proteins showing the effect of mutation to further confirm this observation.

The effect of mutation observed on *RAB7A* indicates the possible effect of mutation on the endosomal pathway. A mutation in Rubicon has already been linked to a neurodegenerative disorder, ataxia, where the mutation abrogates the last domain of Rubicon that binds to Rab7 and impairs the endosomal localisation of Rubicon (Assoum et al., 2013). Rubicon binds to the UVRAG containing PI3KC3 complex to negatively regulate endosomal pathway. Active Rab7 competes with UVRAG for binding to Rubicon and releases UVRAG from Rubicon, which leads to endosomal maturation (Sun et al., 2010b).

We have used NOX2 as a marker for both LAP and oxidative stress as it is involved in ROS production. The effect of the mutation observed on *NOX2* indicates the possible effect of the *RUBCN* mutation on the LAP pathway. NOX2 is a key marker of phagocytes. Very low NOX2 activity has been proposed to promote autoimmune neurodegeneration (Sorce et al., 2017) and very high expression of NOX2 has been reported in mouse models of prion disease (Sorce et al., 2014) and in mouse models of familial ALS (Sorce et al., 2017). We have found a downregulation in the expression of *NOX2* at the mRNA level in the presence of the mutation. Unlike canonical autophagy where Rubicon plays an inhibitory role, Rubicon is required for LAP as the cells lacking Rubicon fail to recruit LC3 II to phagosomes that contained cargo for degradation (Martinez et al., 2015, Yang et al., 2012). The Rubicon containing PI3KC3 complex produces PI(3)P which stabilizes and activates the NOX2 complex leading to the production of (ROS) in the lumen of phagosomes. Both PI(3)P and ROS are required for LAP

(Martinez et al., 2015). Hence, if Rubicon activity is impaired, then PI(3)P will not be produced by the Rubicon containing PI3KC3 complex, which will lead to impaired ROS production. Since we have seen no effect of mutation on the expression of PI3KC3 complex proteins, this may not be affected by the mutation but studies have also shown that Rubicon interacts directly with a subunit of NOX2, $p22^{phox}$, via its serine rich domain and stabilizes the NOX2 complex for optimal ROS production (Yang et al., 2012). Thus, impaired Rubicon can still lead to impaired ROS production affecting LAP, as absence of ROS has been reported to cause impaired recruitment of downstream LAP components (Martinez et al., 2015, Yang et al., 2012). Hence, Rubicon plays a vital role in the LAP pathway by its involvement in two complexes required for PI(3)P and ROS production. Disturbance of the LAP pathway has been linked to the auto-immune disease, systemic lupus erythematosus (SLE) (Martinez et al., 2016), but not to ALS so far and disturbance in the activity of the NOX2 complex has been reported to cause autoimmune chronic inflammatory conditions (Martinez et al., 2016).

Our observations that correlations between *RUBCN* and *NOX2* are lost in the presence of the mutation further strengthens the assumption that the mutation is probably affecting the LAP pathway and its possible link to ALS, which requires further investigation.

We also observed a significant effect of mutation on the expression of *DNAJC10*. In Sporadic ALS cases, DNAJC10 expression was shown to be upregulated in a recent study (Montibeller and de Belleroche, 2018), whereas, we found a significant downregulation in the expression of *DNAJC10* in the presence of mutation indicating the possible effect of the mutation on ER stress activated pathways. In a study using the zebrafish model, increased autophagy dependent protein degradation was observed with knock-down of the analogue of DNAJC10 (Munoz-Lobato et al., 2014) which indicates a possible interaction between DNAJC10 and regulation of autophagy pathway, and hence, with Rubicon. Although the pathways of autophagy and ER

stress are tightly linked (Smith and Wilkinson, 2017), no link has been reported between the function of the co-chaperone DNAJC10 and Rubicon so far.

6.4.3 Correlation between the expression of different pathway genes

The correlation between *RUBCN* and *NOX2* was lost in the presence of mutation indicating a possible effect of mutation on the interaction between the two genes. The same effect was obtained under oxidative stress but that could be because of the absence of any significant t-BH effect observed on the expression of both genes. Whether the correlation between the two genes is lost or not under oxidative stress will require the expression of the two genes to be studied with exposure to strong oxidative stress.

Since an effect of mutation was observed on the expression of *DNAJC10*, we tested the correlation between expression profiles of *VPS34* (autophagy gene) and *XBP1*s (ER stress gene) especially under TN induced ER stress. A strong positive correlation was observed between the mRNA expression of the two genes in control and mutant cell lines at basal levels and also under ER stress independent of the presence of the mutation. This correlation indicated the link between ER stress and autophagy, that has already been reported in literature, and could also help in investigating further the possible link between Rubicon and DNAJC10 since Rubicon interacts with VPS34 and DNAJC10 is a part of the endoplasmic reticulum-associated degradation complex (ERAD complex) induced by ER stress.

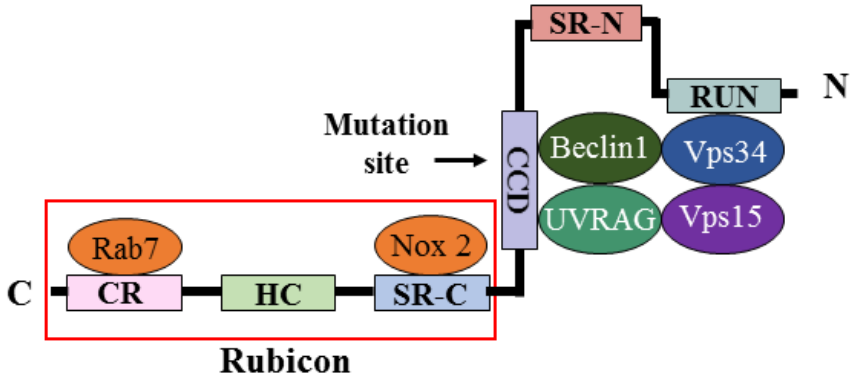

Figure 6-9 Interaction of Rubicon with UVRAG containing PI3KC3 complex, Rab7 and Nox2

Rubicon interacts with multiple proteins of the UVRAG containing PI3KC3 complex including Vps34, the catalytic subunit of the complex, near the N terminal. Hence, even if the mutation we have detected in Rubicon affects the interaction of Rubicon with UVRAG and Beclin 1, Rubicon may still bind to the complex through its interaction with Vps34 which in turn interacts on its own with other components of PI3KC3 complex. Effect of the mutation has been found on two other proteins that interact with Rubicon but are not a part of PI3KC3 complex, Nox2 and Rab7 (indicated in red box).

6.4.4 Effect of mutation on cell survival

We also investigated effects of mutation on cell survival. In this experiment, we treated cells with tunicamycin, n-BP, t-BH and rapamycin in addition to staurosporine. Staurosporine is used in assays of apoptosis as a positive control for apoptosis induction (Kabir et al., 2002). As described in chapter 5, we hypothesized that the presence of mutation could disrupt the normal cellular processes by the formation of protein aggregates. On the other hand, as the role of the gene is to act as a negative regulator of autophagy, a loss of function mutation at basal levels could result in an upregulated level of autophagy. Continuous upregulated autophagy may be a signal of an unresolved problem inside the cell which can trigger apoptotic cell death. We wanted to investigate the effect of mutation on cell survival under oxidative stress, ER stress, under induced autophagy by mTOR dependant pathway and with autophagy inhibition to see if the effect could be reversed by inhibition of autophagy. The presence of a constant ER stress and oxidative stress leads to apoptosis (Cao and Kaufman, 2014).

In our LCL model, staurosporine (data shown already in Chapter 5), tunicamycin and t-BH showed a significant increase in cell death but n-BP and rapamycin did not show a significant effect on cell survival. n-BP has been shown to downregulate autophagy and caspase-3 (Hsueh KW et al., 2016) and may thus have protected cells from apoptotic cell death. Since the mode of action of rapamycin is not directly related to induction of apoptosis, rapamycin is not necessarily expected to kill cells either. Overall, our results suggest that the presence of the mutation does not affect cell viability.

In conclusion, the identified mutation in *RUBCN* significantly decreased the mRNA expression levels of *DNJC10*, *NOX2* and *RAB7A,* which are the marker genes for ER stress, oxidative stress and endosomal pathways, the three neuroprotective pathways. These results indicate that

RUBCN is most probably relevant to FALS but further experiments are needed to confirm the relation of *RUBCN* with the disease.

Chapter 7: Functional characterisation of *CLCN6* in FALS lymphoblastoid cell lines (LCLs)

7.1 Introduction

CLCN6 encodes for chloride transport protein 6 (ClC-6) that belongs to the family of chloride channel (CLC) proteins. The ClC family consists of 9 genes and based on their cellular localisation and function, they can be classified into two groups. The first group consists of ClC-1, ClC-2, ClC-Ka, and ClC-Kb proteins that are localised to plasma membrane and function as chloride channels. Proteins in the other group consisting of ClC-3 to ClC-7 are localised to the membranes of the endosomal-lysosomal system. ClC-3 is localised in late endosomes (Stobrawa et al., 2001), ClC-4 and ClC-5 are expressed in early and recycling endosomes (Mohammad-Panah et al., 2009, Piwon et al., 2000) and ClC-7 is prominently expressed in late endosomes and lysosomes (Kasper et al., 2005). These proteins are thought to facilitate in the acidification of the endosomal-lysosomal compartments by providing an electric shunt for the efficient pumping of the H^+-ATPase (Figure 7-1) (Jentsch et al., 2002, Zhao et al., 2009).

ClC-6 is localised to the endoplasmic reticulum (Buyse et al., 1998) and late endosomal membrane (Ignoul et al., 2007), where it functions as a Cl^-/H^+ antiporter (Neagoe et al., 2010). The protein is broadly expressed in different tissues (Brandt and Jentsch, 1995) but predominantly in the nervous system (Poet et al., 2006). It has four isoforms but only one of them encodes for the 869-amino-acid canonical ClC-6 protein while the remaining three isoforms are truncated (Eggermont et al., 1997). The closest homolog of *CLCN6* is *CLCN7* which shows 45% sequence homology with *CLCN6* (Brandt and Jentsch, 1995).

ClC-6 is the least well characterised member of ClC protein family, therefore, very little is known about the activity of the protein inside the cell. Based on the available literature and some studies performed in our laboratory, we hypothesized that ClC-6 is involved in the ER stress activated unfolded protein response (UPR) pathway since the *CLCN6* gene contains a consensus sequence that is recognised by the transcription factors that are activated in response to ER stress. For the functional characterisation of the identified mutation, we used lymphoblastoid cell lines (LCLs) as our cellular model which were derived from individuals harbouring the mutation and family members lacking the mutation of pedigree SM821. LCLs are a good model for studying the effects of a mutation as they contain the pathways that have been linked to neurodegeneration. The LCLs were previously established by the in-vitro infection of B-cells with Epstein-Barr virus (EBV) resulting in the immortalisation of the cells. We investigated the effect of the FALS-associated mutation on the ER stress activated UPR pathway, autophagy/endocytosis pathways and on cell survival. Please refer to the introduction section of chapter 5 for the description of ER stress and its activated pathways, the endosomal pathway, autophagy pathway, apoptosis and for the mode of action of the drugs used.

7.1.1 Objectives

We hypothesized that if the mutation is a loss of function mutation, it will disrupt aspects of endoplasmic reticulum function and/or endosomal pathway by effecting their pH or Cl^- concentration owing to the role of *CLCN6* as a Cl^-/H^+ antiporter and will also effect cell survival. To test this hypothesis, we performed the following experiments

3. Analysis of the cell survival using flow cytometry with the FITC- Annexin V assay.
4. Analysis of the changes in gene expression using two techniques: quantitative PCR (qPCR) and western blotting.

We designed these experiments to test the effects of the mutation under both basal and stress conditions. We used tunicamycin and thapsigargin to induce ER stress and the downstream autophagy pathway and rapamycin was used to induce autophagy.

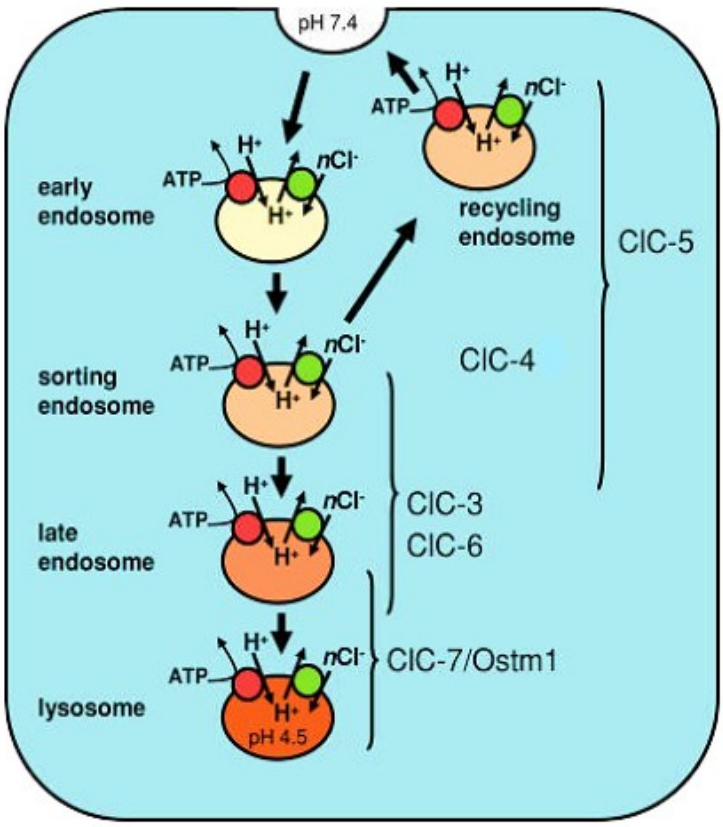

Figure 7-1 Subcellular localization of ClC-3 to ClC-7 proteins in endosomal-lysosomal system

The endosomal-lysosomal system contains different vesicles consisting of early endosomes, recycling endosomes, sorting endosomes, late endosomes, and the lysosome. The vesicles in the endosomal pathway have a decreasing pH along the way to lysosomes starting from the neutral extracellular pH of ~7.4 to the acidic pH of ~4.5. The decreasing pH is achieved mainly by the activity of the ATP-dependent proton pumps which require a net influx of negative charge for maintaining electroneutrality thought to be mediated by ClC family proteins. ClC-3 to ClC-7 are the Cl^-–H^+ antiporters. ClC-3 resides in late endosomes, ClC-4 and ClC-5 are expressed in early and recycling endosomes, ClC-6 predominantly on late endosomes and ClC-7 is expressed in late endosomes and lysosomes. Adapted from (Eggermont et al., 1997).

7.2 Materials and methods

The materials and methods used for the experiments described in this chapter are the same as previously described in Chapter 5. The only difference is in the samples used. The LCLs used for the study of *CLCN6* mutation were derived from pedigree SM821. LCLs from eight cell lines were used, five with the mutation and three without the mutation. LCLs were unavailable from one at-risk and one control individual, so they could not be included in this functional study. In order to increase the number of controls, two additional control LCLs from other families were included in the study. This provided the two groups used for the functional studies, five cell lines with a mutation and five without mutation. The Western blotting experiment described in this chapter was performed together with Ayesha Hashmi, an MSc research student, as part of her research project under my supervision.

The drugs and concentrations used for inducing cell stress were the same as described before in chapter 5. The primer pairs used to investigate the expression of genes investigated in this chapter are given in Table 7-1 and the antibodies used for the protein expression analysis are as follows:

7.2.1 Primary antibodies

Rabbit polyclonal anti-DNAJC10 antibody (1:1000, Proteintech$^{TM)}$, rabbit polyclonal anti-GRP78/BIP antibody (1:1000, Proteintech^{TM}), rabbit polyclonal anti-Rab7 antibody (1:1000, Cell Signalling), rabbit polyclonal anti-LC3B antibody (1:2000, Sigma Aldrich), mouse monoclonal anti GAPDH antibody (1:2000, Santa Cruz).

7.2.2 Secondary antibodies

Peroxidase labelled anti-mouse IgG (H+L) (Vector laboratories), peroxidase labelled anti-rabbit IgG (H+L) (Vector laboratories).

7.2.3 Statistical analysis

We used Two-way ANOVA along with a Bonferroni post-hoc to analyse the effect of the interaction of drug and mutation on cell survival. Confirmation of the effect of drugs and investigation of the effect of mutations was performed using Student's t-test where there was normal distribution of data. Where it was not normally distributed or the variance between the groups being tested did not show equal variance, nonparametric Mann-Whitney test was used. Results were given as mean ± Standard error of mean (SEM). The changes in gene expression have been given as fold change (FC) value. GraphPad Prism 5 software was used for performing the tests and for drawing graphs. Inverse of ΔCt values were used to draw graphs as the inverse represents the right direction of the gene expression change compared to ΔCt values. There was a lot of variation in the expression of some genes we tested but the variation was very reasonable and similar in most groups and therefore were comparable for statistical analysis.

Table 7-1 Primer sequences for qPCR

Gene	Primers	Product size (bp)
Candidate gene		
CLCN6	Forward: GAGTCTTAGAGAGCCTCCTTGTGTC Reverse: ACACAGCAGAGAAGGCACAA	365
ER stress genes		
XBP1 total	Forward: GCTCAGACTGCCAGAGATCG Reverse: TCTTCAGCAACCAGGGCATC	188
XBP1 spliced	Forward: AGAGTCTGATATCCTGTTGG Reverse: AGTTCATTAATGGCTTCCAG	189
HSPA5	Forward: TCAAGTTCTTGCCGTTCAAGG Reverse: AAATAAGCCTCAGCGGTTTCTT	148
DNAJB9	Forward: TTTCCAGACACGCCAGGATG Reverse: GTCCTGCAGTGCTTGCTAGA	195
Autophagy genes		
LAMP2	Forward: CGTTCTGGTCTGCCTAGTCC Reverse: CAGTGCCATGGTCTGAAATG	173
SQSTM1 (P62)	Forward: CAGTCCCTACAGATGCCAGA Reverse: TCTGGGAGAGGGACTCAATC	142
Endosomal pathway gene		
RAB7A	Forward: CACTCATGAACCAGTATGTG Reverse: CATATCTGCATTGTGACTAGC	118
House-keeping gene		
ACTB	Forward: GACAACGGCTCCGGCATGTG Reverse: CCTTCTGACCCATGCCCAC	121

Primers used to amplify the exome regions of genes by qPCR to study their expression at the mRNA level for investigating the effect of the mutation in LCLs from the individuals of pedigree SM821.

7.3 Results

7.3.1 Confirmation of DNA sequence in LCLs

The DNA sequence of LCLs from eight cell lines was determined. LCLs were unavailable from one at-risk and one control individual. The presence of the mutation in the index case and a further family member with FALS, found through lymphocyte sequencing, was confirmed in LCLs. In addition, the mutation was also present in three other individuals, putting them at risk of developing the disease, but absent from three further individuals (Figure 7-2). This provided the two groups for the functional studies, five cell lines with mutation and three without (see chapter 3 for further details). In order to increase the number of controls, two additional controls from other families were included in the study.

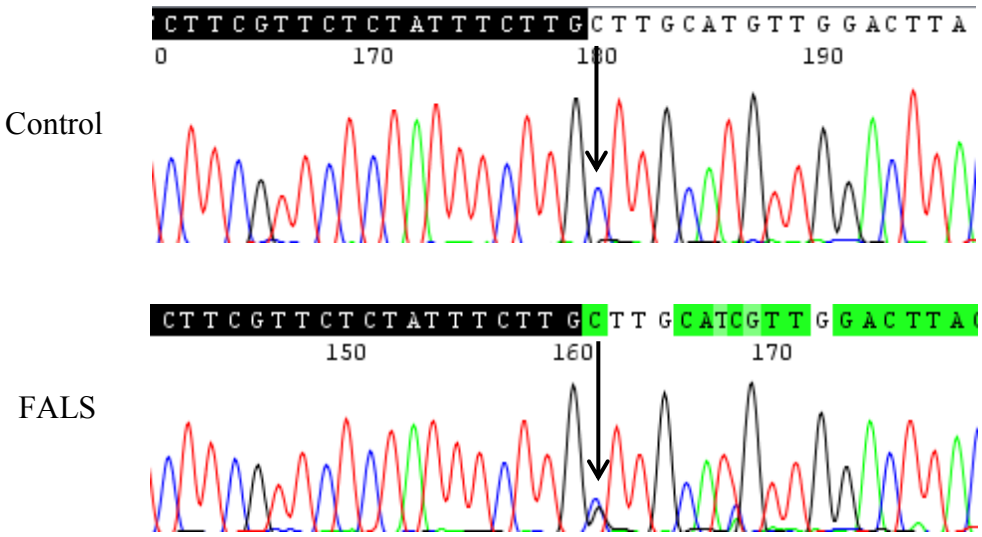

Figure 7-2 Chromatograms of *CLCN6* sequence indicating the nucleotide transversion in a FALS case compared to a control from pedigree SM821.

DNA was extracted from the LCLs of two FALS cases, three at-risk individuals and three controls from pedigree SM821. A *CLCN6* gene segment containing the mutation was sequenced using primer set given in Table 7-1. The two chromatograms shown here indicate the difference between the DNA sequence of *CLCN6* in LCLs from a control and a FALS case. The arrows indicate the position of a heterozygous transversion, C to G, present in a FALS case compared to control.

7.3.2 Investigation of the effect of the mutation on cell survival

We performed flow cytometry analysis on LCLs to investigate the effect of the mutation on cell survival under basal and stress conditions. We hypothesized that the presence of the mutation could lead to increased cell death under cell stress conditions. LCLs were exposed to ER stress by tunicamycin and thapsigargin and autophagy was induced by rapamycin. Staurosporine was used as a positive control for apoptotic cell death. Staurosporine, tunicamycin, thapsigargin and rapamycin caused a significant increase in cell death (Table 7-2).

The presence of the mutation caused a significant increase in cell death ($p<0.05$) at basal levels (10% increase) and under thapsigargin treatment (8% increase) (Table 7-2) (Figure 7-3 to Figure 7-6). These results strongly suggest an impairment in cellular mechanisms caused by the mutation affecting cell survival both under basal and cell stress conditions.

Table 7-2 Investigation of the effect of mutation on cell survival

Stage	Interaction between mutation and drug	Effect of drug	Effect of mutation
TN total apoptosis	0.3130	P<0.0001 ↑	0.2174
TN early apoptosis	0.1471	P<0.0001 ↑	0.5421
TN late apoptosis	0.7295	P<0.0001 ↑	0.1658
TN viable cells	0.2044	P<0.0001 ↓	0.1549
TG total apoptosis	0.5633	0.0037 ↑	0.0494 ↑
TG early apoptosis	0.6342	0.0009 ↑	0.8000
TG late apoptosis	0.5741	0.0692	0.0920
TG viable cells	0.5538	0.0049 ↓	0.0351 ↓
R total apoptosis	0.4054	0.0299 ↑	0.1009
R early apoptosis	0.6491	0.0114 ↑	0.9685
R late apoptosis	0.3856	0.0947	0.1177
R viable cells	0.3263	0.0864	0.0670
S total apoptosis	0.9020	0.0059 ↑	0.0666
S early apoptosis	0.8670	0.0017 ↑	0.9645
S late apoptosis	0.9402	0.4609	0.0642
S viable cells	0.8621	0.0082 ↓	0.0554

P values obtained from a two-way ANOVA test along with Bonferroni post-hoc correction for investigating the effect of the interaction of drug and *CLCN6* mutation on cell survival. Ten LCLs, five mutant and five wild type individuals, of pedigree SM281, were treated with staurosporine for 4 hours, thapsigargin for 6 hours, tunicamycin and rapamycin for 24 hours with the addition of vehicle, DMSO, simultaneously in the relevant experimental controls. Fluorescence-activated cell sorting (FACS) was performed with FITC-Annexin V assay was for cell survival analysis. Values in red indicate significant values, $p<0.05$. Arrows indicate an upregulation or downregulation in the expression of the gene. Values in red indicate a significant effect, $p<0.05$.

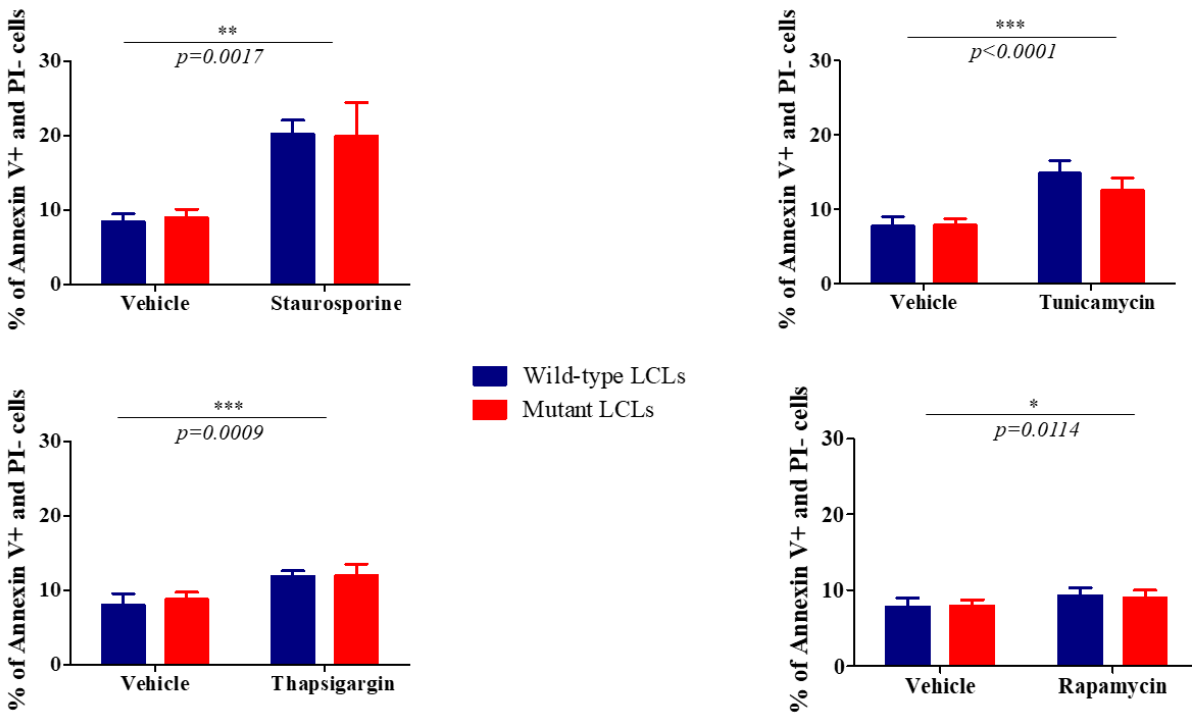

Figure 7-3 Investigation of the effect of the *CLCN6* mutation on early apoptosis

Annexin V positive cells undergoing early apoptosis measured from fluorescence-activated cell sorting (FACS) profiles in ten LCLs, five mutant and five wild type individuals, of pedigree SM821, to investigate the effect of mutation on cell viability. LCLs were treated with staurosporine for 4 hours, thapsigargin for 6 hours, tunicamycin and rapamycin for 24 hours with the addition of vehicle, DMSO, simultaneously in the relevant experimental controls. The data is represented by means and standard deviation (SD). Two-way ANOVA along with a Bonferroni post-hoc test was used to analyse the effect of the interaction of drug and *CLCN6* mutation on cell survival. P-values indicate the effect of drug. *p<0.05; **p<0.005; ***p<0.005.

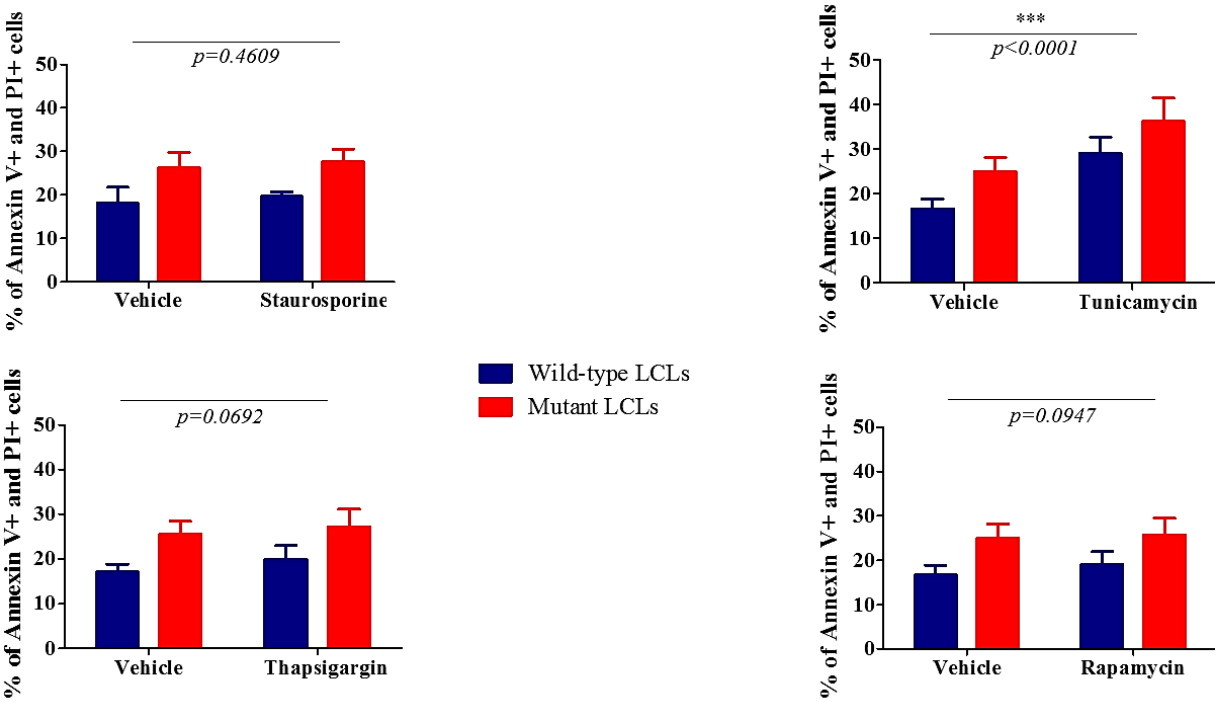

Figure 7-4 Investigation of the effect of the *CLCN6* mutation on late apoptosis

Annexin V positive cells undergoing late apoptosis measured from fluorescence-activated cell sorting (FACS) profiles in ten LCLs, five mutant and five wild type individuals, of pedigree SM821, to investigate the effect of mutation on cell viability. LCLs were treated with staurosporine for 4 hours, thapsigargin for 6 hours, tunicamycin and rapamycin for 24 hours with the addition of vehicle, DMSO, simultaneously in the relevant experimental controls. The data is represented by means and standard deviation (SD). Two-way ANOVA along with a Bonferroni post-hoc test was used to analyse the effect of the interaction of drug and *CLCN6* mutation on cell survival. P-values given in black indicate the effect of drug. ***p<0.005.

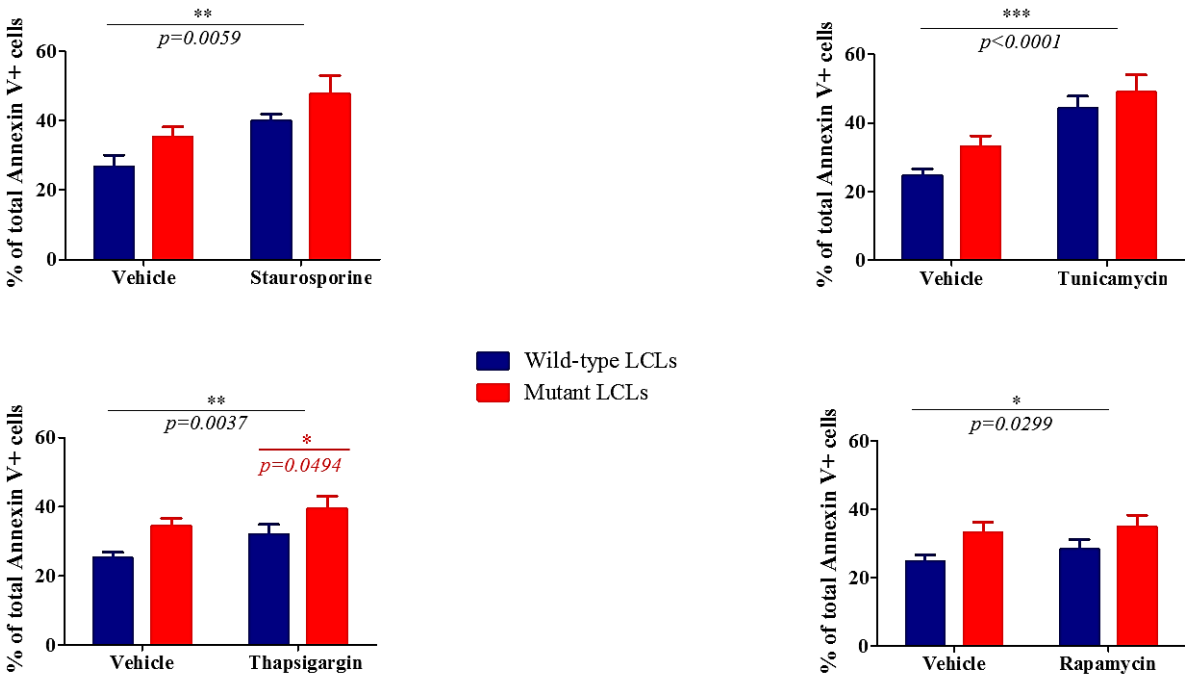

Figure 7-5 Investigation of the effect of the *CLCN6* mutation on total Annexin V positive cells

Annexin V positive cells undergoing both early and late apoptosis measured from fluorescence-activated cell sorting (FACS) profiles in ten LCLs, five mutant and five wild type individuals, of pedigree SM821, to investigate the effect of mutation on cell viability. LCLs were treated with staurosporine for 4 hours, thapsigargin for 6 hours, tunicamycin and rapamycin for 24 hours with the addition of vehicle, DMSO, simultaneously in the relevant experimental controls. The data is represented by means and standard deviation (SD). Two-way ANOVA along with a Bonferroni post-hoc test was used to analyse the effect of the interaction of drug and *CLCN6* mutation on cell survival. P-values given in black indicate the effect of drug and in red and green indicate the effect of mutation. *p<0.05; **p<0.005; ***p<0.005.

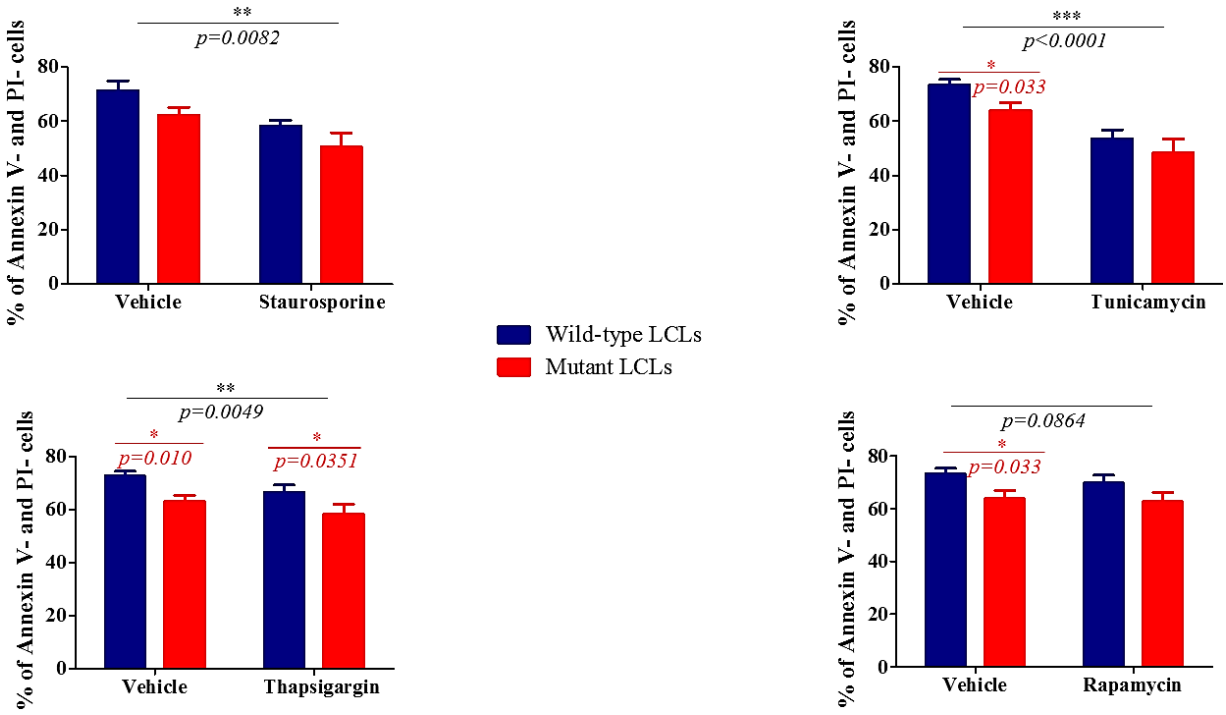

Figure 7-6 Investigation of the effect of the *CLCN6* mutation on viable cells

Annexin V and PI negative viable cells that did not undergo apoptosis measured from fluorescence-activated cell sorting (FACS) profiles in ten LCLs, five mutant and five wild type individuals, of pedigree SM821, to investigate the effect of mutation on cell viability. LCLs were treated with staurosporine for 4 hours, thapsigargin for 6 hours, tunicamycin and rapamycin for 24 hours with the addition of vehicle, DMSO, simultaneously in the relevant experimental controls. The data is represented by means and standard deviation (SD). Two-way ANOVA along with a Bonferroni post-hoc test was used to analyse the effect of the interaction of drug and *CLCN6* mutation on cell survival. Unpaired Student's t-test was performed for the effect of mutation at basal levels. P-values given in black indicate the effect of drug and in red indicate the effect of mutation. *p<0.05; **p<0.005; ***p<0.005.

7.3.3 Investigation of the effect of mutation on cellular pathways

We investigated the effect of the identified mutation on the autophagy/endosomal pathways in LCLs obtained from pedigree SM821. The LCLs were treated with tunicamycin, thapsigargin and rapamycin along with the selection of following marker proteins to investigate the effect on pathways: ER stress (*XBP1*, *DNAJB9*, *HSPA5*), autophagy pathway (*SQSTM1*), endosomal pathway (*RAB7A*) and lysosomal pathway (*LAMP2*) for this study. We investigated the effect of the mutation at both mRNA and protein level. Each gene studied was a separate experiment and functions in a different way in the pathways. The effect of the drugs was confirmed in the control cell lines as described in chapter 5 and showed the expected results as explained below.

7.3.3.1 Expression of UPR genes at the mRNA level

7.3.3.1.1 Effect of drugs

Tunicamycin caused a significant upregulation (p=<0.05) of ER stress markers *XBP1* total, *XBP1*s and *HSPA5* in control (FC=2.59, 4.43, 3.07 respectively) and mutant cell lines (FC=4.15, 2.18, 3.30 respectively) and in *DNAJB9* (p=<0.05, FC=4.15) in control cell lines. Thapsigargin caused a significant upregulation in the expression of *XBP1 total* in both control (FC=2.87) and mutant LCLs (FC=5.09) and in *XBP1s* in mutant LCLs (FC=1.84). The upregulation of these genes by both drugs confirmed the activation of UPR pathway. Rapamycin caused a significant downregulation in the expression levels of *XBP1s* (p=0.04, FC=0.67) and a small but non-significant change in the expression levels of *HSPA5* in mutant LCLs (p=0.052) (Table 7-3).

7.3.3.1.2 Effect of mutation

We observe a significant downregulation in the expression levels of *DNAJB9* (p=0.05, FC= 0.46) in the presence of the mutation under tunicamycin treatment. We also observed a

significant downregulation in the expression levels of *HSPA5* (FC=0.43) with mutation under rapamycin treatment (Table 7-4). These findings illustrate that the ER stress response is impaired by the mutation.

7.3.3.2 Expression of autophagy and endosomal pathway genes at the mRNA levels

7.3.3.2.1 Effect of drugs

Thapsigargin caused a significant upregulation in the expression levels of *RAB7A* (p= 0.015, FC=1.66) in mutant LCLs. Tunicamycin caused a small but non-significant change in the expression levels of *LAMP2* in both wild type and mutant cell lines (p=0.07). It caused no effect on the expression of *CLCN6*, *SQSTM1* and *RAB7A*. Rapamycin did not have an effect on the expression of any gene (Table 7-3).

7.3.3.2.2 Effect of mutation

No significant effect of the mutation was observed on the expression of any of the genes investigated (*CLCN6, SQSTM1, RAB7A, LAMP2*) at basal levels or under cell stress (Table 7-5) (Figure 7-7). These findings suggest that the autophagy and endosomal pathways are probably not affected by the mutation at mRNA expression levels.

7.3.3.3 Effect of mutation on cellular pathways at protein level

We observed a significant downregulation in the protein expression of DNAJC10 ($p<0.05$, FC=0.23) in the presence of thapsigargin treatment that suggests that the mutation disrupts the UPR pathway (Figure 7-8). No effects of the mutation were observed on the expression of other genes. Unfortunately, we were not able to analyse the effect of mutation on the expression of all genes under basal and stress conditions because of the poor quality of sample protein extraction. We don't know what caused this and because time did not allow we were unable to

repeat them but we plan to repeat this in future. Please refer to the appendix section for the graphs on protein expression.

Table 7-3 Investigation of the effect of drug treatment on cellular pathways at the mRNA level.

	Wild type			Mutant		
	TN	TG	R	TN	TG	R
LAMP2	0.074	0.919	0.363	0.075	0.572	0.598
CLCN6	0.411	0.766	0.405	0.103	0.284	0.549
DNAJB9	0.009 ↑	0.632	0.453	0.232	0.628	0.370
HSPA5	0.009 ↑	0.236	0.742	0.005	0.834	0.053
***XBP1* total**	0.021 ↑	0.007 ↑	0.121	0.006 ↑	0.0134 ↑	0.675
***XBP1* spliced**	0.003 ↑	0.135	0.215	0.002 ↑	0.018 ↑	0.040 ↓
RAB7A	0.712	0.850	0.370	0.293	0.015 ↑	0.270
SQSTM1	0.642	0.824	0.826	0.772	0.094	0.718

P-values obtained from paired t-tests for investigating the effect of drug treatment on cellular pathways. LCLs were treated with tunicamycin and rapamycin for 24 hours and thapsigargin for 6 hours with the addition of vehicle in the relevant experimental controls simultaneously. The values of gene expression were normalised to the house-keeping gene β-actin. TN, tunicamycin treatment; TG, thapsigargin treatment; R, rapamycin treatment. Arrows indicate an upregulation or downregulation in the expression of the gene. Values in red indicate significant values, $p<0.05$.

Table 7-4 Investigation of the effect of *CLCN6* mutation on ER stress activated UPR pathway.

P values obtained by comparing the wild-type LCLs to mutant LCLs under different drug treatments				
	M	**TN**	**TG**	**R**
DNAJB9	0.8565	0.0496 ↓	0.7006	0.2784
HSPA5	0.6169	0.4288	0.7533	0.0315 ↓
***XBP1* total**	0.9230	0.9309	0.6657	0.4704
***XBP1*s**	0.8284	0.1178	0.3089	0.2222

Table 7-5 Investigation of the effect of *CLCN6* mutation on autophagy/endosomal pathway.

P values obtained by comparing the wild-type LCLs to mutant LCLs under different drug treatments				
	M	**TN**	**TG**	**R**
CLCN6	0.4271	0.3816	0.9175	0.6308
SQSTM1	0.1413	0.4974	0.5476	0.9750
RAB7A	0.9682	0.6901	0.6905	0.4127
LAMP2	0.7359	0.7705	0.8903	0.7102

P-values obtained from unpaired Student's t-tests investigating the effect of *CLCN6* mutation on autophagy/endosomal pathway. LCLs were treated with tunicamycin and rapamycin for 24 hours and thapsigargin for 6 hours with the addition of vehicle in respective experimental controls simultaneously. The values of gene expression were normalised to the house-keeping gene β-actin. M, no drug medium (basal levels); TN, tunicamycin treatment; TG, thapsigargin treatment; R, rapamycin treatment. Values in red indicate significant values, $p \geq 0.05$.

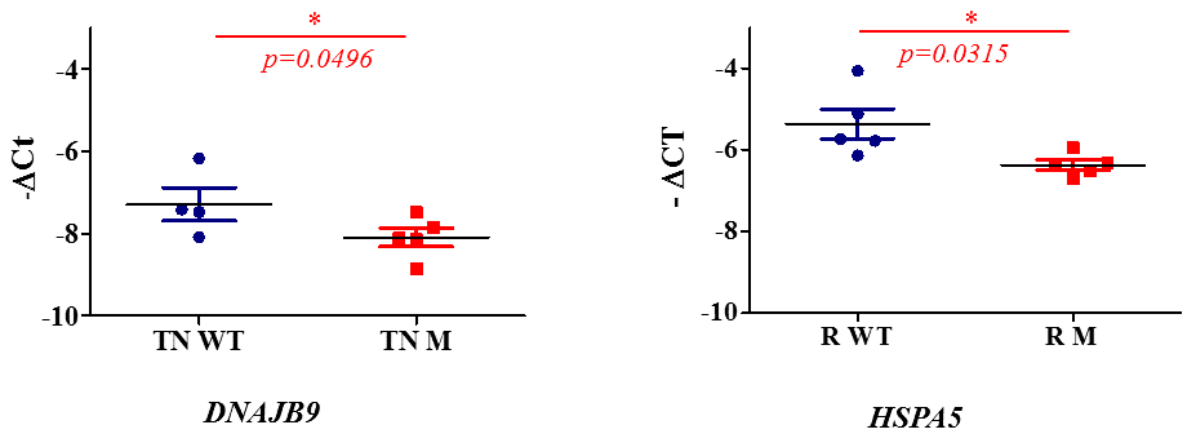

Figure 7-7 Effect of the mutation on the mRNA expression levels of the ER stress activated molecular chaperones in LCLs.

The mRNA expression levels of the ER stress activated molecular chaperones, *DNAJB9* and *HSPA5* in ten LCLs, five mutant and five wild type individuals, of pedigree SM821 to investigate the effect of mutation on UPR. The values of the mRNA expression of *DNAJB9* and *HSPA5* normalised to the house-keeping gene β-actin (-delta Ct) are represented by means and SEMs. Circles and squares show individual samples in the presence of ER stress inducers, tunicamycin and rapamycin. WT, wild type; M, mutant; TN, tunicamycin treatment; R, rapamycin treatment. Unpaired Student's t-tests was used for investigating the effect of mutation. P-values given above each graph in red indicate the effect of mutation. *p<0.05

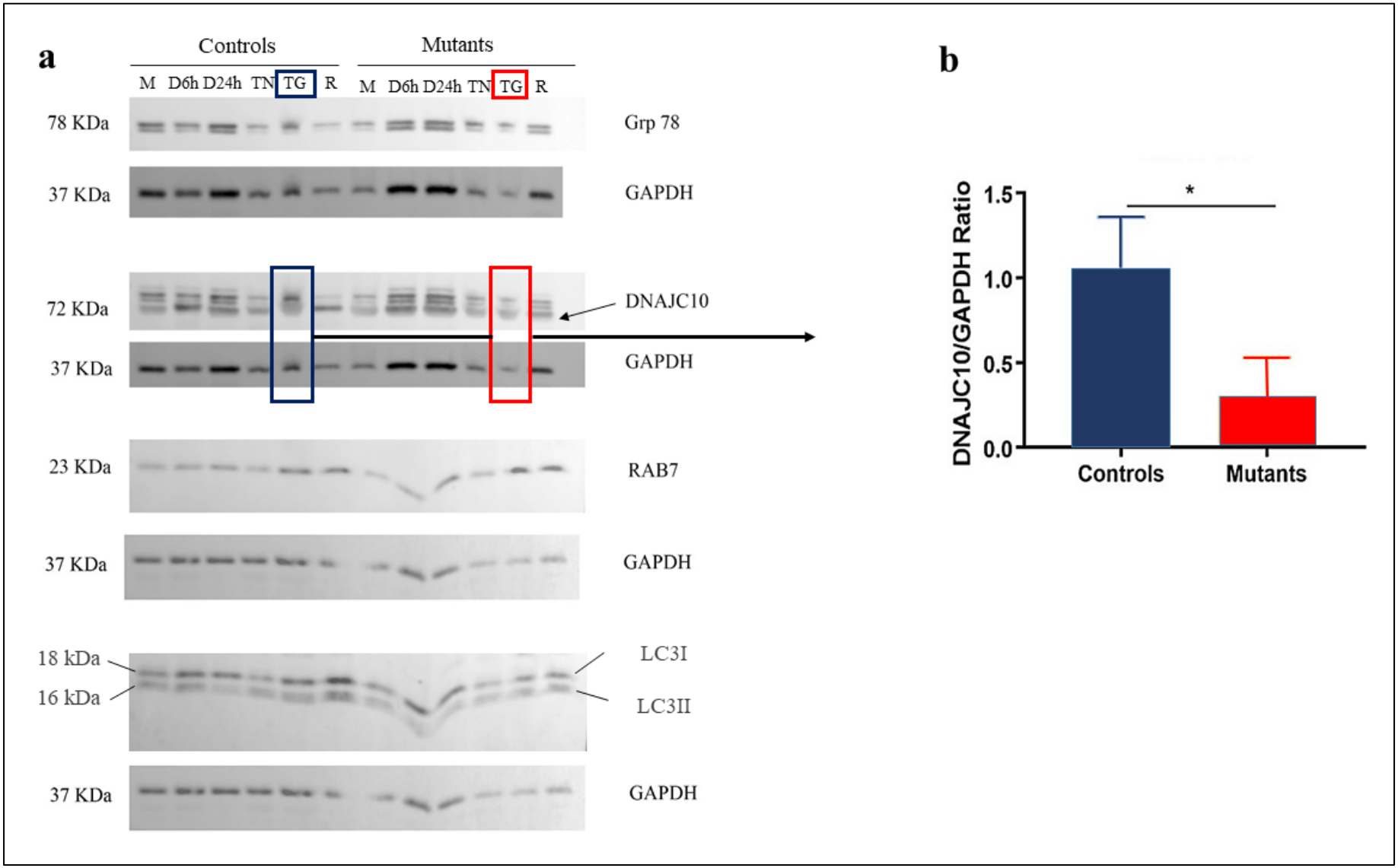
a
Controls
Mutants
M D6h D24h TN TG R
M D6h D24h TN TG R
78 KDa
Grp 78
37 KDa
GAPDH
72 KDa
DNAJC10
37 KDa
GAPDH
23 KDa
RAB7
37 KDa
GAPDH
18 kDa
16 kDa
LC3I
LC3II
37 KDa
GAPDH
b
DNAJC10/GAPDH Ratio
1.5
1.0
0.5
0.0
*
Controls
Mutants

Figure 7-8 Western blots of the UPR, autophagy and endosomal pathway genes in LCLs.

a) Western blot analysis for investigating the protein levels of UPR pathway markers, Grp78 and DNAJC10; autophagy markers, LC3II; and endosomal pathway marker, Rab7 in ten LCLs treated with tunicamycin, thapsigargin and rapamycin. LCLs were treated with tunicamycin and rapamycin for 24 hours and thapsigargin for 6 hours with the addition of vehicle, DMSO, simultaneously in the relevant experimental controls. The figure shows a representative control and a representative mutant cell line in each blot with all treatments. Quantitative analysis of protein bands was performed by densitometry and each protein was normalised against reference gene, GAPDH. M, untreated LCLs; D6h, Vehicle addition for 6 hours; D24h, vehicle added for 24 hours; TN, tunicamycin treatment; TG, thapsigargin treatment; R, rapamycin treatment. **Note:** The multiple bands visible in DNAJC10 blot above the bands for DNAJC10 are from Grp78.

b) Protein level analysis of DNAJC10 under thapsigargin treatment in LCLs, five mutant and five wild type individuals, of pedigree SM821. One sample from each group is indicated in a blue and a red box in part a. The data is represented by means and SEMs. Quantitative analysis of protein bands was performed by densitometry and the values were normalised against reference gene GAPDH. The unpaired Student's t-test was used for investigating the effect of mutation.

7.4 Discussion

In this chapter we have investigated the effects of the *CLCN6* mutation identified in FALS in pedigree SM821 on cell viability and the cellular pathways we expect to be linked to *CLCN6* activity at basal and cell stress conditions. The concentration of the drugs used for tissue treatment to induce cell stress was selected based on dose-response curves produced by Intan Barul Akma Bakhtiar previously in our lab (unpublished data).

7.4.1 Effect of drugs

In cell survival experiments, all the drugs used (staurosporine, tunicamycin, thapsigargin and rapamycin) showed a significant increase in cell death. In experiments on cellular pathways, we observed a significant upregulation in the expression of ER stress marker proteins with tunicamycin and thapsigargin indicating that both drug treatments induced the required ER stress in the tissues. The differences observed in the expression of ER marker genes under tunicamycin and thapsigargin treatment indicate the difference in the mode of action of the two drugs. A significant upregulation in the expression of *RAB7A* in mutant LCLs with thapsigargin treatment suggests a possible activation of the autophagy/endosomal pathway by ER stress inducers that has been illustrated in previous studies (Rashid et al., 2015). The effect of rapamycin on autophagy/endosomal pathway could not be confirmed as there were large variations in the data sets. Overall, we got good evidence of the presence of the desired cell stresses in our LCL model.

7.4.2 Effect of mutation on cell survival

Based on our hypothesis, we investigated whether the presence of mutation disrupts cellular mechanisms that eventually affect cell survival. We were highly encouraged to find that the mutant *CLCN6* caused significant increase in cell death both under basal conditions and with

thapsigargin treatment. The cell death may or may not have occurred as a result of apoptosis. Further studies are required to differentiate apoptosis from necroptosis as the Annexin V assay cannot differentiate the cause of cell death between apoptosis and necroptosis in the late stages of the disease. We then performed further investigation on the cellular pathways involved in the action of *CLCN6* to characterise the pathogenic mechanism involved underlying the cell death caused by the mutation.

7.4.3 Effect of mutation on cellular pathways

A significant downregulation in the expression of *DNAJB9* under tunicamycin treatment along with a significant downregulation in the expression of *HSPA5* under rapamycin treatment indicated the impairment of UPR pathway by the mutation. In addition, *XBP1s* and *HSPA5* mRNA levels were significantly downregulated in mutant LCLs compared to controls under rapamycin treatment. Furthermore, a significant downregulation in the protein expression of *DNAJC10* observed under thapsigargin treatment gave further evidence of the impaired UPR pathway. We were, unfortunately, not able to investigate the effect of the mutation on the expression of ClC-6 protein because of the time shortage. The anti-CLCN6 antibody we used initially for ClC-6 protein expression gave multiple bands and made it very difficult to distinguish the right band from the rest. ClC-6 protein expression will thus be investigated in further studies with a different antibody.

The most important finding is that the mutation causes a significant decrease in cell survival at basal levels and under thapsigargin treatment which is involved in the inhibition of calcium pumps in the ER. Considering the role of ClC-6, the connection of the mutation with the inhibition of calcium pumps gives a valuable insight into the pathogenesis associated with the mutation. In the endoplasmic reticulum, ClC-6 is thought to be involved in dispersing the electrical gradient that is created by Ca^{2+} uptake or Ca^{2+} release across the ER membrane

maintaining the internal pH (Buyse, Trouet et al. 1998). It is possible that when the calcium pumps are blocked by thapsigargin and the chloride antiporter ClC-6 is also mutated simultaneously, then a severe ER stress is generated that the cell is unable to resolve and induces apoptosis.

Another possible cause for the increased cell death could be the disruption of the endosomal-lysosomal pathway due to the change in pH inside the late endosomes as a result of mutation in *CLCN6*. ClC family members, ClC-3 to ClC-7, are all present in the endosomal/lysosomal system and are Cl^{-}–H^{+} antiporters. Impaired acidification of endosomes on disruption of ClC-3, ClC-4 and ClC-5 has been reported in various studies (Gunther et al., 2003, Hara-Chikuma et al., 2005b, Hara-Chikuma et al., 2005a, Mohammad-Panah et al., 2009). CLC-6 also plays a role in the acidification of endosomes and lysosomes as it is localised to late endosomes. The endosomal-lysosomal system contains different compartments consisting of early endosomes, recycling endosomes, late endosomes, and the lysosome. The vesicles in the endosomal pathway have a decreasing pH from 6.5 to 4.5 compared to the cytoplasmic pH of ~7. The low pH is required for the enzymatic activities, trafficking of cargo and for receptor–ligand interactions along the pathway. The decreasing pH is achieved mainly by the activity of the ATP-dependent proton pumps present in the membranes of the endosomal vesicles and lysosomes. As these pumps transfer protons inside the lumen, they create a positive voltage. Chloride ions are thus required in the lumen to generate a neutralising current to achieve an efficient luminal acidification. This is mediated by vesicular Cl^{-}–H^{+} antiporter which keep the vesicular Cl^{-} concentration higher for as long as the inside-acidic pH gradient is maintained under steady-state conditions (Jentsch, 2007, Hu et al., 2015). There is, therefore, a high possibility that the presence of mutation in *CLCN6* affects the Cl^{-}–H^{+} transport disturbing pH inside the late endosomal lumen resulting in the disruption of endosomal-lysosomal pathway and triggering apoptosis. The upregulation in the mRNA expression of *RAB7A* under

thapsigargin treatment in mutant cell lines may also give a clue to the disturbed endosomal pathway.

ER and endosomal pathways are interlinked as changes in Rab7a expression are known to modulate ER morphology (Mateus et al., 2018). We found a significant upregulation of *RAB7A* mRNA expression in mutant LCLs with thapsigargin treatment, which also indicates a link between ER and endosomal pathways. Therefore, a change in Rab7a mRNA expression with mutated ClC-6 could indicate an effect of mutation on both the ER and endocytosis. We conclude that the blockage of calcium pumps along with the impaired Cl^{-}–H^{+} antiporters leads to a change in the pH of ER causing ER stress that can also affect endosomal pathway which is linked to ER. At the same time, the impaired Cl^{-}–H^{+} antiporters in the late endosomes can also cause pH change affecting the endosomal pathway and subsequently the ER. This disturbance in the ER leads to the activation of UPR pathway, but as a result of the failure of the UPR pathway in the cell in the presence of the mutation, the cell eventually triggers ER stress-mediated apoptotic pathway leading to cell death (Figure 7-9Figure 7-9).

The significant downregulation of *DNAJB9* and *HSPA5* mRNA expression and DNAJC10 protein expression in the presence of mutation under cell stress gives evidence to disrupted UPR by the mutation and strongly supports our conclusion that the disruption of the UPR pathway is the molecular mechanism underlying the pathogenesis caused by *CLCN6* mutation.

Previous studies have already reported variations in the *CLCN6* gene in some neurological disorders that further emphasises the importance of this gene in relation to ALS keeping in consideration our novel findings. Examples include single nucleotide variants in *CLCN6* that were linked to benign partial epilepsies in infancy (Yamamoto et al., 2015) and to West syndrome, a classic form of early infantile epileptic encephalopathy (Peng et al., 2018). In addition, mutations in *CLCN6* were linked to mild forms of neuronal ceroid lipofuscinosis

(NCL), a lysosomal storage disease (Poet et al., 2006, Pressey et al., 2010, Yamamoto et al., 2015). Furthermore, the disruption in ER stress activated pathways and endosomal-lysosomal systems have both been associated with neurodegenerative disorders in previous studies (Cabral-Miranda and Hetz, 2018, Hu et al., 2015). In summary, our findings show strong evidence of the association of *CLCN6* mutation with Familial ALS.

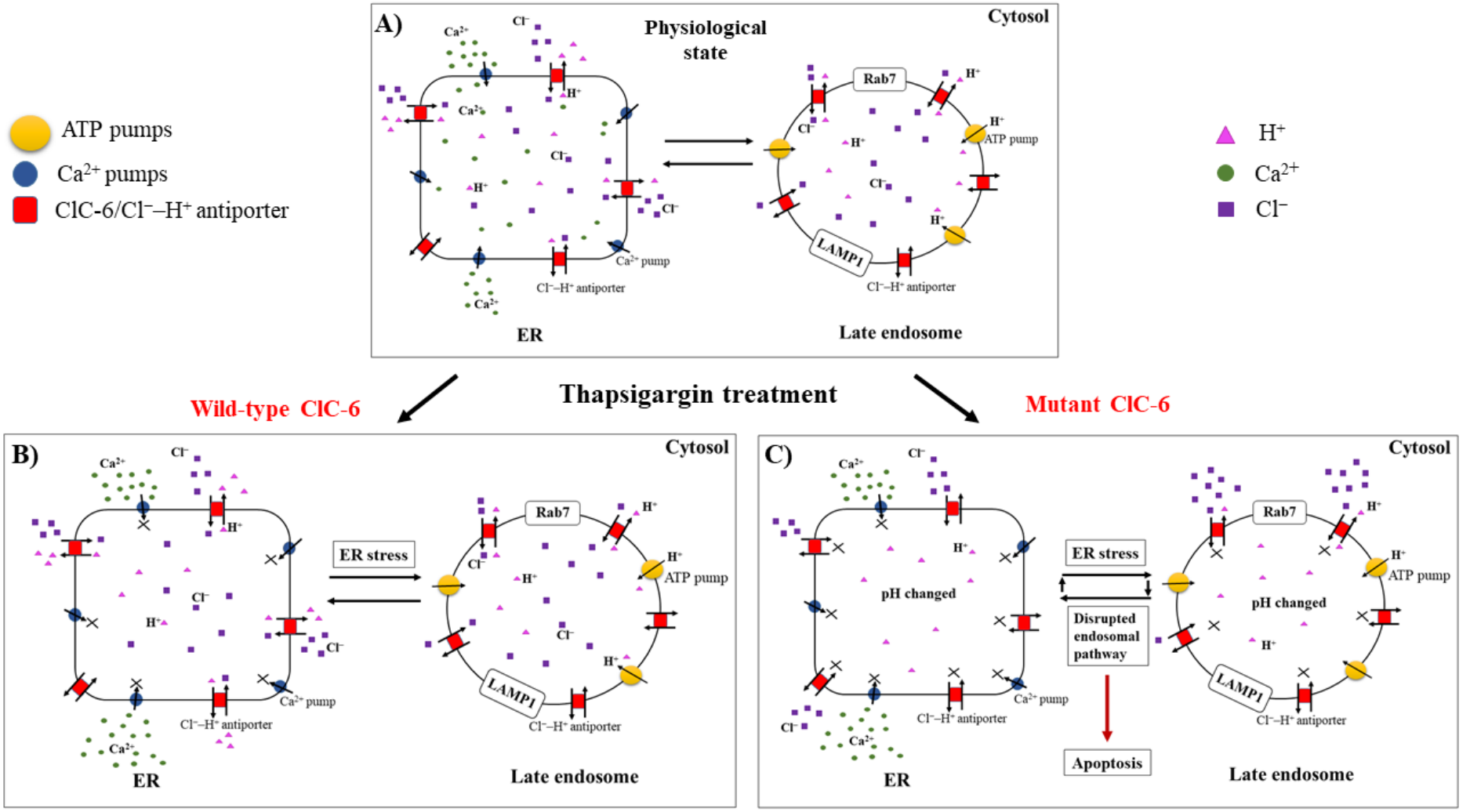
ATP pumps
Ca2+ pumps
ClC-6/Cl−–H+ antiporter
H+
Ca2+
Cl−
A)
Physiological state
Cytosol
Rab7
ATP pump
LAMP1
Cl−–H+ antiporter
Ca2+ pump
ER
Late endosome
Thapsigargin treatment
Wild-type ClC-6
Mutant ClC-6
B)
ER stress
C)
pH changed
Disrupted endosomal pathway
Apoptosis

Figure 7-9 Effect of *CLCN6* mutation on cell survival

A) At physiological state, the calcium pumps and Cl^{-}–H^{+} antiporters perform their function of keeping the calcium levels and pH of ER stable. In the same way, the ATP pumps and Cl^{-}–H^{+} antiporters in late endosomes maintain the pH inside the late endosomal lumen. B) On treating cells with thapsigargin, calcium pumps are blocked depriving the ER lumen from Ca^{2+} that leads to increase in the misfolded proteins inside ER causing ER stress. C) The blockage of calcium pumps under thapsigargin treatment along with the impaired Cl^{-}–H^{+} antiporters due to the mutant ClC-6 could lead to a change in the pH of ER and ER stress. This can subsequently also affect endosomal pathway which is linked to ER. At the same time, the impaired Cl^{-}–H^{+} antiporters in the presence of mutant ClC-6 in the late endosomes will also cause pH change affecting the endosomal pathway and subsequently ER. This cycle can lead to an unresolved ER stress in the cell that can eventually trigger ER stress-mediated apoptotic pathway and cell death.

Chapter 8: General Discussion

Although a couple of drugs are available for ALS, there is still a lack of an effective treatments indicating the need for a greater understanding of the molecular pathogenesis of the disease. We, therefore, started this thesis project with the aim of characterising putative novel mutations of familial ALS to elucidate the mechanisms through which they contribute to the disease pathogenesis. We focused on the predicted pathogenic mutations obtained from the Imperial College FALS cohort and started the project from six short-listed genes, but found the transmission of the mutation with the disease in only two genes, *CLCN6* and *RUBCN*. We, therefore, selected the novel mutations in these two genes for characterisation in FALS.

All cells require a properly functioning protein quality control system for maintaining cellular homeostasis. The quality control system ensures the removal of misfolded proteins, protein aggregates and damaged organelles from the cell. This system is especially important in the case of neurons which are post-mitotic cells and cannot thus dilute the damage accumulating inside them by cell division like other cells of the body that continuously undergo mitosis. As a result, waste and toxic material accumulate inside neurons and make efficient activity of quality control system vital for neuronal life (Martinez-Vicente, 2015). Among the quality control systems, autophagy plays a pivotal role in maintaining cellular homeostasis. It is involved in the clearance of damaged organelles, turnover of old organelles and removal of protein aggregates. Autophagy takes place continuously at basal levels in all cell types, termed as basal autophagy. It is only fully activated when the cell is exposed to stress conditions like starvation, oxidative damage, protein aggregation and hypoxia in order to maintain cellular homeostasis and is termed as induced autophagy (Martinez-Vicente, 2017). Since it plays such an important role in maintenance of neuronal homeostasis, defects in this pathway have been linked to many neurodegenerative diseases including Parkinson's disease, Huntington’s

disease, Alzheimer's disease and amyotrophic lateral sclerosis (ALS) (Martinez-Vicente, 2015).

Another important pathway for maintaining normal cellular functions is the endosomal pathway that is involved in membrane trafficking inside the cell. This pathway is especially important for neurons because of their unique morphology. Alterations in the pathway disrupt membrane trafficking and results in accumulation of organelles and proteins consequently leading to neuronal cell death (Schreij et al., 2016).

8.1 *RUBCN*

Rubicon is involved in multiple signalling pathways inside the cell. It is a component of the PI3KC3 complex involved in both canonical autophagy and endosomal pathways where it acts as a negative regulator of autophagosome and endosome maturation respectively (Sun et al., 2010a, Matsunaga et al., 2009, Zhong et al., 2009). It is also required as a critical component in the non-canonical autophagy pathway called LC3-associated phagocytosis (Martinez et al., 2015). In addition, Rubicon acts as a key modulator in the inflammatory response (Yang et al., 2012). In our studies, we focused on investigating the effect of a *RUBCN* mutation on canonical autophagy, non-canonical autophagy and endosomal pathways since autophagy and endosomal pathways have been linked extensively with neurodegenerative disorders including ALS.

In order to functionally characterise the *RUBCN* mutation, we first investigated the known actions of *RUBCN* that have been established in the regulation of autophagy and endosomal pathways in spinal cord samples from sporadic ALS cases (SALS). We found highly encouraging results from this study as the mRNA expression of *RUBCN* was significantly upregulated while the protein expression was significantly downregulated in SALS cases compared to controls. A significant negative correlation obtained between the mRNA expression of Rubicon and LAMP2 suggested an increase in the activity of the

autophagy/endosomal pathway whereby a decrease in a negative regulator probably increases the activity of the pathway. These results provided evidence of the involvement of the gene in SALS disease mechanisms and encouraged us to characterise the *RUBCN* mutation in FALS cases.

We used lymphoblastoid cell lines (LCLs) derived from the individuals of pedigree SM331 harbouring the mutation and the healthy family members lacking the mutation for the functional characterisation of the mutation. A high expression of *RUBCN* in LCLs made them an excellent model for characterising *RUBCN* mutation. Since Rubicon negatively regulates autophagy and endocytosis at basal conditions, we hypothesized that the mutation may result in the loss of function of Rubicon in inhibiting the pathways at basal levels and may trigger cell death. Under cell stress, however, there may not be an effect of *RUBCN* mutation on the activity of the pathways. We then tested our hypothesis under both basal and cell stress conditions.

We investigated the effect of mutation on oxidative stress, ER stress activated UPR pathways, canonical and noncanonical autophagy, endosomal pathways and on cell survival. We used tunicamycin and thapsigargin to induce ER stress. Both drugs gave the expected results of induced ER stress and autophagy. Rapamycin treatment showed a significant downregulation in the mRNA expression of *RUBCN* suggesting a possible activation of the pathways. We did not obtain any significant effect of oxidative stress by tertiary-butyl hydroperoxide (t-BH) on the expression of oxidative stress or autophagy markers. The autophagy inhibitor, n-butylidenephtalide (n-BP) also did not show a significant downregulation in the expression of the autophagy genes, which might indicate a different dosage or exposure time required to obtain the desired effects although the doses used gave expected results in the cell survival experiments. Overall, we found clear evidence of the induction of the relevant pathways and

the disruptive effects on cell survival using the drugs proving the cellular model suitable for the investigation of the effect of the mutation.

8.1.1 Effect of mutation

Each gene studied was a separate experiment and functions in different ways in the pathways. The mutation caused a significant downregulation in the mRNA expression of *DNAJC10*, *NOX2* and *RAB7A* which are the marker genes for the three neuroprotective pathways; ER stress, oxidative stress and endosomal pathways respectively. A small change towards a decreased mRNA expression was also caused by the mutation in *RUBCN* ($p=0.081$) but it was non-significant. We were also encouraged to find a small though non-significant upregulation in the expression of Rubicon protein at basal levels ($p=0.06$). At basal levels, the mutation effects were present either in medium without vehicle or medium with added vehicle, DMSO, but not in all basal conditions, which suggested a possible interference of the vehicle with the activity of the pathway to some extent although we found no significant effect of DMSO on the expression of any gene (data not shown). The vehicle, DMSO, still seemed to exert some protective role when added for 24 hours in the culture medium compared to the shorter exposure of 4 or 6 hours. As Rubicon does not have an inhibitory role on pathways under cell stress conditions, it was not surprising to find the absence of effect of mutation on the expression of the genes investigated from autophagy and endocytic pathway under cell stress conditions.

An interesting finding regarding the protein structure of Rubicon was that the proteins interacting at its N-terminal (Vps34, Beclin1 and UVRAG) had no effect of mutation on their expression while the proteins interacting at the C-terminal (NOX2 and Rab7) showed downregulation in their gene expression in the presence of mutation. This might occur as a result of the multiple protein-protein interactions between the protein components of the

PI3KC3 complex that interacts with Rubicon at its N-terminal resulting in intact activity of the complex despite the possible effect of the mutation on UVRAG or Beclin-1. Since the complex is involved in regulating autophagy, the autophagy pathway remained unaffected by the mutation. The significant downregulation in the mRNA expression of *RAB7A* indicates a possible effect of the mutation on endosomal pathway where Rab7 may not be able to interact with Rubicon leading to failure of endosomal maturation and disrupted endocytosis (Figure 8-1). The significant downregulation in the mRNA expression of *NOX2* indicates a possible effect of *RUBCN* mutation on LC3-associated phagocytosis (LAP) pathway where it is involved as a positive regulator (Figure 8-2). Rubicon interacts directly with a subunit of NOX2 stabilizing the NOX2 complex for optimal production of reactive oxygen species required by LAP pathway, therefore, impaired Rubicon can lead to impaired ROS production affecting LAP. Our observation of the lost correlation between *RUBCN* and *NOX2* in the presence the of mutation strengthens our assumption of a possibility of impairment in LAP pathway and the possible link of the pathway to ALS but this will require further investigation. Our finding of a significant downregulation in the mRNA expression of *DNAJC10* indicates either a possible effect of the mutation on the UPR pathway or a possible interaction between Rubicon and DNAJC10. We found an absence of a toxic effect of mutation on cell viability.

Rubicon and the genes affected by the mutation in Rubicon have previously been reported to be involved in several neurological diseases in both human and mouse models which further emphasises the possible association of Rubicon with ALS. In summary, our novel findings in SALS and FALS are highly suggestive of the relevance of the *RUBCN* mutation to FALS.

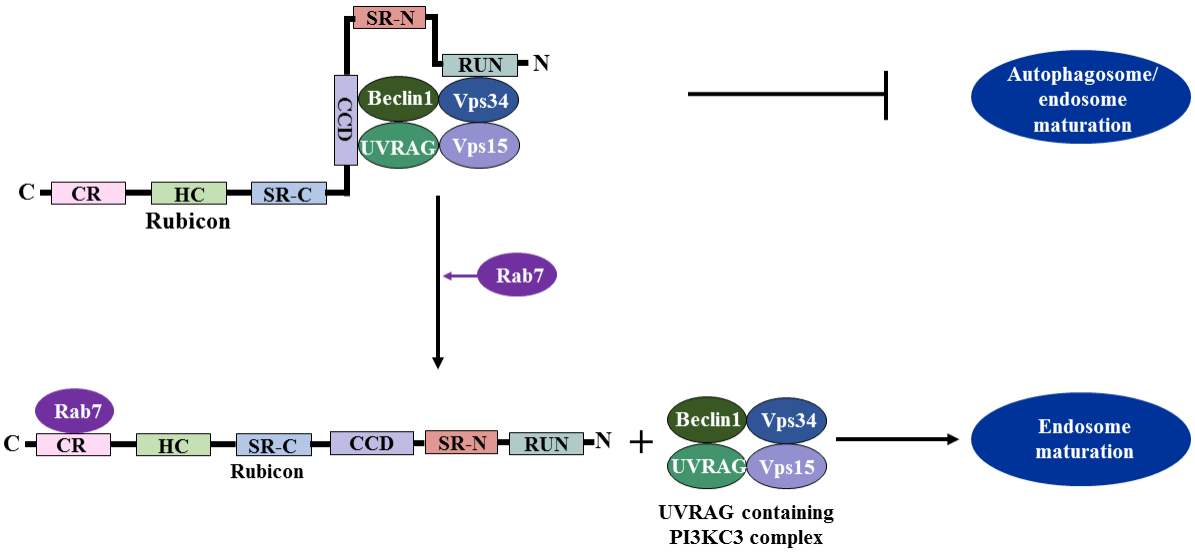

Figure 8-1 Rubicon negatively regulates endosome maturation

Rubicon binds to a subpopulation of UVRAG containing PI3KC3 complex to negatively regulate endosomal maturation. When endosomal maturation is required, active Rab7 competes with UVRAG for binding to Rubicon and releases UVRAG containing PI3KC3 complex from Rubicon, leading to endosomal maturation.

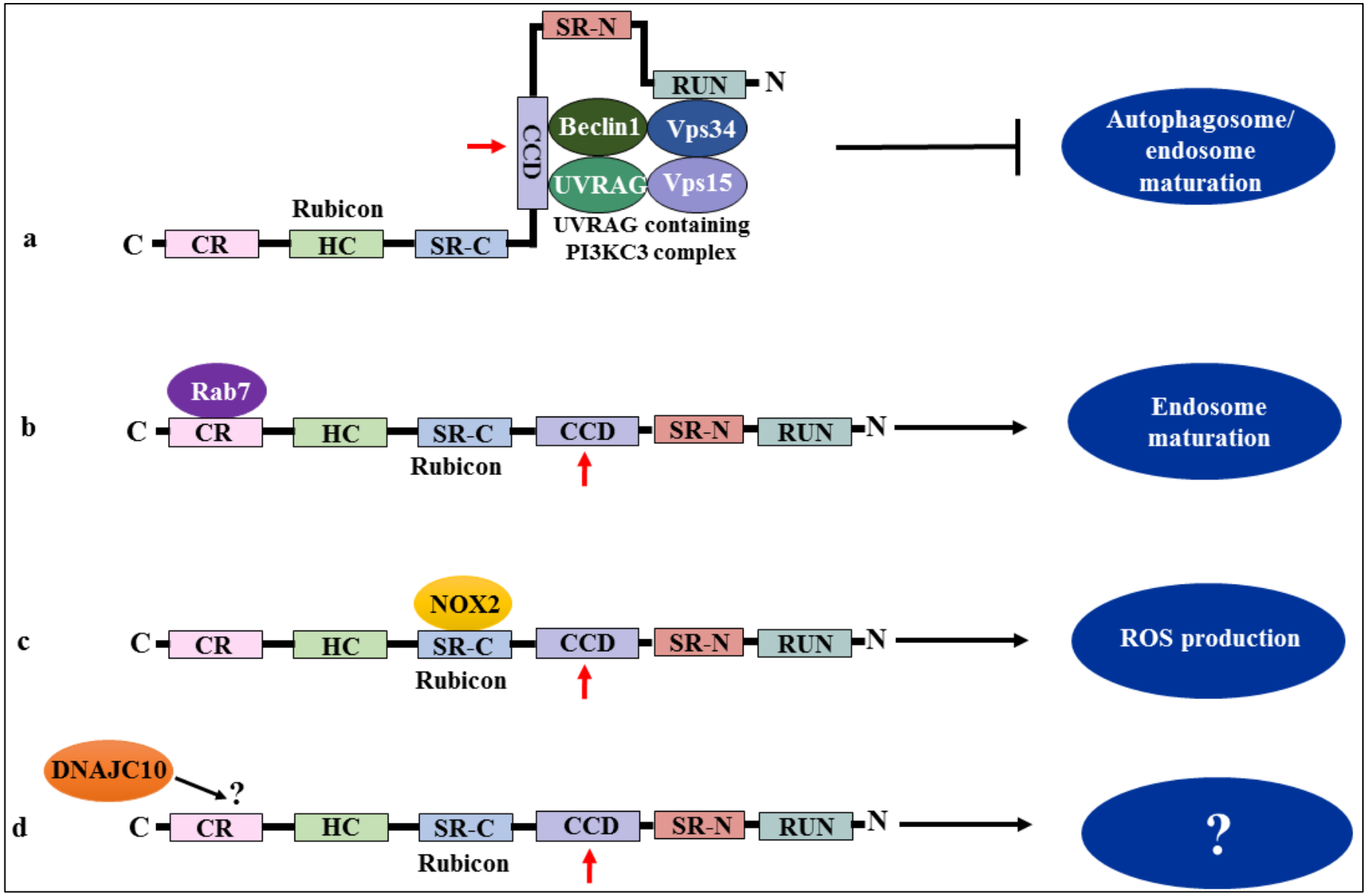
a
C
CR
HC
SR-C
Rubicon
CCD
SR-N
RUN
N
Beclin1
Vps34
UVRAG
Vps15
UVRAG containing
PI3KC3 complex
Autophagosome/
endosome
maturation
b
Rab7
C
CR
HC
SR-C
CCD
SR-N
RUN
N
Rubicon
Endosome
maturation
c
NOX2
C
CR
HC
SR-C
CCD
SR-N
RUN
N
Rubicon
ROS production
d
DNAJC10
?
C
CR
HC
SR-C
CCD
SR-N
RUN
N
Rubicon
?

Figure 8-2 Role of Rubicon in various pathways inside a cell

Rubicon is involved in various pathways in the cell active as both positive and negative regulator. a) Rubicon acts as a negative regulator in autophagy and endosomal pathway. Binding of Rubicon to UVRAG containing PI3KC3 complex inhibits autophagosome and endosome maturation. The mutation is present as the site of UVRAG binding to Rubicon but we found no effect of the mutation on the mRNA expression of *UVRAG*. No effect was found on the mRNA expression of *VPS34* either which might indicate that the UVRAG containing VIPKC3 complex is able to bind to Rubicon via VPS34 because of multiple interactions present within the complex even if the interaction of UVRAG to Rubicon is affected by the mutation leading eventually to inhibition of autophagy and endosomal pathway. b) In case of endosomal pathway, active Rab7 competes with UVRAG for binding to Rubicon and releases UVRAG from Rubicon, which leads to endosomal maturation. Since we found a significant effect of mutation on the mRNA expression of *RAB7A*, it might indicate that the Rab7 may not be able to interact with Rubicon and replace UVRAG leading to failure of endosomal maturation. c) Rubicon interacts with NOX2 and causes activation of NOX2 complex that is required for the production of reactive oxygen species (ROS). The significant effect of mutation observed on NOX2 mRNA expression indicates a possible effect of *RUBCN* mutation on LAP pathway as failure in the activation of NOX2 complex will lead to failure in the production of ROS required for the embedding of LC3-II on LAPosomes and subsequent fusion of LAPosomes with lysosomes. d) We found a significant effect of the mutation on the mRNA expression of *DNAJC10*. Although the pathways of autophagy and ER stress are tightly linked, no link has been reported between the function of co-chaperone DNAJC10, activated as a result of ER stress, and Rubicon so far. The mutation effect on DNAJC10 indicates a possible effect of the mutation on ER stress activated pathways. The red arrow indicates the site of identified mutation.

8.2 *CLCN6*

The protein ClC-6 encoded by *CLCN6* is localised to the endoplasmic reticulum and late endosome membranes (Buyse et al., 1998, Ignoul et al., 2007). The protein is predominantly expressed in the nervous system and functions as a Cl^-/H^+ antiporter (Neagoe et al., 2010, Poet et al., 2006). It is involved in facilitating the acidification of the late endosomal vesicle by providing an electric shunt for the efficient pumping of the H^+-ATPase (Jentsch et al., 2002). Because of its function, we hypothesized that the mutant ClC-6 may disrupt aspects of endoplasmic reticulum function and/or endosomal pathway by effecting their pH or Cl- concentration and will eventually affecting cell survival.

In order to functionally characterise the *CLCN6* mutation, we first profiled the expression of *CLCN6* and the pathways associated with the action of *CLCN6*, ER stress and endosomal pathways, in spinal cord samples from sporadic ALS cases (SALS). Our results were highly suggestive of the involvement of *CLCN6* in SALS disease mechanisms as we found a significant downregulation in the protein expression level of CLC-6 in SALS cases compared to controls and the presence of ER stress. Our findings in SALS encouraged us to characterise the effects of the *CLCN6* mutation in cellular model.

For functional characterisation of the mutation, we used LCLs as cellular models that were derived from the FALS cases of pedigree SM821 carrying the mutations and healthy controls lacking the mutations. We investigated the effect of the mutation on ER stress activated UPR, autophagy and endosomal pathways, and on cell survival. The drugs used to induce the pathways and increased cell death were the same as mentioned earlier in *RUBCN* section with the same expected results.

8.2.1 Effect of mutation

Expression of each gene studied was a separate experiment and performs a different function in the pathways. We found a significant downregulation in the mRNA expression of *DNAJB9* and *HSPA5* and in the protein expression of DNAJC10 in the presence of mutation under cell stress. The observation of the upregulated mRNA expression of *RAB7A* under thapsigargin treatment in mutant cell lines also gave a clue of the disturbed endosomal pathway. Our other important finding was the significant decrease in cell survival at basal levels and under thapsigargin treatment. We concluded that the blockage of calcium pumps under thapsigargin treatment along with the impaired Cl^{-}–H^{+} antiporters due to the mutant ClC-6 could be causing a change in the pH of ER leading to the ER stress. This might be consequently affecting the endosomal pathway as the ER and endosomal pathways are interlinked. At the same time, the impaired Cl^{-}–H^{+} antiporters due to the mutant ClC-6 in the late endosomes may be causing pH change affecting the endosomal pathway and subsequently ER. This cycle of disrupted ER affecting the late endosome and vice versa may be leading to an unresolved ER stress in the cell that eventually triggers ER stress-mediated apoptotic pathway and cell death (Figure 7-9). Therefore, our findings of increased cell death in the presence of the mutation along with the defective UPR pathway strongly supports the conclusion that the disruption of the UPR pathway is the molecular mechanism underlying the pathogenesis caused by *CLCN6* mutation.

Variations in the *CLCN6* gene have previously been associated with neurological disorders, which further emphasises the strong possibility of the association of this gene with ALS while keeping in view our novel findings. In summary, our findings in SALS and FALS show a strong evidence of the association of *CLCN6* mutation with familial ALS.

8.3 Correlation between *RUBCN* and *CLCN6*

As *RUBCN* and *CLCN6* are both localised to late endosomes, we determined the correlation between the mRNA expression of these two genes. We found a significant positive correlation between the mRNA expression levels of *CLCN6* and *RUBCN* in SALS cases. In addition, mutations in both genes led to the defective UPR pathway. These observations suggest a strong possibility of a close functional link between the two genes.

8.4 Limitations of the study

In our experiments performed on spinal cord samples from the SALS cases, RNA samples had previously been screened for pH (agonal status) and RNA quality. 15% of samples did not satisfy quality control but amongst the remaining samples there was no significant effect of post-mortem delay found. On the whole, expression results were reliable but other factors could have contributed to sample reduction, such as storage of cDNA and protein extracts. On the whole the expression studies gave good reproducible results. However, use of a large cohort would have enhanced the project.

We performed the functional characterisation of the mutations in lymphoblastoid cell lines (LCLs) which were available from the families carrying the mutation. LCLs were a good model for our studies since they allowed us to investigate the effect of the mutations on the universal pathways. However, we were limited by the number of individuals with these mutations that were known and hence available for study. However, as motor neurons are the main cells that degenerate in ALS, it is crucial to replicate the study in motor neurons to understand the specific effects of the mutations on cellular mechanisms leading to pathogenesis of the disease.

For the analysis of apoptotic cell death, FITC-Annexin V assay is currently preferred but it has the limitation of not differentiating apoptotic cell death from necrotic cell death thus making it

difficult to eliminate necrosis as a route for cell death. Alternative experiments could be performed to test if the cell death occurred as a result of apoptosis such as staining the cells with DAPI to see small apoptotic bodies formed by nuclear fragmentation.

As the studies we have performed were on isolated cells grown in culture, the results could also be replicated on organoids instead of isolated cells to characterise the mutations especially for the studies on cell death as the cells grown in cell culture are isolated cells and thus may or may not be prone to cell death compared to the cells in tissues.

8.5 Future work

8.5.1 *RUBCN*

We were not able to investigate the effect of the mutation on protein levels of *DNAJC10* and *NOX2* because of the time limitation but in order to confirm our findings, we will perform these experiments in future. We also plan to investigate the expression of NOX2 in spinal cord samples from sporadic ALS cases to investigate the role of NOX2 in SALS disease mechanism. We will also perform protein-protein interactions studies to investigate the effect of the mutation on Rubicon binding with Rab7, NOX2. The protein-protein interaction of Rubicon with VPS34, Beclin 1 and UVRAG was investigated by our collaborator Professor Christopher Shaw (King's College London, UK, data not shown) but the mutation did not disrupt the interaction of Rubicon with these three proteins and was in accordance with our observations of unaffected expression of these genes in the presence of the mutation. We also plan to perform immunohistochemistry to investigate the effect of the mutation on cellular localisation of Rubicon.

In this thesis project, we have focused on the role of Rubicon in autophagy/endosomal pathways and LCL-associated phagocytosis pathway because of the known relevance of the

autophagy and endosomal pathways with neurodegenerative disorders. In addition to these three pathways, Rubicon is also involved in the feedback inhibition of CARD9-mediated PRR-signal transduction which is an inflammatory response. The effect of the *RUBCN* mutation on this pathway is still required to be investigated.

We used lymphoblastoid cell lines (LCLs) as a cellular model for the functional characterisation of the mutation as an initial step because of the ease of obtaining LCLs from lymphocytes that carry the mutation. Although LCLs have all the important pathways relevant to neurological disorders, which makes them a good model for investigation, they have limitations being not the neuronal cells. In future, we thus plan to replicate the results obtained from this study in motor neurons to confirm the findings as ALS results from the degeneration of motor neurons. This could either be done by using transgenic mouse motor neuron-like hybrid cell line (NSC-34) or by using iPSCs derived from the lymphoblastoid cell lines of pedigree SM331.

8.5.2 *CLCN6*

We plan to investigate the effect of the mutation on the protein expression of CLCN6 in LCLs which we were unable to perform because of the time shortage. We may also measure the pH of endoplasmic reticulum and late endosomes in order to confirm our assumption of disturbed pH caused by the mutant ClC-6. We also plan to replicate the results obtained by this study in motor neurons to confirm our findings using the techniques explained earlier for *RUBCN*.

Bibliography

ADOLPH, T. E., TOMCZAK, M. F., NIEDERREITER, L., KO, H. J., BOCK, J., MARTINEZ-NAVES, E., GLICKMAN, J. N., TSCHURTSCHENTHALER, M., HARTWIG, J., HOSOMI, S., FLAK, M. B., CUSICK, J. L., KOHNO, K., IWAWAKI, T., BILLMANN-BORN, S., RAINE, T., BHARTI, R., LUCIUS, R., KWEON, M. N., MARCINIAK, S. J., CHOI, A., HAGEN, S. J., SCHREIBER, S., ROSENSTIEL, P., KASER, A. & BLUMBERG, R. S. 2013. Paneth cells as a site of origin for intestinal inflammation. *Nature,* 503**,** 272-6.

AL-CHALABI, A., ANDERSEN, P. M., NILSSON, P., CHIOZA, B., ANDERSSON, J. L., RUSS, C., SHAW, C. E., POWELL, J. F. & LEIGH, P. N. 1999. Deletions of the heavy neurofilament subunit tail in amyotrophic lateral sclerosis. *Hum Mol Genet,* 8**,** 157-64.

AL-CHALABI, A., CALVO, A., CHIO, A., COLVILLE, S., ELLIS, C. M., HARDIMAN, O., HEVERIN, M., HOWARD, R. S., HUISMAN, M. H. B., KEREN, N., LEIGH, P. N., MAZZINI, L., MORA, G., ORRELL, R. W., ROONEY, J., SCOTT, K. M., SCOTTON, W. J., SEELEN, M., SHAW, C. E., SIDLE, K. S., SWINGLER, R., TSUDA, M., VELDINK, J. H., VISSER, A. E., VAN DEN BERG, L. H. & PEARCE, N. 2014. Analysis of amyotrophic lateral sclerosis as a multistep process: a population-based modelling study. *The Lancet. Neurology,* 13**,** 1108-1113.

AL-CHALABI, A. & HARDIMAN, O. 2013. The epidemiology of ALS: a conspiracy of genes, environment and time. *Nat Rev Neurol,* 9**,** 617-28.

AL-CHALABI, A., HARDIMAN, O., KIERNAN, M. C., CHIO, A., RIX-BROOKS, B. & VAN DEN BERG, L. H. 2016. Amyotrophic lateral sclerosis: moving towards a new classification system. *Lancet Neurol,* 15**,** 1182-94.

AL-SAIF, A., AL-MOHANNA, F. & BOHLEGA, S. 2011. A mutation in sigma-1 receptor causes juvenile amyotrophic lateral sclerosis. *Ann Neurol,* 70**,** 913-9.

ALBO, F., PIERI, M. & ZONA, C. 2004. Modulation of AMPA receptors in spinal motor neurons by the neuroprotective agent riluzole. *J Neurosci Res,* 78**,** 200-7.

ALSULTAN, A. A., WALLER, R., HEATH, P. R. & KIRBY, J. 2016. The genetics of amyotrophic lateral sclerosis: current insights. *Degenerative neurological and neuromuscular disease,* 6**,** 49-64.

AMICK, J., ROCZNIAK-FERGUSON, A. & FERGUSON, S. M. 2016. C9orf72 binds SMCR8, localizes to lysosomes, and regulates mTORC1 signaling. *Mol Biol Cell,* 27**,** 3040-3051.

ANDERSEN, J. K. 2004. Oxidative stress in neurodegeneration: cause or consequence? *Nat Med,* 10 Suppl**,** S18-25.

ANDERSEN, P. M. & AL-CHALABI, A. 2011. Clinical genetics of amyotrophic lateral sclerosis: what do we really know? *Nat Rev Neurol,* 7**,** 603-15.

ANDERSEN, P. M., FORSGREN, L., BINZER, M., NILSSON, P., ALA-HURULA, V., KERANEN, M. L., BERGMARK, L., SAARINEN, A., HALTIA, T., TARVAINEN, I., KINNUNEN, E., UDD, B. & MARKLUND, S. L. 1996. Autosomal recessive adult-onset amyotrophic lateral sclerosis associated with homozygosity for Asp90Ala CuZn-superoxide dismutase mutation. A clinical and genealogical study of 36 patients. *Brain,* 119 (Pt 4)**,** 1153-72.

ARAI, T., NONAKA, T., HASEGAWA, M., AKIYAMA, H., YOSHIDA, M., HASHIZUME, Y., TSUCHIYA, K., ODA, T. & IKEDA, K. 2003. Neuronal and glial inclusions in

frontotemporal dementia with or without motor neuron disease are immunopositive for p62. *Neurosci Lett,* 342**,** 41-4.

ARIAS, E. & CUERVO, A. M. 2011. Chaperone-mediated autophagy in protein quality control. *Curr Opin Cell Biol,* 23**,** 184-9.

ASHE, P. C. & BERRY, M. D. 2003. Apoptotic signaling cascades. *Prog Neuropsychopharmacol Biol Psychiatry,* 27**,** 199-214.

ASSOUM, M., SALIH, M. A., DROUOT, N., HNIA, K., MARTELLI, A. & KOENIG, M. 2013. The Salih ataxia mutation impairs Rubicon endosomal localization. *Cerebellum,* 12**,** 835-40.

ATKIN, J. D., FARG, M. A., WALKER, A. K., MCLEAN, C., TOMAS, D. & HORNE, M. K. 2008. Endoplasmic reticulum stress and induction of the unfolded protein response in human sporadic amyotrophic lateral sclerosis. *Neurobiol Dis,* 30**,** 400-7.

AYALA, Y. M., DE CONTI, L., AVENDANO-VAZQUEZ, S. E., DHIR, A., ROMANO, M., D'AMBROGIO, A., TOLLERVEY, J., ULE, J., BARALLE, M., BURATTI, E. & BARALLE, F. E. 2011. TDP-43 regulates its mRNA levels through a negative feedback loop. *Embo j,* 30**,** 277-88.

BALENDRA, R. & ISAACS, A. M. 2018. C9orf72-mediated ALS and FTD: multiple pathways to disease. *Nat Rev Neurol,* 14**,** 544-558.

BANERJEE, A., LANG, J. Y., HUNG, M. C., SENGUPTA, K., BANERJEE, S. K., BAKSI, K. & BANERJEE, D. K. 2011. Unfolded protein response is required in nu/nu mice microvasculature for treating breast tumor with tunicamycin. *J Biol Chem,* 286**,** 29127-38.

BANNWARTH, S., AIT-EL-MKADEM, S., CHAUSSENOT, A., GENIN, E. C., LACAS-GERVAIS, S., FRAGAKI, K., BERG-ALONSO, L., KAGEYAMA, Y., SERRE, V., MOORE, D. G., VERSCHUEREN, A., ROUZIER, C., LE BER, I., AUGE, G., COCHAUD, C., LESPINASSE, F., N'GUYEN, K., DE SEPTENVILLE, A., BRICE, A., YU-WAI-MAN, P., SESAKI, H., POUGET, J. & PAQUIS-FLUCKLINGER, V. 2014. A mitochondrial origin for frontotemporal dementia and amyotrophic lateral sclerosis through CHCHD10 involvement. *Brain,* 137**,** 2329-45.

BANSAL, M., SWARUP, G. & BALASUBRAMANIAN, D. 2015. Functional analysis of optineurin and some of its disease-associated mutants. *IUBMB Life,* 67**,** 120-8.

BARBEITO, L. 2018. Astrocyte-based cell therapy: new hope for amyotrophic lateral sclerosis patients? *Stem cell research & therapy,* 9**,** 241-241.

BARTOLOME, F., WU, H. C., BURCHELL, V. S., PREZA, E., WRAY, S., MAHONEY, C. J., FOX, N. C., CALVO, A., CANOSA, A., MOGLIA, C., MANDRIOLI, J., CHIO, A., ORRELL, R. W., HOULDEN, H., HARDY, J., ABRAMOV, A. Y. & PLUN-FAVREAU, H. 2013. Pathogenic VCP mutations induce mitochondrial uncoupling and reduced ATP levels. *Neuron,* 78**,** 57-64.

BASKOYLU, S. N., YERSAK, J., O'HERN, P., GROSSER, S., SIMON, J., KIM, S., SCHUCH, K., DIMITRIADI, M., YANAGI, K. S., LINS, J. & HART, A. C. 2018. Single copy/knock-in models of ALS SOD1 in C. elegans suggest loss and gain of function have different contributions to cholinergic and glutamatergic neurodegeneration. *PLoS Genet,* 14**,** e1007682.

BASSO, M., MASSIGNAN, T., SAMENGO, G., CHERONI, C., DE BIASI, S., SALMONA, M., BENDOTTI, C. & BONETTO, V. 2006. Insoluble mutant SOD1 is partly oligoubiquitinated in amyotrophic lateral sclerosis mice. *J Biol Chem,* 281**,** 33325-35.

BAUMER, D., HILTON, D., PAINE, S. M., TURNER, M. R., LOWE, J., TALBOT, K. & ANSORGE, O. 2010. Juvenile ALS with basophilic inclusions is a FUS proteinopathy with FUS mutations. *Neurology,* 75**,** 611-8.

BÄUMER, D., HILTON, D., PAINE, S. M. L., TURNER, M. R., LOWE, J., TALBOT, K. & ANSORGE, O. 2010. Juvenile ALS with basophilic inclusions is a FUS proteinopathy with FUS mutations. *Neurology,* 75**,** 611-618.

BELZIL, V. V., BAUER, P. O., PRUDENCIO, M., GENDRON, T. F., STETLER, C. T., YAN, I. K., PREGENT, L., DAUGHRITY, L., BAKER, M. C., RADEMAKERS, R., BOYLAN, K., PATEL, T. C., DICKSON, D. W. & PETRUCELLI, L. 2013. Reduced C9orf72 gene expression in c9FTD/ALS is caused by histone trimethylation, an epigenetic event detectable in blood. *Acta Neuropathol,* 126**,** 895-905.

BENDOTTI, C., MARINO, M., CHERONI, C., FONTANA, E., CRIPPA, V., POLETTI, A. & DE BIASI, S. 2012. Dysfunction of constitutive and inducible ubiquitin-proteasome system in amyotrophic lateral sclerosis: implication for protein aggregation and immune response. *Prog Neurobiol,* 97**,** 101-26.

BENSIMON, G., LACOMBLEZ, L. & MEININGER, V. 1994. A controlled trial of riluzole in amyotrophic lateral sclerosis. ALS/Riluzole Study Group. *N Engl J Med,* 330**,** 585-91.

BOGDANOV, M., BROWN, R. H., MATSON, W., SMART, R., HAYDEN, D., O'DONNELL, H., FLINT BEAL, M. & CUDKOWICZ, M. 2000. Increased oxidative damage to DNA in ALS patients. *Free Radic Biol Med,* 29**,** 652-8.

BOOPATHY, S., SILVAS, T. V., TISCHBEIN, M., JANSEN, S., SHANDILYA, S. M., ZITZEWITZ, J. A., LANDERS, J. E., GOODE, B. L., SCHIFFER, C. A. & BOSCO,

D. A. 2015. Structural basis for mutation-induced destabilization of profilin 1 in ALS. *Proc Natl Acad Sci U S A,* 112**,** 7984-9.

BORGHERO, G., PUGLIATTI, M., MARROSU, F., MARROSU, M. G., MURRU, M. R., FLORIS, G., CANNAS, A., PARISH, L. D., CAU, T. B., LOI, D., TICCA, A., TRACCIS, S., MANERA, U., CANOSA, A., MOGLIA, C., CALVO, A., BARBERIS, M., BRUNETTI, M., RENTON, A. E., NALLS, M. A., TRAYNOR, B. J., RESTAGNO, G. & CHIO, A. 2015. ATXN2 is a modifier of phenotype in ALS patients of Sardinian ancestry. *Neurobiol Aging,* 36**,** 2906.e1-5.

BOSCO, D. A., LEMAY, N., KO, H. K., ZHOU, H., BURKE, C., KWIATKOWSKI, T. J., JR., SAPP, P., MCKENNA-YASEK, D., BROWN, R. H., JR. & HAYWARD, L. J. 2010a. Mutant FUS proteins that cause amyotrophic lateral sclerosis incorporate into stress granules. *Hum Mol Genet,* 19**,** 4160-75.

BOSCO, D. A., MORFINI, G., KARABACAK, N. M., SONG, Y., GROS-LOUIS, F., PASINELLI, P., GOOLSBY, H., FONTAINE, B. A., LEMAY, N., MCKENNA-YASEK, D., FROSCH, M. P., AGAR, J. N., JULIEN, J.-P., BRADY, S. T. & BROWN, R. H., JR. 2010b. Wild-type and mutant SOD1 share an aberrant conformation and a common pathogenic pathway in ALS. *Nature neuroscience,* 13**,** 1396-1403.

BRANDT, S. & JENTSCH, T. J. 1995. ClC-6 and ClC-7 are two novel broadly expressed members of the CLC chloride channel family. *FEBS Lett,* 377**,** 15-20.

BRENNER, D., MULLER, K., WIELAND, T., WEYDT, P., BOHM, S., LULE, D., HUBERS, A., NEUWIRTH, C., WEBER, M., BORCK, G., WAHLQVIST, M., DANZER, K. M., VOLK, A. E., MEITINGER, T., STROM, T. M., OTTO, M., KASSUBEK, J., LUDOLPH, A. C., ANDERSEN, P. M. & WEISHAUPT, J. H. 2016. NEK1 mutations in familial amyotrophic lateral sclerosis. *Brain,* 139**,** e28.

BRENNER, D., YILMAZ, R., MULLER, K., GREHL, T., PETRI, S., MEYER, T., GROSSKREUTZ, J., WEYDT, P., RUF, W., NEUWIRTH, C., WEBER, M., PINTO, S., CLAEYS, K. G., SCHRANK, B., JORDAN, B., KNEHR, A., GUNTHER, K., HUBERS, A., ZELLER, D., KUBISCH, C., JABLONKA, S., SENDTNER, M., KLOPSTOCK, T., DE CARVALHO, M., SPERFELD, A., BORCK, G., VOLK, A. E., DORST, J., WEIS, J., OTTO, M., SCHUSTER, J., DEL TREDICI, K., BRAAK, H., DANZER, K. M., FREISCHMIDT, A., MEITINGER, T., STROM, T. M., LUDOLPH, A. C., ANDERSEN, P. M. & WEISHAUPT, J. H. 2018. Hot-spot KIF5A mutations cause familial ALS. *Brain,* 141**,** 688-697.

BRETTSCHNEIDER, J., DEL TREDICI, K., TOLEDO, J. B., ROBINSON, J. L., IRWIN, D. J., GROSSMAN, M., SUH, E., VAN DEERLIN, V. M., WOOD, E. M., BAEK, Y., KWONG, L., LEE, E. B., ELMAN, L., MCCLUSKEY, L., FANG, L., FELDENGUT, S., LUDOLPH, A. C., LEE, V. M., BRAAK, H. & TROJANOWSKI, J. Q. 2013. Stages of pTDP-43 pathology in amyotrophic lateral sclerosis. *Ann Neurol,* 74**,** 20-38.

BRETTSCHNEIDER, J., VAN DEERLIN, V. M., ROBINSON, J. L., KWONG, L., LEE, E. B., ALI, Y. O., SAFREN, N., MONTEIRO, M. J., TOLEDO, J. B., ELMAN, L., MCCLUSKEY, L., IRWIN, D. J., GROSSMAN, M., MOLINA-PORCEL, L., LEE, V. M. & TROJANOWSKI, J. Q. 2012. Pattern of ubiquilin pathology in ALS and FTLD indicates presence of C9ORF72 hexanucleotide expansion. *Acta Neuropathol,* 123**,** 825-39.

BROWN, R. H. & AL-CHALABI, A. 2017. Amyotrophic Lateral Sclerosis. *N Engl J Med,* 377**,** 162-172.

BRUNETEAU, G., SIMONET, T., BAUCHE, S., MANDJEE, N., MALFATTI, E., GIRARD, E., TANGUY, M. L., BEHIN, A., KHIAMI, F., SARIALI, E., HELL-REMY, C.,

SALACHAS, F., PRADAT, P. F., FOURNIER, E., LACOMBLEZ, L., KOENIG, J., ROMERO, N. B., FONTAINE, B., MEININGER, V., SCHAEFFER, L. & HANTAI, D. 2013. Muscle histone deacetylase 4 upregulation in amyotrophic lateral sclerosis: potential role in reinnervation ability and disease progression. *Brain,* 136**,** 2359-68.

BURATTI, E. & BARALLE, F. E. 2010. The multiple roles of TDP-43 in pre-mRNA processing and gene expression regulation. *RNA Biol,* 7**,** 420-9.

BUYSE, G., TROUET, D., VOETS, T., MISSIAEN, L., DROOGMANS, G., NILIUS, B. & EGGERMONT, J. 1998. Evidence for the intracellular location of chloride channel (ClC)-type proteins: co-localization of ClC-6a and ClC-6c with the sarco/endoplasmic-reticulum Ca2+ pump SERCA2b. *Biochem J,* 330 (Pt 2)**,** 1015-21.

CABRAL-MIRANDA, F. & HETZ, C. 2018. ER Stress and Neurodegenerative Disease: A Cause or Effect Relationship? *Curr Top Microbiol Immunol,* 414**,** 131-157.

CAI, H., SHIM, H., LAI, C., XIE, C., LIN, X., YANG, W. J. & CHANDRAN, J. 2008. ALS2/alsin knockout mice and motor neuron diseases. *Neuro-degenerative diseases,* 5**,** 359-366.

CAO, S. S. & KAUFMAN, R. J. 2014. Endoplasmic reticulum stress and oxidative stress in cell fate decision and human disease. *Antioxid Redox Signal,* 21**,** 396-413.

CHANG, Y., KONG, Q., SHAN, X., TIAN, G., ILIEVA, H., CLEVELAND, D. W., ROTHSTEIN, J. D., BORCHELT, D. R., WONG, P. C. & LIN, C. L. 2008. Messenger RNA oxidation occurs early in disease pathogenesis and promotes motor neuron degeneration in ALS. *PLoS One,* 3**,** e2849.

CHEN, H. J., ANAGNOSTOU, G., CHAI, A., WITHERS, J., MORRIS, A., ADHIKAREE, J., PENNETTA, G. & DE BELLEROCHE, J. S. 2010. Characterization of the

properties of a novel mutation in VAPB in familial amyotrophic lateral sclerosis. *J Biol Chem,* 285**,** 40266-81.

CHEN, S., SAYANA, P., ZHANG, X. & LE, W. 2013. Genetics of amyotrophic lateral sclerosis: an update. *Mol Neurodegener,* 8**,** 28.

CHEN, S., ZHANG, X., SONG, L. & LE, W. 2012. Autophagy dysregulation in amyotrophic lateral sclerosis. *Brain Pathol,* 22**,** 110-6.

CHEN, Y., DENG, J., WANG, P., YANG, M., CHEN, X., ZHU, L., LIU, J., LU, B., SHEN, Y., FUSHIMI, K., XU, Q. & WU, J. Y. 2016a. PINK1 and Parkin are genetic modifiers for FUS-induced neurodegeneration. *Hum Mol Genet,* 25**,** 5059-5068.

CHEN, Y., WEI, Q., CHEN, X., LI, C., CAO, B., OU, R., HADANO, S. & SHANG, H.-F. 2016b. Aberration of miRNAs Expression in Leukocytes from Sporadic Amyotrophic Lateral Sclerosis. *Frontiers in molecular neuroscience,* 9**,** 69-69.

CHEN, Y., YANG, M., DENG, J., CHEN, X., YE, Y., ZHU, L., LIU, J., YE, H., SHEN, Y., LI, Y., RAO, E. J., FUSHIMI, K., ZHOU, X., BIGIO, E. H., MESULAM, M., XU, Q. & WU, J. Y. 2011. Expression of human FUS protein in Drosophila leads to progressive neurodegeneration. *Protein Cell,* 2**,** 477-86.

CHEN, Y. Z., BENNETT, C. L., HUYNH, H. M., BLAIR, I. P., PULS, I., IROBI, J., DIERICK, I., ABEL, A., KENNERSON, M. L., RABIN, B. A., NICHOLSON, G. A., AUER-GRUMBACH, M., WAGNER, K., DE JONGHE, P., GRIFFIN, J. W., FISCHBECK, K. H., TIMMERMAN, V., CORNBLATH, D. R. & CHANCE, P. F. 2004. DNA/RNA helicase gene mutations in a form of juvenile amyotrophic lateral sclerosis (ALS4). *Am J Hum Genet,* 74**,** 1128-35.

CHERONI, C., PEVIANI, M., CASCIO, P., DEBIASI, S., MONTI, C. & BENDOTTI, C. 2005. Accumulation of human SOD1 and ubiquitinated deposits in the spinal cord of SOD1G93A mice during motor neuron disease progression correlates with a decrease of proteasome. *Neurobiol Dis,* 18**,** 509-22.

CHIA, R., CHIO, A. & TRAYNOR, B. J. 2018. Novel genes associated with amyotrophic lateral sclerosis: diagnostic and clinical implications. *Lancet Neurol,* 17**,** 94-102.

CHIO, A., CALVO, A., MAZZINI, L., CANTELLO, R., MORA, G., MOGLIA, C., CORRADO, L., D'ALFONSO, S., MAJOUNIE, E., RENTON, A., PISANO, F., OSSOLA, I., BRUNETTI, M., TRAYNOR, B. J. & RESTAGNO, G. 2012. Extensive genetics of ALS: a population-based study in Italy. *Neurology,* 79**,** 1983-9.

CHIO, A., LOGROSCINO, G., TRAYNOR, B. J., COLLINS, J., SIMEONE, J. C., GOLDSTEIN, L. A. & WHITE, L. A. 2013. Global epidemiology of amyotrophic lateral sclerosis: a systematic review of the published literature. *Neuroepidemiology,* 41**,** 118-30.

CHOW, C. Y., LANDERS, J. E., BERGREN, S. K., SAPP, P. C., GRANT, A. E., JONES, J. M., EVERETT, L., LENK, G. M., MCKENNA-YASEK, D. M., WEISMAN, L. S., FIGLEWICZ, D., BROWN, R. H. & MEISLER, M. H. 2009. Deleterious variants of FIG4, a phosphoinositide phosphatase, in patients with ALS. *American journal of human genetics,* 84**,** 85-88.

CIECHANOVER, A. & BRUNDIN, P. 2003. The ubiquitin proteasome system in neurodegenerative diseases: sometimes the chicken, sometimes the egg. *Neuron,* 40**,** 427-46.

CIRULLI, E. T., LASSEIGNE, B. N., PETROVSKI, S., SAPP, P. C., DION, P. A., LEBLOND, C. S., COUTHOUIS, J., LU, Y. F., WANG, Q., KRUEGER, B. J., REN,

Z., KEEBLER, J., HAN, Y., LEVY, S. E., BOONE, B. E., WIMBISH, J. R., WAITE, L. L., JONES, A. L., CARULLI, J. P., DAY-WILLIAMS, A. G., STAROPOLI, J. F., XIN, W. W., CHESI, A., RAPHAEL, A. R., MCKENNA-YASEK, D., CADY, J., VIANNEY DE JONG, J. M., KENNA, K. P., SMITH, B. N., TOPP, S., MILLER, J., GKAZI, A., AL-CHALABI, A., VAN DEN BERG, L. H., VELDINK, J., SILANI, V., TICOZZI, N., SHAW, C. E., BALOH, R. H., APPEL, S., SIMPSON, E., LAGIER-TOURENNE, C., PULST, S. M., GIBSON, S., TROJANOWSKI, J. Q., ELMAN, L., MCCLUSKEY, L., GROSSMAN, M., SHNEIDER, N. A., CHUNG, W. K., RAVITS, J. M., GLASS, J. D., SIMS, K. B., VAN DEERLIN, V. M., MANIATIS, T., HAYES, S. D., ORDUREAU, A., SWARUP, S., LANDERS, J., BAAS, F., ALLEN, A. S., BEDLACK, R. S., HARPER, J. W., GITLER, A. D., ROULEAU, G. A., BROWN, R., HARMS, M. B., COOPER, G. M., HARRIS, T., MYERS, R. M. & GOLDSTEIN, D. B. 2015. Exome sequencing in amyotrophic lateral sclerosis identifies risk genes and pathways. *Science,* 347**,** 1436-41.

CLAGUE, M. J. & URBE, S. 2010. Ubiquitin: same molecule, different degradation pathways. *Cell,* 143**,** 682-5.

COELHO, M. B., ATTIG, J., BELLORA, N., KONIG, J., HALLEGGER, M., KAYIKCI, M., EYRAS, E., ULE, J. & SMITH, C. W. 2015. Nuclear matrix protein Matrin3 regulates alternative splicing and forms overlapping regulatory networks with PTB. *Embo j,* 34**,** 653-68.

COHEN, T. J., HWANG, A. W., UNGER, T., TROJANOWSKI, J. Q. & LEE, V. M. 2012. Redox signalling directly regulates TDP-43 via cysteine oxidation and disulphide cross-linking. *Embo j,* 31**,** 1241-52.

COLOMBRITA, C., ZENNARO, E., FALLINI, C., WEBER, M., SOMMACAL, A., BURATTI, E., SILANI, V. & RATTI, A. 2009. TDP-43 is recruited to stress granules in conditions of oxidative insult. *J Neurochem,* 111**,** 1051-61.

COX, L. E., FERRAIUOLO, L., GOODALL, E. F., HEATH, P. R., HIGGINBOTTOM, A., MORTIBOYS, H., HOLLINGER, H. C., HARTLEY, J. A., BROCKINGTON, A., BURNESS, C. E., MORRISON, K. E., WHARTON, S. B., GRIERSON, A. J., INCE, P. G., KIRBY, J. & SHAW, P. J. 2010. Mutations in CHMP2B in lower motor neuron predominant amyotrophic lateral sclerosis (ALS). *PLoS One,* 5**,** e9872.

CULLINAN, S. B. & DIEHL, J. A. 2006. Coordination of ER and oxidative stress signaling: the PERK/Nrf2 signaling pathway. *Int J Biochem Cell Biol,* 38**,** 317-32.

DAMIANO, M., STARKOV, A. A., PETRI, S., KIPIANI, K., KIAEI, M., MATTIAZZI, M., FLINT BEAL, M. & MANFREDI, G. 2006. Neural mitochondrial Ca2+ capacity impairment precedes the onset of motor symptoms in G93A Cu/Zn-superoxide dismutase mutant mice. *J Neurochem,* 96**,** 1349-61.

DAOUD, H. & ROULEAU, G. A. 2011. A role for ubiquilin 2 mutations in neurodegeneration. *Nature Reviews Neurology,* 7**,** 599.

DAOUD, H., SUHAIL, H., SZUTO, A., CAMU, W., SALACHAS, F., MEININGER, V., BOUCHARD, J. P., DUPRE, N., DION, P. A. & ROULEAU, G. A. 2012. UBQLN2 mutations are rare in French and French-Canadian amyotrophic lateral sclerosis. *Neurobiol Aging,* 33**,** 2230.e1-2230.e5.

DAVIDSON, Y., ROBINSON, A. C., LIU, X., WU, D., TROAKES, C., ROLLINSON, S., MASUDA-SUZUKAKE, M., SUZUKI, G., NONAKA, T., SHI, J., TIAN, J., HAMDALLA, H., EALING, J., RICHARDSON, A., JONES, M., PICKERING-BROWN, S., SNOWDEN, J. S., HASEGAWA, M. & MANN, D. M. 2016.

Neurodegeneration in frontotemporal lobar degeneration and motor neurone disease associated with expansions in C9orf72 is linked to TDP-43 pathology and not associated with aggregated forms of dipeptide repeat proteins. *Neuropathol Appl Neurobiol,* 42**,** 242-54.

DE MAJO, M., TOPP, S. D., SMITH, B. N., NISHIMURA, A. L., CHEN, H. J., GKAZI, A. S., MILLER, J., WONG, C. H., VANCE, C., BAAS, F., TEN ASBROEK, A., KENNA, K. P., TICOZZI, N., REDONDO, A. G., ESTEBAN-PEREZ, J., TILOCA, C., VERDE, F., DUGA, S., MORRISON, K. E., SHAW, P. J., KIRBY, J., TURNER, M. R., TALBOT, K., HARDIMAN, O., GLASS, J. D., DE BELLEROCHE, J., GELLERA, C., RATTI, A., AL-CHALABI, A., BROWN, R. H., SILANI, V., LANDERS, J. E. & SHAW, C. E. 2018. ALS-associated missense and nonsense TBK1 mutations can both cause loss of kinase function. *Neurobiol Aging,* 71**,** 266.e1-266.e10.

DEJESUS-HERNANDEZ, M., MACKENZIE, I. R., BOEVE, B. F., BOXER, A. L., BAKER, M., RUTHERFORD, N. J., NICHOLSON, A. M., FINCH, N. A., FLYNN, H., ADAMSON, J., KOURI, N., WOJTAS, A., SENGDY, P., HSIUNG, G. Y., KARYDAS, A., SEELEY, W. W., JOSEPHS, K. A., COPPOLA, G., GESCHWIND, D. H., WSZOLEK, Z. K., FELDMAN, H., KNOPMAN, D. S., PETERSEN, R. C., MILLER, B. L., DICKSON, D. W., BOYLAN, K. B., GRAFF-RADFORD, N. R. & RADEMAKERS, R. 2011. Expanded GGGGCC hexanucleotide repeat in noncoding region of C9ORF72 causes chromosome 9p-linked FTD and ALS. *Neuron,* 72**,** 245-56.

DENG, H. X., CHEN, W., HONG, S. T., BOYCOTT, K. M., GORRIE, G. H., SIDDIQUE, N., YANG, Y., FECTO, F., SHI, Y., ZHAI, H., JIANG, H., HIRANO, M., RAMPERSAUD, E., JANSEN, G. H., DONKERVOORT, S., BIGIO, E. H., BROOKS, B. R., AJROUD, K., SUFIT, R. L., HAINES, J. L., MUGNAINI, E., PERICAK-

VANCE, M. A. & SIDDIQUE, T. 2011. Mutations in UBQLN2 cause dominant X-linked juvenile and adult-onset ALS and ALS/dementia. *Nature,* 477**,** 211-5.

DENG, J., YANG, M., CHEN, Y., CHEN, X., LIU, J., SUN, S., CHENG, H., LI, Y., BIGIO, E. H., MESULAM, M., XU, Q., DU, S., FUSHIMI, K., ZHU, L. & WU, J. Y. 2015. FUS Interacts with HSP60 to Promote Mitochondrial Damage. *PLoS Genet,* 11**,** e1005357.

DEWEY, C. M., CENIK, B., SEPHTON, C. F., DRIES, D. R., MAYER, P., 3RD, GOOD, S. K., JOHNSON, B. A., HERZ, J. & YU, G. 2011. TDP-43 is directed to stress granules by sorbitol, a novel physiological osmotic and oxidative stressor. *Mol Cell Biol,* 31**,** 1098-108.

DIERING, G. H. & NUMATA, M. 2014. Endosomal pH in neuronal signaling and synaptic transmission: role of Na(+)/H(+) exchanger NHE5. *Frontiers in physiology,* 4**,** 412-412.

DOBLE, A. 1996. The pharmacology and mechanism of action of riluzole. *Neurology,* 47**,** S233-41.

DOLINAR, A., RAVNIK-GLAVAC, M. & GLAVAC, D. 2018. Epigenetic mechanisms in amyotrophic lateral sclerosis: A short review. *Mech Ageing Dev,* 174**,** 103-110.

DOLS-ICARDO, O., NEBOT, I., GOROSTIDI, A., ORTEGA-CUBERO, S., HERNANDEZ, I., ROJAS-GARCIA, R., GARCIA-REDONDO, A., POVEDANO, M., LLADO, A., ALVAREZ, V., SANCHEZ-JUAN, P., PARDO, J., JERICO, I., VAZQUEZ-COSTA, J., SEVILLA, T., CARDONA, F., INDAKOECHEA, B., MORENO, F., FERNANDEZ-TORRON, R., MUNOZ-LLAHUNA, L., MORENO-GRAU, S., ROSENDE-ROCA, M., VELA, A., MUNOZ-BLANCO, J. L., COMBARROS, O., COTO, E., ALCOLEA, D., FORTEA, J., LLEO, A., SANCHEZ-VALLE, R.,

ESTEBAN-PEREZ, J., RUIZ, A., PASTOR, P., LOPEZ DE MUNAIN, A., PEREZ-TUR, J. & CLARIMON, J. 2015. Analysis of the CHCHD10 gene in patients with frontotemporal dementia and amyotrophic lateral sclerosis from Spain. *Brain,* 138**,** e400.

EGGERMONT, J., BUYSE, G., VOETS, T., TYTGAT, J., DE SMEDT, H., DROOGMANS, G. & NILIUS, B. 1997. Alternative splicing of ClC-6 (a member of the CIC chloride-channel family) transcripts generates three truncated isoforms one of which, ClC-6c, is kidney-specific. *Biochem J,* 325 (Pt 1)**,** 269-76.

EKHTIARI BIDHENDI, E., BERGH, J., ZETTERSTROM, P., FORSBERG, K., PAKKENBERG, B., ANDERSEN, P. M., MARKLUND, S. L. & BRANNSTROM, T. 2018. Mutant superoxide dismutase aggregates from human spinal cord transmit amyotrophic lateral sclerosis. *Acta Neuropathol*.

ELDEN, A. C., KIM, H. J., HART, M. P., CHEN-PLOTKIN, A. S., JOHNSON, B. S., FANG, X., ARMAKOLA, M., GESER, F., GREENE, R., LU, M. M., PADMANABHAN, A., CLAY-FALCONE, D., MCCLUSKEY, L., ELMAN, L., JUHR, D., GRUBER, P. J., RUB, U., AUBURGER, G., TROJANOWSKI, J. Q., LEE, V. M., VAN DEERLIN, V. M., BONINI, N. M. & GITLER, A. D. 2010. Ataxin-2 intermediate-length polyglutamine expansions are associated with increased risk for ALS. *Nature,* 466**,** 1069-75.

ELKIN, S. R., LAKODUK, A. M. & SCHMID, S. L. 2016. Endocytic pathways and endosomal trafficking: a primer. *Wien Med Wochenschr,* 166**,** 196-204.

ESTEVEZ, A. G., CROW, J. P., SAMPSON, J. B., REITER, C., ZHUANG, Y., RICHARDSON, G. J., TARPEY, M. M., BARBEITO, L. & BECKMAN, J. S. 1999.

Induction of nitric oxide-dependent apoptosis in motor neurons by zinc-deficient superoxide dismutase. *Science,* 286**,** 2498-500.

EZZI, S. A., URUSHITANI, M. & JULIEN, J. P. 2007. Wild-type superoxide dismutase acquires binding and toxic properties of ALS-linked mutant forms through oxidation. *J Neurochem,* 102**,** 170-8.

FARG, M. A., SOO, K. Y., WARRAICH, S. T., SUNDARAMOORTHY, V., BLAIR, I. P. & ATKIN, J. D. 2013. Ataxin-2 interacts with FUS and intermediate-length polyglutamine expansions enhance FUS-related pathology in amyotrophic lateral sclerosis. *Hum Mol Genet,* 22**,** 717-28.

FARG, M. A., SUNDARAMOORTHY, V., SULTANA, J. M., YANG, S., ATKINSON, R. A., LEVINA, V., HALLORAN, M. A., GLEESON, P. A., BLAIR, I. P., SOO, K. Y., KING, A. E. & ATKIN, J. D. 2014. C9ORF72, implicated in amytrophic lateral sclerosis and frontotemporal dementia, regulates endosomal trafficking. *Hum Mol Genet,* 23**,** 3579-95.

FECTO, F., YAN, J., VEMULA, S. P., LIU, E., YANG, Y., CHEN, W., ZHENG, J. G., SHI, Y., SIDDIQUE, N., ARRAT, H., DONKERVOORT, S., AJROUD-DRISS, S., SUFIT, R. L., HELLER, S. L., DENG, H. X. & SIDDIQUE, T. 2011. SQSTM1 mutations in familial and sporadic amyotrophic lateral sclerosis. *Arch Neurol,* 68**,** 1440-6.

FERGUSON, T. A. & ELMAN, L. B. 2007. Clinical presentation and diagnosis of amyotrophic lateral sclerosis. *NeuroRehabilitation,* 22**,** 409-16.

FIGLEWICZ, D. A., KRIZUS, A., MARTINOLI, M. G., MEININGER, V., DIB, M., ROULEAU, G. A. & JULIEN, J. P. 1994. Variants of the heavy neurofilament subunit are associated with the development of amyotrophic lateral sclerosis. *Hum Mol Genet,* 3**,** 1757-61.

FIGLEY, M. D., BIERI, G., KOLAITIS, R. M., TAYLOR, J. P. & GITLER, A. D. 2014. Profilin 1 associates with stress granules and ALS-linked mutations alter stress granule dynamics. *J Neurosci,* 34**,** 8083-97.

FIGUEROA-ROMERO, C., HUR, J., LUNN, J. S., PAEZ-COLASANTE, X., BENDER, D. E., YUNG, R., SAKOWSKI, S. A. & FELDMAN, E. L. 2016. Expression of microRNAs in human post-mortem amyotrophic lateral sclerosis spinal cords provides insight into disease mechanisms. *Mol Cell Neurosci,* 71**,** 34-45.

FREISCHMIDT, A., WIELAND, T., RICHTER, B., RUF, W., SCHAEFFER, V., MULLER, K., MARROQUIN, N., NORDIN, F., HUBERS, A., WEYDT, P., PINTO, S., PRESS, R., MILLECAMPS, S., MOLKO, N., BERNARD, E., DESNUELLE, C., SORIANI, M. H., DORST, J., GRAF, E., NORDSTROM, U., FEILER, M. S., PUTZ, S., BOECKERS, T. M., MEYER, T., WINKLER, A. S., WINKELMAN, J., DE CARVALHO, M., THAL, D. R., OTTO, M., BRANNSTROM, T., VOLK, A. E., KURSULA, P., DANZER, K. M., LICHTNER, P., DIKIC, I., MEITINGER, T., LUDOLPH, A. C., STROM, T. M., ANDERSEN, P. M. & WEISHAUPT, J. H. 2015. Haploinsufficiency of TBK1 causes familial ALS and fronto-temporal dementia. *Nat Neurosci,* 18**,** 631-6.

FUKUNAGA, K., SHINODA, Y. & TAGASHIRA, H. 2015. The role of SIGMAR1 gene mutation and mitochondrial dysfunction in amyotrophic lateral sclerosis. *J Pharmacol Sci,* 127**,** 36-41.

GANLEY, I. G., LAM DU, H., WANG, J., DING, X., CHEN, S. & JIANG, X. 2009. ULK1.ATG13.FIP200 complex mediates mTOR signaling and is essential for autophagy. *J Biol Chem,* 284**,** 12297-305.

GENIN, E. C., PLUTINO, M., BANNWARTH, S., VILLA, E., CISNEROS-BARROSO, E., ROY, M., ORTEGA-VILA, B., FRAGAKI, K., LESPINASSE, F., PINERO-MARTOS, E., AUGÉ, G., MOORE, D., BURTÉ, F., LACAS-GERVAIS, S., KAGEYAMA, Y., ITOH, K., YU-WAI-MAN, P., SESAKI, H., RICCI, J.-E., VIVES-BAUZA, C. & PAQUIS-FLUCKLINGER, V. 2016. CHCHD10 mutations promote loss of mitochondrial cristae junctions with impaired mitochondrial genome maintenance and inhibition of apoptosis. *EMBO molecular medicine,* 8**,** 58-72.

GHAVAMI, S., CUNNINGTON, R. H., YEGANEH, B., DAVIES, J. J., RATTAN, S. G., BATHE, K., KAVOSH, M., LOS, M. J., FREED, D. H., KLONISCH, T., PIERCE, G. N., HALAYKO, A. J. & DIXON, I. M. 2012. Autophagy regulates trans fatty acid-mediated apoptosis in primary cardiac myofibroblasts. *Biochim Biophys Acta,* 1823**,** 2274-86.

GHAVAMI, S., SHOJAEI, S., YEGANEH, B., ANDE, S. R., JANGAMREDDY, J. R., MEHRPOUR, M., CHRISTOFFERSSON, J., CHAABANE, W., MOGHADAM, A. R., KASHANI, H. H., HASHEMI, M., OWJI, A. A. & LOS, M. J. 2014. Autophagy and apoptosis dysfunction in neurodegenerative disorders. *Prog Neurobiol,* 112**,** 24-49.

GIJSELINCK, I., VAN MOSSEVELDE, S., VAN DER ZEE, J., SIEBEN, A., PHILTJENS, S., HEEMAN, B., ENGELBORGHS, S., VANDENBULCKE, M., DE BAETS, G., BAUMER, V., CUIJT, I., VAN DEN BROECK, M., PEETERS, K., MATTHEIJSSENS, M., ROUSSEAU, F., VANDENBERGHE, R., DE JONGHE, P., CRAS, P., DE DEYN, P. P., MARTIN, J. J., CRUTS, M. & VAN BROECKHOVEN, C. 2015. Loss of TBK1 is a frequent cause of frontotemporal dementia in a Belgian cohort. *Neurology,* 85**,** 2116-25.

GILPIN, K. M., CHANG, L. & MONTEIRO, M. J. 2015. ALS-linked mutations in ubiquilin-2 or hnRNPA1 reduce interaction between ubiquilin-2 and hnRNPA1. *Hum Mol Genet,* 24**,** 2565-77.

GIORDANA, M. T., PICCININI, M., GRIFONI, S., DE MARCO, G., VERCELLINO, M., MAGISTRELLO, M., PELLERINO, A., BUCCINNA, B., LUPINO, E. & RINAUDO, M. T. 2010. TDP-43 redistribution is an early event in sporadic amyotrophic lateral sclerosis. *Brain Pathol,* 20**,** 351-60.

GITLER, A. D. & SHORTER, J. 2011. RNA-binding proteins with prion-like domains in ALS and FTLD-U. *Prion,* 5**,** 179-87.

GLASS, J. D., HERTZBERG, V. S., BOULIS, N. M., RILEY, J., FEDERICI, T., POLAK, M., BORDEAU, J., FOURNIER, C., JOHE, K., HAZEL, T., CUDKOWICZ, M., ATASSI, N., BORGES, L. F., RUTKOVE, S. B., DUELL, J., PATIL, P. G., GOUTMAN, S. A. & FELDMAN, E. L. 2016. Transplantation of spinal cord-derived neural stem cells for ALS: Analysis of phase 1 and 2 trials. *Neurology,* 87**,** 392-400.

GLICK, D., BARTH, S. & MACLEOD, K. F. 2010. Autophagy: cellular and molecular mechanisms. *J Pathol,* 221**,** 3-12.

GORDON, P. H., CHENG, B., KATZ, I. B., PINTO, M., HAYS, A. P., MITSUMOTO, H. & ROWLAND, L. P. 2006. The natural history of primary lateral sclerosis. *Neurology,* 66**,** 647-53.

GREENWAY, M. J., ANDERSEN, P. M., RUSS, C., ENNIS, S., CASHMAN, S., DONAGHY, C., PATTERSON, V., SWINGLER, R., KIERAN, D., PREHN, J., MORRISON, K. E., GREEN, A., ACHARYA, K. R., BROWN, R. H., JR. & HARDIMAN, O. 2006. ANG mutations segregate with familial and 'sporadic' amyotrophic lateral sclerosis. *Nat Genet,* 38**,** 411-3.

GROS-LOUIS, F., KRIZ, J., KABASHI, E., MCDEARMID, J., MILLECAMPS, S., URUSHITANI, M., LIN, L., DION, P., ZHU, Q., DRAPEAU, P., JULIEN, J. P. & ROULEAU, G. A. 2008. Als2 mRNA splicing variants detected in KO mice rescue severe motor dysfunction phenotype in Als2 knock-down zebrafish. *Hum Mol Genet,* 17**,** 2691-702.

GUÉGAN, C. & PRZEDBORSKI, S. 2003. Programmed cell death in amyotrophic lateral sclerosis. *The Journal of clinical investigation,* 111**,** 153-161.

GUNTHER, W., PIWON, N. & JENTSCH, T. J. 2003. The ClC-5 chloride channel knock-out mouse - an animal model for Dent's disease. *Pflugers Arch,* 445**,** 456-62.

GUO, J. L. & LEE, V. M. Y. 2014. Cell-to-cell transmission of pathogenic proteins in neurodegenerative diseases. *Nature medicine,* 20**,** 130-138.

GURNEY, M. E. 1997. The use of transgenic mouse models of amyotrophic lateral sclerosis in preclinical drug studies. *J Neurol Sci,* 152 Suppl 1**,** S67-73.

HADANO, S., HAND, C. K., OSUGA, H., YANAGISAWA, Y., OTOMO, A., DEVON, R. S., MIYAMOTO, N., SHOWGUCHI-MIYATA, J., OKADA, Y., SINGARAJA, R., FIGLEWICZ, D. A., KWIATKOWSKI, T., HOSLER, B. A., SAGIE, T., SKAUG, J., NASIR, J., BROWN, R. H., JR., SCHERER, S. W., ROULEAU, G. A., HAYDEN, M. R. & IKEDA, J. E. 2001. A gene encoding a putative GTPase regulator is mutated in familial amyotrophic lateral sclerosis 2. *Nat Genet,* 29**,** 166-73.

HAMMER, R. P., JR., TOMIYASU, U. & SCHEIBEL, A. B. 1979. Degeneration of the human Betz cell due to amyotrophic lateral sclerosis. *Exp Neurol,* 63**,** 336-46.

HANADA, T., NODA, N. N., SATOMI, Y., ICHIMURA, Y., FUJIOKA, Y., TAKAO, T., INAGAKI, F. & OHSUMI, Y. 2007. The Atg12-Atg5 conjugate has a novel E3-like activity for protein lipidation in autophagy. *J Biol Chem,* 282**,** 37298-302.

HANS, F., ECKERT, M., VON ZWEYDORF, F., GLOECKNER, C. J. & KAHLE, P. J. 2018. Identification and characterization of ubiquitinylation sites in TAR DNA-binding protein of 43 kDa (TDP-43). *J Biol Chem,* 293**,** 16083-16099.

HARA-CHIKUMA, M., WANG, Y., GUGGINO, S. E., GUGGINO, W. B. & VERKMAN, A. S. 2005a. Impaired acidification in early endosomes of ClC-5 deficient proximal tubule. *Biochem Biophys Res Commun,* 329**,** 941-6.

HARA-CHIKUMA, M., YANG, B., SONAWANE, N. D., SASAKI, S., UCHIDA, S. & VERKMAN, A. S. 2005b. ClC-3 chloride channels facilitate endosomal acidification and chloride accumulation. *J Biol Chem,* 280**,** 1241-7.

HARDING, H. P., ZHANG, Y. & RON, D. 1999. Protein translation and folding are coupled by an endoplasmic-reticulum-resident kinase. *Nature,* 397**,** 271-4.

HART, M. P. & GITLER, A. D. 2012. ALS-associated ataxin 2 polyQ expansions enhance stress-induced caspase 3 activation and increase TDP-43 pathological modifications. *J Neurosci,* 32**,** 9133-42.

HENAULT, J., MARTINEZ, J., RIGGS, J. M., TIAN, J., MEHTA, P., CLARKE, L., SASAI, M., LATZ, E., BRINKMANN, M. M., IWASAKI, A., COYLE, A. J., KOLBECK, R., GREEN, D. R. & SANJUAN, M. A. 2012. Noncanonical Autophagy Is Required for Type I Interferon Secretion in Response to DNA-Immune Complexes. *Immunity,* 37**,** 986-997.

HETZ, C. 2012. The unfolded protein response: controlling cell fate decisions under ER stress and beyond. *Nat Rev Mol Cell Biol,* 13**,** 89-102.

HETZ, C., CHEVET, E. & OAKES, S. A. 2015. Proteostasis control by the unfolded protein response. *Nat Cell Biol,* 17**,** 829-38.

HETZ, C. & MOLLEREAU, B. 2014. Disturbance of endoplasmic reticulum proteostasis in neurodegenerative diseases. *Nat Rev Neurosci,* 15**,** 233-49.

HETZ, C., THIELEN, P., MATUS, S., NASSIF, M., COURT, F., KIFFIN, R., MARTINEZ, G., CUERVO, A. M., BROWN, R. H. & GLIMCHER, L. H. 2009. XBP-1 deficiency in the nervous system protects against amyotrophic lateral sclerosis by increasing autophagy. *Genes Dev,* 23**,** 2294-306.

HIGASHI, S., TSUCHIYA, Y., ARAKI, T., WADA, K. & KABUTA, T. 2010. TDP-43 physically interacts with amyotrophic lateral sclerosis-linked mutant CuZn superoxide dismutase. *Neurochem Int,* 57**,** 906-13.

HIGELIN, J., CATANESE, A., SEMELINK-SEDLACEK, L. L., OEZTUERK, S., LUTZ, A. K., BAUSINGER, J., BARBI, G., SPEIT, G., ANDERSEN, P. M., LUDOLPH, A. C., DEMESTRE, M. & BOECKERS, T. M. 2018. NEK1 loss-of-function mutation induces DNA damage accumulation in ALS patient-derived motoneurons. *Stem Cell Res,* 30**,** 150-162.

HIGGINS, C. M., JUNG, C., DING, H. & XU, Z. 2002. Mutant Cu, Zn superoxide dismutase that causes motoneuron degeneration is present in mitochondria in the CNS. *J Neurosci,* 22**,** Rc215.

HIGGINS, C. M., JUNG, C. & XU, Z. 2003. ALS-associated mutant SOD1G93A causes mitochondrial vacuolation by expansion of the intermembrane space and by involvement of SOD1 aggregation and peroxisomes. *BMC Neurosci,* 4**,** 16.

HIPP, M. S., PARK, S. H. & HARTL, F. U. 2014. Proteostasis impairment in protein-misfolding and -aggregation diseases. *Trends Cell Biol,* 24**,** 506-14.

HIRANO, M., QUINZII, C. M., MITSUMOTO, H., HAYS, A. P., ROBERTS, J. K., RICHARD, P. & ROWLAND, L. P. 2011. Senataxin mutations and amyotrophic lateral sclerosis. *Amyotroph Lateral Scler,* 12**,** 223-7.

HONDA, H., HAMASAKI, H., WAKAMIYA, T., KOYAMA, S., SUZUKI, S. O., FUJII, N. & IWAKI, T. 2015. Loss of hnRNPA1 in ALS spinal cord motor neurons with TDP-43-positive inclusions. *Neuropathology,* 35**,** 37-43.

HOSOI, T., NOMURA, J., TANAKA, K., OZAWA, K., NISHI, A. & NOMURA, Y. 2017. Link between endoplasmic reticulum stress and autophagy in neurodegenerative diseases. *Endoplasmic Reticulum Stress in Diseases.*

HOWLAND, D. S., LIU, J., SHE, Y., GOAD, B., MARAGAKIS, N. J., KIM, B., ERICKSON, J., KULIK, J., DEVITO, L., PSALTIS, G., DEGENNARO, L. J., CLEVELAND, D. W. & ROTHSTEIN, J. D. 2002. Focal loss of the glutamate transporter EAAT2 in a transgenic rat model of SOD1 mutant-mediated amyotrophic lateral sclerosis (ALS). *Proc Natl Acad Sci U S A,* 99**,** 1604-9.

HOYER-HANSEN, M. & JAATTELA, M. 2007. Connecting endoplasmic reticulum stress to autophagy by unfolded protein response and calcium. *Cell Death Differ,* 14**,** 1576-82.

HSUEH, K. W., CHIOU, T. W., CHIANG, S. F., YAMASHITA, T., ABE, K., BORLONGAN, C. V., SANBERG, P. R., HUANG, A. Y., LIN, S. Z. & HARN, H. J. 2016. Autophagic

down-regulation in motor neurons remarkably prolongs the survival of ALS mice. *Neuropharmacology,* 108**,** 152-60.

HU, Y. B., DAMMER, E. B., REN, R. J. & WANG, G. 2015. The endosomal-lysosomal system: from acidification and cargo sorting to neurodegeneration. *Transl Neurodegener,* 4**,** 18.

HUANG, C., ZHOU, H., TONG, J., CHEN, H., LIU, Y. J., WANG, D., WEI, X. & XIA, X. G. 2011. FUS transgenic rats develop the phenotypes of amyotrophic lateral sclerosis and frontotemporal lobar degeneration. *PLoS Genet,* 7**,** e1002011.

HULISZ, D. 2018. Amyotrophic lateral sclerosis: disease state overview. *Am J Manag Care,* 24**,** S320-s326.

HUOTARI, J. & HELENIUS, A. Endosome maturation. *The EMBO journal,* 30**,** 3481-3500.

HUSSAIN, T. & MULHERKAR, R. 2012. Lymphoblastoid Cell lines: a Continuous in Vitro Source of Cells to Study Carcinogen Sensitivity and DNA Repair. *Int J Mol Cell Med,* 1**,** 75-87.

IGNOUL, S., SIMAELS, J., HERMANS, D., ANNAERT, W. & EGGERMONT, J. 2007. Human ClC-6 is a late endosomal glycoprotein that associates with detergent-resistant lipid domains. *PLoS One,* 2**,** e474.

ILIEVA, E. V., AYALA, V., JOVE, M., DALFO, E., CACABELOS, D., POVEDANO, M., BELLMUNT, M. J., FERRER, I., PAMPLONA, R. & PORTERO-OTIN, M. 2007. Oxidative and endoplasmic reticulum stress interplay in sporadic amyotrophic lateral sclerosis. *Brain,* 130**,** 3111-23.

ILIEVA, H., POLYMENIDOU, M. & CLEVELAND, D. W. 2009. Non-cell autonomous toxicity in neurodegenerative disorders: ALS and beyond. *J Cell Biol,* 187**,** 761-72.

INGRE, C., ROOS, P. M., PIEHL, F., KAMEL, F. & FANG, F. 2015. Risk factors for amyotrophic lateral sclerosis. *Clinical epidemiology,* 7**,** 181-193.

ITAKURA, E., KISHI, C., INOUE, K. & MIZUSHIMA, N. 2008. Beclin 1 forms two distinct phosphatidylinositol 3-kinase complexes with mammalian Atg14 and UVRAG. *Mol Biol Cell,* 19**,** 5360-72.

JENTSCH, T. J. 2007. Chloride and the endosomal-lysosomal pathway: emerging roles of CLC chloride transporters. *J Physiol,* 578**,** 633-40.

JENTSCH, T. J., STEIN, V., WEINREICH, F. & ZDEBIK, A. A. 2002. Molecular structure and physiological function of chloride channels. *Physiol Rev,* 82**,** 503-68.

JIANG, J., ZHU, Q., GENDRON, T. F., SABERI, S., MCALONIS-DOWNES, M., SEELMAN, A., STAUFFER, J. E., JAFAR-NEJAD, P., DRENNER, K., SCHULTE, D., CHUN, S., SUN, S., LING, S. C., MYERS, B., ENGELHARDT, J., KATZ, M., BAUGHN, M., PLATOSHYN, O., MARSALA, M., WATT, A., HEYSER, C. J., ARD, M. C., DE MUYNCK, L., DAUGHRITY, L. M., SWING, D. A., TESSAROLLO, L., JUNG, C. J., DELPOUX, A., UTZSCHNEIDER, D. T., HEDRICK, S. M., DE JONG, P. J., EDBAUER, D., VAN DAMME, P., PETRUCELLI, L., SHAW, C. E., BENNETT, C. F., DA CRUZ, S., RAVITS, J., RIGO, F., CLEVELAND, D. W. & LAGIER-TOURENNE, C. 2016. Gain of Toxicity from ALS/FTD-Linked Repeat Expansions in C9ORF72 Is Alleviated by Antisense Oligonucleotides Targeting GGGGCC-Containing RNAs. *Neuron,* 90**,** 535-50.

JOHNSON, J. O., MANDRIOLI, J., BENATAR, M., ABRAMZON, Y., VAN DEERLIN, V. M., TROJANOWSKI, J. Q., GIBBS, J. R., BRUNETTI, M., GRONKA, S., WUU, J., DING, J., MCCLUSKEY, L., MARTINEZ-LAGE, M., FALCONE, D., HERNANDEZ, D. G., AREPALLI, S., CHONG, S., SCHYMICK, J. C., ROTHSTEIN,

J., LANDI, F., WANG, Y. D., CALVO, A., MORA, G., SABATELLI, M., MONSURRO, M. R., BATTISTINI, S., SALVI, F., SPATARO, R., SOLA, P., BORGHERO, G., GALASSI, G., SCHOLZ, S. W., TAYLOR, J. P., RESTAGNO, G., CHIO, A. & TRAYNOR, B. J. 2010. Exome sequencing reveals VCP mutations as a cause of familial ALS. *Neuron,* 68**,** 857-64.

JOHNSON, J. O., PIORO, E. P., BOEHRINGER, A., CHIA, R., FEIT, H., RENTON, A. E., PLINER, H. A., ABRAMZON, Y., MARANGI, G., WINBORN, B. J., GIBBS, J. R., NALLS, M. A., MORGAN, S., SHOAI, M., HARDY, J., PITTMAN, A., ORRELL, R. W., MALASPINA, A., SIDLE, K. C., FRATTA, P., HARMS, M. B., BALOH, R. H., PESTRONK, A., WEIHL, C. C., ROGAEVA, E., ZINMAN, L., DRORY, V. E., BORGHERO, G., MORA, G., CALVO, A., ROTHSTEIN, J. D., DREPPER, C., SENDTNER, M., SINGLETON, A. B., TAYLOR, J. P., COOKSON, M. R., RESTAGNO, G., SABATELLI, M., BOWSER, R., CHIO, A. & TRAYNOR, B. J. 2014. Mutations in the Matrin 3 gene cause familial amyotrophic lateral sclerosis. *Nat Neurosci,* 17**,** 664-666.

JONAS, S. & IZAURRALDE, E. 2015. Towards a molecular understanding of microRNA-mediated gene silencing. *Nat Rev Genet,* 16**,** 421-33.

KABIR, J., LOBO, M. & ZACHARY, I. 2002. Staurosporine induces endothelial cell apoptosis via focal adhesion kinase dephosphorylation and focal adhesion disassembly independent of focal adhesion kinase proteolysis. *Biochemical Journal,* 367**,** 145-155.

KANEKURA, K., NISHIMOTO, I., AISO, S. & MATSUOKA, M. 2006. Characterization of amyotrophic lateral sclerosis-linked P56S mutation of vesicle-associated membrane protein-associated protein B (VAPB/ALS8). *J Biol Chem,* 281**,** 30223-33.

KANG, R., ZEH, H. J., LOTZE, M. T. & TANG, D. 2011. The Beclin 1 network regulates autophagy and apoptosis. *Cell Death Differ,* 18**,** 571-80.

KANG, S. H., LI, Y., FUKAYA, M., LORENZINI, I., CLEVELAND, D. W., OSTROW, L. W., ROTHSTEIN, J. D. & BERGLES, D. E. 2013. Degeneration and impaired regeneration of gray matter oligodendrocytes in amyotrophic lateral sclerosis. *Nat Neurosci,* 16**,** 571-9.

KAPELI, K., MARTINEZ, F. J. & YEO, G. W. 2017. Genetic mutations in RNA-binding proteins and their roles in ALS. *Hum Genet,* 136**,** 1193-1214.

KASPER, D., PLANELLS-CASES, R., FUHRMANN, J. C., SCHEEL, O., ZEITZ, O., RUETHER, K., SCHMITT, A., POET, M., STEINFELD, R., SCHWEIZER, M., KORNAK, U. & JENTSCH, T. J. 2005. Loss of the chloride channel ClC-7 leads to lysosomal storage disease and neurodegeneration. *Embo j,* 24**,** 1079-91.

KATO, S., TAKIKAWA, M., NAKASHIMA, K., HIRANO, A., CLEVELAND, D. W., KUSAKA, H., SHIBATA, N., KATO, M., NAKANO, I. & OHAMA, E. 2000. New consensus research on neuropathological aspects of familial amyotrophic lateral sclerosis with superoxide dismutase 1 (SOD1) gene mutations: inclusions containing SOD1 in neurons and astrocytes. *Amyotroph Lateral Scler Other Motor Neuron Disord,* 1**,** 163-84.

KAUFMAN, R. J. 1999. Stress signaling from the lumen of the endoplasmic reticulum: coordination of gene transcriptional and translational controls. *Genes Dev,* 13**,** 1211-33.

KAUFMAN, R. J. 2002. Orchestrating the unfolded protein response in health and disease. *The Journal of Clinical Investigation,* 110**,** 1389-1398.

KAWAHARA, Y. & MIEDA-SATO, A. 2012. TDP-43 promotes microRNA biogenesis as a component of the Drosha and Dicer complexes. *Proc Natl Acad Sci U S A,* 109**,** 3347-52.

KAWAMATA, T., AKIYAMA, H., YAMADA, T. & MCGEER, P. L. 1992. Immunologic reactions in amyotrophic lateral sclerosis brain and spinal cord tissue. *Am J Pathol,* 140**,** 691-707.

KENNA, K. P., VAN DOORMAAL, P. T., DEKKER, A. M., TICOZZI, N., KENNA, B. J., DIEKSTRA, F. P., VAN RHEENEN, W., VAN EIJK, K. R., JONES, A. R., KEAGLE, P., SHATUNOV, A., SPROVIERO, W., SMITH, B. N., VAN ES, M. A., TOPP, S. D., KENNA, A., MILLER, J. W., FALLINI, C., TILOCA, C., MCLAUGHLIN, R. L., VANCE, C., TROAKES, C., COLOMBRITA, C., MORA, G., CALVO, A., VERDE, F., AL-SARRAJ, S., KING, A., CALINI, D., DE BELLEROCHE, J., BAAS, F., VAN DER KOOI, A. J., DE VISSER, M., TEN ASBROEK, A. L., SAPP, P. C., MCKENNA-YASEK, D., POLAK, M., ASRESS, S., MUNOZ-BLANCO, J. L., STROM, T. M., MEITINGER, T., MORRISON, K. E., CONSORTIUM, S., LAURIA, G., WILLIAMS, K. L., LEIGH, P. N., NICHOLSON, G. A., BLAIR, I. P., LEBLOND, C. S., DION, P. A., ROULEAU, G. A., PALL, H., SHAW, P. J., TURNER, M. R., TALBOT, K., TARONI, F., BOYLAN, K. B., VAN BLITTERSWIJK, M., RADEMAKERS, R., ESTEBAN-PEREZ, J., GARCIA-REDONDO, A., VAN DAMME, P., ROBBERECHT, W., CHIO, A., GELLERA, C., DREPPER, C., SENDTNER, M., RATTI, A., GLASS, J. D., MORA, J. S., BASAK, N. A., HARDIMAN, O., LUDOLPH, A. C., ANDERSEN, P. M., WEISHAUPT, J. H., BROWN, R. H., JR., AL-CHALABI, A., SILANI, V., SHAW, C. E., VAN DEN BERG, L. H., VELDINK, J. H. & LANDERS, J. E. 2016a. NEK1 variants confer susceptibility to amyotrophic lateral sclerosis. *Nat Genet,* 48**,** 1037-42.

KENNA, K. P., VAN DOORMAAL, P. T., DEKKER, A. M., TICOZZI, N., KENNA, B. J., DIEKSTRA, F. P., VAN RHEENEN, W., VAN EIJK, K. R., JONES, A. R., KEAGLE, P., SHATUNOV, A., SPROVIERO, W., SMITH, B. N., VAN ES, M. A., TOPP, S. D., KENNA, A., MILLER, J. W., FALLINI, C., TILOCA, C., MCLAUGHLIN, R. L., VANCE, C., TROAKES, C., COLOMBRITA, C., MORA, G., CALVO, A., VERDE, F., AL-SARRAJ, S., KING, A., CALINI, D., DE BELLEROCHE, J., BAAS, F., VAN DER KOOI, A. J., DE VISSER, M., TEN ASBROEK, A. L., SAPP, P. C., MCKENNA-YASEK, D., POLAK, M., ASRESS, S., MUNOZ-BLANCO, J. L., STROM, T. M., MEITINGER, T., MORRISON, K. E., LAURIA, G., WILLIAMS, K. L., LEIGH, P. N., NICHOLSON, G. A., BLAIR, I. P., LEBLOND, C. S., DION, P. A., ROULEAU, G. A., PALL, H., SHAW, P. J., TURNER, M. R., TALBOT, K., TARONI, F., BOYLAN, K. B., VAN BLITTERSWIJK, M., RADEMAKERS, R., ESTEBAN-PEREZ, J., GARCIA-REDONDO, A., VAN DAMME, P., ROBBERECHT, W., CHIO, A., GELLERA, C., DREPPER, C., SENDTNER, M., RATTI, A., GLASS, J. D., MORA, J. S., BASAK, N. A., HARDIMAN, O., LUDOLPH, A. C., ANDERSEN, P. M., WEISHAUPT, J. H., BROWN, R. H., JR., AL-CHALABI, A., SILANI, V., SHAW, C. E., VAN DEN BERG, L. H., VELDINK, J. H. & LANDERS, J. E. 2016b. NEK1 variants confer susceptibility to amyotrophic lateral sclerosis. *Nat Genet,* 48**,** 1037-42.

KERR, J. F., WYLLIE, A. H. & CURRIE, A. R. 1972. Apoptosis: a basic biological phenomenon with wide-ranging implications in tissue kinetics. *Br J Cancer,* 26**,** 239-57.

KIM, G. H., KIM, J. E., RHIE, S. J. & YOON, S. 2015a. The Role of Oxidative Stress in Neurodegenerative Diseases. *Experimental Neurobiology,* 24**,** 325-340.

KIM, H. J., KIM, N. C., WANG, Y. D., SCARBOROUGH, E. A., MOORE, J., DIAZ, Z., MACLEA, K. S., FREIBAUM, B., LI, S., MOLLIEX, A., KANAGARAJ, A. P., CARTER, R., BOYLAN, K. B., WOJTAS, A. M., RADEMAKERS, R., PINKUS, J. L., GREENBERG, S. A., TROJANOWSKI, J. Q., TRAYNOR, B. J., SMITH, B. N., TOPP, S., GKAZI, A. S., MILLER, J., SHAW, C. E., KOTTLORS, M., KIRSCHNER, J., PESTRONK, A., LI, Y. R., FORD, A. F., GITLER, A. D., BENATAR, M., KING, O. D., KIMONIS, V. E., ROSS, E. D., WEIHL, C. C., SHORTER, J. & TAYLOR, J. P. 2013. Mutations in prion-like domains in hnRNPA2B1 and hnRNPA1 cause multisystem proteinopathy and ALS. *Nature,* 495**,** 467-73.

KIM, N. H., JEONG, M. S., CHOI, S. Y. & HOON KANG, J. 2004. Oxidative modification of neurofilament-L by the Cu,Zn-superoxide dismutase and hydrogen peroxide system. *Biochimie,* 86**,** 553-9.

KIM, Y. M., JUNG, C. H., SEO, M., KIM, E. K., PARK, J. M., BAE, S. S. & KIM, D. H. 2015b. mTORC1 phosphorylates UVRAG to negatively regulate autophagosome and endosome maturation. *Mol Cell,* 57**,** 207-18.

KING, O. D., GITLER, A. D. & SHORTER, J. 2012. The tip of the iceberg: RNA-binding proteins with prion-like domains in neurodegenerative disease. *Brain Res,* 1462**,** 61-80.

KONDORI, N. R., PAUL, P., ROBBINS, J. P., LIU, K., HILDYARD, J. C. W., WELLS, D. J. & DE BELLEROCHE, J. S. 2018. Focus on the Role of D-serine and D-amino Acid Oxidase in Amyotrophic Lateral Sclerosis/Motor Neuron Disease (ALS). *Frontiers in molecular biosciences,* 5**,** 8-8.

KOPPERS, M., VAN BLITTERSWIJK, M. M., VLAM, L., ROWICKA, P. A., VAN VUGHT, P. W., GROEN, E. J., SPLIET, W. G., ENGELEN-LEE, J., SCHELHAAS, H. J., DE VISSER, M., VAN DER KOOI, A. J., VAN DER POL, W. L., PASTERKAMP, R. J.,

VELDINK, J. H. & VAN DEN BERG, L. H. 2012. VCP mutations in familial and sporadic amyotrophic lateral sclerosis. *Neurobiol Aging,* 33**,** 837.e7-13.

KORAC, J., SCHAEFFER, V., KOVACEVIC, I., CLEMENT, A. M., JUNGBLUT, B., BEHL, C., TERZIC, J. & DIKIC, I. 2013. Ubiquitin-independent function of optineurin in autophagic clearance of protein aggregates. *J Cell Sci,* 126**,** 580-92.

KOSTIC, V., JACKSON-LEWIS, V., DE BILBAO, F., DUBOIS-DAUPHIN, M. & PRZEDBORSKI, S. 1997. Bcl-2: prolonging life in a transgenic mouse model of familial amyotrophic lateral sclerosis. *Science,* 277**,** 559-62.

KUČERA, O., ENDLICHER, R., ROUŠAR, T., LOTKOVÁ, H., GARNOL, T., DRAHOTA, Z. & ČERVINKOVÁ, Z. 2014. The Effect of tert-Butyl Hydroperoxide-Induced Oxidative Stress on Lean and Steatotic Rat Hepatocytes In Vitro. *Oxidative Medicine and Cellular Longevity,* 2014**,** 752506.

KWIATKOWSKI, T. J., JR., BOSCO, D. A., LECLERC, A. L., TAMRAZIAN, E., VANDERBURG, C. R., RUSS, C., DAVIS, A., GILCHRIST, J., KASARSKIS, E. J., MUNSAT, T., VALDMANIS, P., ROULEAU, G. A., HOSLER, B. A., CORTELLI, P., DE JONG, P. J., YOSHINAGA, Y., HAINES, J. L., PERICAK-VANCE, M. A., YAN, J., TICOZZI, N., SIDDIQUE, T., MCKENNA-YASEK, D., SAPP, P. C., HORVITZ, H. R., LANDERS, J. E. & BROWN, R. H., JR. 2009. Mutations in the FUS/TLS gene on chromosome 16 cause familial amyotrophic lateral sclerosis. *Science,* 323**,** 1205-8.

LAGIER-TOURENNE, C., BAUGHN, M., RIGO, F., SUN, S., LIU, P., LI, H. R., JIANG, J., WATT, A. T., CHUN, S., KATZ, M., QIU, J., SUN, Y., LING, S. C., ZHU, Q., POLYMENIDOU, M., DRENNER, K., ARTATES, J. W., MCALONIS-DOWNES, M., MARKMILLER, S., HUTT, K. R., PIZZO, D. P., CADY, J., HARMS, M. B.,

BALOH, R. H., VANDENBERG, S. R., YEO, G. W., FU, X. D., BENNETT, C. F., CLEVELAND, D. W. & RAVITS, J. 2013. Targeted degradation of sense and antisense C9orf72 RNA foci as therapy for ALS and frontotemporal degeneration. *Proc Natl Acad Sci U S A,* 110**,** E4530-9.

LAGIER-TOURENNE, C., POLYMENIDOU, M. & CLEVELAND, D. W. 2010. TDP-43 and FUS/TLS: emerging roles in RNA processing and neurodegeneration. *Hum Mol Genet,* 19**,** R46-64.

LAGIER-TOURENNE, C., POLYMENIDOU, M., HUTT, K. R., VU, A. Q., BAUGHN, M., HUELGA, S. C., CLUTARIO, K. M., LING, S. C., LIANG, T. Y., MAZUR, C., WANCEWICZ, E., KIM, A. S., WATT, A., FREIER, S., HICKS, G. G., DONOHUE, J. P., SHIUE, L., BENNETT, C. F., RAVITS, J., CLEVELAND, D. W. & YEO, G. W. 2012. Divergent roles of ALS-linked proteins FUS/TLS and TDP-43 intersect in processing long pre-mRNAs. *Nat Neurosci,* 15**,** 1488-97.

LAI, C., LIN, X., CHANDRAN, J., SHIM, H., YANG, W. J. & CAI, H. 2007. The G59S mutation in p150(glued) causes dysfunction of dynactin in mice. *J Neurosci,* 27**,** 13982-90.

LAI, C., XIE, C., SHIM, H., CHANDRAN, J., HOWELL, B. W. & CAI, H. 2009. Regulation of endosomal motility and degradation by amyotrophic lateral sclerosis 2/alsin. *Mol Brain,* 2**,** 23.

LANSON, N. A., JR. & PANDEY, U. B. 2012. FUS-related proteinopathies: lessons from animal models. *Brain Res,* 1462**,** 44-60.

LATTANTE, S., DE CALBIAC, H., LE BER, I., BRICE, A., CIURA, S. & KABASHI, E. 2015. Sqstm1 knock-down causes a locomotor phenotype ameliorated by rapamycin in a zebrafish model of ALS/FTLD. *Hum Mol Genet,* 24**,** 1682-90.

LAUTENSCHLAEGER, J., PRELL, T. & GROSSKREUTZ, J. 2012. Endoplasmic reticulum stress and the ER mitochondrial calcium cycle in amyotrophic lateral sclerosis. *Amyotroph Lateral Scler,* 13**,** 166-77.

LEBLOND, C. S., KANEB, H. M., DION, P. A. & ROULEAU, G. A. 2014. Dissection of genetic factors associated with amyotrophic lateral sclerosis. *Exp Neurol,* 262 Pt B**,** 91-101.

LEE, A. H., IWAKOSHI, N. N. & GLIMCHER, L. H. 2003. XBP-1 regulates a subset of endoplasmic reticulum resident chaperone genes in the unfolded protein response. *Mol Cell Biol,* 23**,** 7448-59.

LEE, E. B., LEE, V. M. Y. & TROJANOWSKI, J. Q. 2011. Gains or losses: molecular mechanisms of TDP43-mediated neurodegeneration. *Nature Reviews Neuroscience,* 13**,** 38.

LEE, Y. B., CHEN, H. J., PERES, J. N., GOMEZ-DEZA, J., ATTIG, J., STALEKAR, M., TROAKES, C., NISHIMURA, A. L., SCOTTER, E. L., VANCE, C., ADACHI, Y., SARDONE, V., MILLER, J. W., SMITH, B. N., GALLO, J. M., ULE, J., HIRTH, F., ROGELJ, B., HOUART, C. & SHAW, C. E. 2013. Hexanucleotide repeats in ALS/FTD form length-dependent RNA foci, sequester RNA binding proteins, and are neurotoxic. *Cell Rep,* 5**,** 1178-86.

LI, L., ZHANG, X. & LE, W. 2008. Altered macroautophagy in the spinal cord of SOD1 mutant mice. *Autophagy,* 4**,** 290-3.

LIANG, C., LEE, J. S., INN, K. S., GACK, M. U., LI, Q., ROBERTS, E. A., VERGNE, I., DERETIC, V., FENG, P., AKAZAWA, C. & JUNG, J. U. 2008. Beclin1-binding UVRAG targets the class C Vps complex to coordinate autophagosome maturation and endocytic trafficking. *Nat Cell Biol,* 10**,** 776-87.

LIN, M. G. & ZHONG, Q. 2011. Interaction between small GTPase Rab7 and PI3KC3 links autophagy and endocytosis: A new Rab7 effector protein sheds light on membrane trafficking pathways. *Small GTPases,* 2**,** 85-88.

LIU-YESUCEVITZ, L., BILGUTAY, A., ZHANG, Y. J., VANDERWEYDE, T., CITRO, A., MEHTA, T., ZAARUR, N., MCKEE, A., BOWSER, R., SHERMAN, M., PETRUCELLI, L. & WOLOZIN, B. 2010. Tar DNA binding protein-43 (TDP-43) associates with stress granules: analysis of cultured cells and pathological brain tissue. *PLoS One,* 5**,** e13250.

LIU, J., LILLO, C., JONSSON, P. A., VANDE VELDE, C., WARD, C. M., MILLER, T. M., SUBRAMANIAM, J. R., ROTHSTEIN, J. D., MARKLUND, S., ANDERSEN, P. M., BRANNSTROM, T., GREDAL, O., WONG, P. C., WILLIAMS, D. S. & CLEVELAND, D. W. 2004. Toxicity of familial ALS-linked SOD1 mutants from selective recruitment to spinal mitochondria. *Neuron,* 43**,** 5-17.

LOPATE, G., BALOH, R. H., AL-LOZI, M. T., MILLER, T. M., FERNANDES FILHO, J. A., NI, O., LESTON, A., FLORENCE, J., SCHIERBECKER, J. & ALLRED, P. 2010. Familial ALS with extreme phenotypic variability due to the I113T SOD1 mutation. *Amyotroph Lateral Scler,* 11**,** 232-6.

LUDOLPH, A., DRORY, V., HARDIMAN, O., NAKANO, I., RAVITS, J., ROBBERECHT, W. & SHEFNER, J. 2015. A revision of the El Escorial criteria - 2015. *Amyotroph Lateral Scler Frontotemporal Degener,* 16**,** 291-2.

LUDOLPH, A. C., BENDOTTI, C., BLAUGRUND, E., HENGERER, B., LOFFLER, J. P., MARTIN, J., MEININGER, V., MEYER, T., MOUSSAOUI, S., ROBBERECHT, W., SCOTT, S., SILANI, V. & VAN DEN BERG, L. H. 2007. Guidelines for the preclinical

in vivo evaluation of pharmacological active drugs for ALS/MND: report on the 142nd ENMC international workshop. *Amyotroph Lateral Scler,* 8**,** 217-23.

LUTY, A. A., KWOK, J. B., DOBSON-STONE, C., LOY, C. T., COUPLAND, K. G., KARLSTROM, H., SOBOW, T., TCHORZEWSKA, J., MARUSZAK, A., BARCIKOWSKA, M., PANEGYRES, P. K., ZEKANOWSKI, C., BROOKS, W. S., WILLIAMS, K. L., BLAIR, I. P., MATHER, K. A., SACHDEV, P. S., HALLIDAY, G. M. & SCHOFIELD, P. R. 2010. Sigma nonopioid intracellular receptor 1 mutations cause frontotemporal lobar degeneration-motor neuron disease. *Ann Neurol,* 68**,** 639-49.

MACKENZIE, I. R., BIGIO, E. H., INCE, P. G., GESER, F., NEUMANN, M., CAIRNS, N. J., KWONG, L. K., FORMAN, M. S., RAVITS, J., STEWART, H., EISEN, A., MCCLUSKY, L., KRETZSCHMAR, H. A., MONORANU, C. M., HIGHLEY, J. R., KIRBY, J., SIDDIQUE, T., SHAW, P. J., LEE, V. M. & TROJANOWSKI, J. Q. 2007. Pathological TDP-43 distinguishes sporadic amyotrophic lateral sclerosis from amyotrophic lateral sclerosis with SOD1 mutations. *Ann Neurol,* 61**,** 427-34.

MAGRANE, J., CORTEZ, C., GAN, W. B. & MANFREDI, G. 2014. Abnormal mitochondrial transport and morphology are common pathological denominators in SOD1 and TDP43 ALS mouse models. *Hum Mol Genet,* 23**,** 1413-24.

MANN, D. M., ROLLINSON, S., ROBINSON, A., BENNION CALLISTER, J., THOMPSON, J. C., SNOWDEN, J. S., GENDRON, T., PETRUCELLI, L., MASUDA-SUZUKAKE, M., HASEGAWA, M., DAVIDSON, Y. & PICKERING-BROWN, S. 2013. Dipeptide repeat proteins are present in the p62 positive inclusions in patients with frontotemporal lobar degeneration and motor neurone disease associated with expansions in C9ORF72. *Acta Neuropathol Commun,* 1**,** 68.

MARANGI, G., LATTANTE, S., DORONZIO, P. N., CONTE, A., TASCA, G., MONFORTE, M., PATANELLA, A. K., BISOGNI, G., MELEO, E., LA SPADA, S., ZOLLINO, M. & SABATELLI, M. 2017. Matrin 3 variants are frequent in Italian ALS patients. *Neurobiol Aging,* 49**,** 218.e1-218.e7.

MARANGI, G. & TRAYNOR, B. J. 2015. Genetic causes of amyotrophic lateral sclerosis: new genetic analysis methodologies entailing new opportunities and challenges. *Brain Res,* 1607**,** 75-93.

MARKGRAF, D. F., PEPLOWSKA, K. & UNGERMANN, C. 2007. Rab cascades and tethering factors in the endomembrane system. *FEBS Lett,* 581**,** 2125-30.

MARTINEZ-VICENTE, M. 2015. Autophagy in neurodegenerative diseases: From pathogenic dysfunction to therapeutic modulation. *Semin Cell Dev Biol,* 40**,** 115-26.

MARTINEZ-VICENTE, M. 2017. Neuronal Mitophagy in Neurodegenerative Diseases. *Front Mol Neurosci,* 10**,** 64.

MARTINEZ, J., ALMENDINGER, J., OBERST, A., NESS, R., DILLON, C. P., FITZGERALD, P., HENGARTNER, M. O. & GREEN, D. R. 2011. Microtubule-associated protein 1 light chain 3 alpha (LC3)-associated phagocytosis is required for the efficient clearance of dead cells. *Proceedings of the National Academy of Sciences of the United States of America,* 108**,** 17396-17401.

MARTINEZ, J., CUNHA, L. D., PARK, S., YANG, M., LU, Q., ORCHARD, R., LI, Q. Z., YAN, M., JANKE, L., GUY, C., LINKERMANN, A., VIRGIN, H. W. & GREEN, D. R. 2016. Corrigendum: Noncanonical autophagy inhibits the autoinflammatory, lupus-like response to dying cells. *Nature,* 539**,** 124.

MARTINEZ, J., MALIREDDI, R. K., LU, Q., CUNHA, L. D., PELLETIER, S., GINGRAS, S., ORCHARD, R., GUAN, J. L., TAN, H., PENG, J., KANNEGANTI, T. D., VIRGIN, H. W. & GREEN, D. R. 2015. Molecular characterization of LC3-associated phagocytosis reveals distinct roles for Rubicon, NOX2 and autophagy proteins. *Nat Cell Biol,* 17**,** 893-906.

MARUYAMA, H., MORINO, H., ITO, H., IZUMI, Y., KATO, H., WATANABE, Y., KINOSHITA, Y., KAMADA, M., NODERA, H., SUZUKI, H., KOMURE, O., MATSUURA, S., KOBATAKE, K., MORIMOTO, N., ABE, K., SUZUKI, N., AOKI, M., KAWATA, A., HIRAI, T., KATO, T., OGASAWARA, K., HIRANO, A., TAKUMI, T., KUSAKA, H., HAGIWARA, K., KAJI, R. & KAWAKAMI, H. 2010. Mutations of optineurin in amyotrophic lateral sclerosis. *Nature,* 465**,** 223.

MASSILAMANY, C., GANGAPLARA, A., KIM, H., STANFORD, C., RATHNAIAH, G., STEFFEN, D., LEE, J. & REDDY, J. 2013. Copper-zinc superoxide dismutase-deficient mice show increased susceptibility to experimental autoimmune encephalomyelitis induced with myelin oligodendrocyte glycoprotein 35-55. *J Neuroimmunol,* 256**,** 19-27.

MATEUS, D., MARINI, E. S., PROGIDA, C. & BAKKE, O. 2018. Rab7a modulates ER stress and ER morphology. *Biochimica et Biophysica Acta (BBA) - Molecular Cell Research,* 1865**,** 781-793.

MATSUNAGA, K., SAITOH, T., TABATA, K., OMORI, H., SATOH, T., KUROTORI, N., MAEJIMA, I., SHIRAHAMA-NODA, K., ICHIMURA, T., ISOBE, T., AKIRA, S., NODA, T. & YOSHIMORI, T. 2009. Two Beclin 1-binding proteins, Atg14L and Rubicon, reciprocally regulate autophagy at different stages. *Nat Cell Biol,* 11**,** 385-96.

MATTIAZZI, M., D'AURELIO, M., GAJEWSKI, C. D., MARTUSHOVA, K., KIAEI, M., BEAL, M. F. & MANFREDI, G. 2002. Mutated human SOD1 causes dysfunction of oxidative phosphorylation in mitochondria of transgenic mice. *J Biol Chem,* 277**,** 29626-33.

MCGEER, P. L. & MCGEER, E. G. 2002. Inflammatory processes in amyotrophic lateral sclerosis. *Muscle Nerve,* 26**,** 459-70.

MELENDEZ, A. & LEVINE, B. 2009. Autophagy in C. elegans. *WormBook, ed.* The C. elegans Research Community, WormBook.

MENZIES, F. M., FLEMING, A., CARICASOLE, A., BENTO, C. F., ANDREWS, S. P., ASHKENAZI, A., FULLGRABE, J., JACKSON, A., JIMENEZ SANCHEZ, M., KARABIYIK, C., LICITRA, F., LOPEZ RAMIREZ, A., PAVEL, M., PURI, C., RENNA, M., RICKETTS, T., SCHLOTAWA, L., VICINANZA, M., WON, H., ZHU, Y., SKIDMORE, J. & RUBINSZTEIN, D. C. 2017. Autophagy and Neurodegeneration: Pathogenic Mechanisms and Therapeutic Opportunities. *Neuron,* 93**,** 1015-1034.

MEYER, H. & WEIHL, C. C. 2014. The VCP/p97 system at a glance: connecting cellular function to disease pathogenesis. *J Cell Sci,* 127**,** 3877-83.

MIGUEL, L., AVEQUIN, T., PONS, M., FREBOURG, T., CAMPION, D. & LECOURTOIS, M. 2018. FTLD/ALS-linked TDP-43 mutations do not alter TDP-43's ability to self-regulate its expression in Drosophila. *Brain Res,* 1695**,** 1-9.

MITCHELL, J., PAUL, P., CHEN, H.-J., MORRIS, A., PAYLING, M., FALCHI, M., HABGOOD, J., PANOUTSOU, S., WINKLER, S., TISATO, V., HAJITOU, A., SMITH, B., VANCE, C., SHAW, C., MAZARAKIS, N. D. & DE BELLEROCHE, J. 2010. Familial amyotrophic lateral sclerosis is associated with a mutation in D-amino

acid oxidase. *Proceedings of the National Academy of Sciences of the United States of America,* 107**,** 7556-7561.

MITSUMOTO, H., SANTELLA, R. M., LIU, X., BOGDANOV, M., ZIPPRICH, J., WU, H. C., MAHATA, J., KILTY, M., BEDNARZ, K., BELL, D., GORDON, P. H., HORNIG, M., MEHRAZIN, M., NAINI, A., FLINT BEAL, M. & FACTOR-LITVAK, P. 2008. Oxidative stress biomarkers in sporadic ALS. *Amyotroph Lateral Scler,* 9**,** 177-83.

MIZIELINSKA, S., LASHLEY, T., NORONA, F. E., CLAYTON, E. L., RIDLER, C. E., FRATTA, P. & ISAACS, A. M. 2013. C9orf72 frontotemporal lobar degeneration is characterised by frequent neuronal sense and antisense RNA foci. *Acta Neuropathol,* 126**,** 845-57.

MIZUNO, Y., AMARI, M., TAKATAMA, M., AIZAWA, H., MIHARA, B. & OKAMOTO, K. 2006. Transferrin localizes in Bunina bodies in amyotrophic lateral sclerosis. *Acta Neuropathol,* 112**,** 597-603.

MIZUNO, Y., FUJITA, Y., TAKATAMA, M. & OKAMOTO, K. 2011. Peripherin partially localizes in Bunina bodies in amyotrophic lateral sclerosis. *J Neurol Sci,* 302**,** 14-8.

MIZUSAWA, H. 1993. Hyaline and Skein-like Inclusions in Amyotrophic Lateral Sclerosis. *Neuropathology,* 13**,** 201-208.

MIZUSHIMA, N. 2007. Autophagy: process and function. *Genes Dev,* 21**,** 2861-73.

MIZUSHIMA, N. & KOMATSU, M. 2011. Autophagy: renovation of cells and tissues. *Cell,* 147**,** 728-41.

MODJTAHEDI, N., TOKATLIDIS, K., DESSEN, P. & KROEMER, G. 2016. Mitochondrial Proteins Containing Coiled-Coil-Helix-Coiled-Coil-Helix (CHCH) Domains in Health and Disease. *Trends Biochem Sci,* 41**,** 245-260.

MOHAMMAD-PANAH, R., WELLHAUSER, L., STEINBERG, B. E., WANG, Y., HUAN, L. J., LIU, X. D. & BEAR, C. E. 2009. An essential role for ClC-4 in transferrin receptor function revealed in studies of fibroblasts derived from Clcn4-null mice. *J Cell Sci,* 122**,** 1229-37.

MOLONEY, C., RAYAPROLU, S., HOWARD, J., FROMHOLT, S., BROWN, H., COLLINS, M., CABRERA, M., DUFFY, C., SIEMIENSKI, Z., MILLER, D., SWANSON, M. S., NOTTERPEK, L., BORCHELT, D. R. & LEWIS, J. 2016. Transgenic mice overexpressing the ALS-linked protein Matrin 3 develop a profound muscle phenotype. *Acta Neuropathol Commun,* 4**,** 122.

MONTIBELLER, L. & DE BELLEROCHE, J. 2018. Amyotrophic lateral sclerosis (ALS) and Alzheimer's disease (AD) are characterised by differential activation of ER stress pathways: focus on UPR target genes. *Cell Stress Chaperones*.

MORAHAN, J. M., YU, B., TRENT, R. J. & PAMPHLETT, R. 2009. A genome-wide analysis of brain DNA methylation identifies new candidate genes for sporadic amyotrophic lateral sclerosis. *Amyotroph Lateral Scler,* 10**,** 418-29.

MORFINI, G. A., BOSCO, D. A., BROWN, H., GATTO, R., KAMINSKA, A., SONG, Y., MOLLA, L., BAKER, L., MARANGONI, M. N., BERTH, S., TAVASSOLI, E., BAGNATO, C., TIWARI, A., HAYWARD, L. J., PIGINO, G. F., WATTERSON, D. M., HUANG, C. F., BANKER, G., BROWN, R. H., JR. & BRADY, S. T. 2013. Inhibition of fast axonal transport by pathogenic SOD1 involves activation of p38 MAP kinase. *PLoS One,* 8**,** e65235.

MORI, F., MIKI, Y., TANJI, K., KAKITA, A., TAKAHASHI, H., UTSUMI, J., SASAKI, H. & WAKABAYASHI, K. 2015. Sortilin-related receptor CNS expressed 2 (SorCS2) is localized to Bunina bodies in amyotrophic lateral sclerosis. *Neurosci Lett,* 608**,** 6-11.

MORI, K., WENG, S. M., ARZBERGER, T., MAY, S., RENTZSCH, K., KREMMER, E., SCHMID, B., KRETZSCHMAR, H. A., CRUTS, M., VAN BROECKHOVEN, C., HAASS, C. & EDBAUER, D. 2013. The C9orf72 GGGGCC repeat is translated into aggregating dipeptide-repeat proteins in FTLD/ALS. *Science,* 339**,** 1335-8.

MORIMOTO, N., NAGAI, M., OHTA, Y., MIYAZAKI, K., KURATA, T., MORIMOTO, M., MURAKAMI, T., TAKEHISA, Y., IKEDA, Y., KAMIYA, T. & ABE, K. 2007. Increased autophagy in transgenic mice with a G93A mutant SOD1 gene. *Brain Res,* 1167**,** 112-7.

MOROTZ, G. M., DE VOS, K. J., VAGNONI, A., ACKERLEY, S., SHAW, C. E. & MILLER, C. C. 2012. Amyotrophic lateral sclerosis-associated mutant VAPBP56S perturbs calcium homeostasis to disrupt axonal transport of mitochondria. *Hum Mol Genet,* 21**,** 1979-88.

MULLER, H. P., TURNER, M. R., GROSSKREUTZ, J., ABRAHAMS, S., BEDE, P., GOVIND, V., PRUDLO, J., LUDOLPH, A. C., FILIPPI, M. & KASSUBEK, J. 2016. A large-scale multicentre cerebral diffusion tensor imaging study in amyotrophic lateral sclerosis. *J Neurol Neurosurg Psychiatry,* 87**,** 570-9.

MUNCH, C. & BERTOLOTTI, A. 2011. Self-propagation and transmission of misfolded mutant SOD1: prion or prion-like phenomenon? *Cell Cycle,* 10**,** 1711.

MUNOZ-LOBATO, F., RODRIGUEZ-PALERO, M. J., NARANJO-GALINDO, F. J., SHEPHARD, F., GAFFNEY, C. J., SZEWCZYK, N. J., HAMAMICHI, S., CALDWELL, K. A., CALDWELL, G. A., LINK, C. D. & MIRANDA-VIZUETE, A. 2014. Protective role of DNJ-27/ERdj5 in Caenorhabditis elegans models of human neurodegenerative diseases. *Antioxid Redox Signal,* 20**,** 217-35.

MURPHY, J. M., HENRY, R. G., LANGMORE, S., KRAMER, J. H., MILLER, B. L. & LOMEN-HOERTH, C. 2007. Continuum of frontal lobe impairment in amyotrophic lateral sclerosis. *Arch Neurol,* 64**,** 530-4.

NAKANISHI, K., KAMIGUCHI, K., TORIGOE, T., NABETA, C., HIROHASHI, Y., ASANUMA, H., TOBIOKA, H., KOGE, N., HARADA, O., TAMURA, Y., NAGANO, H., YANO, S., CHIBA, S., MATSUMOTO, H. & SATO, N. 2004. Localization and function in endoplasmic reticulum stress tolerance of ERdj3, a new member of Hsp40 family protein. *Cell Stress Chaperones,* 9**,** 253-64.

NASSIF, M., MATUS, S., CASTILLO, K. & HETZ, C. 2010. Amyotrophic lateral sclerosis pathogenesis: a journey through the secretory pathway. *Antioxid Redox Signal,* 13**,** 1955-89.

NEAGOE, I., STAUBER, T., FIDZINSKI, P., BERGSDORF, E.-Y. & JENTSCH, T. J. 2010. The Late Endosomal ClC-6 Mediates Proton/Chloride Countertransport in Heterologous Plasma Membrane Expression. *Journal of Biological Chemistry,* 285**,** 21689-21697.

NEUMANN, M., RADEMAKERS, R., ROEBER, S., BAKER, M., KRETZSCHMAR, H. A. & MACKENZIE, I. R. 2009. A new subtype of frontotemporal lobar degeneration with FUS pathology. *Brain,* 132**,** 2922-31.

NISHIMURA, A. L., MITNE-NETO, M., SILVA, H. C. A., RICHIERI-COSTA, A., MIDDLETON, S., CASCIO, D., KOK, F., OLIVEIRA, J. R. M., GILLINGWATER, T., WEBB, J., SKEHEL, P. & ZATZ, M. 2004. A mutation in the vesicle-trafficking protein VAPB causes late-onset spinal muscular atrophy and amyotrophic lateral sclerosis. *American journal of human genetics,* 75**,** 822-831.

OAKES, J. A., DAVIES, M. C. & COLLINS, M. O. 2017. TBK1: a new player in ALS linking autophagy and neuroinflammation. *Molecular Brain,* 10**,** 5.

ORLACCHIO, A., BABALINI, C., BORRECA, A., PATRONO, C., MASSA, R., BASARAN, S., MUNHOZ, R. P., ROGAEVA, E. A., ST GEORGE-HYSLOP, P. H., BERNARDI, G. & KAWARAI, T. 2010. SPATACSIN mutations cause autosomal recessive juvenile amyotrophic lateral sclerosis. *Brain,* 133**,** 591-8.

ORRENIUS, S., ZHIVOTOVSKY, B. & NICOTERA, P. 2003. Regulation of cell death: the calcium-apoptosis link. *Nat Rev Mol Cell Biol,* 4**,** 552-65.

OSKARSSON, B., GENDRON, T. F. & STAFF, N. P. 2018. Amyotrophic Lateral Sclerosis: An Update for 2018. *Mayo Clinic Proceedings,* 93**,** 1617-1628.

OTOMO, A., KUNITA, R., SUZUKI-UTSUNOMIYA, K., MIZUMURA, H., ONOE, K., OSUGA, H., HADANO, S. & IKEDA, J. E. 2008. ALS2/alsin deficiency in neurons leads to mild defects in macropinocytosis and axonal growth. *Biochem Biophys Res Commun,* 370**,** 87-92.

OYANAGI, K., YAMAZAKI, M., TAKAHASHI, H., WATABE, K., WADA, M., KOMORI, T., MORITA, T. & MIZUTANI, T. 2008. Spinal anterior horn cells in sporadic amyotrophic lateral sclerosis show ribosomal detachment from, and cisternal distention of the rough endoplasmic reticulum. *Neuropathol Appl Neurobiol,* 34**,** 650-8.

PAEZ-COLASANTE, X., FIGUEROA-ROMERO, C., SAKOWSKI, S. A., GOUTMAN, S. A. & FELDMAN, E. L. 2015. Amyotrophic lateral sclerosis: mechanisms and therapeutics in the epigenomic era. *Nat Rev Neurol,* 11**,** 266-79.

PAJARES, M., CUADRADO, A., ENGEDAL, N., JIRSOVA, Z. & CAHOVA, M. 2018. The Role of Free Radicals in Autophagy Regulation: Implications for Ageing. *Oxidative Medicine and Cellular Longevity,* 2018**,** 2450748.

PANKIV, S., CLAUSEN, T. H., LAMARK, T., BRECH, A., BRUUN, J. A., OUTZEN, H., OVERVATN, A., BJORKOY, G. & JOHANSEN, T. 2007. p62/SQSTM1 binds directly to Atg8/LC3 to facilitate degradation of ubiquitinated protein aggregates by autophagy. *J Biol Chem,* 282**,** 24131-45.

PASINELLI, P. & BROWN, R. H. 2006. Molecular biology of amyotrophic lateral sclerosis: insights from genetics. *Nat Rev Neurosci,* 7**,** 710-23.

PAUL, P., MURPHY, T., OSENI, Z., SIVALOKANATHAN, S. & DE BELLEROCHE, J. S. 2014. Pathogenic effects of amyotrophic lateral sclerosis-linked mutation in D-amino acid oxidase are mediated by D-serine. *Neurobiol Aging,* 35**,** 876-85.

PENG, J., WANG, Y., HE, F., CHEN, C., WU, L. W., YANG, L. F., MA, Y. P., ZHANG, W., SHI, Z. Q., CHEN, C., XIA, K., GUO, H., YIN, F. & PANG, N. 2018. Novel West syndrome candidate genes in a Chinese cohort. *CNS Neurosci Ther*.

PENSATO, V., TILOCA, C., CORRADO, L., BERTOLIN, C., SARDONE, V., DEL BO, R., CALINI, D., MANDRIOLI, J., LAURIA, G., MAZZINI, L., QUERIN, G., CERONI, M., CANTELLO, R., CORTI, S., CASTELLOTTI, B., SOLDA, G., DUGA, S., COMI, G. P., CEREDA, C., SORARU, G., D'ALFONSO, S., TARONI, F., SHAW, C. E., LANDERS, J. E., TICOZZI, N., RATTI, A., GELLERA, C. & SILANI, V. 2015. TUBA4A gene analysis in sporadic amyotrophic lateral sclerosis: identification of novel mutations. *J Neurol,* 262**,** 1376-8.

PEREZ-BRANGULI, F., MISHRA, H. K., PROTS, I., HAVLICEK, S., KOHL, Z., SAUL, D., RUMMEL, C., DORCA-AREVALO, J., REGENSBURGER, M., GRAEF, D., SOCK,

E., BLASI, J., GROEMER, T. W., SCHLOTZER-SCHREHARDT, U., WINKLER, J. & WINNER, B. 2014. Dysfunction of spatacsin leads to axonal pathology in SPG11-linked hereditary spastic paraplegia. *Hum Mol Genet,* 23**,** 4859-74.

PETERS, O. M., GHASEMI, M. & BROWN, R. H., JR. 2015. Emerging mechanisms of molecular pathology in ALS. *J Clin Invest,* 125**,** 1767-79.

PHILIPS, T. & ROTHSTEIN, J. D. 2014. Glial cells in amyotrophic lateral sclerosis. *Experimental neurology,* 262 Pt B**,** 111-120.

PICKLES, S., SEMMLER, S., BROOM, H. R., DESTROISMAISONS, L., LEGROUX, L., ARBOUR, N., MEIERING, E., CASHMAN, N. R. & VANDE VELDE, C. 2016. ALS-linked misfolded SOD1 species have divergent impacts on mitochondria. *Acta Neuropathol Commun,* 4**,** 43.

PIWON, N., GUNTHER, W., SCHWAKE, M., BOSL, M. R. & JENTSCH, T. J. 2000. ClC-5 Cl- -channel disruption impairs endocytosis in a mouse model for Dent's disease. *Nature,* 408**,** 369-73.

POET, M., KORNAK, U., SCHWEIZER, M., ZDEBIK, A. A., SCHEEL, O., HOELTER, S., WURST, W., SCHMITT, A., FUHRMANN, J. C., PLANELLS-CASES, R., MOLE, S. E., HUBNER, C. A. & JENTSCH, T. J. 2006. Lysosomal storage disease upon disruption of the neuronal chloride transport protein ClC-6. *Proc Natl Acad Sci U S A,* 103**,** 13854-9.

POLYMENIDOU, M. & CLEVELAND, D. W. 2012. Prion-like spread of protein aggregates in neurodegeneration. *J Exp Med,* 209**,** 889-93.

POLYMENIDOU, M., LAGIER-TOURENNE, C., HUTT, K. R., HUELGA, S. C., MORAN, J., LIANG, T. Y., LING, S. C., SUN, E., WANCEWICZ, E., MAZUR, C.,

KORDASIEWICZ, H., SEDAGHAT, Y., DONOHUE, J. P., SHIUE, L., BENNETT, C. F., YEO, G. W. & CLEVELAND, D. W. 2011. Long pre-mRNA depletion and RNA missplicing contribute to neuronal vulnerability from loss of TDP-43. *Nat Neurosci,* 14**,** 459-68.

PRESSEY, S. N., O'DONNELL, K. J., STAUBER, T., FUHRMANN, J. C., TYYNELA, J., JENTSCH, T. J. & COOPER, J. D. 2010. Distinct neuropathologic phenotypes after disrupting the chloride transport proteins ClC-6 or ClC-7/Ostm1. *J Neuropathol Exp Neurol,* 69**,** 1228-46.

PRUDENCIO, M., HART, P. J., BORCHELT, D. R. & ANDERSEN, P. M. 2009. Variation in aggregation propensities among ALS-associated variants of SOD1: correlation to human disease. *Hum Mol Genet,* 18**,** 3217-26.

PULS, I., JONNAKUTY, C., LAMONTE, B. H., HOLZBAUR, E. L., TOKITO, M., MANN, E., FLOETER, M. K., BIDUS, K., DRAYNA, D., OH, S. J., BROWN, R. H., JR., LUDLOW, C. L. & FISCHBECK, K. H. 2003. Mutant dynactin in motor neuron disease. *Nat Genet,* 33**,** 455-6.

RABIZADEH, S., GRALLA, E. B., BORCHELT, D. R., GWINN, R., VALENTINE, J. S., SISODIA, S., WONG, P., LEE, M., HAHN, H. & BREDESEN, D. E. 1995. Mutations associated with amyotrophic lateral sclerosis convert superoxide dismutase from an antiapoptotic gene to a proapoptotic gene: studies in yeast and neural cells. *Proceedings of the National Academy of Sciences of the United States of America,* 92**,** 3024-3028.

RAKHIT, R., CUNNINGHAM, P., FURTOS-MATEI, A., DAHAN, S., QI, X. F., CROW, J. P., CASHMAN, N. R., KONDEJEWSKI, L. H. & CHAKRABARTTY, A. 2002. Oxidation-induced misfolding and aggregation of superoxide dismutase and its implications for amyotrophic lateral sclerosis. *J Biol Chem,* 277**,** 47551-6.

RAO, S. D. & WEISS, J. H. 2004. Excitotoxic and oxidative cross-talk between motor neurons and glia in ALS pathogenesis. *Trends Neurosci,* 27**,** 17-23.

RASHID, H. O., YADAV, R. K., KIM, H. R. & CHAE, H. J. 2015. ER stress: Autophagy induction, inhibition and selection. *Autophagy,* 11**,** 1956-1977.

RAVID, T. & HOCHSTRASSER, M. 2008. Diversity of degradation signals in the ubiquitin-proteasome system. *Nat Rev Mol Cell Biol,* 9**,** 679-90.

REMBACH, A., TURNER, B. J., BRUCE, S., CHEAH, I. K., SCOTT, R. L., LOPES, E. C., ZAGAMI, C. J., BEART, P. M., CHEUNG, N. S., LANGFORD, S. J. & CHEEMA, S. S. 2004. Antisense peptide nucleic acid targeting GluR3 delays disease onset and progression in the SOD1 G93A mouse model of familial ALS. *J Neurosci Res,* 77**,** 573-82.

RENTON, A. E., CHIO, A. & TRAYNOR, B. J. 2014. State of play in amyotrophic lateral sclerosis genetics. *Nat Neurosci,* 17**,** 17-23.

RENTON, A. E., MAJOUNIE, E., WAITE, A., SIMON-SANCHEZ, J., ROLLINSON, S., GIBBS, J. R., SCHYMICK, J. C., LAAKSOVIRTA, H., VAN SWIETEN, J. C., MYLLYKANGAS, L., KALIMO, H., PAETAU, A., ABRAMZON, Y., REMES, A. M., KAGANOVICH, A., SCHOLZ, S. W., DUCKWORTH, J., DING, J., HARMER, D. W., HERNANDEZ, D. G., JOHNSON, J. O., MOK, K., RYTEN, M., TRABZUNI, D., GUERREIRO, R. J., ORRELL, R. W., NEAL, J., MURRAY, A., PEARSON, J., JANSEN, I. E., SONDERVAN, D., SEELAAR, H., BLAKE, D., YOUNG, K., HALLIWELL, N., CALLISTER, J. B., TOULSON, G., RICHARDSON, A., GERHARD, A., SNOWDEN, J., MANN, D., NEARY, D., NALLS, M. A., PEURALINNA, T., JANSSON, L., ISOVIITA, V. M., KAIVORINNE, A. L., HOLTTA-VUORI, M., IKONEN, E., SULKAVA, R., BENATAR, M., WUU, J.,

CHIO, A., RESTAGNO, G., BORGHERO, G., SABATELLI, M., HECKERMAN, D., ROGAEVA, E., ZINMAN, L., ROTHSTEIN, J. D., SENDTNER, M., DREPPER, C., EICHLER, E. E., ALKAN, C., ABDULLAEV, Z., PACK, S. D., DUTRA, A., PAK, E., HARDY, J., SINGLETON, A., WILLIAMS, N. M., HEUTINK, P., PICKERING-BROWN, S., MORRIS, H. R., TIENARI, P. J. & TRAYNOR, B. J. 2011. A hexanucleotide repeat expansion in C9ORF72 is the cause of chromosome 9p21-linked ALS-FTD. *Neuron,* 72**,** 257-68.

REYES, N. A., FISHER, J. K., AUSTGEN, K., VANDENBERG, S., HUANG, E. J. & OAKES, S. A. 2010. Blocking the mitochondrial apoptotic pathway preserves motor neuron viability and function in a mouse model of amyotrophic lateral sclerosis. *J Clin Invest,* 120**,** 3673-9.

RINK, J., GHIGO, E., KALAIDZIDIS, Y. & ZERIAL, M. 2005. Rab conversion as a mechanism of progression from early to late endosomes. *Cell,* 122**,** 735-49.

ROBBERECHT, W. & PHILIPS, T. 2013. The changing scene of amyotrophic lateral sclerosis. *Nat Rev Neurosci,* 14**,** 248-64.

RON, D. & WALTER, P. 2007. Signal integration in the endoplasmic reticulum unfolded protein response. *Nat Rev Mol Cell Biol,* 8**,** 519-29.

ROSEN, D. R., SIDDIQUE, T., PATTERSON, D., FIGLEWICZ, D. A., SAPP, P., HENTATI, A., DONALDSON, D., GOTO, J., O'REGAN, J. P., DENG, H. X. & ET AL. 1993. Mutations in Cu/Zn superoxide dismutase gene are associated with familial amyotrophic lateral sclerosis. *Nature,* 362**,** 59-62.

ROTHSTEIN, J. D., TSAI, G., KUNCL, R. W., CLAWSON, L., CORNBLATH, D. R., DRACHMAN, D. B., PESTRONK, A., STAUCH, B. L. & COYLE, J. T. 1990.

Abnormal excitatory amino acid metabolism in amyotrophic lateral sclerosis. *Ann Neurol,* 28**,** 18-25.

RUEGSEGGER, C. & SAXENA, S. 2016. Proteostasis impairment in ALS. *Brain Res,* 1648**,** 571-579.

SABERI, S., STAUFFER, J. E., SCHULTE, D. J. & RAVITS, J. 2015. Neuropathology of Amyotrophic Lateral Sclerosis and Its Variants. *Neurol Clin,* 33**,** 855-76.

SANO, R. & REED, J. C. 2013. ER stress-induced cell death mechanisms. *Biochim Biophys Acta,* 1833**,** 3460-3470.

SARKAR, S. 2013. Regulation of autophagy by mTOR-dependent and mTOR-independent pathways: autophagy dysfunction in neurodegenerative diseases and therapeutic application of autophagy enhancers. *Biochem Soc Trans,* 41**,** 1103-30.

SASAKI, S. 2010. Endoplasmic reticulum stress in motor neurons of the spinal cord in sporadic amyotrophic lateral sclerosis. *J Neuropathol Exp Neurol,* 69**,** 346-55.

SASAKI, S. & IWATA, M. 2007. Mitochondrial alterations in the spinal cord of patients with sporadic amyotrophic lateral sclerosis. *J Neuropathol Exp Neurol,* 66**,** 10-6.

SATHASIVAM, S. & SHAW, P. J. 2005. Apoptosis in amyotrophic lateral sclerosis--what is the evidence? *Lancet Neurol,* 4**,** 500-9.

SCHIFFER, D. & FIANO, V. 2004. Astrogliosis in ALS: possible interpretations according to pathogenetic hypotheses. *Amyotroph Lateral Scler Other Motor Neuron Disord,* 5**,** 22-5.

SCHREIJ, A. M., FON, E. A. & MCPHERSON, P. S. 2016. Endocytic membrane trafficking and neurodegenerative disease. *Cell Mol Life Sci,* 73**,** 1529-45.

SCHRODER, M. & KAUFMAN, R. J. 2005. The mammalian unfolded protein response. *Annu Rev Biochem,* 74**,** 739-89.

SCHWENK, B. M., HARTMANN, H., SERDAROGLU, A., SCHLUDI, M. H., HORNBURG, D., MEISSNER, F., OROZCO, D., COLOMBO, A., TAHIROVIC, S., MICHAELSEN, M., SCHREIBER, F., HAUPT, S., PEITZ, M., BRUSTLE, O., KUPPER, C., KLOPSTOCK, T., OTTO, M., LUDOLPH, A. C., ARZBERGER, T., KUHN, P. H. & EDBAUER, D. 2016. TDP-43 loss of function inhibits endosomal trafficking and alters trophic signaling in neurons. *Embo j,* 35**,** 2350-2370.

SELLIER, C., CAMPANARI, M. L., JULIE CORBIER, C., GAUCHEROT, A., KOLB-CHEYNEL, I., OULAD-ABDELGHANI, M., RUFFENACH, F., PAGE, A., CIURA, S., KABASHI, E. & CHARLET-BERGUERAND, N. 2016. Loss of C9ORF72 impairs autophagy and synergizes with polyQ Ataxin-2 to induce motor neuron dysfunction and cell death. *Embo j,* 35**,** 1276-97.

SELVARAJ, B. T., LIVESEY, M. R., ZHAO, C., GREGORY, J. M., JAMES, O. T., CLEARY, E. M., CHOUHAN, A. K., GANE, A. B., PERKINS, E. M., DANDO, O., LILLICO, S. G., LEE, Y. B., NISHIMURA, A. L., PORECI, U., THANKAMONY, S., PRAY, M., VASISTHA, N. A., MAGNANI, D., BOROOAH, S., BURR, K., STORY, D., MCCAMPBELL, A., SHAW, C. E., KIND, P. C., AITMAN, T. J., WHITELAW, C. B. A., WILMUT, I., SMITH, C., MILES, G. B., HARDINGHAM, G. E., WYLLIE, D. J. A. & CHANDRAN, S. 2018. C9ORF72 repeat expansion causes vulnerability of motor neurons to Ca(2+)-permeable AMPA receptor-mediated excitotoxicity. *Nat Commun,* 9**,** 347.

SHANG, Y. & HUANG, E. J. 2016. Mechanisms of FUS mutations in familial amyotrophic lateral sclerosis. *Brain Res,* 1647**,** 65-78.

SHARMA, A., LYASHCHENKO, A. K., LU, L., NASRABADY, S. E., ELMALEH, M., MENDELSOHN, M., NEMES, A., TAPIA, J. C., MENTIS, G. Z. & SHNEIDER, N. A. 2016. ALS-associated mutant FUS induces selective motor neuron degeneration through toxic gain of function. *Nat Commun,* 7**,** 10465.

SHEN, W. C., LI, H. Y., CHEN, G. C., CHERN, Y. & TU, P. H. 2015. Mutations in the ubiquitin-binding domain of OPTN/optineurin interfere with autophagy-mediated degradation of misfolded proteins by a dominant-negative mechanism. *Autophagy,* 11**,** 685-700.

SHIBATA, N., HIRANO, A., KOBAYASHI, M., ASAYAMA, K., UMAHARA, T., KOMORI, T. & IKEMOTO, A. 1993. IMMUNOHISTOCHEMICAL DEMONSTRATION OF Cu/Zn SUPEROXIDE DISMUTASE IN THE SPINAL CORD OF PATIENTS WITH FAMILIAL AMYOTRO-PHIC LATERAL SCLEROSIS. *Acta Histochemica et Cytochemica,* 26**,** 619-624.

SHORE, G. C., PAPA, F. R. & OAKES, S. A. 2011. Signaling cell death from the endoplasmic reticulum stress response. *Curr Opin Cell Biol,* 23**,** 143-9.

SKIBINSKI, G., PARKINSON, N. J., BROWN, J. M., CHAKRABARTI, L., LLOYD, S. L., HUMMERICH, H., NIELSEN, J. E., HODGES, J. R., SPILLANTINI, M. G., THUSGAARD, T., BRANDNER, S., BRUN, A., ROSSOR, M. N., GADE, A., JOHANNSEN, P., SORENSEN, S. A., GYDESEN, S., FISHER, E. M. & COLLINGE, J. 2005. Mutations in the endosomal ESCRTIII-complex subunit CHMP2B in frontotemporal dementia. *Nat Genet,* 37**,** 806-8.

SKOURTI-STATHAKI, K., PROUDFOOT, N. J. & GROMAK, N. 2011. Human senataxin resolves RNA/DNA hybrids formed at transcriptional pause sites to promote Xrn2-dependent termination. *Mol Cell,* 42**,** 794-805.

SMITH, B. N., TICOZZI, N., FALLINI, C., GKAZI, A. S., TOPP, S., KENNA, K. P., SCOTTER, E. L., KOST, J., KEAGLE, P., MILLER, J. W., CALINI, D., VANCE, C., DANIELSON, E. W., TROAKES, C., TILOCA, C., AL-SARRAJ, S., LEWIS, E. A., KING, A., COLOMBRITA, C., PENSATO, V., CASTELLOTTI, B., DE BELLEROCHE, J., BAAS, F., TEN ASBROEK, A. L., SAPP, P. C., MCKENNA-YASEK, D., MCLAUGHLIN, R. L., POLAK, M., ASRESS, S., ESTEBAN-PEREZ, J., MUNOZ-BLANCO, J. L., SIMPSON, M., CONSORTIUM, S., VAN RHEENEN, W., DIEKSTRA, F. P., LAURIA, G., DUGA, S., CORTI, S., CEREDA, C., CORRADO, L., SORARU, G., MORRISON, K. E., WILLIAMS, K. L., NICHOLSON, G. A., BLAIR, I. P., DION, P. A., LEBLOND, C. S., ROULEAU, G. A., HARDIMAN, O., VELDINK, J. H., VAN DEN BERG, L. H., AL-CHALABI, A., PALL, H., SHAW, P. J., TURNER, M. R., TALBOT, K., TARONI, F., GARCIA-REDONDO, A., WU, Z., GLASS, J. D., GELLERA, C., RATTI, A., BROWN, R. H., JR., SILANI, V., SHAW, C. E. & LANDERS, J. E. 2014a. Exome-wide rare variant analysis identifies TUBA4A mutations associated with familial ALS. *Neuron,* 84**,** 324-31.

SMITH, B. N., TICOZZI, N., FALLINI, C., GKAZI, A. S., TOPP, S., KENNA, K. P., SCOTTER, E. L., KOST, J., KEAGLE, P., MILLER, J. W., CALINI, D., VANCE, C., DANIELSON, E. W., TROAKES, C., TILOCA, C., AL-SARRAJ, S., LEWIS, E. A., KING, A., COLOMBRITA, C., PENSATO, V., CASTELLOTTI, B., DE BELLEROCHE, J., BAAS, F., TEN ASBROEK, A. L., SAPP, P. C., MCKENNA-YASEK, D., MCLAUGHLIN, R. L., POLAK, M., ASRESS, S., ESTEBAN-PEREZ, J., MUNOZ-BLANCO, J. L., SIMPSON, M., VAN RHEENEN, W., DIEKSTRA, F. P., LAURIA, G., DUGA, S., CORTI, S., CEREDA, C., CORRADO, L., SORARU, G., MORRISON, K. E., WILLIAMS, K. L., NICHOLSON, G. A., BLAIR, I. P., DION, P.

A., LEBLOND, C. S., ROULEAU, G. A., HARDIMAN, O., VELDINK, J. H., VAN DEN BERG, L. H., AL-CHALABI, A., PALL, H., SHAW, P. J., TURNER, M. R., TALBOT, K., TARONI, F., GARCIA-REDONDO, A., WU, Z., GLASS, J. D., GELLERA, C., RATTI, A., BROWN, R. H., JR., SILANI, V., SHAW, C. E. & LANDERS, J. E. 2014b. Exome-wide rare variant analysis identifies TUBA4A mutations associated with familial ALS. *Neuron,* 84**,** 324-31.

SMITH, B. N., TOPP, S. D., FALLINI, C., SHIBATA, H., CHEN, H. J., TROAKES, C., KING, A., TICOZZI, N., KENNA, K. P., SORAGIA-GKAZI, A., MILLER, J. W., SATO, A., DIAS, D. M., JEON, M., VANCE, C., WONG, C. H., DE MAJO, M., KATTUAH, W., MITCHELL, J. C., SCOTTER, E. L., PARKIN, N. W., SAPP, P. C., NOLAN, M., NESTOR, P. J., SIMPSON, M., WEALE, M., LEK, M., BAAS, F., VIANNEY DE JONG, J. M., TEN ASBROEK, A., REDONDO, A. G., ESTEBAN-PEREZ, J., TILOCA, C., VERDE, F., DUGA, S., LEIGH, N., PALL, H., MORRISON, K. E., AL-CHALABI, A., SHAW, P. J., KIRBY, J., TURNER, M. R., TALBOT, K., HARDIMAN, O., GLASS, J. D., DE BELLEROCHE, J., MAKI, M., MOSS, S. E., MILLER, C., GELLERA, C., RATTI, A., AL-SARRAJ, S., BROWN, R. H., JR., SILANI, V., LANDERS, J. E. & SHAW, C. E. 2017a. Mutations in the vesicular trafficking protein annexin A11 are associated with amyotrophic lateral sclerosis. *Sci Transl Med,* 9.

SMITH, E. F., SHAW, P. J. & DE VOS, K. J. 2017b. The role of mitochondria in amyotrophic lateral sclerosis. *Neurosci Lett*.

SMITH, M. & WILKINSON, S. 2017. ER homeostasis and autophagy. *Essays Biochem,* 61**,** 625-635.

SORCE, S., NUVOLONE, M., KELLER, A., FALSIG, J., VAROL, A., SCHWARZ, P., BIERI, M., BUDKA, H. & AGUZZI, A. 2014. The Role of the NADPH Oxidase NOX2 in Prion Pathogenesis. *PLoS Pathogens,* 10**,** e1004531.

SORCE, S., STOCKER, R., SEREDENINA, T., HOLMDAHL, R., AGUZZI, A., CHIO, A., DEPAULIS, A., HEITZ, F., OLOFSSON, P., OLSSON, T., DUVEAU, V., SANOUDOU, D., SKOSGATER, S., VLAHOU, A., WASQUEL, D., KRAUSE, K. H. & JAQUET, V. 2017. NADPH oxidases as drug targets and biomarkers in neurodegenerative diseases: What is the evidence? *Free Radic Biol Med,* 112**,** 387-396.

SREEDHARAN, J., BLAIR, I. P., TRIPATHI, V. B., HU, X., VANCE, C., ROGELJ, B., ACKERLEY, S., DURNALL, J. C., WILLIAMS, K. L., BURATTI, E., BARALLE, F., DE BELLEROCHE, J., MITCHELL, J. D., LEIGH, P. N., AL-CHALABI, A., MILLER, C. C., NICHOLSON, G. & SHAW, C. E. 2008. TDP-43 mutations in familial and sporadic amyotrophic lateral sclerosis. *Science,* 319**,** 1668-72.

STENMARK, H. 2009. Rab GTPases as coordinators of vesicle traffic. *Nat Rev Mol Cell Biol,* 10**,** 513-25.

STOBRAWA, S. M., BREIDERHOFF, T., TAKAMORI, S., ENGEL, D., SCHWEIZER, M., ZDEBIK, A. A., BOSL, M. R., RUETHER, K., JAHN, H., DRAGUHN, A., JAHN, R. & JENTSCH, T. J. 2001. Disruption of ClC-3, a chloride channel expressed on synaptic vesicles, leads to a loss of the hippocampus. *Neuron,* 29**,** 185-96.

STOICA, R., DE VOS, K. J., PAILLUSSON, S., MUELLER, S., SANCHO, R. M., LAU, K. F., VIZCAY-BARRENA, G., LIN, W. L., XU, Y. F., LEWIS, J., DICKSON, D. W., PETRUCELLI, L., MITCHELL, J. C., SHAW, C. E. & MILLER, C. C. 2014. ER-mitochondria associations are regulated by the VAPB-PTPIP51 interaction and are disrupted by ALS/FTD-associated TDP-43. *Nat Commun,* 5**,** 3996.

STOICA, R., PAILLUSSON, S., GOMEZ-SUAGA, P., MITCHELL, J. C., LAU, D. H., GRAY, E. H., SANCHO, R. M., VIZCAY-BARRENA, G., DE VOS, K. J., SHAW, C. E., HANGER, D. P., NOBLE, W. & MILLER, C. C. 2016. ALS/FTD-associated FUS activates GSK-3beta to disrupt the VAPB-PTPIP51 interaction and ER-mitochondria associations. *EMBO Rep,* 17**,** 1326-42.

STROMHAUG, P. E., BERG, T. O., FENGSRUD, M. & SEGLEN, P. O. 1998. Purification and characterization of autophagosomes from rat hepatocytes. *Biochem J,* 335 (Pt 2)**,** 217-24.

SUBRAMANIAN, V., CRABTREE, B. & ACHARYA, K. R. 2008. Human angiogenin is a neuroprotective factor and amyotrophic lateral sclerosis associated angiogenin variants affect neurite extension/pathfinding and survival of motor neurons. *Hum Mol Genet,* 17**,** 130-49.

SULLIVAN, P. M., ZHOU, X., ROBINS, A. M., PAUSHTER, D. H., KIM, D., SMOLKA, M. B. & HU, F. 2016. The ALS/FTLD associated protein C9orf72 associates with SMCR8 and WDR41 to regulate the autophagy-lysosome pathway. *Acta Neuropathol Commun,* 4**,** 51.

SUN, Q., WESTPHAL, W., WONG, K. N., TAN, I. & ZHONG, Q. 2010a. Rubicon controls endosome maturation as a Rab7 effector. *Proc Natl Acad Sci U S A,* 107**,** 19338-43.

SUN, Q., WESTPHAL, W., WONG, K. N., TAN, I. & ZHONG, Q. 2010b. Rubicon controls endosome maturation as a Rab7 effector. *Proceedings of the National Academy of Sciences,* 107**,** 19338.

SUN, Q., ZHANG, J., FAN, W., WONG, K. N., DING, X., CHEN, S. & ZHONG, Q. 2011a. The RUN domain of rubicon is important for hVps34 binding, lipid kinase inhibition, and autophagy suppression. *J Biol Chem,* 286**,** 185-91.

SUN, Z., DIAZ, Z., FANG, X., HART, M. P., CHESI, A., SHORTER, J. & GITLER, A. D. 2011b. Molecular determinants and genetic modifiers of aggregation and toxicity for the ALS disease protein FUS/TLS. *PLoS Biol,* 9**,** e1000614.

SUZUKI, H., LEE, K. & MATSUOKA, M. 2011. TDP-43-induced death is associated with altered regulation of BIM and Bcl-xL and attenuated by caspase-mediated TDP-43 cleavage. *J Biol Chem,* 286**,** 13171-83.

TAKALO, M., SALMINEN, A., SOININEN, H., HILTUNEN, M. & HAAPASALO, A. 2013. Protein aggregation and degradation mechanisms in neurodegenerative diseases. *American journal of neurodegenerative disease,* 2**,** 1-14.

TALBOT, K., FENEBERG, E., SCABER, J., THOMPSON, A. G. & TURNER, M. R. 2018. Amyotrophic lateral sclerosis: the complex path to precision medicine. *J Neurol,* 265**,** 2454-2462.

TAN, C. C., YU, J. T., TAN, M. S., JIANG, T., ZHU, X. C. & TAN, L. 2014. Autophagy in aging and neurodegenerative diseases: implications for pathogenesis and therapy. *Neurobiol Aging,* 35**,** 941-57.

TANAKA, S., HIKITA, H., TATSUMI, T., SAKAMORI, R., NOZAKI, Y., SAKANE, S., SHIODE, Y., NAKABORI, T., SAITO, Y., HIRAMATSU, N., TABATA, K., KAWABATA, T., HAMASAKI, M., EGUCHI, H., NAGANO, H., YOSHIMORI, T. & TAKEHARA, T. 2016. Rubicon inhibits autophagy and accelerates hepatocyte apoptosis and lipid accumulation in nonalcoholic fatty liver disease in mice. *Hepatology,* 64**,** 1994-2014.

TATENO, M., SADAKATA, H., TANAKA, M., ITOHARA, S., SHIN, R.-M., MIURA, M., MASUDA, M., AOSAKI, T., URUSHITANI, M., MISAWA, H. & TAKAHASHI, R. 2004. Calcium-permeable AMPA receptors promote misfolding of mutant SOD1

protein and development of amyotrophic lateral sclerosis in a transgenic mouse model. *Human Molecular Genetics,* 13**,** 2183-2196.

TEYSSOU, E., TAKEDA, T., LEBON, V., BOILLEE, S., DOUKOURE, B., BATAILLON, G., SAZDOVITCH, V., CAZENEUVE, C., MEININGER, V., LEGUERN, E., SALACHAS, F., SEILHEAN, D. & MILLECAMPS, S. 2013. Mutations in SQSTM1 encoding p62 in amyotrophic lateral sclerosis: genetics and neuropathology. *Acta Neuropathol,* 125**,** 511-22.

THASTRUP, O., CULLEN, P. J., DROBAK, B. K., HANLEY, M. R. & DAWSON, A. P. 1990. Thapsigargin, a tumor promoter, discharges intracellular Ca2+ stores by specific inhibition of the endoplasmic reticulum Ca2(+)-ATPase. *Proc Natl Acad Sci U S A,* 87**,** 2466-70.

TIWARI, A., XU, Z. & HAYWARD, L. J. 2005. Aberrantly increased hydrophobicity shared by mutants of Cu,Zn-superoxide dismutase in familial amyotrophic lateral sclerosis. *J Biol Chem,* 280**,** 29771-9.

TOLLERVEY, J. R., CURK, T., ROGELJ, B., BRIESE, M., CEREDA, M., KAYIKCI, M., KÖNIG, J., HORTOBÁGYI, T., NISHIMURA, A. L., ŽUPUNSKI, V., PATANI, R., CHANDRAN, S., ROT, G., ZUPAN, B., SHAW, C. E. & ULE, J. 2011. Characterizing the RNA targets and position-dependent splicing regulation by TDP-43. *Nature Neuroscience,* 14**,** 452.

TOMONAGA, M., SAITO, M., YOSHIMURA, M., SHIMADA, H. & TOHGI, H. 1978. Ultrastructure of the Bunina bodies in anterior horn cells of amyotrophic lateral sclerosis. *Acta Neuropathol,* 42**,** 81-6.

TRADEWELL, M. L., YU, Z., TIBSHIRANI, M., BOULANGER, M. C., DURHAM, H. D. & RICHARD, S. 2012. Arginine methylation by PRMT1 regulates nuclear-cytoplasmic

localization and toxicity of FUS/TLS harbouring ALS-linked mutations. *Hum Mol Genet,* 21**,** 136-49.

TSAO, W., JEONG, Y. H., LIN, S., LING, J., PRICE, D. L., CHIANG, P. M. & WONG, P. C. 2012. Rodent models of TDP-43: recent advances. *Brain Res,* 1462**,** 26-39.

TSVETANOVA, N. G. 2013. The secretory pathway in control of endoplasmic reticulum homeostasis. *Small GTPases,* 4**,** 28-33.

TURNER, M. R., HARDIMAN, O., BENATAR, M., BROOKS, B. R., CHIO, A., DE CARVALHO, M., INCE, P. G., LIN, C., MILLER, R. G., MITSUMOTO, H., NICHOLSON, G., RAVITS, J., SHAW, P. J., SWASH, M., TALBOT, K., TRAYNOR, B. J., VAN DEN BERG, L. H., VELDINK, J. H., VUCIC, S. & KIERNAN, M. C. 2013. Controversies and priorities in amyotrophic lateral sclerosis. *Lancet Neurol,* 12**,** 310-22.

VAN BLITTERSWIJK, M., VAN VUGHT, P. W., VAN ES, M. A., SCHELHAAS, H. J., VAN DER KOOI, A. J., DE VISSER, M., VELDINK, J. H. & VAN DEN BERG, L. H. 2012. Novel optineurin mutations in sporadic amyotrophic lateral sclerosis patients. *Neurobiol Aging,* 33**,** 1016.e1-7.

VAN ENGELAND, M., RAMAEKERS, F. C., SCHUTTE, B. & REUTELINGSPERGER, C. P. 1996. A novel assay to measure loss of plasma membrane asymmetry during apoptosis of adherent cells in culture. *Cytometry,* 24**,** 131-9.

VANCE, C., ROGELJ, B., HORTOBAGYI, T., DE VOS, K. J., NISHIMURA, A. L., SREEDHARAN, J., HU, X., SMITH, B., RUDDY, D., WRIGHT, P., GANESALINGAM, J., WILLIAMS, K. L., TRIPATHI, V., AL-SARAJ, S., AL-CHALABI, A., LEIGH, P. N., BLAIR, I. P., NICHOLSON, G., DE BELLEROCHE, J., GALLO, J. M., MILLER, C. C. & SHAW, C. E. 2009. Mutations in FUS, an RNA

processing protein, cause familial amyotrophic lateral sclerosis type 6. *Science,* 323**,** 1208-1211.

VOLK, A. E., WEISHAUPT, J. H., ANDERSEN, P. M., LUDOLPH, A. C. & KUBISCH, C. 2018. Current knowledge and recent insights into the genetic basis of amyotrophic lateral sclerosis. *Med Genet,* 30**,** 252-258.

WALTER, P. & RON, D. 2011. The unfolded protein response: from stress pathway to homeostatic regulation. *Science,* 334**,** 1081-6.

WANG, W., LI, L., LIN, W. L., DICKSON, D. W., PETRUCELLI, L., ZHANG, T. & WANG, X. 2013. The ALS disease-associated mutant TDP-43 impairs mitochondrial dynamics and function in motor neurons. *Hum Mol Genet,* 22**,** 4706-19.

WANG, W., WANG, L., LU, J., SIEDLAK, S. L., FUJIOKA, H., LIANG, J., JIANG, S., MA, X., JIANG, Z., DA ROCHA, E. L., SHENG, M., CHOI, H., LEROU, P. H., LI, H. & WANG, X. 2016. The inhibition of TDP-43 mitochondrial localization blocks its neuronal toxicity. *Nat Med,* 22**,** 869-78.

WATE, R., ITO, H., ZHANG, J. H., OHNISHI, S., NAKANO, S. & KUSAKA, H. 2005. Expression of an endoplasmic reticulum-resident chaperone, glucose-regulated stress protein 78, in the spinal cord of a mouse model of amyotrophic lateral sclerosis. *Acta Neuropathol,* 110**,** 557-62.

WEN, X., TAN, W., WESTERGARD, T., KRISHNAMURTHY, K., MARKANDAIAH, S. S., SHI, Y., LIN, S., SHNEIDER, N. A., MONAGHAN, J., PANDEY, U. B., PASINELLI, P., ICHIDA, J. K. & TROTTI, D. 2014. Antisense proline-arginine RAN dipeptides linked to C9ORF72-ALS/FTD form toxic nuclear aggregates that initiate in vitro and in vivo neuronal death. *Neuron,* 84**,** 1213-25.

WIEDEMANN, F. R., MANFREDI, G., MAWRIN, C., BEAL, M. F. & SCHON, E. A. 2002. Mitochondrial DNA and respiratory chain function in spinal cords of ALS patients. *J Neurochem,* 80**,** 616-25.

WILLIAMS, K. L., TOPP, S., YANG, S., SMITH, B., FIFITA, J. A., WARRAICH, S. T., ZHANG, K. Y., FARRAWELL, N., VANCE, C., HU, X., CHESI, A., LEBLOND, C. S., LEE, A., RAYNER, S. L., SUNDARAMOORTHY, V., DOBSON-STONE, C., MOLLOY, M. P., VAN BLITTERSWIJK, M., DICKSON, D. W., PETERSEN, R. C., GRAFF-RADFORD, N. R., BOEVE, B. F., MURRAY, M. E., POTTIER, C., DON, E., WINNICK, C., MCCANN, E. P., HOGAN, A., DAOUD, H., LEVERT, A., DION, P. A., MITSUI, J., ISHIURA, H., TAKAHASHI, Y., GOTO, J., KOST, J., GELLERA, C., GKAZI, A. S., MILLER, J., STOCKTON, J., BROOKS, W. S., BOUNDY, K., POLAK, M., MUNOZ-BLANCO, J. L., ESTEBAN-PEREZ, J., RABANO, A., HARDIMAN, O., MORRISON, K. E., TICOZZI, N., SILANI, V., DE BELLEROCHE, J., GLASS, J. D., KWOK, J. B., GUILLEMIN, G. J., CHUNG, R. S., TSUJI, S., BROWN, R. H., JR., GARCIA-REDONDO, A., RADEMAKERS, R., LANDERS, J. E., GITLER, A. D., ROULEAU, G. A., COLE, N. J., YERBURY, J. J., ATKIN, J. D., SHAW, C. E., NICHOLSON, G. A. & BLAIR, I. P. 2016. CCNF mutations in amyotrophic lateral sclerosis and frontotemporal dementia. *Nat Commun,* 7**,** 11253.

WONG, S. W., SIL, P. & MARTINEZ, J. 2017. Rubicon: LC3-associated phagocytosis and beyond. *Febs j*.

WONG, S. W., SIL, P. & MARTINEZ, J. 2018. Rubicon: LC3-associated phagocytosis and beyond. *Febs j,* 285**,** 1379-1388.

WOO, J.-A. A., LIU, T., TROTTER, C., FANG, C. C., DE NARVAEZ, E., LEPOCHAT, P., MASLAR, D., BUKHARI, A., ZHAO, X., DEONARINE, A., WESTERHEIDE, S. D. & KANG, D. E. 2017. Loss of function CHCHD10 mutations in cytoplasmic TDP-43 accumulation and synaptic integrity. *Nature Communications,* 8**,** 15558.

WOOLLACOTT, I. O. & MEAD, S. 2014. The C9ORF72 expansion mutation: gene structure, phenotypic and diagnostic issues. *Acta Neuropathol,* 127**,** 319-32.

WROE, R., WAI-LING BUTLER, A., ANDERSEN, P. M., POWELL, J. F. & AL-CHALABI, A. 2008. ALSOD: the Amyotrophic Lateral Sclerosis Online Database. *Amyotroph Lateral Scler,* 9**,** 249-50.

WU, C. H., FALLINI, C., TICOZZI, N., KEAGLE, P. J., SAPP, P. C., PIOTROWSKA, K., LOWE, P., KOPPERS, M., MCKENNA-YASEK, D., BARON, D. M., KOST, J. E., GONZALEZ-PEREZ, P., FOX, A. D., ADAMS, J., TARONI, F., TILOCA, C., LECLERC, A. L., CHAFE, S. C., MANGROO, D., MOORE, M. J., ZITZEWITZ, J. A., XU, Z. S., VAN DEN BERG, L. H., GLASS, J. D., SICILIANO, G., CIRULLI, E. T., GOLDSTEIN, D. B., SALACHAS, F., MEININGER, V., ROSSOLL, W., RATTI, A., GELLERA, C., BOSCO, D. A., BASSELL, G. J., SILANI, V., DRORY, V. E., BROWN, R. H., JR. & LANDERS, J. E. 2012. Mutations in the profilin 1 gene cause familial amyotrophic lateral sclerosis. *Nature,* 488**,** 499-503.

YAMAGUCHI, A. & TAKANASHI, K. 2016. FUS interacts with nuclear matrix-associated protein SAFB1 as well as Matrin3 to regulate splicing and ligand-mediated transcription. *Sci Rep,* 6**,** 35195.

YAMAMOTO, T., SHIMOJIMA, K., SANGU, N., KOMOIKE, Y., ISHII, A., ABE, S., YAMASHITA, S., IMAI, K., KUBOTA, T., FUKASAWA, T., OKANISHI, T., ENOKI, H., TANABE, T., SAITO, A., FURUKAWA, T., SHIMIZU, T., MILLIGAN,

C. J., PETROU, S., HERON, S. E., DIBBENS, L. M., HIROSE, S. & OKUMURA, A. 2015. Single nucleotide variations in CLCN6 identified in patients with benign partial epilepsies in infancy and/or febrile seizures. *PLoS One,* 10**,** e0118946.

YANG, C.-S., RODGERS, M., MIN, C.-K., LEE, J.-S., KINGETER, L., LEE, J.-Y., JONG, A., KRAMNIK, I., LIN, X. & JUNG, J. U. 2012. The Autophagy Regulator Rubicon Is a Feedback Inhibitor of CARD9-Mediated Host Innate Immunity. *Cell host & microbe,* 11**,** 277-289.

YANG, Y., HENTATI, A., DENG, H. X., DABBAGH, O., SASAKI, T., HIRANO, M., HUNG, W. Y., OUAHCHI, K., YAN, J., AZIM, A. C., COLE, N., GASCON, G., YAGMOUR, A., BEN-HAMIDA, M., PERICAK-VANCE, M., HENTATI, F. & SIDDIQUE, T. 2001. The gene encoding alsin, a protein with three guanine-nucleotide exchange factor domains, is mutated in a form of recessive amyotrophic lateral sclerosis. *Nat Genet,* 29**,** 160-5.

YONEKAWA, T. & THORBURN, A. 2013. Autophagy and Cell Death. *Essays in biochemistry,* 55**,** 105-117.

YOUNG, P. E., KUM JEW, S., BUCKLAND, M. E., PAMPHLETT, R. & SUTER, C. M. 2017. Epigenetic differences between monozygotic twins discordant for amyotrophic lateral sclerosis (ALS) provide clues to disease pathogenesis. *PLoS One,* 12**,** e0182638.

ZHANG, K., DONNELLY, C. J., HAEUSLER, A. R., GRIMA, J. C., MACHAMER, J. B., STEINWALD, P., DALEY, E. L., MILLER, S. J., CUNNINGHAM, K. M., VIDENSKY, S., GUPTA, S., THOMAS, M. A., HONG, I., CHIU, S.-L., HUGANIR, R. L., OSTROW, L. W., MATUNIS, M. J., WANG, J., SATTLER, R., LLOYD, T. E. & ROTHSTEIN, J. D. 2015. The C9orf72 repeat expansion disrupts nucleocytoplasmic transport. *Nature,* 525**,** 56.

ZHAO, Q., WEI, Q., HE, A., JIA, R. & XIAO, Y. 2009. CLC-7: a potential therapeutic target for the treatment of osteoporosis and neurodegeneration. *Biochem Biophys Res Commun,* 384**,** 277-9.

ZHONG, Y., WANG, Q. J., LI, X., YAN, Y., BACKER, J. M., CHAIT, B. T., HEINTZ, N. & YUE, Z. 2009. Distinct regulation of autophagic activity by Atg14L and Rubicon associated with Beclin 1-phosphatidylinositol-3-kinase complex. *Nat Cell Biol,* 11**,** 468-76.

ZHOU, Q. M., ZHANG, J. J., LI, S., CHEN, S. & LE, W. D. 2017. n-butylidenephthalide treatment prolongs life span and attenuates motor neuron loss in SOD1(G93A) mouse model of amyotrophic lateral sclerosis. *CNS Neurosci Ther,* 23**,** 375-385.

ZI, Z., SONG, Z., ZHANG, S., YE, Y., LI, C., XU, M., ZOU, Y., HE, L. & ZHU, H. 2015. Rubicon deficiency enhances cardiac autophagy and protects mice from lipopolysaccharide-induced lethality and reduction in stroke volume. *J Cardiovasc Pharmacol,* 65**,** 252-61.

ZOU, Z. Y., ZHOU, Z. R., CHE, C. H., LIU, C. Y., HE, R. L. & HUANG, H. P. 2017. Genetic epidemiology of amyotrophic lateral sclerosis: a systematic review and meta-analysis. *J Neurol Neurosurg Psychiatry,* 88**,** 540-549.

Appendix I

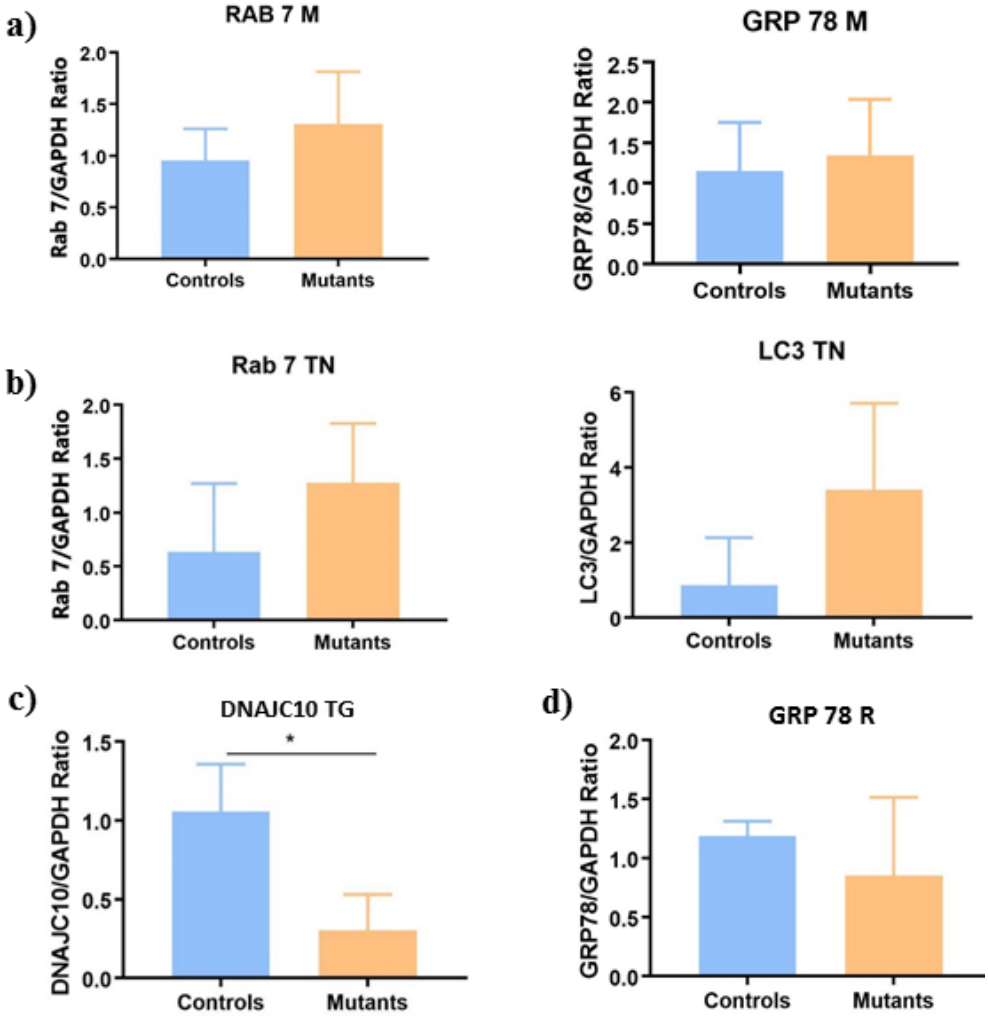

Analysis of protein levels of the UPR, autophagy and endosomal pathway genes in LCLs.

Protein level analysis of proteins under basal levels and drug treatments in LCLs of pedigree SM821. The data is represented by means and SEMs. Quantitative analysis of protein bands was performed by densitometry and the values were normalised against reference gene, GAPDH. The unpaired Student's t-test was used for investigating the effect of mutation. a) Expression of Rab7 and Grp78, at basal levels. b) Expression of Rab7 and LC3II with tunicamycin treatment. c) Expression of DNAJC10 with thapsigargin treatment. d) Expression of Grp78 with rapamycin treatment. M, basal levels; TN, tunicamycin treatment; TG, thapsigargin treatment; R, rapamycin treatment *$p<0.05$.

Appendix II

Protein expression from the spinal cord samples of SALS cases

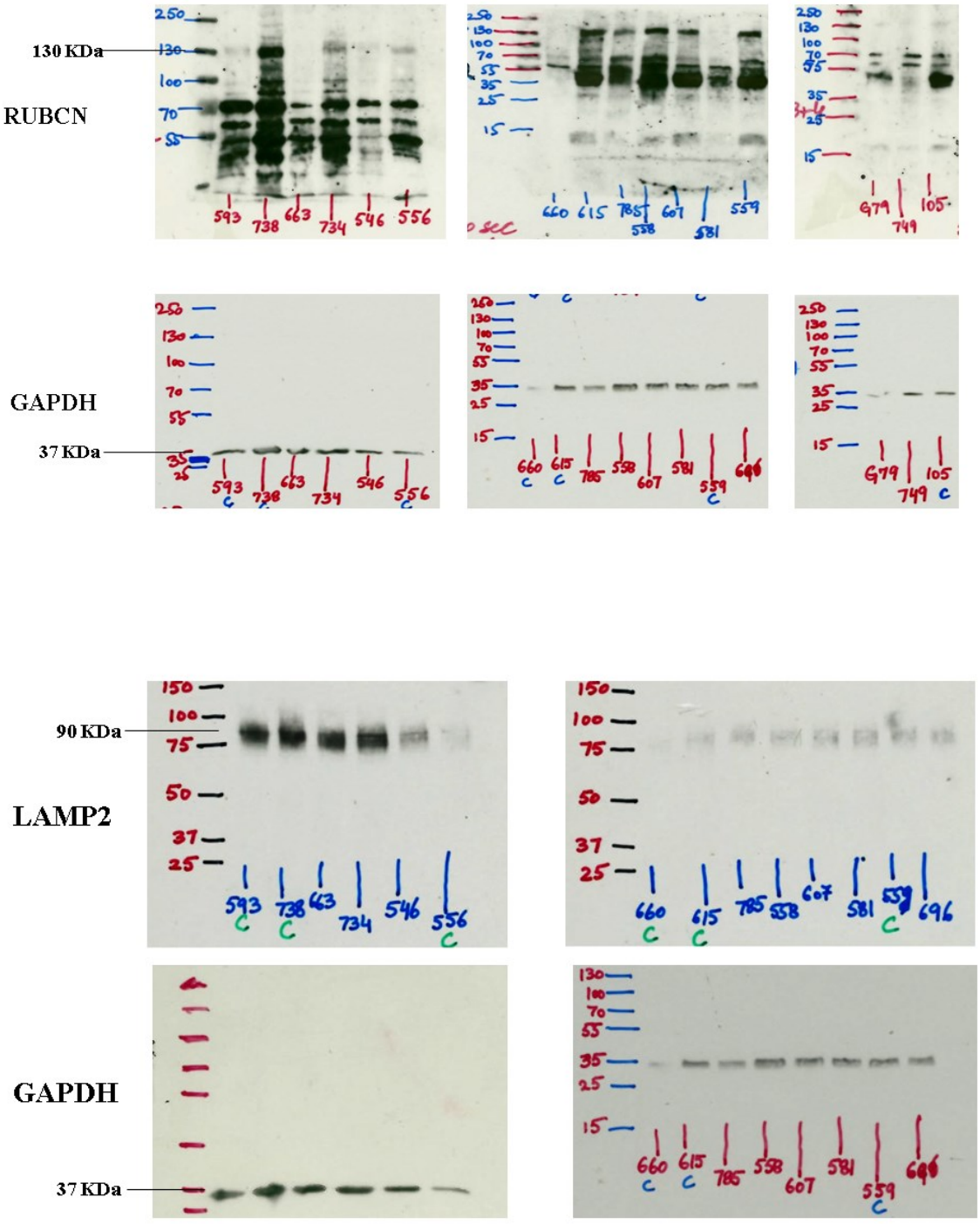

CLCN6

70 KDa

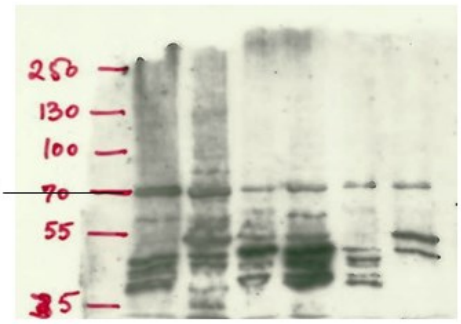

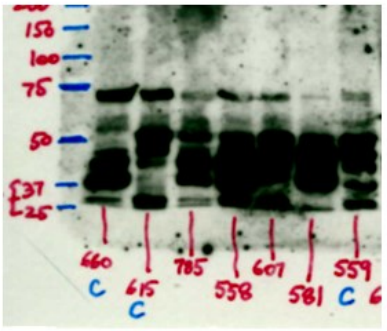

GAPDH

37 kDa

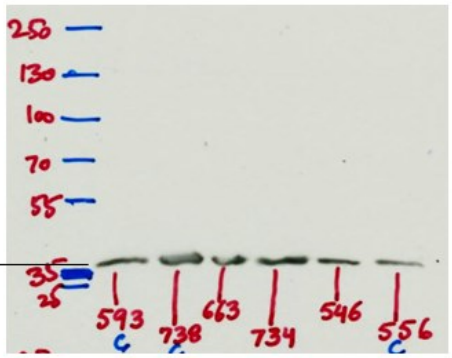

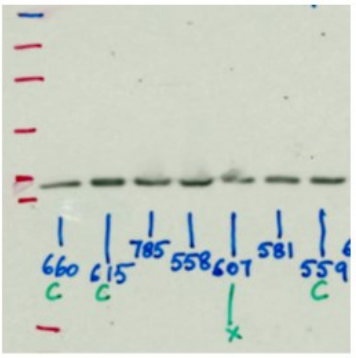

Protein expression in the lymphoblastoid cell lines from pedigree SM331

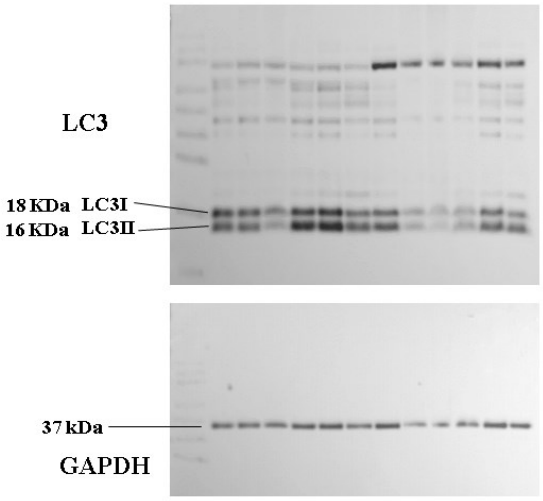

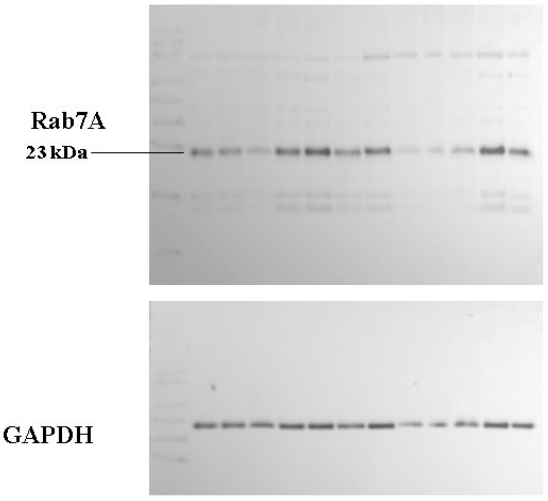

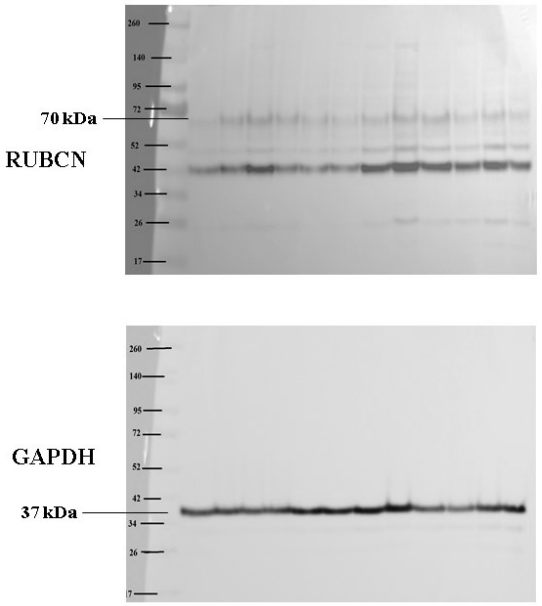

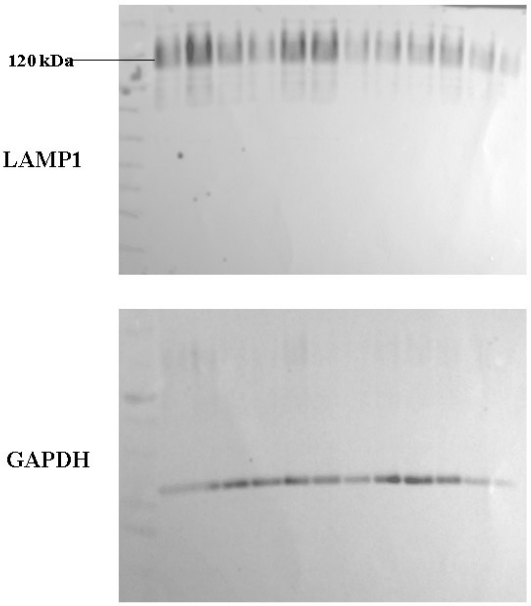

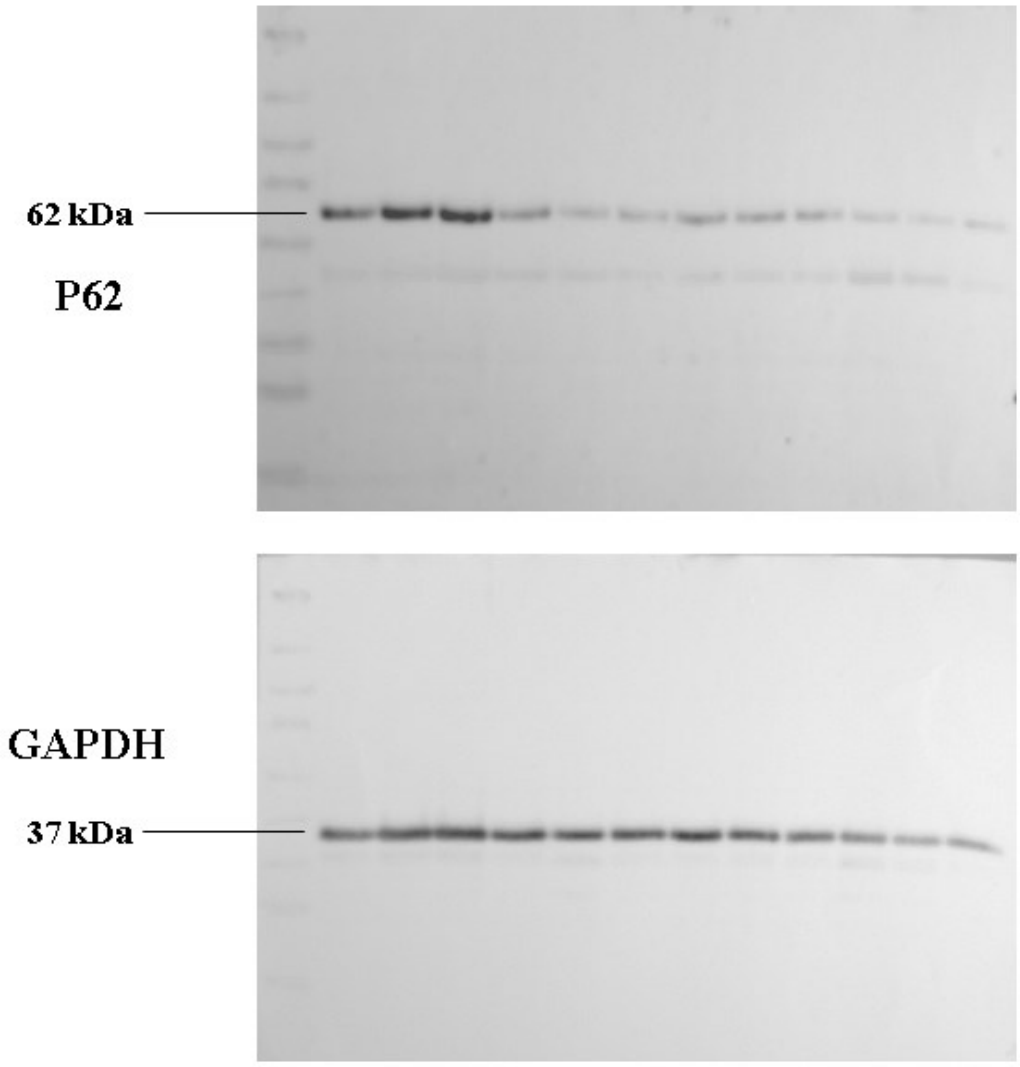
62 kDa
P62
GAPDH
37 kDa

Protein expression in the lymphoblastoid cell lines from pedigree SM821

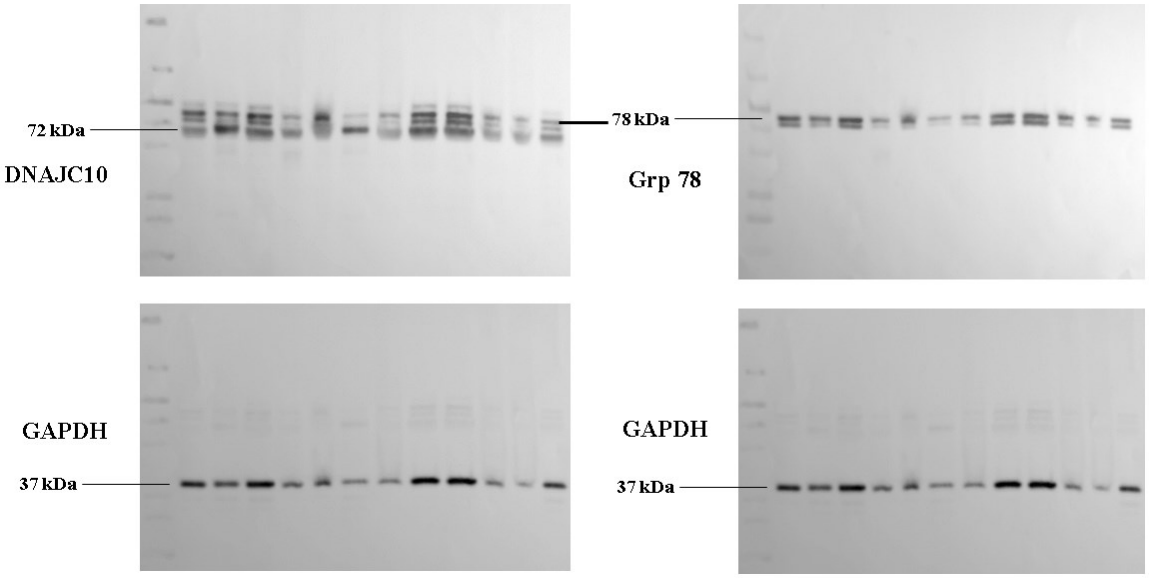

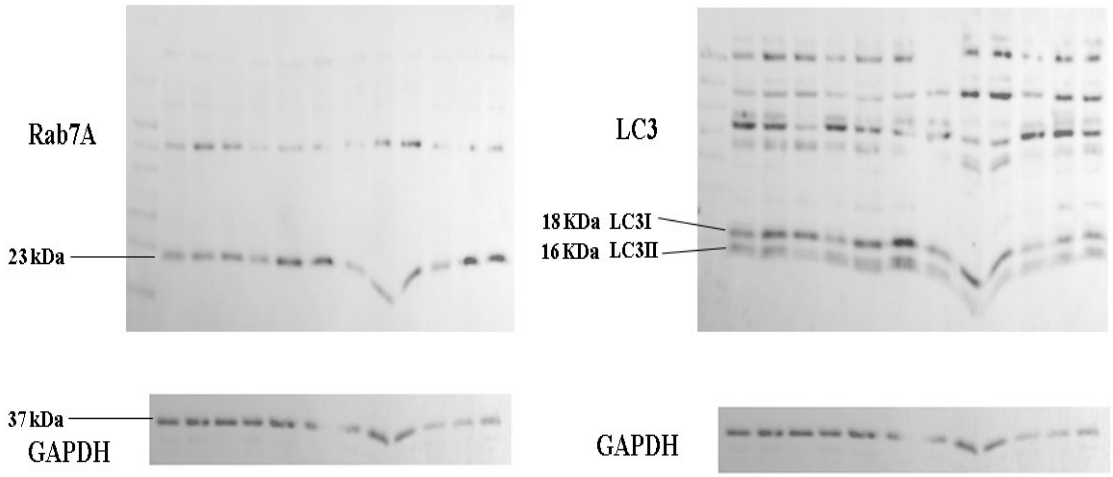

Scientific Contributions

Conferences and guest talks

Guest talk

Delivered a guest talk on my PhD project at University of Health Sciences Lahore, Pakistan (17 January, 2017).

Poster presentation

Salman M, Morris A, Topp S, Smith B, Shaw C, de Belleroche J. The identification of novel mutations causing familial ALS and the elucidation of common disease mechanisms. Poster presentation in 28th international symposium on ALS/MND held in Boston, USA (8-10 December, 2017).